THE EXTRUSION OF

Ti-6Al-4V

by

JULIAN NORLEY B.Sc.(Eng.), A.R.S.M.

A Thesis Submitted For The Degree Of Doctor Of Philosophy Of The University Of London And For The Diploma Of Membership Of The Imperial College

John Percy Research Group,
Department of Metallurgy
and Materials Science,
Royal School of Mines,
Imperial College,
London, SW7 2BP

June 1985

ABSTRACT

The glass-lubricated extrusion of the titanium alloy Ti-6Al-4V has been investigated in the two phase alpha+beta regime and the single phase beta regime.

This has involved the development of an extrusion practice for titanium, based on the Ugine-Sejournet process for steel extrusion. Die wear problems were encountered in the development of the extrusion techniques, and the factors influencing die wear have been discussed. A technique was finally perfected which resulted in the elimination of die wear and a product of excellent surface quality.

Glass was employed as the main lubricant and the variation in the lubricating behaviour of several glasses with the extrusion variables has been studied, the lubricating characteristics being related to the viscosity of the glass at the extrusion temperature.

Hot torsion tests were carried out in the alpha+beta and beta regimes to evaluate suitable constitutive equations to describe the hot working behaviour of the alloy. Structural studies were carried out on the torsion specimens to identify the dynamic restoration mechanisms operative in the two regimes.

The variation in the extrusion pressure with the extrusion variables has been investigated in the two regimes. Empirical relationships have been established between the peak pressure and the extrusion variables using the values of flow stress and temperature compensated strain rate z obtained from the torsion analysis.

The structure and properties of the extrudes have been investigated in the two regimes, following both air cooling and water quenching from the extrusion temperature. Property evaluation has been by tensile testing. The structure and properties of the extrudes have been related to the extrusion variables through the z-parameter.

The temperature changes occurring during extrusion have been investigated using an integral profile technique. An axisymmetric upper bound solution for lubricated extrusion has been developed and used in the prediction of the extrusion pressure and the mean strain rate.

ACKNOWLEDGEMENTS

The author wishes to express his sincere appreciation to all those who have made this work possible, in particular :-

1) Professor T. Sheppard
For his initiation of the project, supervision throughout the work, and influence in obtaining material.

2) S.E.R.C.
For providing the funding.

3) Royal Aircraft Establishment, Farnborough
For provision of the C.A.S.E. award and the use of the tensile testing equipment.

4) Industrial Contacts (see Appendix IV)
For their unselfish and very constructive advice.

5) The Technical Staff at Imperial College
For the quality of their workmanship and their readiness to assist. The author would like to single out Alec Neve for help and advice which was way beyond the call of duty.

6) All the Members of the John Percy Group and J.P.D.C.
For being a great bunch of people and making my time in the group such a happy one.

7) Sandra
For struggling through my scrawl and making such an excellent job of the typing.

And most of all to Jenny - words fail me

CONTENTS

PAGE

CHAPTER THREE - EXPERIMENTAL PROCEDURE

PAGE

SECTION FOUR - STRUCTURE AND PROPERTIES OF EXTRUDED Ti-6Al-4V

LIST OF FIGURES

LIST OF TABLES

CHAPTER ONE

LITERATURE SURVEY

CHAPTER ONE

LITERATURE SURVEY

1.1 TITANIUM AND ITS ALLOYS

1.1.1 INTRODUCTION[1-4]

Titanium and its alloys are used primarily in two areas of application:- strength efficient structures and corrosion resistance service.

Titanium alloys have a higher strength to weight ratio compared with aluminium alloys, steels and nickel alloys, an advantage which is maintained to around 500°C. As a result they have found extensive use in the aerospace industry as airframe and jet engine parts at low to moderately elevated temperatures.

Titanium has excellent corrosion resistance due to its ability to form a very stable self-healing oxide film. It is more resistant to attack than aluminium, stainless steels and copper which has led to an expansion of its use by the chemical industry. Typical applications include tubing in steam condensers and heat exchangers. Titanium also shows an outstanding resistance to corrosion by body fluids and this has led to its use for prosthetic devices.

The main disadvantage of titanium is that it is expensive compared with other common metals, due to the high cost of its extraction and refinement. Hence, in general, it is only used in applications either where weight saving is the primary concern, such as in the aerospace industry where reduced weight results in reduced fuel costs, or in corrosion service where its longer life justifies its selection.

1.1.2 CLASSIFICATION OF TITANIUM ALLOYS[1-5]

Pure titanium undergoes an allotropic phase transformation from the low temperature hexagonal close packed (h.c.p.) alpha-phase to the high temperature body centred cubic (b.c.c.) beta-phase at 882°C. This

transition temperature can be greatly altered by the addition of alloying elements and forms the basis for alloy classification.

Elements which increase the transition temperature and hence stabilise the low temperature alpha-phase are termed alpha-stabilisers. Aluminium, together with the interstitials oxygen, nitrogen and carbon are strong alpha-stabilising elements (Figure 1.1a).

Elements which decrease the transition temperature are termed beta-stabilisers. The beta-stabilising elements may be divided into the beta isomorphous types, e.g. vanadium, molybdenum (Figure 1.1b) or beta-eutectoid types, e.g. manganese, iron, copper, hydrogen (Figure 1.1c) on the basis of the binary equilibrium diagrams which are obtained. The eutectoid reactions which occur, however, are extremely sluggish, and with a few exceptions (e.g. titanium-copper system) are not made use of in the heat treatment of commercial titanium alloys.

So called neutral elements which have little or no effect on the transition temperature include zirconium and tin (Figure 1.1d).

It is customary to classify titanium alloys into three main groups, designated alpha and near alpha, beta and alpha+beta, according to the predominant phases present in the microstructure.

1.1.2.1. ALPHA AND NEAR ALPHA ALLOYS

Fully alpha-alloys consist wholly of the h.c.p. alpha phase and are produced by additions of alpha-stabilising elements and neutral elements which confer solid solution strengthening. As the alloys are single phase, tensile strengths are relatively low, although their high thermal stability leads to reasonable creep strengths. They display good ductility down to very low temperatures and are readily weldable. Formability is limited, however, because of their hexagonal crystal structure and the fact that they exhibit a high rate of strain hardening.

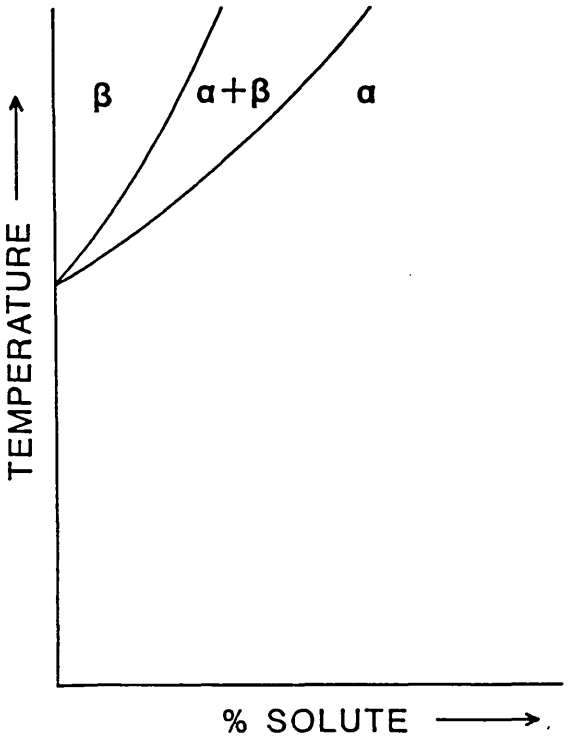

(a) Alpha Stabilizing e.g. Al, O, N, C

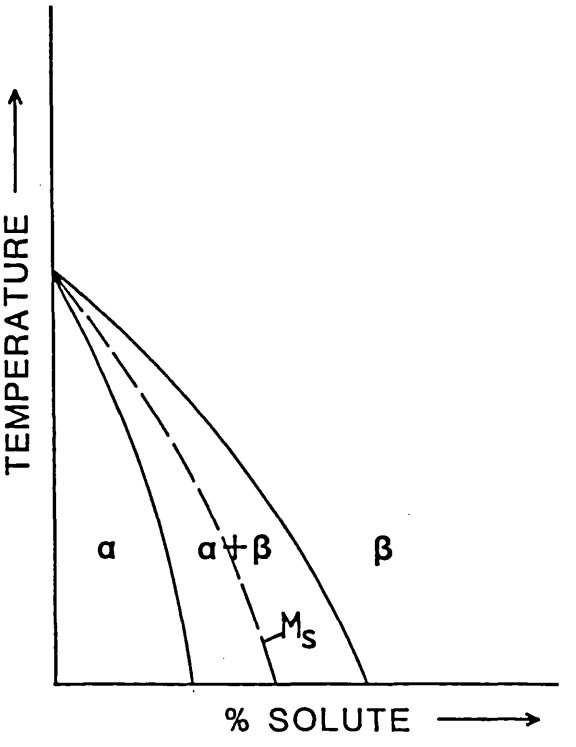

(b) Beta-Isomorphous e.g. V, Mo

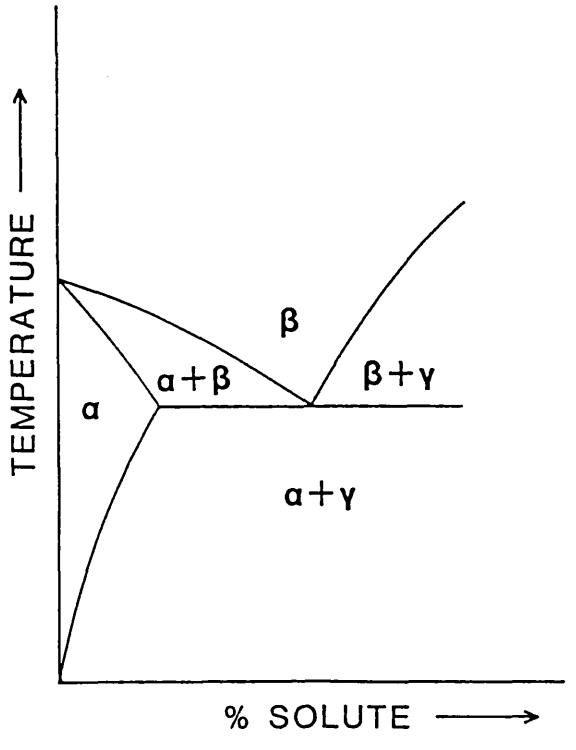

(c) Beta-Eutectoid e.g. Fe, Cu, Mn

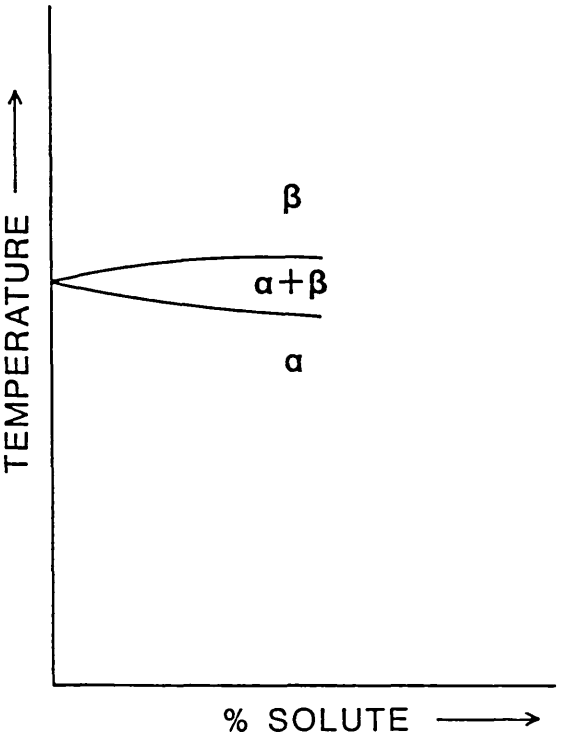

(d) Neutral e.g. Sn, Zr

Figure 1.1 BINARY TITANIUM ALLOY SYSTEMS

Near alpha-alloys, containing up to 2% of beta-stabilising elements, were developed to meet demands for higher operating temperatures in the compressor section of aircraft gas turbine engines. They possess higher room temperature tensile strength than the fully alpha-alloys and show the greatest creep resistance of all titanium alloys at temperatures above approximately 400°C. The presence of the beta-stabilising elements serves to introduce small amounts of the more ductile b.c.c. beta phase into the microstructure which improves formability and allows a limited response to heat treatment.

1.1.2.2 ALPHA+BETA ALLOYS

Most alpha+beta alloys contain elements to stabilise and strengthen the alpha-phase, together with 4-6% of a beta-stabilising element which allows a substantial amount of this phase to be retained on cooling to room temperature. The alloys have good formability and can develop relatively high strengths on heat treatment, although some sacrifice in creep strength occurs above 400°C as well as reduced weldability. Their principal use is for forged components, e.g. in the fan blades of jet engines. Ti-6Al-4V is an alpha+beta alloy, and will be discussed in detail in a later section.

1.1.2.3 BETA ALLOYS

The addition of sufficient beta-stabilising elements to titanium can produce a fully beta structure at room temperature. They are characterized by excellent formability due to the presence of* a high content of solute elements, which allows through hardening of thick sections during heat treatment. The strength levels developed on heat treatment are comparable or superior to those of alpha+beta alloys. The chief disadvantages of beta alloys are higher density, lower creep strength and lower tensile ductility.

* the b.c.c. beta phase, and high hardenability due to the presence of

1.2 TITANIUM - 6 ALUMINIUM - 4 VANADIUM

1.2.1 INTRODUCTION[6-7]

Ti-6Al-4V is the most widely used of all titanium alloys. It has good tensile properties at room temperature and a useful creep resistance up to 300°C. Its resistance to fatigue and crack propagation is excellent and it also has outstanding corrosion resistance. It can be readily formed or forged and is easily welded. Applications are numerous in the aerospace and chemical industries.

1.2.2 GENERAL METALLURGY

Ti-6Al-4V is an alpha+beta alloy containing 6 wt % aluminium and 4 wt % vanadium. The aluminium stabilises and strengthens the alpha phase, so raising the transition temperature, as well as reducing the density of the alloy. The vanadium is a beta stabiliser, which leads to a greater amount of the more ductile beta phase during hot working. The alpha+beta transus temperature is 995±15°C.

1.2.3 PHASE TRANSFORMATIONS IN Ti-6Al-4V

The major phase transformations occurring in titanium alloys have been reviewed by Williams[8]. The phase transformations occurring in Ti-6Al-4V are well documented[6-14] and will only be briefly discussed here.

1.2.3.1 ON COOLING FROM THE BETA-PHASE FIELD

Above the transus temperature the structure is single phase b.c.c. beta. On cooling from the beta phase field, the beta may transform to alpha either by a nucleation and growth process or for more rapid cooling rates by a martensitic transformation process.

Diffusional transformations give rise to Widmanstatten α and 'basket weave' structures. The Widmanstatten structure consists of large colonies of parallel sided plates and is often accompanied by grain boundary alpha. At faster cooling rates the colonies become smaller, contain fewer parallel sided platelets and appear to nucleate independently of the grain boundaries. The distribution of the colonies over all variants of the α/β orientation relationship gives rise to a 'basket weave' structure. The orientation relationship between the alpha and beta phases is the characteristic Burgers relation :-

$$(110)_\beta \,//(0001)_\alpha \;\; ; \;\; [111]_\beta \,//\, [11\bar{2}0]_\alpha$$

During growth of the alpha phase, the vanadium partitions to the beta phase and a vanadium rich beta layer is formed alongside each alpha plate. This results in stabilization of the beta phase and its retention at room temperature.

With rapid quenching rates the b.c.c. beta phase undergoes a martensitic transformation. An acicular hexagonal martensite is the most commonly observed form[8,9]. The martensite occurs as an intimate mixture of individual plates each having a different variant of the Burgers orientation relation. The plates which form first are called primary plates. The primary plates extend for large distances across the parent beta grains and effectively partition the remaining untransformed beta. The partitioned beta subsequently transforms to a series of shorter, thinner secondary plates. The martensite is found to be frequently internally twinned on $\{10\bar{1}1\}_\alpha$

1.2.3.2 ON COOLING FROM THE TWO PHASE ALPHA+BETA FIELD

Solution treatment in the alpha+beta phase field results in the formation of an equiaxed structure of h.c.p. alpha and b.c.c. beta. As the solution treatment temperature is decreased the proportion of the alpha phase increases and the composition of the beta phase becomes more vanadium rich.

On rapid cooling from the solution treatment temperature, the alpha phase remains untransformed, and is termed 'primary α'. The beta phase, however, is either transformed to martensite or, if the vanadium content of the beta phase is above a critical value, it is retained. The approximate temperature at which the beta phase is retained is 815°C[9], the vanadium content of the beta phase being approximately 10%.

On slower cooling from the solution treatment temperature, the alpha phase again remains untransformed, although primary alpha regrowth can occur[7], depending on the cooling rate. The beta phase transforms to plates of alpha and beta by a nucleation and growth process.

1.2.3.3 AGEING TREATMENTS

The martensite formed during rapid cooling of the beta phase will respond to ageing, producing an increase in strength. The martensite decomposes to the equilibrium alpha+beta structure of acicular morphology, the beta being formed directly by nucleation and growth processes. The beta is mostly nucleated heterogeneously at the martensite plate boundaries and at the internal martensite substructure[8]. During the precipitation of the beta phase, the composition of the hexagonal martensite approaches the equilibrium composition of the alpha phase in equilibrium with the beta phase at the ageing temperature. The acicular alpha+beta structure formed in this manner is much finer than that obtained on air-cooling.

The strengthening response obtained depends on the solution treatment temperature, i.e. the amount of martensite present, and the ageing temperature and time. This will be discussed in more detail in the heat treatment section.

1.2.4 HOT WORKING OF Ti-6Al-4V

This subject has been divided into two sections. In the first section, the basic laboratory hot working approach is discussed, i.e. the establishment of empirical relationships between flow stress, strain rate and temperature, and the study of structural changes occurring during deformation in the identification of the operative high temperature restoration mechanisms. In the second section large scale hot working of Ti-6Al-4V is discussed and the interrelationship between the process variables and the structure and properties of the alloy.

1.2.4.1 INTRODUCTION

The subject of hot working of metals and alloys has been extensively reviewed[15-17], and only the basic principles will be discussed here and their applicability to the hot working of Ti-6Al-4V.

The main feature of hot working is that extremely large strains are applied to material at high rates of strain at temperatures above approximately 0.6 Tm, where Tm is the melting temperature in degrees Kelvin. These large strains can be achieved with little or no strain hardening, indicating that dynamic softening processes can operate sufficiently rapidly to balance the strain hardening processes. It is these restoration mechanisms that have been studied in investigations into hot working.

The approach to hot working has generally been to establish empirical relationships between flow stress, strain rate and temperature by using standard laboratory testing techniques adapted for high temperature and high strain rate work. In addition, a knowledge of any structural changes may aid the interpretation of the empirical relationship. The most commonly employed laboratory hot workability tests are tension, compression and torsion, the advantages and disadvantages of each

technique having been reviewed[16]. In general, the stress systems in practice are complex and the laboratory hot-workability tests tend to simplify the situation. However, in may cases, suitable correlations can be obtained between practical behaviour and laboratory tests.

1.2.4.2 EMPIRICAL APPROACH TO HOT WORKING

The similarity between steady state creep and steady state hot working led Sellars and Tegart[15] to propose the relationship :-

$$\dot{\varepsilon} = A\,[\sinh(\alpha\sigma)]^n \exp\frac{-Q}{RT} \qquad 1.1$$

where A, α and n are stress and temperature independent constants, and Q was referred to as the activation energy for the hot working process. This can be rewritten in the form :-

$$z = \dot{\varepsilon} \exp\frac{Q}{RT} = A\,[\sinh(\alpha\sigma)]^n \qquad 1.2$$

where z is the temperature compensated strain rate parameter. The presence of the Arrhenius term in the above equation implies that hot working is a thermally activated process and Q is the activation energy of the rate controlling dynamic softening mechanism. The values of activation energy have been evaluated for many metals and alloys and it was found that they fell into two classes, the classes being characterized by their stacking fault energy.

When a dislocation dissociates into partials there will be a ribbon of stacking fault between them which has a characteristic energy called the stacking fault energy α which provides a force tending to pull the dislocations together. In materials of high stacking fault energy the ribbon widths are small, i.e. the dislocations behave essentially as unit dislocations, while in materials of low stacking fault energy, the ribbon widths are large and extended dislocations are formed. Recovery involves dislocation climb and cross slip. For these processes to occur

the partials must form a constriction, this occurring much more readily in high stacking fault energy materials, so that recovery is much easier in this class of material.

Thus in the first class of material, characterized by high stacking fault energy, the activation energy for hot working, creep and self-diffusion were found to be similar, indicating that dynamic recovery is operational over the whole range as a result of the ease of dislocation climb and cross slip in these materials. This group includes aluminium and its alloys, commercial purity α-iron and ferritic alloys. They are observed to develop subgrains when specimens are cooled rapidly after either small or large amounts of deformation.

In the second class of material of low stacking fault energy there is a marked difference between the values of activation energy for creep and hot working, indicating that while dynamic recovery is the softening process during creep, dynamic recrystallization may well occur during hot working. This is attributed to the difficulty of dislocation climb and cross-slip in these materials. This group includes copper and its alloys, nickel and its alloys and austenitic steels. They show a substructure within the distorted original grains after low deformation, but it is poorly developed and after high deformation when steady state conditions have been attained, they develop an equiaxed recrystallised grain structure.

All the structural observations on metals have been made at room temperature, usually after rapid quenching following the high temperature deformation. Hot worked structures are unstable and tend to recrystallise if held at temperature after deformation, and hence structural modifications may well occur during cooling. Thus while the observations of substructure constitute fairly unambiguous evidence of dynamic recovery, the observation of recrystallised grains could result from either dynamic or static recrystallisation.

1.2.4.3 APPLICABILITY TO THE HOT WORKING OF Ti-6Al-4V

The structural changes occurring during the hot deformation of Ti-6Al-4V, and indeed titanium alloys in general, have received scant attention. Programmes of laboratory hot workability tests have been few and have lacked structural interpretation, so that the dynamic restoration mechanisms are poorly understood.

Titanium is reported to have a stacking fault energy of 300 mJm^{-2} in the basal plane of the h.c.p. alpha phase[18] which puts it in the high stacking fault energy class of materials and suggests that dynamic recovery should occur in the alpha phase. Stacking fault energy measurements have not been carried out on the b.c.c. beta phase of titanium, however b.c.c. metals in general have very high stacking fault energies[19], as illustrated by the ease of cross slip in these materials, which suggests that dynamic recovery should also occur in the b.c.c. phase of titanium. However, as discussed in section 1.2.3 the beta phase undergoes a phase transformation during cooling which appears to remove all trace of a deformation substructure.

In the alloy Ti-6Al-4V, the addition of aluminium and vanadium contribute to produce a two phase structure of h.c.p. alpha and b.c.c. beta below the beta transus, the additions conferring substantial solid solution strengthening to the two phases. The influence of additions of aluminium and vanadium on the individual stacking fault energies of the two phases has not been investigated, but the two phase structure exhibits markedly different hot deformation behaviour compared to the single phases in unalloyed titanium, which would suggest that different dynamic restoration mechanisms may well be operative in the two phase structure. Above the transus in Ti-6Al-4V the structure is single phase b.c.c. beta, albeit a solid solution of aluminium and vanadium, and hence some similarity with the b.c.c. phase in unalloyed titanium might be expected.

The activation energies for self-diffusion in super-pure titanium in the alpha and beta phases are 169, 147 J/mole and 152, 818 J/mole respectively[20, 21]. Several authors have made use of these values in their interpretation of the hot deformation behaviour of Ti-6Al-4V.

Sastry et al[22] carried out compression testing of Ti-6Al-4V in the alpha+beta regime using strain rates of 0.005 s^{-1} to 0.5 s^{-1}. Activation energies were obtained from plots of $\ln \dot{\varepsilon}$ versus $\frac{1}{T}$, values of 470,000 J/mole and 572,000 J/mole being obtained at flow stresses of 200 and 100 MPa respectively. They concluded that since these values were much higher than those for self-diffusion in the alpha and beta phases, dynamic recrystallisation might be occurring. Electron microscopy studies above 850°C, indicated both dynamic recovery and dynamic recrystallisation as evidenced by hexagonal networks of dislocations in the alpha phase and the formation of small equiaxed alpha.

Bryant[23] correlated the available hot deformation data on Ti-6Al-4V in terms of the Zener-Holloman parameter. The activation energies were obtained at constant flow stress from plots of $\ln \dot{\varepsilon}$ versus $\frac{1}{T}$. The vast majority of the data was obtained from testing in the alpha+beta regime. He was able to divide the data into two regions, described as "low temperature mechanism" and "high temperature mechanism" for which the former had an activation energy of 355,878 J/mole and the latter 711,756 J/mole. Again comparison was made with the activation energies for self-diffusion in the alpha and beta phases, and he concluded that deformation rate control by dislocation climb was unlikely. He was not able to identify a mechanism for the low temperature deformation activation energy, but suggested that the high temperature mechanism might be dynamic recrystallisation. No structural studies were carried out to verify these claims.

Hence the limited data available would suggest that dynamic recrystallisation occurs in the two phase alpha+beta regime of Ti-6Al-4V. No work has been done on obtaining the activation energy for hot working in the beta regime.

1.2.4.4 LARGE SCALE HOT DEFORMATION OF Ti-6Al-4V

The most important feature of the hot working of Ti-6Al-4V is the comparative merits of working in the two phase alpha+beta regime (termed alpha+beta working) and the single phase beta regime (termed

beta working), with regard to the pressure requirements and the resultant structure and properties of the alloy. Most of the work done on the hot deformation of Ti-6Al-4V relates to the forging process[6,7, 24-29], with only Gurney and Male having published any substantial work on extrusion[30-33]. The same general principles were observed in forging and extrusion and are summarized below.

Deformation in the single phase beta regime where the starting structure consists of coarse beta grains results in substantially lower working loads compared to alpha+beta working. This permits the fabrication of more complex shapes to closer dimensional tolerances and hence economies in material utilization.

The major problem with finish working in the beta regime is that on air-cooling a coarse Widmanstatten alpha+beta structure is produced (section 1.2.3.1) which has lower attendant ductility and reduction of area values than alpha+beta worked material. Refinement of this structure, and hence an increase in ductility, can be achieved by increasing the severity of deformation in the beta phase field. Thus it is essential in beta working processes, and this is particularly the case in forging, where lower strains are employed compared to extrusion, that sufficient deformation is given to all sections of the work piece to ensure adequate refinement of the structure.

The beta worked structure is reported to have substantially higher fracture toughness and improved creep strength compared to alpha+beta worked material. This improved fracture toughness is attributed to the increased crack tortuosity occurring within the Widmanstatten structure.

If high ductility and R.of A. values are the primary requirement, however, then alpha+beta working with its higher attendant loads is required. The R. of A. and ductility values increase with an increase in the proportion of alpha phase, i.e. lower working temperatures, however the fracture toughness deteriorates.

1.2.4.5 HEAT TREATMENT OF Ti-6Al-4V[3,6-14,34]

Most of the applications of Ti-6Al-4V call for it in the annealed condition, and the properties specified in the British Standards refer to a heat treatment at 700°C followed by air-cooling to room temperature. Annealing serves primarily to provide adequate toughness, maximum ductility at room temperature, dimensional and structural stability at room temperature and improved machinability.

The tensile strength of small sections such as bolts and other fasteners can be improved by heat treatment high in the alpha+beta field, followed by water quenching, the beta phase transforming to martensite (section 1.2.3), and ageing (section 1.2.3.2). The strengthening response obtained depends on three factors :- the solution treatment temperature and the ageing temperature and time. These variables have been investigated by several authors[6,7,10-13,34]. The solution treatment temperature governs the proportion of beta phase, and its vanadium content, and hence the proportion of martensite formed on quenching. Increasing the solution treatment temperature in the alpha+beta phase field increases the proportion of martensite and hence increases the strengthening response on ageing, although the reduced proportion of alpha phase results in lower ductility[6,7,34].

I.M.I.[6] recommend for their Ti-6Al-4V alloy, IMI 318, a solution treatment at 900°C for ½ hour followed by water quenching and ageing for 8 hours at 500°C. Timet[7] recommend for their Ti-6Al-4V alloy, a solution treatment at 955 ± 15°C followed by water quenching and ageing for 4 hours at 540°C.

The strengthening effect can only be obtained following a rapid quench from the solution treatment temperature[6,7,34]. In addition, the alloy is of relatively low hardenability, and although some strength increase can be obtained in sections as large as 50 mm, the effect gets progressively less and is negligible in thicker sections[6,7].

Gurney and Male in their work on the extrusion of Ti-6Al-4V[30-33] looked at the effect of water quenching of the extrudes on the resultant properties and compared them with air cooled extrusions. The extrudes were given a direct ageing treatment of 4 hours at 540°C. They observed an increase in tensile strength of approximately 15%, with only a slight loss in ductility, although at the expense of reduced toughness.

1.3 TITANIUM EXTRUSION

1.3.1 INTRODUCTION

This section concentrates predominantly on the practical aspects of titanium extrusion. Published information on the subject is scarce, with a large proportion of it dealing mainly in generalities rather than the important specifics of lubricant selection and surface quality.

The only published works of any substance were conducted by Gurney and Male[30-33] and Adair et al[35-37], all of whom worked at the Air Force Materials Laboratory in Ohio. They investigated the extrusion of several alpha, alpha+beta and beta alloys, including Ti-6Al-4V. The technique they employed for extruding titanium, however, although successful, is very unconventional and hence an alternative technique was sought in this work.

Titanium is normally extruded using a modified version of steel extrusion practices and this was the approach adopted in this work. The subject of steel extrusion is well documented, with excellent work on a laboratory scale having been done by Hughes and Sellars[38-43]. In addition, several papers have been published on the industrial scale extrusion of steel[44-47].

Thus this survey is derived mainly from steel extrusion papers, modified to apply to titanium extrusion where appropriate.

1.3.2 TITANIUM EXTRUDERS AND USES OF TITANIUM EXTRUSIONS

Martin Marietta Titanium of America is the free worlds largest supplier of titanium extrusions[48-50]. In this country, IMI Titanium[51], in association with Osborne Steel Extrusions[44-46], have recently started to provide titanium extrusions after a break of several years.

Most of the available alloys of titanium can be extruded and a wide variety of extruded shapes can be produced[48-57]. The major uses of titanium extrusions are in airframe and aircraft engine parts. Typical applications are in flash butt welded rings used in compressor casings for jet engines, and flaptracks[48-51]. Ti-6Al-4V extruded angle chords are used in landing gear support beams[56,57]. Extruded titanium pipe and hollow shapes find use in the pulp and paper, petrochemical, chemical and marine environments, for such applications as heat exchangers, condensers and piping systems[48-50,53,54].

1.3.3 THE EXTRUSION PROCESS FOR TITANIUM

1.3.3.1 INTRODUCTION - EARLY ATTEMPTS TO EXTRUDE TITANIUM BASED ON ALUMINIUM EXTRUSION PRACTICES

Initial efforts to extrude titanium were based on the assumption that it would extrude like aluminium[54]. The extrusion of aluminium is accomplished using flat-faced dies with no lubrication and is shown schematically in Figure 1.2[59,60]. This type of metal flow is known as unlubricated or turbulent flow. The central portion of the billet travels forward through the die more rapidly than the sides which are restrained by friction at the container walls. This results in the formation of a dead metal zone under the shoulders of the die in which the metal layers are stagnant, and a zone of highly sheared metal which flows through the die to form the outer surface of the extrude. Towards the end of the extrusion the oxidised sheared metal skin of the billet bulges in towards the centre, manifesting itself as an annulus of defective material within the extrude. This extrusion defect or "piping" can result in up to 30 per cent of the extrusion being rejected[61].

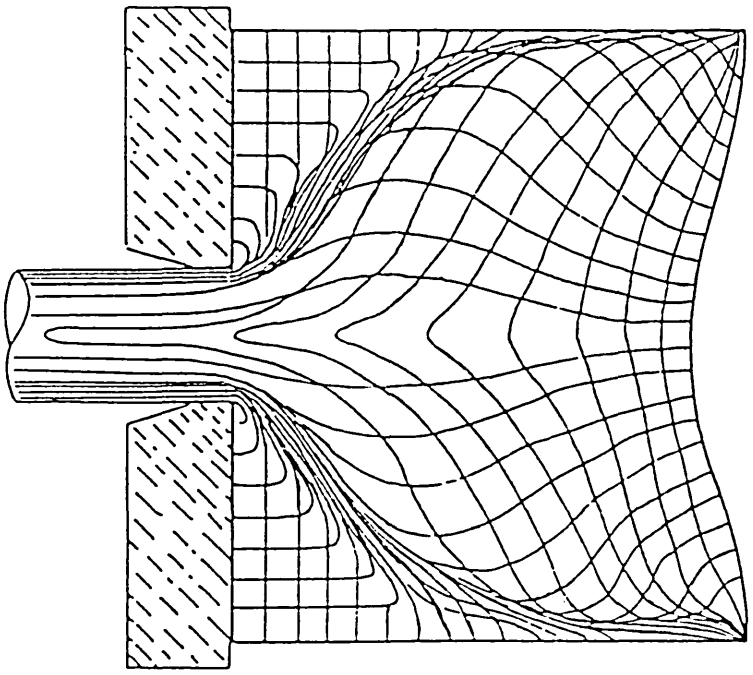

Figure 1.2 SCHEMATIC OF UNLUBRICATED METAL FLOW[59]

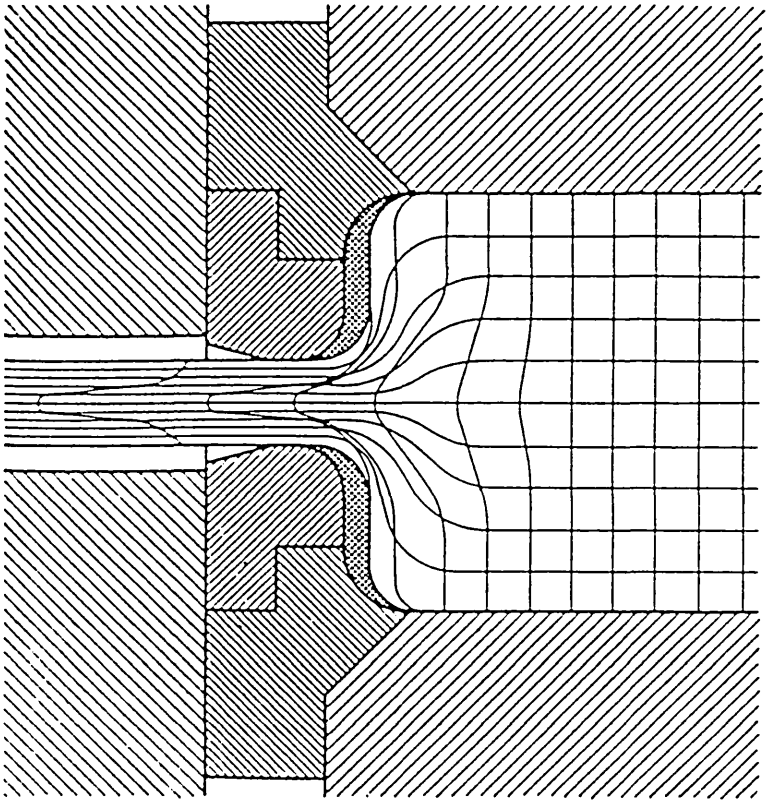

Figure 1.4 SCHEMATIC OF LUBRICATED METAL FLOW[59]

The main advantage of this type of flow is a cosmetic one. The oxidised skin of the billet is sheared off during extrusion, and metal from the interior of the billet forms the surface of the extrude. This gives an attractive, bright, defect-free surface to the extrude that makes it a "net" extrusion, requiring little or no machining.

Another important feature of aluminium extrusion is that it is carried out at temperatures close to its melting temperature, and therefore very low speeds have to be employed to avoid incipient melting, which occurs as a result of large temperature rises.

Titanium has a much higher melting temperature than alminium (1678°C c.f. 660°C), and hence its hot working range is much higher (850°C - 1100°C c.f. 250°C - 500°C). When initial efforts to extrude titanium were made using variations on the aluminium practice, the titanium galled and welded to the tools. The dies changed drastically from initial configuration during the stroke because of seizing and galling. The product lacked dimensional integrity and revealed many surface defects[54].

Much greater success was achieved using techniques similar to those employed for steel extrusion. Steel is extruded in the temperature range 1000°C - 1300°C, and hence there is some degree of overlap of the extrusion ranges. Steel extrusion is well documented[38-47,59-65] and since the principles applying to steel, are appropriate in the main to titanium extrusion, much use can be made of this literature.

1.3.3.2 THE USE OF GLASS AS AN EXTRUSION LUBRICANT

1.3.3.2.1 INTRODUCTION

To avoid seizing between the hot billet and tooling during extrusion, lubrication must be employed. Experiments have been made with a wide variety of lubricants[60,65], but in general the most satisfactory form of lubrication for high temperature extrusion is glass and this has become the standard practice for the extrusion of titanium[29,30,52-55].

The main advantage of glass derives from its very low coefficient of friction, less than 0.01, at extrusion temperatures[41,44]. In addition, the glass insulates the tooling from the hot billet during extrusion, thereby preventing overheating and hence wear.

1.3.3.2.2 THE UGINE - SEJOURNET PROCESS FOR GLASS LUBRICATED EXTRUSION

The technique employed for titanium extrusion is a modification of the Ugine-Sejournet process which was developed for the extrusion of steel[60]. This is shown schematically in Figure 1.3.

Glass is applied to the billet/liner interface by rolling the hot billet down an inclined table covered with powdered glass which softens and adheres to the billet. The die/billet interface is lubricated by means of a preformed pad of glass powder or a wad of glass fibre placed between the die and billet[38-46,52].

During extrusion the billet slides through the container without appreciable friction, while at its front end, the glass pad melts down layer by layer, and coats the extruded product with a film of approximately 20 - 100 microns thickness[38-46,60,64,65].

1.3.3.2.3 METAL FLOW IN GLASS - LUBRICATED EXTRUSION

In aluminium extrusion, as discussed in section 1.3.3.1, a substantial proportion of the required energy is consumed in overcoming the internal shear of metal near the container wall. With glass lubrication the element of friction is greatly reduced, so that the power required for extrusion is more efficiently used in deforming the metal. The type of flow obtaining in glass lubricated extrusion, known as streamlined or lubricated metal flow, is shown schematically in Figure 1.4[59]. A regular flow pattern is obtained with the surface of the billet extruding to form the surface of the extrude. No dead metal zone is formed and the extrusion defect is essentially eliminated, resulting in a higher product yield compared to aluminium extrusion[38,61,62].

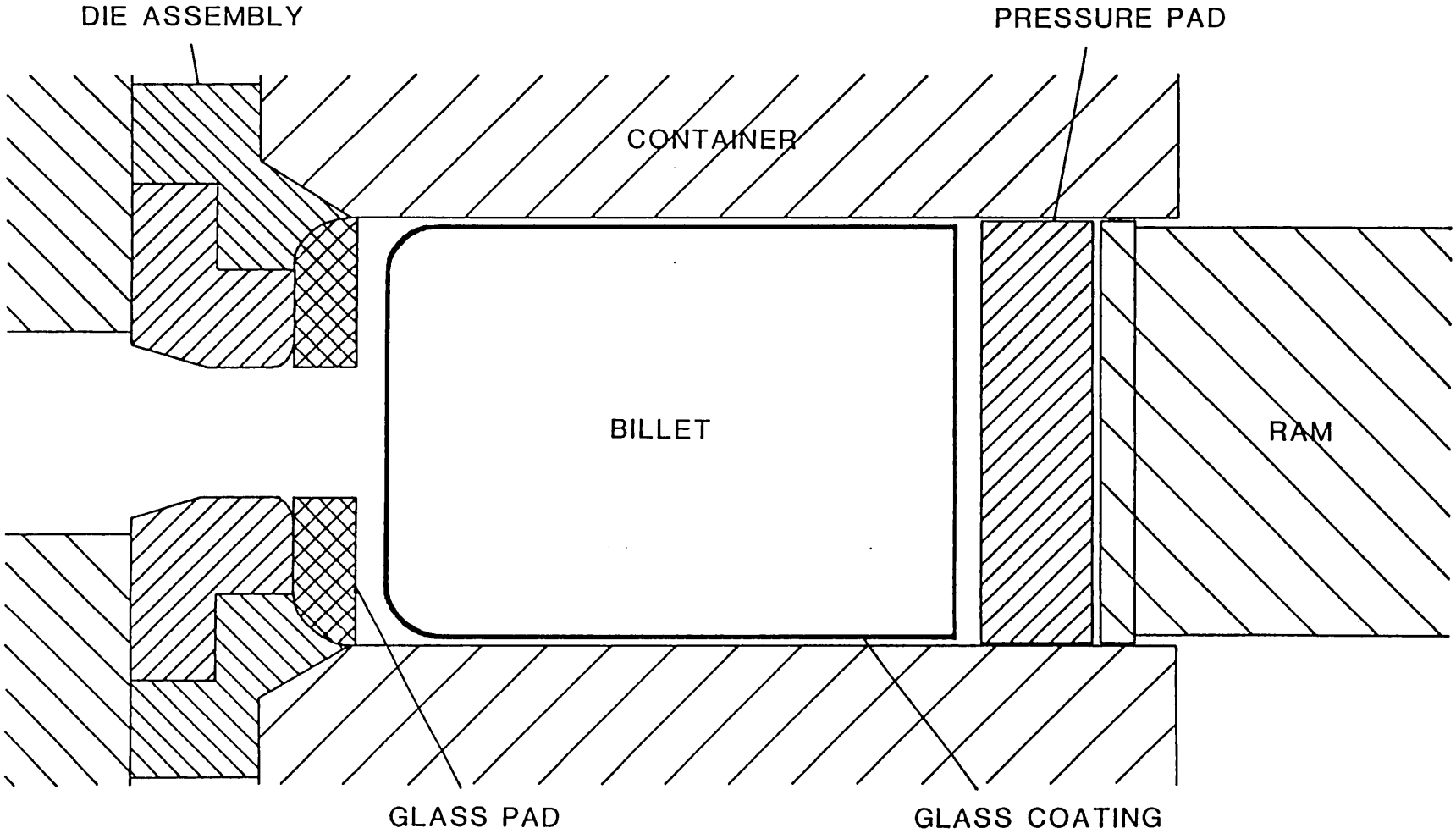

Figure 1.3 UGINE-SEJOURNET PROCESS FOR GLASS-LUBRICATED EXTRUSION

To assist streamlined metal flow, industrial die assemblies are normally dish-shaped with a radiused entry to the orifice (Figure 1.4)[38].

1.3.3.2.4 CLASSIFICATION OF EXTRUSION GLASSES

Two methods are used for categorising glasses as to their suitability as extrusion lubricants - measurement of the softening point and measurement of the viscosity variation with temperature. This is shown schematically in Figure 1.5. The softening point of the glass is usually defined as the temperature at which the viscosity of the glass is $10^{7.6}$ poise[38,64-65]. Bayer U.K., the major supplier of extrusion glasses, define their softening point as the temperature at which the glass just adheres to a biscuit tile placed in a furnace. There would appear to be a reasonable agreement between these two definitions. If the softening point of the glass is too high, the glass will act as an abrasive, however, if the softening point is too low, the glass will flow through the die too quickly leaving an unlubricated back end. Similar considerations apply to the softening rate of the glass, a rapid softening rate leading to early exhaustion of the glass reservoir, and a slow one to the glass not being melted in sufficient quantity to provide adequate lubrication. Experience has shown that the ideal glasses are ones having a softening point of approximately $\frac{2}{3}$ of the billet temperature for the pad glass, and approximately $\frac{1}{2}$ of the billet temperature for the tray glass[38,64,65].

The second method involves the measurement of the viscosity variation with temperature. Opinions vary regarding the appropriate degree of viscosity that the glass should exhibit at the extrusion temperature[63,66,67], but an overall range of 10^2 - 10^4 poise viscosity is usually suggested.

Glasses are made in a wide variety of compositions so that it is possible to provide efficient lubrication over an extremely wide range of temperatures[38,43,63-67]. Typical glasses are shown in Table 1.1[66]. They have an average viscosity of 10^4 poise over the corresponding temperature range.

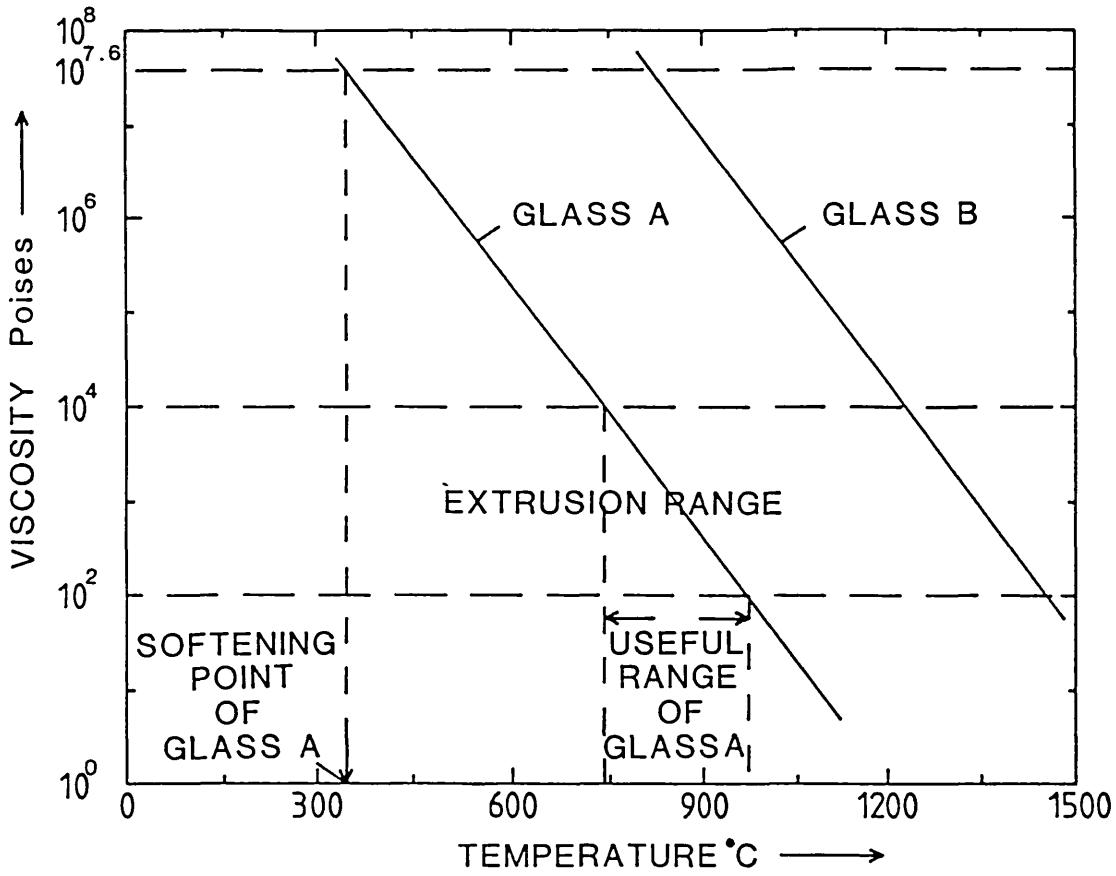

GLASS A - Low Softening Point, Low Working Range

GLASS B - High Softening Point, High Working Range

Figure 1.5 SCHEMATIC CATEGORIZATION OF EXTRUSION GLASSES

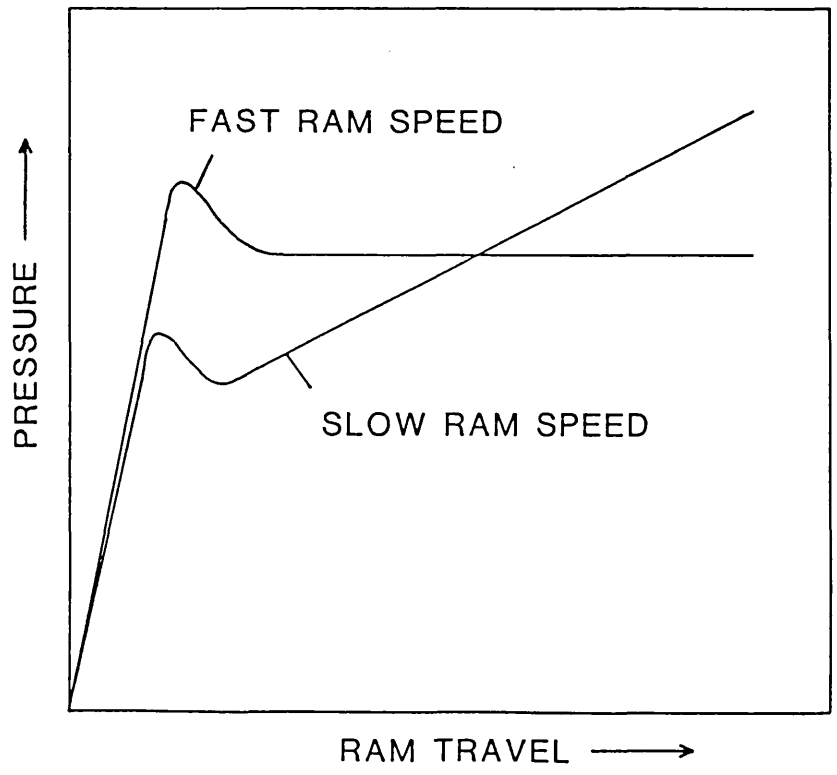

Figure 1.6 EFFECT OF RAM SPEED ON EXTRUSION PRESSURE

Temp. °C	SiO_2	B_2O_3	BaO	Al_2O_3	CaO	MgO	PbO	Na_2O	K_2O	Rest
450 - 600		20.0					80.0			
600 - 750	27.3						71.0		1.5	0.2
850 - 1000	69.0		3.4	3.4	6.1	3.2		16.2	0.7	0.2
1000-1100	80.0	12.0		3.0				4.0	0.3	0.7
1100-1200	50.0	7.0	3.0	21.0	14.0					5.0

TABLE 1.1 EXAMPLES OF LUBRICATING GLASSES[66]

1.3.3.3 THE USE OF MOLYBDENUM DISULPHIDE GREASE[38]

The application of molybdenum disulphide grease to the liner when glass is used as the main lubricant results in a very smooth pressure stroke and the complete absence of jarring and juddering during ejection of discards or stickers. It also probably provides some lubrication if the skin temperature of the extruding billet falls to a level where glass lubrication is no longer effective. The grease is applied to the liner and die by swabbing, the heat of the container causing the more volatile hydrocarbons to burn off leaving a dark grey deposit of graphite and molybdenum disulphide. This is held in place by the bentonite clay which such greases usually contain.

1.3.3.4 EXTRUSION TEMPERATURES

Titanium and its alloys are extruded at temperatures of 870°C - 1100°C[52-55]. The temperature selected depends on the alloy composition, press capacity, lubricant and die performance. In general, higher temperatures are more demanding on lubricants and dies, but the resulting lower pressures allow the extrusion of thinner, more complex shapes and hence economies in material utilization.

The influence of extrusion temperature on the structure and properties of Ti-6Al-4V was discussed in section 1.2.4.4.

1.3.3.5 EXTRUSION SPEEDS

Most of the following observations have been made on steel extrusions, but are equally applicable to titanium extrusion.

The tooling temperatures employed in titanium extrusion are in the range 200°C - 500°C[52]. Thus during extrusion there is a balance between the heat losses from the billet to the tooling and heat generated due to deformation work. For a given extrusion temperature the ram speed employed controls this heat balance and can markedly influence the shape of the pressure-displacement curve.

A peak is always observed after the billet upsetting stage (Figure 1.6), the peak increasing with increasing ram speed[30,38,44,45]. However, while at high ram speed, after an initial fall, the pressure remains essentially constant; at low ram speed the pressure progressively increases until it may become higher than the peak pressure obtained at higher ram speed[38,46]. In the former case, there is a balance between heat losses and heat generation, but in the latter case the contact time between the billet and tooling is prolonged and severe billet chilling occurs, outweighing any heat generation. At slow ram speeds, therefore, marked heterogeniety of structure amy occur between the front and back ends of the extrude. In addition, overheating of the tooling can occur, resulting in wear. As a final disadvantage the chilling of the billet may prevent the glass from softening adequately during extrusion, resulting in a dry back end[38,43,45].

These problems can be overcome by the use of fast ram speeds, which reduce the contact time between the billet and tooling, thereby reducing billet chilling and overheating of the tooling.

Commercially extrusion speeds of 100 mm/sec - 250 mm/sec are employed, with the extrusion being complete in typically 2-3 seconds[29,55]. These fast ram speeds are achieved by the use of nitrogen/hydraulic oil accumulator systems that are capable of delivering large volumes of oil under high pressure in a short time[29,38,45,53,55].

1.3.3.6 BILLET PREPARATION

Since the billet surface extrudes to form the surface of the product, billet preparation is very important.

The starting material for the extrusion billets is in the form of as-rolled or as-forged bar. This is smooth turned to eliminate any surface defects.

On heating titanium billets in air, a brittle oxide contaminated layer is formed on the surface of the billet. During extrusion the scale cracks and prevents proper lubrication. This results in poor

surface finish and may even cause tool wear[29,44-47]. In addition, many glasses in the molten state react with the oxide scale thereby altering the glass's thermal properties and viscosity and rendering it unsuitable[29].

To minimise scale formation during heating, the billets are heated rapidly by induction under a protective argon atmosphere. On removal from the coil, the billet is immediately rolled through glass powder to minimise oxidation during transfer. Alternatively, the billets can be pre-coated with a glass slurry prior to heating[30,52,64,67], however this normally necessitates grit blasting of the billet to prevent the glass flowing off during heating.

Possibly the greatest advantage of induction heating is the possibility of introducing radial and axial temperature gradients in the billet. This is shown schematically in Figure 1.7[44,45].

During transfer of the billet, and also during the extrusion stroke, the surface of the billet cools much more rapidly than the core. This creates problems in the extrusion of hollow sections and externally finned tubes, which extrude better if the bore is cooler than the surface. Induction heating makes possible the introduction of a radial temperature gradient with the billet centre being cooler than the outer surface to compensate for heat losses from the surface[44,45].

1.3.3.7 EXTRUSION DIES

One of the major problems associated with the extrusion of steels and titanium alloys is die wear. The wear that can be allowed depends on the dimensional requirements of the extruded sections. If the extrusion is to be machined all over, considerable die wear can be tolerated. However, if a precision extrusion is required for use in the as-extruded condition or for further drawing, little die wear can be permitted.

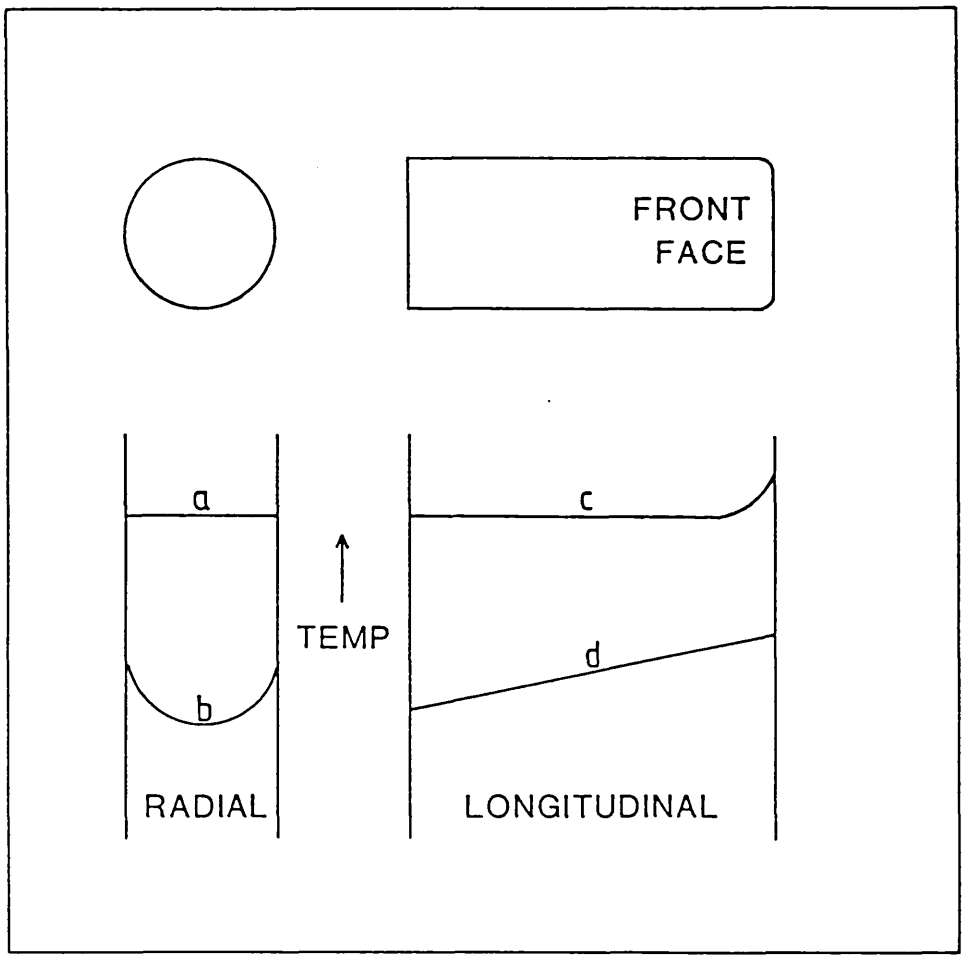

RADIAL :-
- a - Evenly Heated Billet
- b - Radial Gradient With Relatively Cool Core

LONGITUDINAL :-
- c - Front End Superheated
- d - Gradual Longitudinal Gradient Cooling From Front to Back

Figure 1.7 TYPICAL BILLET TEMPERATURE GRADIENTS POSSIBLE WITH INDUCTION HEATING[44]

Extrusion dies are normally heated to around 200°C[45]. During extrusion the temperature at the radiused entry of the die orifice rises to above 600°C[45] and can be as high as 1000°C[41]. If the die material employed does not have sufficient wear resistance, softening of the die metal occurs at the radiused entry, leading to erosion of the die ("wash-in").

The die material employed must therefore combine adequate resistance to softening and wear with adequate toughness, to avoid cracking of the die during service.

There are three classes of hot work steels :- chromium, tungsten and molybdenum. Typical examples are given in Table 1.2, while Table 1.3 shows typical in-service characteristics of these steels[68]. The most commonly used hot work steels for the manufacture of dies used in the extrusion of steel are the 5% Cr-V-Mo steel H13[69] or, for improved wear resistance, the 9% W steel H21[38,45,64,65].

The alloying elements added are strong carbide formers and increase the resistance of the steel to softening when it is heated, the precipitation of alloy carbides promoting secondary hardening at approximately 550°C[70].

Dies can be manufactured in single pieces or built up, i.e. a die insert, a support ring and a die backer[45]. The use of die inserts saves money as the support ring and die backer need not be made from the expensive hot die steel.

The dies are inspected and dressed after each extrusion. If the die is not out of tolerance it can be welded up and ground back to profile, repair work being possible several times on the same die[44-47].

For the extrusion of complex, thin sections improved wear resistance is sometimes required. This can be achieved by flame spraying the dies with a thin coating, approximately 50 - 100 microns thick, of ceramic such as alumina or zirconia[30,52,67]. Flame sprayed coatings have been used to extrude refractory metals at 2350°C[67]. Recoating of the die is possible if the coating is damaged.

Hot Work Steel Type	A.I.S.I. Number	% C	% W	% Mo	% Cr	% V	% Other
Cr	H13	0.35		1.50	5.0	1.0	
Cr	H19	0.40	4.25		4.25	2.0	4.25 Co
W	H21	0.35	9.0		2.0		
W	H26	0.50	18.0		4.0	1.0	
Mo	H42	0.60	6.0	5.0	4.0	2.0	

TABLE 1.2 TYPICAL HOT-WORK STEELS[68]

Hot Work Steel Type	A.I.S.I. Number	Approx. Hardness After Tempering	Machin-ability	Toughness	Resistance To Softening	Resistance To Wear
Cr	H13	38 - 53	Medium/High	Very High	High	Medium
Cr	H19	40 - 57	Medium	High	High	Medium/High
W	H21	36 - 54	Medium	High	High	Medium/High
W	H26	43 - 58	Medium	Medium	Very High	High
Mo	H42	50 - 60	Medium	Medium	Very High	High

TABLE 1.3 IN SERVICE CHARACTERISTICS OF HOT-WORK TOOL STEELS[68]

Various other techniques are employed for improving wear resistance, including surface hardening by carburising or nitriding[68], and the use of nimonic, cemented tungsten carbide and nickel-bonded titanium carbide dies[69].

1.3.3.8 SECONDARY OPERATIONS

Extruded sections are usually air cooled on the runout table of the extrusion press. The extrusion is covered by a thin film of glass, which has to be removed before any heat treatment is carried out. Two methods are available; grit blasting followed by an etch in a solution of hydrofluoric and nitric acids, and molten salt deglassing in sodium hydride and sodium hydroxide at 450°C[52]. After de-glassing the extrusions are heat treated and straightened by isothermally hot stretching at elevated temperatures[52,53]. Warm drawing of the finished extrusion is sometimes carried out to improve the dimensional tolerances and the surface quality[29.54].

1.3.3.9 "NET" EXTRUSIONS

Aluminium extrusions can be provided in the form of "net" extrusions of great complexity. In the earlier days of titanium extrusion, "net" extrusions could not be produced[29,52,53], the shape being delivered as a "gross" extrusion with sufficient metal to permit machining to final shape. This machining was expensive and wasteful of material and was the main reason for the poor economic competitiveness of extruded titanium shapes. Nowadays some producers claim they can provide close tolerance "net" extrusions that can be used as received. In practice, however, it would appear that some machining is still necessary.

Dimensional tolerances established by various producers vary from $\pm$ 0.38 mm/0.76 mm for sections under 25 mm to $\pm$ 1.0/2.0 mm for sections over 75 mm[28,48,52,53].

1.3.3.10 ALTERNATIVE TECHNIQUES FOR EXTRUDING TITANIUM

An alternative technique for extruding titanium was employed by Gurney and Male[30-33] and Adair et al[35-37] using conical extrusion dies. No glass pad was employed at the die face, but the billet was pre-coated with a glass slurry, which together with a high temperature grease applied to the liner and die, provided the lubrication. To assist metal flow the front face of the billet was machined to match the profile of the die. The dies were flame sprayed with zirconia to improve their wear resistance. Extrusions were carried out over the temperature range of 870°C - 1175°C, with the surface qualities being generally very good.

The flow pattern obtaining when conical dies are used is shown schematically in Figure 1.8[59]. The similarity with Figure 1.4, for extrusion with a glass pad at the die face, is apparent with the surface of the billet extruding to form the surface of the extrude with no dead metal zone formation.

Conical dies have also been employed to extrude steels in the temperature range of 600°C - 950°C[38-39]. In this case no glass was employed with molybdenum disulphide grease being the sole lubricant. Superior surface qualities were reported compared to glass lubricated extrusions.

Titanium can also be extruded, using copper as a sheath material[61], the copper extruding to form the surface of the extrude. The extrusion temperature is necessarily lower to avoid alloying between the copper and titanium, and in the case of Ti-6Al-4V extrusion is limited to the alpha+beta regime. The copper is usually removed by cutting and stripping followed by acid pickling.

1.3.3.11 LIMIT DIAGRAMS FOR GLASS - LUBRICATED EXTRUSION

Limit diagrams were originally proposed by Hirst and Ursell to represent graphically the extrusion limit within which products with an adequate surface finish could be produced for a specific press capacity[71].

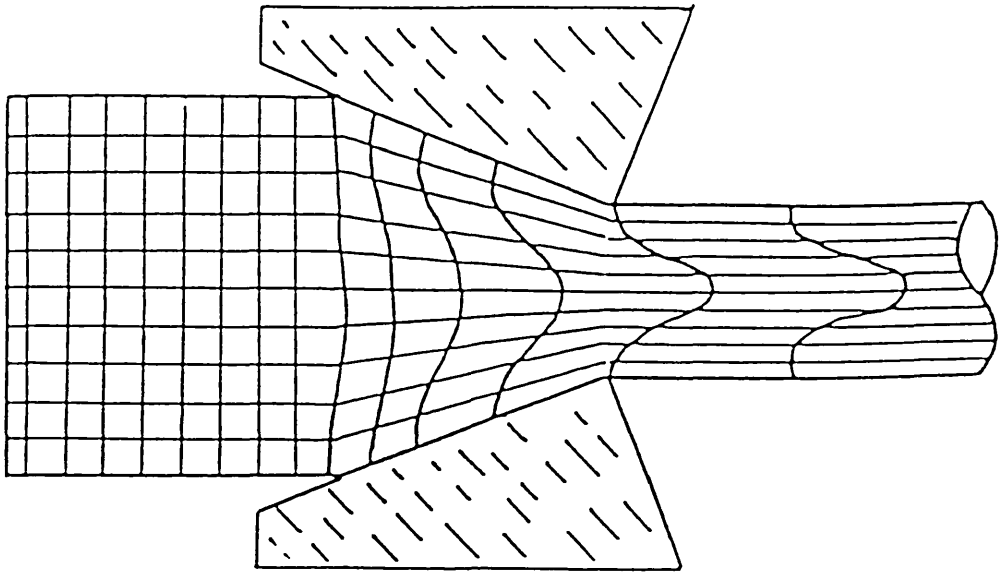

Figure 1.8 SCHEMATIC OF FLOW PRODUCED USING CONICAL DIES[59]

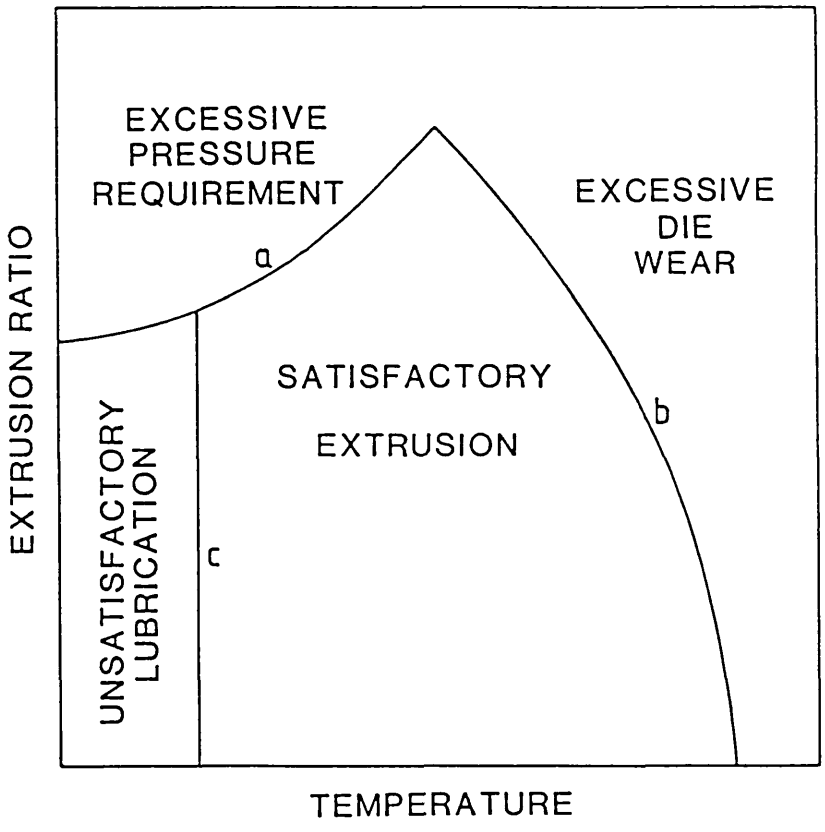

Figure 1.9 SCHEMATIC OF LIMIT DIAGRAM FOR GLASS LUBRICATED EXTRUSION

The basic parameters which limit the extrusion ratio are the available pressure and the extrusion temperature. In the case of high temperature extrusion additional constraints are imposed by lubricants and die wear.

Limit diagrams have been produced for steel extrusion[40], and the principles applying are the same for titanium extrusion. A typical extrusion limit diagram is shown schematically in Figure 1.9. This applies to specific conditions of ram speed, billet dimensions, extrusion shape and glass softening point. Three lines define the extrusion limits;

a) Excessive Pressure Requirement Line

The maximum pressure that can be used depends either on the capacity of the press or on the strength of the thrust rod. The pressure required increases with decreasing temperature and increasing extrusion ratio.

b) Die Wear Line

As discussed in section 1.3.3.7, increasing the extrusion temperature and extrusion ratio increases the possibility of die wear due to softening of the die material. This puts an upper constraint on the temperature and extrusion ratio that can be employed to satisfy the dimensional tolerances imposed. This limit can be extended by improving the die material, e.g. by applying a ceramic coating to the die or by using a higher softening point glass which will provide better thermal insulation to the die.

c) Unsatisfactory Lubrication Line

As discussed in section 1.3.3.2, below a certain temperature, depending on the softening point of the glass, the glass does not soften adequately and ceases to be an effective lubricant, leading to a poor surface on the extrude. This lower limit can be extended, within the pressure constraints by using a glass of lower softening point. Alternatively, a conical die may be employed with molybdenum disulphide grease as the lubricant.

CHAPTER TWO

THEORY

CHAPTER TWO

THEORY

2.1 INTRODUCTION

In this chapter the various analyses used in the work are presented in detail. The derivation of upper bound solutions and temperature rise models for glass-lubricated extrusion are described and a general hot working theory is presented which relates flow stress to strain rate and temperature. The evaluation of data from hot torsion tests is also discussed.

2.2 ANALYSIS OF HOT WORKING CHARACTERISTICS

Before any extensive investigation can be made of the behaviour of a metal during extrusion it is necessary to determine its stress-strain behaviour at high temperatures.

2.2.1 GENERAL HOT WORKING EQUATION

The similarity between steady state creep and steady state hot working led Sellars and Tegart[15] to propose the following relationship between strain rate, flow stress and temperature during the hot deformation of metals

$$\dot{\varepsilon} = A\,[\sinh(\alpha\sigma)]^n \exp(-Q/RT) \qquad 2.1$$

where A, α and n are temperature and stress independent constants and Q is the activation energy of the rate controlling dynamic softening mechanism which is also assumed to be independent of temperature and stress.

The equation can be rewritten in the form :-

$$z = \dot{\varepsilon} \exp(Q/RT) = A \sinh(\alpha\sigma)^n \qquad 2.2$$

where z is the temperature compensated strain rate. To make use of these equations the four constants must be evaluated.

2.2.2 EVALUATION OF THE CONSTANTS IN THE HOT WORKING EQUATION

Prior to the constants in the hot working equation being evaluated a method must be found for assessing the flow stress-strain behaviour of the material at high temperatures. The method chosen was that of hot torsion since the ability to achieve high strains at high constant surface strain rates is of prime importance.

The theory of the mathematical minimization technique employed in the evaluation of the hot working constants from raw torque-twist data is given in reference 72. Allowance was made for temperature rises during testing, using a finite difference method developed by Wright[73] and extended by Vierod[72], to allow for a strain dependence of the hot working constants, and Richards[74] who allowed for radiant heat losses from the test piece. The computer programme has been slightly modified to allow for the temperature dependence of the specific heat and thermal conductivity of Ti-6Al-4V[75], the modifications being given in Appendix I.

2.3 AXISYMMETRIC UPPER BOUND SOLUTION

2.3.1 INTRODUCTION

The formulation of the axisymmetric upper bound model for extrusion has been discussed by several authors[76-78] and only its applicability to lubricated extrusion will be discussed here.

In the upper bound analysis elements of material are assumed to offer maximum resistance to deformation, i.e. they deform in such a way as to require the maximum amount of work to produce a given strain. Hence the upperbound solutions produce loads which are in excess of the true values.

The models developed to date have all been applicable to unlubricated extrusion, both direct and indirect[76-78]. In a number of respects, however, the type of metal flow occurring in glass lubricated extrusion is similar to that obtaining in indirect extrusion. No dead metal zone is observed to form and the element of billet/container friction is eliminated in the case of indirect extrusion and substantially reduced in the glass lubricated case. The difference occurs in relation to the billet/die interface, where in glass lubricated extrusion friction is substantially reduced by the glass pad, but in indirect extrusion shearing occurs across the die face, i.e. sticking friction occurs. This feature, however, requires only a small modification to the indirect extrusion model.

Thus the model employed is that developed for indirect extrusion[78], but with allowance for frictionless condition at the die face.

2.3.2 PREDICTION OF PRESSURE FOR GLASS LUBRICATED EXTRUSION

The derivation of the equations employed in the model is available in references 76, 78, and only a basic outline will be given here.

The single triangle deformation field employed and associated hodograph is shown in Figure 2.1. The die has been assumed to have a flat face with a 90° angle at the die orifice, for simplicity of analysis. Frictionless conditions have been assumed at the billet/liner interface.

The total rate of energy dissipation can be found by summing the energies dissipated by shearing at the velocity discontinuities 12, 23 and 24 and by circumferential straining in region 2. The best upper bound solution will be that which minimizes the expression for the internal rate of energy dissipation and may be expressed :-

$$\dot{E} = \iiint_V \bar{\sigma}\, \bar{\dot{\varepsilon}}_i \, dV + \sum_{i,j=1} \tau_{ij} V_{ij} \, ds \qquad 2.3$$

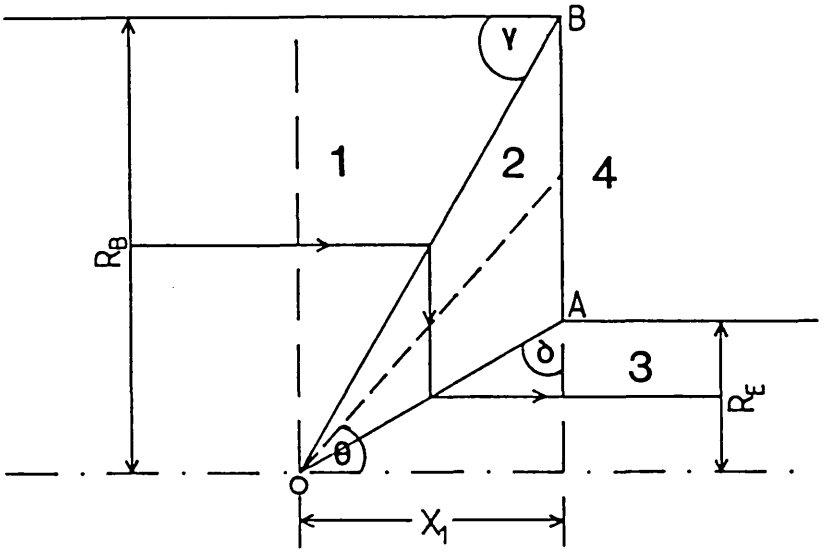

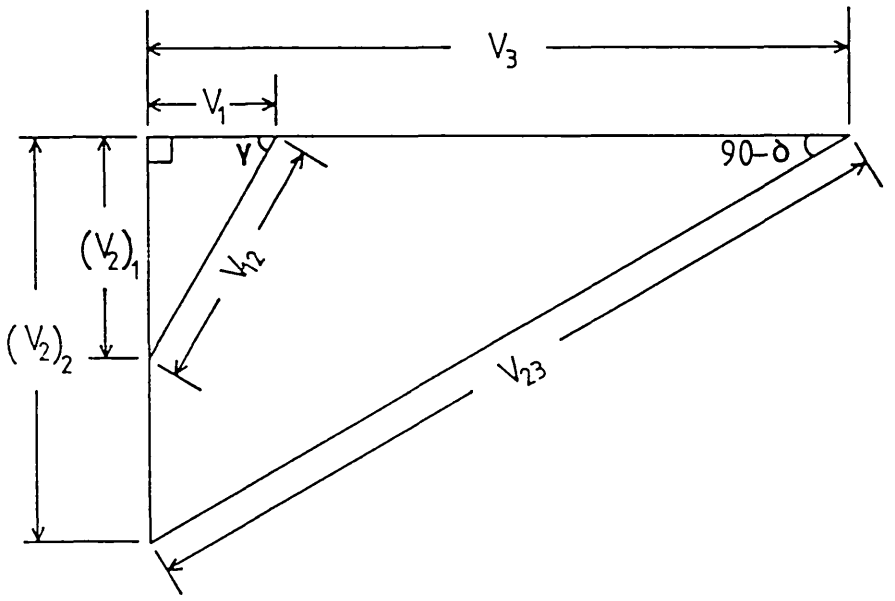

Figure 2.1 SINGLE TRIANGLE UPPER BOUND VELOCITY FIELD AND HODOGRAPH FOR GLASS-LUBRICATED EXTRUSION

The rate of energy input on the left hand side can be expressed :-

$$\dot{E} = PVA_B \qquad 2.4$$

where P = extrusion pressure, V = ram velocity, A_B = cross sectional area of billet.

The first term on the right hand side of the equation 2.3 represents the rate of energy dissipation within region 2. This is given by :-

$$\dot{E}_2 = \pi\bar{\sigma}_2 \sqrt{\frac{2}{3}} \int_{\theta_1}^{\theta_2} [r^2]_{r_1(\theta)}^{r_2(\theta)} \dot{\varepsilon}_i \, (\theta) \sin\theta d\theta \qquad 2.5$$

The limits $r_1(\theta)$ and $r_2(\theta)$, θ_1 and θ_2 define the boundaries of region 2, the deformation zone. Equation 2.5 can be evaluated by the use of Simpson's rule.

The second term on the right hand side of equation 2.3 may also be evaluated. The material deforming in region 2 is assumed to obey the Von Mises yield criterion. Therefore, at all discontinuities within the material

$$k_{ij} = \overline{\sigma y} \; / \sqrt{3} \qquad 2.6$$

All the velocity discontinuities are either constants or functions of r. Therefore :-

$$\dot{E}_{ij} = \iint_S \tau_{ij} \; V_{ij} \, ds \qquad 2.7$$

can be evaluated exactly.

The velocity discontinuities are given below

$$(V_2)_1 = V_1 \tan \gamma \qquad 2.8(a)$$

$$(V_2)_2 = V_1 \frac{R_B^2}{R_E^2} \tan \delta \qquad 2.8(b)$$

$$V_{\overline{12}} = V_1 \sec \gamma \qquad 2.8(c)$$

$$V_{\overline{23}} = V_1 \frac{R_B^2}{R_E^2} \sec \delta \qquad 2.8(d)$$

$$V_{\overline{24}} = (V_2)_1 \frac{R_B}{t} \qquad 2.8(e)$$

where $t = \times \tan \theta$.

Hence the rate of energy dissipation terms are :-

$$\dot{E}_{12} = \frac{\pi}{\sqrt{3}} \sigma_{12} \frac{V_{\overline{12}} R_B^2}{\sin \gamma} \qquad 2.9$$

$$\dot{E}_{23} = \frac{\pi}{\sqrt{3}} \frac{\sigma_{23} V_{\overline{23}} R_E^2}{\sin \delta} \qquad 2.10$$

$$\dot{E}_{24} = m. \frac{2\pi}{\sqrt{3}} \sigma_{24} (V_2)_1 R_B (R_B - R_E) \qquad 2.11$$

where $0 < m < 1$.

$\dot{E}_{24}$ represents the energy associated with shear across the die face. For indirect extrusion sticking friction is assumed and m = 1. However, for fully lubricated extrusion, m = 0 and E_{24} is zero.

Therefore, the total energy dissipated may be evaluated by summing $\dot{E}_{12}$, $\dot{E}_{23}$, $\dot{E}_{24}$ and $\dot{E}_2$ and equating to the rate of energy input. By varying the length ×, the value of energy dissipated may be minimized and a value of P/k obtained.

A computer programme[78] was used to perform the numerical calculations. The programme has been modified to allow for frictionless conditions at the die face, and a new minimization routine employed called MINVAR, available in the Cern Computer Centre program library.

2.4 STRAIN RATE DETERMINATION

The strain rate during extrusion is difficult to define because it varies throughout the deformation zone and so it is necessary to use a mean strain rate. The strain rate in indirect extrusion can be evaluated in a similar manner to that employed by Feltham[79] for direct extrusion, and modified to allow for inhomogeneity of strain[80], and a variation of semi-angle with extrusion ratio[81].

Referring to Figure 2.1, this yields :-

$$\dot{\bar{\varepsilon}} = \frac{6(a + b\ln R)\tan\theta .\ V.\ D_B}{D_B^2 - D_E^2} \qquad 2.12$$

Where θ is the deformation zone semi-angle

D_B is the billet diameter

D_E is the extrude diameter

V is the ram speed

R is the extrusion ratio

The values of $(a + b\ln R)$ and the deformation zone semi-angle are obtained from upper bound theory. This strain rate will be referred to as Feltham's strain rate.

2.5 TEMPERATURE CHANGES OCCURRING DURING EXTRUSION

2.5.1 INTRODUCTION

An understanding of the temperature changes occurring during extrusion is particularly important in high temperature extrusion, where the billet and tooling temperatures are so markedly different. As will be discussed in the results section, the extrusion pressure increases continuously throughout the stroke, reaching a peak at the end of extrusion. Hence the peak pressure for extrusion will be more dependent upon the temperature at the end of the extrusion, rather than at the start. In addition because all the tensile specimens and metallography samples were taken from the middle of the extrude length, then it is necessary to have some idea of the temperatures obtaining at this point if the interrelationship between the extrusion variables and the structure and properties is to be properly interpreted.

The temperature changes occurring during high temperature glass-lubricated extrusion are extremely difficult to predict, because of the large number of variables involved, and the difficulty of definition of some of the parameters. Hence it is not practicable to expect an accurate prediction of the temperatures at each point in the extrusion stroke, and only some idea of the temperature changes occurring during extrusion can be hoped for.

2.5.2 PREDICTION OF TEMPERATURE CHANGES DURING EXTRUSION USING AN INTEGRAL PROFILE TECHNIQUE

The technique employed to evaluate the temperature changes occurring during extrusion is based on Sheppard and Wood's integral profile method[82], which was developed for the unlubricated extrusion of aluminium. The method has been extended by Paterson[76] to accommodate indirect extrusion and further developed by Cooper[83] to allow prediction of the temperatures at various stages of the extrusion stroke.

In adapting this method to allow for glass lubricated extrusion, allowance has to be made for a glass pad at the die face. The basic theory and derivation of equations used in the analysis are given in references 76, 82 and 83, and only a brief outline of the method and its adaption to high temperature glass lubricated extrusion will be given here. A few minor corrections have also been made to the original analysis.

Figure 2.2 shows the assumed heat flow situation for glass lubricated extrusion, the various heat flows Q_1 - Q_7 being defined in the Figure. A control volume is placed around the deformation zone, the dimensions of which are given by the upper bound analysis, and the heat losses to the tooling and glass pad are equated to the work done. All the work is assumed to be done in this volume. A second control volume is placed around the remainder of the billet, to allow for heat losses to the container and pressure pad, and heat flow from control volume one.

The following assumptions have been made in the analysis :-

1) As the mode of deformation occurring during extrusion is very complex, it is difficult to analyse mathematically. The deformation is, therefore, assumed to be homogeneous.

2) Perfect thermal contact between the billet and surrounding tooling is assumed. This is reasonable as high pressures are obtained during extrusion.

3) The material leaving the deformation zone is assumed to be at the same temperature as that of the deformation zone.

4) 90% of the work done is converted to heat

5) Heat conduction between the two control volumes is assumed to occur.

The interface temperatures between the billet and the steel tooling may be calculated from equations of the form :-

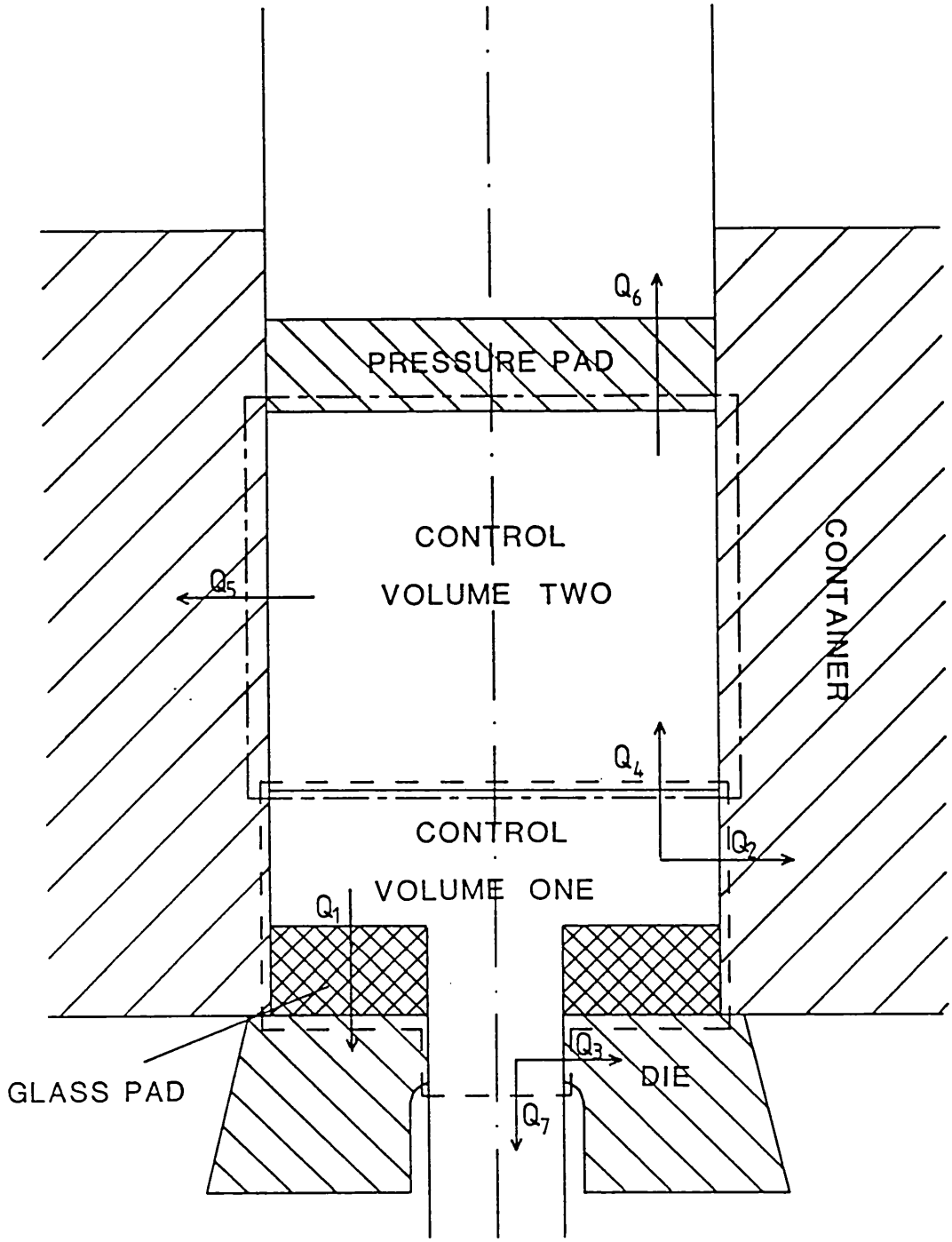

Q_1 = Heat Loss to Glass Pad from Deformation Zone
Q_2 = Heat Loss to Container from Deformation Zone
Q_3 = Heat Loss to Die Land from Deformation Zone
Q_4 = Back Conduction from Deformation Zone to Non-Deforming Zone
Q_5 = Heat Loss to Container from Non-Deforming Zone
Q_6 = Heat Loss to Pressure Pad from Non-Deforming Zone
Q_7 = Heat Loss to Extrude from Deformation Zone

Figure 2.2 SCHEMATIC OF HEAT FLOW IN GLASS-LUBRICATED EXTRUSION

$$\frac{T_B - T_I}{T_I - T_S} = \frac{(KCp)^{\frac{1}{2}}_{STEEL}}{(KCp)_{BILLET}} \qquad 2.13$$

where T_B = billet temperature

T_I = interface temperature

T_S = steel tooling temperature

This corrects the error made in previous analyses[76,82,83], which assumed :-

$$\frac{T_B - T_I}{T_I - T_S} = \frac{\alpha_{STEEL}}{\alpha_{BILLET}}$$

where $\alpha = \frac{K}{Cp}$ for each material

The temperature rise in the deformation zone is ΔT_1 and hence the temperature of the deformation zone is $\Delta T_1 + T_{B1}$. The temperature differential between the interface of the billet and the adjacent tooling $T_I - T_S$ is designated ΔT_D. Thus the temperature differential between the deformation zone and the tooling is $\Delta T_D + \Delta T_1$ or ΔT_1^*. Simiarly, the temperature of the non-deforming zone is $\Delta T_2 + T_{B2}$.

The temperature profile around a heat source may be assumed to be represented by :-

$$\Delta T\ (x\ ,\ t) = a_o + a_1 x + a_2 x^2 \qquad 2.14$$

where $\Delta T(x,t)$ is the temperature at a point distance x from the heat source at a time t. the constants a_o, a_1, and a_2 may be found by consideration of the boundary conditions, and it can be shown that

$$\Delta T\ (x,t) = \Delta T^*\ (1 - \frac{x}{s})^2 \qquad 2.15$$

where s is the maximum penetration distance of the heat front, and can be shown to be :-

$$s = \left(\frac{12\ K_t}{pC} \right)^{\frac{1}{2}} \qquad 2.16$$

when the contact area does not vary with x (Q_1, Q_4, Q_6, Q_7)

$$\text{or } s = \left(\frac{18\ KAt}{\pi l p C} \right)^{\frac{1}{3}} \qquad 2.17$$

when A varies with x (Q_2, Q_3, Q_5)

Knowing these penetrations distances the heat losses from each control volume can now be calculated.

CONTROL VOLUME ONE

Since all the work is assumed to be done in this volume, the temperature of the deformation zone rises by an amount ΔT_1. There is thus an accumulation of heat inthis zone given by :-

$$(Q_{ACC})_1 = \Delta T_1\ \rho_{Ti}\ C_{Ti} V_1 \qquad 2.18$$

where V_1 = the volume of the deformation zone

$$= \frac{1}{4}\ \pi D_B^{\,2} \cdot x \qquad 2.19$$

where x is the deformation zone depth obtained from upper bound. It has been assumed that the entire deformation zone extends to this depth.

Thus performing the heat balance for control volume one :-

$$0.9\ L_m\ V_B\ \Delta t = (Q_{ACC})_1 + Q_1 + Q_2 + Q_3 + Q_4 + Q_7 \qquad 2.20$$

where L_m is the mean load for the nth time increment

V_B is the ram speed

The term $L_m V_B \Delta t$ is the work done during extrusion in a time interval Δt, which is equal to the area under the load-displacement curve, it being assumed that 90% of this work done is converted into heat. An idealised load-displacement curve is shown in Figure 2.3 to illustrate evaluation of the work input. If the ram speed is constant throughout the extrusion stroke, then the load-displacement curve can be split up into increments of equal time Δt $(= \frac{\Delta\delta}{V_B})$ and the area under the curve evaluated for each increment. In the current analysis 10 intervals have been used.

The area under the load-displacement curve for the nth increment is given by :-

$$\text{Area} = \frac{1}{2}[L_n + L_{n+1}].V\Delta t \qquad 2.21$$

where n varies from 1 to 11

The various heat flows from control volume 1 will now be considered.

Heat Loss Q_1

The problem is similar to that encountered for indirect extrusion[76], there being no dead metal zone formation, except that the die is insulated by a glass pad. Rather than considering the conduction of heat through the glass pad to the die, it is simpler to assume that the pad behaves like a semi-infinite body. The general criterion for the semi-infinite solution to apply to a body of finite thickness subjected to one dimensional heat transfer is[84] :-

$$\frac{2L}{(4\alpha t)^{\frac{1}{2}}} \geq 0.5 \qquad 2.22$$

where 2L is the thickness of the body. α for glass using typical values is given by :-

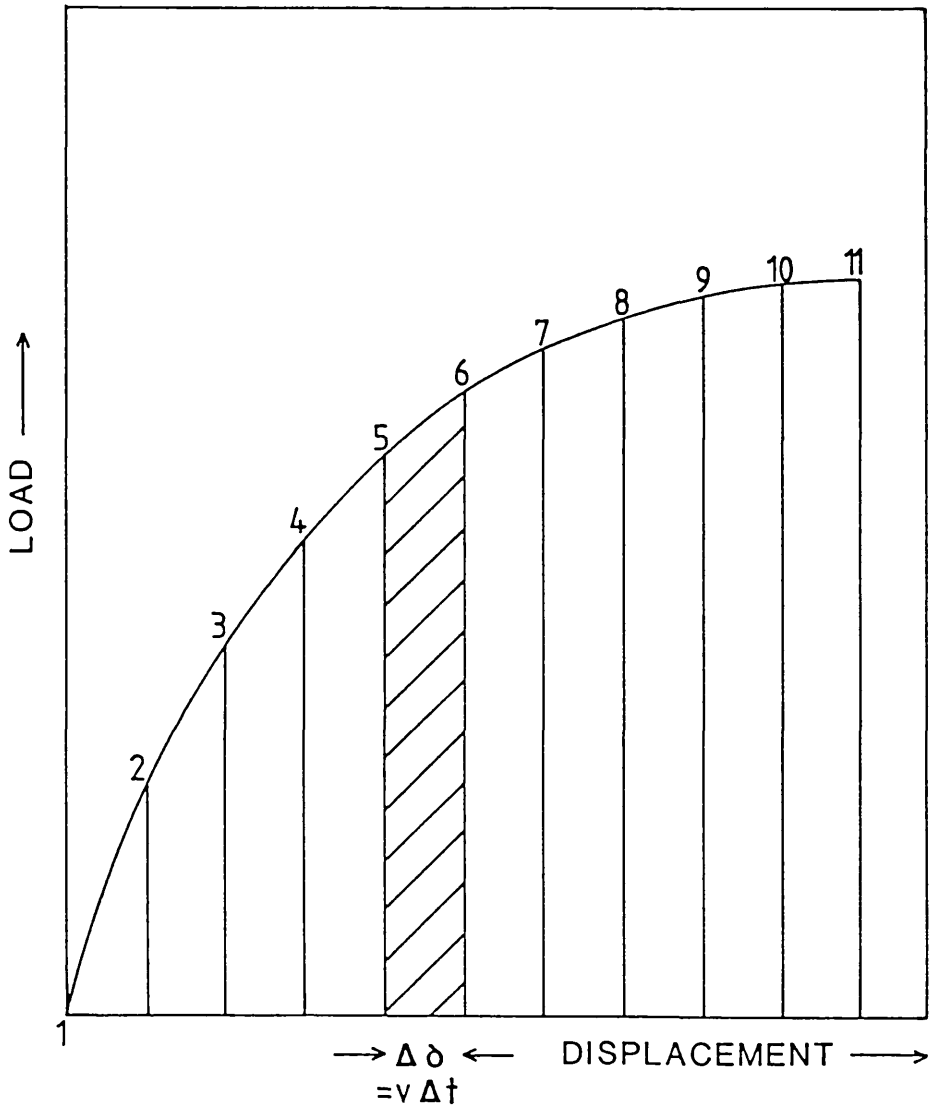

Figure 2.3 SIMPLIFIED LOAD-DISPLACEMENT CURVE TO ILLUSTRATE CALCULATION OF WORK DONE DURING EXTRUSION

$$\alpha \text{ GLASS} = \frac{K}{Cp} = \frac{1.4}{750 \times 2500} = 7.47 \times 10^{-7} \text{ m}^2 \text{ s}^{-1}$$

The time for extrusion is typically 1 second and therefore

$$2L \geq 8.64 \times 10^{-4} \text{ m}$$

i.e. the thickness of the glass pad has to be greater than 0.86 mm for semi-infinitism to apply. Apart from the extrusions carried out at lower temperatures, when the glass did not soften adequately, and was pushed out of the die before the extruding metal, the pad thickness was well in excess of 0.86 mm at the end of extrusion, and hence it is reasonable to assume the billet is in contact with a semi-infinite body of glass at the die face.

Hence the equation for Q_1 becomes

$$Q_1 = \pi(D_B^2 - D_E^2) \frac{(K_G p_G C_G)^{\frac{1}{2}}}{12} (\Delta T_1 + \Delta T_{D1}) t^{\frac{1}{2}} \qquad 2.23$$

$$= (\Delta T_1 + \Delta T_{D1}) k_1 t^{\frac{1}{2}} \qquad 2.24$$

where $\Delta T_{D1} = T_I - T_G$

The interface temperature will accordingly be modified, being given by :-

$$\frac{T_B - T_I}{T_I - T_G} = \frac{(KCp)^{\frac{1}{2}}_{\text{GLASS}}}{(KCp)^{\frac{1}{2}}_{\text{TITANIUM}}} \qquad 2.25$$

where T_G is the temperature of the glass pad, which is assumed to be at the die temperature. For the cases where the glass does not soften adequately during extrusion and therefore offers very little insulation, it can be assumed that the billet is in direct contact with the steel die, the constants for glass in the above equation being substituted by those of steel.

Heat Loss Q_2

This is the heat lost to the container from the deformation zone and is given by :-

$$Q_2 = \frac{\pi}{6} \cdot x. \ (\Delta T_1 + \Delta T_{D2})[(18K_s D_B (p_s C_s)^{\frac{1}{2}} t)^{\frac{2}{3}} + (18K_s D_B^{\ 4} (p_s C_s)^2 t)^{\frac{1}{3}}] \quad 2.26$$

$$= \Delta T_1 \ (k_{2A} t^{\frac{2}{3}} + k_{2B} t^{\frac{1}{3}}) + \Delta T_{D2} (k_{2A} t^{\frac{2}{3}} + k_{2B} t^{\frac{1}{3}}) \quad 2.27$$

where $\Delta T_{D2} = T_{I2} - T_C$

where T_C is the container temperature.

Heat Loss Q_3

This is the heat lost to the die land from the deformation zone. The billet is in fact separated from the die land by a thin layer of viscous glass approximately 50 microns thick. An upper and lower estimate of Q_3 can be obtained by using both the steel and glass constants in the equation for Q_3. The equation for glass is :-

$$Q_3 = \frac{\pi}{6} L_1 (\Delta T_1 + \Delta T_{D1}) \ [(18K_G D_E (p_G C_G)^{\frac{1}{2}} t)^{\frac{2}{3}} + (18K_G D_E^{\ 4} (p_G C_G)^2 t)^{\frac{1}{3}}] \quad 2.28$$

$$= \Delta T_1 \ (k_{3A} t^{\frac{2}{3}} + k_{3B} t^{\frac{1}{3}}) + \Delta T_{D1} \ (k_{3A} t^{\frac{2}{3}} + k_{3B} t^{\frac{1}{3}}) \quad 2.29$$

Heat Loss Q_4

A temperature differential exists between the two control volumes and hence a heat loss Q_4 from control volume 1 to control volume 2 can

be calculated. The temperature differential across the control volume boundary is assumed to be zero in the first iteration, since the billet is originally at a uniform temperature. For subsequent iterations :-

$$Q_4 = \pi D_B^2 \, \Delta T_4 \, (K_{Ti} p_{Ti} C_{Ti}/_{12})^{\frac{1}{2}} t^{\frac{1}{2}} \qquad 2.30$$

$$= \Delta T_4 \, k_4 \, t^{\frac{1}{2}} \qquad 2.31$$

For each iteration, $\Delta T_4 = T_{B1} - T_{B2}$. Thus Q_4 must be calculated from a consideration of the heat balance in control volume 2.

Heat Loss Q_7

This is the heat lost to the extrude from the deformation zone and is given by :-

$$Q_7 = \Delta T_1 \, p_{Ti} \, C_{Ti} \, RV_B \, t \, \frac{\pi D_E^2}{4} \qquad 2.32$$

$$= \Delta T_1 \, k_7 \, t \qquad 2.33$$

CONTROL VOLUME 2

The temperature of control volume 2 rises by an amount ΔT_2. There is thus an accumulation of heat in this zone given by :-

$$(Q_{ACC})_2 = \Delta T_2 \, p_{Ti} \, C_{Ti} \, V_2 \qquad 2.34$$

where $V_2 = \frac{\pi D_B^2}{4} \cdot L_T \qquad 2.35$

Thus performing the heat balance on control volume 2 :-

$$Q_4 = (Q_{ACC})_2 + Q_5 + Q_6 \qquad 2.36$$

The various heat flows in control volume 2 will now be considered.

Heat Loss Q_5

This is the heat lost from the non-deforming zone to the container. If the height of control volume 2 at the start of extrusion is L_T, then the height of the control volume at time t after the extrusion L_E will be :-

$$L_E = L_T - V_B \Delta t \qquad 2.37$$

Hence :-

$$Q_5 = \frac{\pi}{6} (\Delta T_2 + \Delta T_{D3})[(18D_B K_s (p_s C_s)^{\frac{1}{2}})^{\frac{2}{3}} (t^{\frac{2}{3}} - \frac{3V_B t^{5/3}}{5L_t})$$

$$+ D_B (18D_B K_s (p_s C_s)^2)^{\frac{1}{3}} (t^{\frac{1}{3}} - \frac{3V_B t^{4/3}}{4L_t}) \qquad 2.38$$

$$= \Delta T_2 (k_{5A} t^{\frac{2}{3}} + k_{5B} t^{5/3} + k_{5C} t^{\frac{1}{3}} + k_{5D} t^{4/3})$$

$$+ \Delta T_{D3} (k_{5A} t^{\frac{2}{3}} + k_{5B} t^{5/3} + k_{5C} t^{\frac{1}{3}} + k_{5D} t^{4/3}) \qquad 2.39$$

where $\Delta T_{D3} = T_{I3} - T_C$

The height of control volume 2, L_E after time t is calculated on each iteration. When L_E becomes zero, then no further calculations are performed on control volume 2.

Heat Loss Q_6

This is the heat lost to the pressure pad from the non-deforming zone, and is given by :-

$$Q_6 = (\Delta T_2 + \Delta T_{D4})\ \pi D_B^{\,2}\ (K_s p_s C_s/_{12})^{\frac{1}{2}}\ t^{\frac{1}{2}} \qquad 2.40$$

$$= (\Delta T_2 + \Delta T_{D4})\ k_6 t^{\frac{1}{2}} \qquad 2.41$$

where $\Delta T_{D4} = T_{I4} - T_p$

where T_p is the pressure pad temperature.

TEMPERATURE CHANGES DURING EXTRUSION

The temperature changes in the two control volumes can now be evaluated from consideration of the heat balances.

TEMPERATURE CHANGE IN CONTROL VOLUME 1

The heat balance equation applies to all increments of time, up to the time when control volume 2 no longer exists :-

$$0.9\ Lm\ V_B\ \Delta t = (Q_{ACC})_1 + Q_1 + Q_2 + Q_3 + Q_4 + Q_7 \qquad 2.20$$

where

$$(Q_{ACC})_1 = \Delta T_1 p_{Ti} C_{Ti} V_1 = \Delta T_1 \cdot C_{ACC1} \qquad 2.42$$

$$Q_1 = (\Delta T_1 + \Delta T_{D1})\ k_1 t^{\frac{1}{2}} = (\Delta T_1 + \Delta T_{D1}).C_1 \qquad 2.43$$

$$Q_2 = (\Delta T_1 + \Delta T_{D2})(k_{2A} t^{\frac{2}{3}} + k_{2B} t^{\frac{1}{3}}) = (\Delta T_1 + \Delta T_{D2}).C_2 \qquad 2.44$$

$$Q_3 = (\Delta T_1 + \Delta T_{D1})(k_{3A}t^{\frac{2}{3}} + k_{3B}t^{\frac{1}{3}}) = (\Delta T_1 + \Delta T_{D1}).C_3 \qquad 2.45$$

$$Q_4 = \Delta T_4.k_4 t^{\frac{1}{2}} = \Delta T_4.C_4 \qquad 2.46$$

$$Q_7 = \Delta T_1 k_7 t = \Delta T_1.C_7 \qquad 2.47$$

Hence the temperature change in the deformation zone is given by :-

$$\Delta T_1 = \frac{0.9\ Lm\ V_B \Delta t - [\Delta T_{D1}(C_1 + C_3) + \Delta T_{D2}C_2 + \Delta T_4 C_4]}{C_1 + C_2 + C_3 + C_7 + C_{ACC1}} \qquad 2.48$$

For the first time increment $Q_4 = 0$ and hence $\Delta T_4.C_4$ is zero in the first iteration.

TEMPERATURE RISE IN CONTROL VOLUME 2

The heat balance applies to all increments of time up to when the control volume 2 no longer exists :-

$$Q_4 = (Q_{ACC})_2 + Q_5 + Q_6 \qquad 2.36$$

where

$$Q_4 = \Delta T_4\ k_4\ t^{\frac{1}{2}} = \Delta T_4.C_4 \qquad 2.49$$

$$(Q_{ACC})_2 = \Delta T_2 \rho_{Ti} C_{Ti} V_2 = \Delta T_2.C_{ACC2} \qquad 2.50$$

$$Q_5 = (\Delta T_2 + \Delta T_{D3})(k_{5A}t^{\frac{2}{3}} + k_{5B}t^{5/3} + k_{5C}t^{\frac{1}{3}} + k_{5D}t^{4/3})$$

$$= (\Delta T_2 + \Delta T_{D3})\ C_5 \qquad 2.51$$

$$Q_6 = (\Delta T_2 + \Delta T_{D4})\ k_6 t^{\frac{1}{2}} = (\Delta T_2 + \Delta T_{D4})\ C_6 \qquad 2.52$$

Hence the temperature change in the non-deforming zone ΔT_2 is given by :-

$$\Delta T_2 = \frac{\Delta T_4 C_4 - [\Delta T_{D3} C_5 + \Delta T_{D4} C_6]}{C_{ACC2} + C_5 + C_6} \qquad 2.53$$

For the first time increment $Q_4 = 0$ and hence $\Delta T_4 C_4$ is zero in the above equation for the first iteration.

TEMPERATURE RISE IN CONTROL VOLUME 1 WHEN CONTROL VOLUME 2 NO LONGER EXISTS

When the height of control volume 2 reaches zero, a new heat balance must be calculated for control volume 1. There is no longer a term Q_4 for conduction to control volume 2, but there is a new term Q_6^1 for conduction to the pressure pad. The heat balance becomes :-

$$0.9 \text{ Lm } V_B \Delta t = (Q_{ACC})_1 + Q_1 + Q_2 + Q_3 + Q_6^1 + Q_7 \qquad 2.54$$

Heat loss Q_6^1 is calculated in a similar manner to Q_6 :-

$$Q_6^1 = (\Delta T_{D5} + \Delta T_1)\, D_B^2\, (K_s \rho_s C_s / 12)^{\frac{1}{2}}\, t^{\frac{1}{2}} \qquad 2.55$$

$$= (\Delta T_{D5} + \Delta T_1)\, k_6\, t^{\frac{1}{2}} = (\Delta T_{D5} + \Delta T_1) C_6^1 \qquad 2.56$$

where $\Delta T_{D5} = T_{I5} - T_p$

Thus the new term for the temperature rise in control volume 1 is :-

$$\Delta T_1 = \frac{0.9 \text{ Lm } V_B \Delta t - [\Delta T_{D1}(C_1 + C_3) + \Delta T_{D2} C_2 + \Delta T_{D5} C_6]}{C_1 + C_2 + C_3 + C_6^1 + C_7 + C_{ACC1}} \qquad 2.57$$

Thus the analysis proceeds as follows. For the first time increment, the work done in extrusion is evaluated from the corresponding area under the load displacement curve (Figure 2.3) and hence the heat generated determined. The interface temperatures are evaluated using the initial billet temperature, and hence values of the differentials ΔT_{D1}, ΔT_{D2} , ΔT_{D3} and ΔT_{D4} obtained. From these the heat losses can be evaluated for the first time increment ($t = \Delta t$). The temperature changes in the two control volumes are then calculated and these represent the new values of T_{B1} and T_{B2} in the next iteration.

For the second time increment, the corresponding area under the load-displacement curve is evaluated as before. As the temperatures of the two control volumes T_{B1} and T_{B2} have changed, there is a change in the interface temperatures in accordance with equation 2.13. Penetration of the heat front is allowed for by adding on the second time increment ($t = 2\Delta t$) and hence the new heat losses evaluated. The new temperatures in the two control volumes are calculated, and the whole procedure repeated for each iteration.

A computer programme was written to perform these calculations and was incorporated in the extrusion results programme. A description of how to use the model, and the thermal constants employed is given in Appendix II.

CHAPTER THREE

EXPERIMENTAL PROCEDURE

CHAPTER THREE

EXPERIMENTAL PROCEDURE

3.1 EXTRUSION

3.1.1 MATERIAL

The chemical composition of the Ti-6Al-4V alloy employed in the extrusion programme is shown in Table 3.1. The commercial composition range for the alloy is also shown.

	Aluminium %	Vanadium %	Iron %	Oxygen %	Nitrogen %	Titanium %
Alloy Composition	6.34	3.92	0.15	0.17	0.017	Remainder
Commercial Range	5.50-6.75	3.50-4.50	0.30 max.	0.20 max.	0.05 max.	Remainder

TABLE 3.1 CHEMICAL COMPOSITION OF THE BILLET MATERIAL EMPLOYED FOR THE EXTRUSION PROGRAMME

The material was provided in two forms :-

1) Smooth turned round billet 75 mm diameter x 100 mm long. This was to be the size of billet employed for the extrusion programme, however initial trials showed that the pressure requirements were too great at lower temperatures to provide an acceptable extrusion range. Further trials were conducted with 55 mm diameter billets which provided an

extrusion range of 850°C - 1150°C, which is the range used commercially (section 1.3.3.4). Hence all the 75 mm diameter billets were turned to 55 mm diameter. The final stages of machining were carried out with sharp tools, low feed rates and plenty of lubrication to ensure a good surface finish to the billet. The front ends of the billet were machined with a $\frac{1}{4}$" radius.

2) Blocks of material, 75 mm square x 200 mm long. These were again machined to 55 mm diameter x 99 mm $\pm$ 2 mm long billets.

3.1.2 THE EXTRUSION PRESS

The extrusion press used in the experimental work was a 5MN fast action ENEFCO hydraulic press mounted vertically over an accessible pit (depth 3 metres). The press tooling was supported by a backing plate and the container could be raised or lowered hydraulically. The press layout is shown in Figure 3.1.

3.1.2.1 THE ACCUMULATOR DRIVE

An auxiliary pump enabled a fast ram approach by the ram prior to the commencement of extrusion. When the ram hit the pressure pad and the pressure in the main cylinder exceeded 0.69 MNm^{-2} the pump was automatically bypassed and the ram slowed down. When the pressure reached 3.45 MNm^{-2}, the accumulator drive was activated, with four nitrogen filled cylinders discharging, resulting in a high rate of oil delivery to the main ram. Ram speeds in the range 67 mm/sec - 160 mm/sec were obtained, which are typical of those encountered commercially.

The ram speed could not be preset, but varied inversely with the extrusion pressure. It was therefore not possible to investigate the variation of extrusion pressure with ram speed for given conditions of temperature and extrusion ratio.

FIGURE 3.1

THE EXTRUSION PRESS

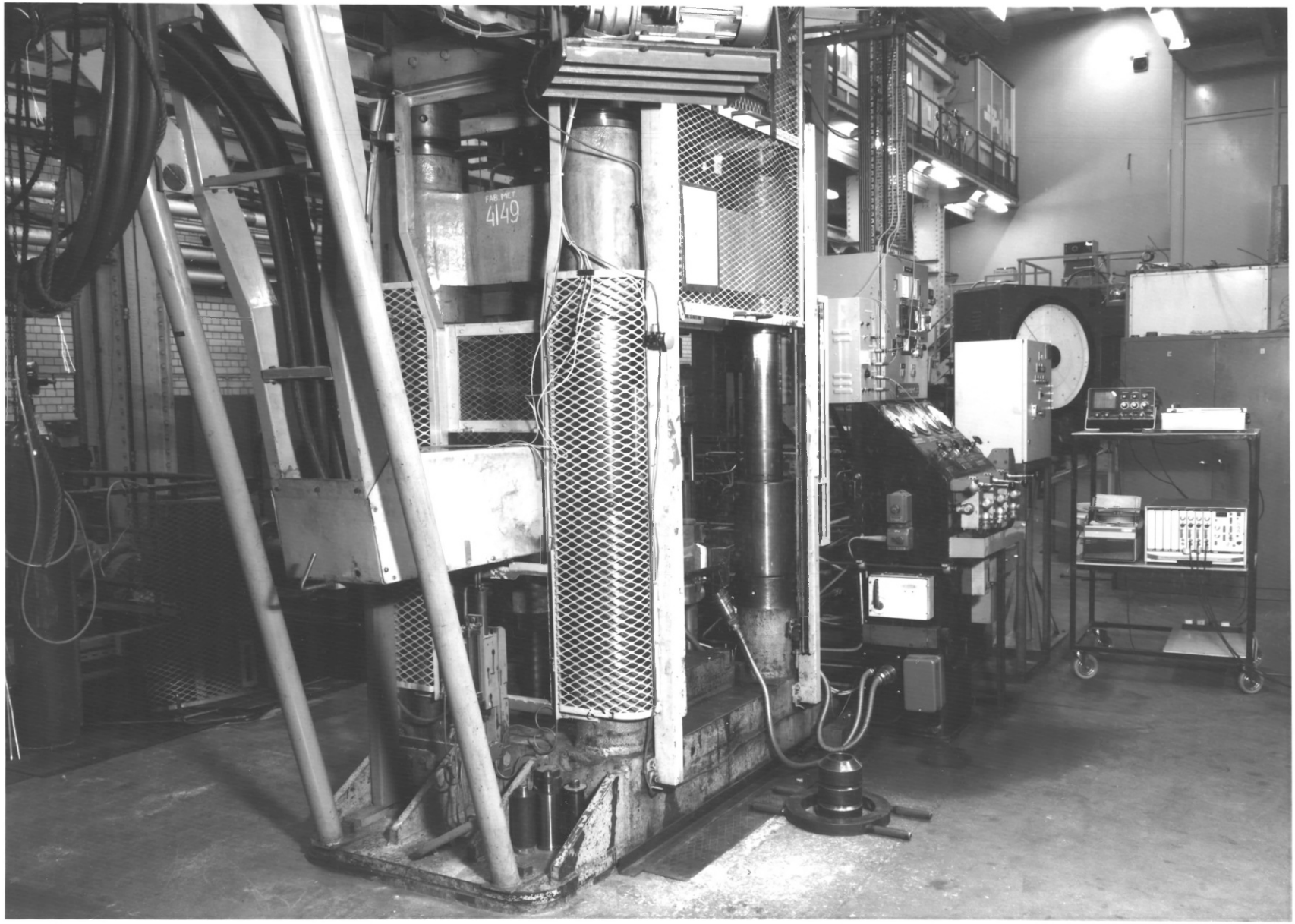
FAB. MET
4149

3.1.2.2 EXTRUSION TOOLING

The extrusion tooling is shown in Figure 3.2. The thrust rod, container and die assemblies are in the background, with the billets, pressure pads, scraper pads and dies in the foreground. The container liner, pressure pads, extrusion dies and thrust rod were all made of K.E.A. 145 (A.I.S.I. No. H13) heat treated to a hardness of 600 Vickers (54 Rockwell C). The composition of the steel and its in-service characteristics are given in Tables 1.2 and 1.3 respectively.

3.1.2.2.1 THE CONTAINER ASSEMBLY

The container assembly was heated by two separate sets of inconel heating elements positioned in the container holder casting (8 elements) and the inner container liner (12 elements) giving a combined power rating of 16 kilowatts. The temperature of the container was controlled by a Eurotherm connected to a thermocouple drilled to within 21.5 mm of the liner bore. The container temperature was set to 525°C, this being the maximum permissible temperature to avoid softening of the steel, which gave a temperature at the liner bore of 466°C. This temperature was used throughout the extrusion programme, the aim being to minimise billet chilling during extrusion.

The liners used had 57 mm diameter bores and permitted a maximum billet length of 158 mm.

3.1.2.2.2 EXTRUSION DIES

The die design employed is shown in Figure 3.3, together with the extrusion ratios used in the extrusion programme. The dies had a short 30° conical lead-in to assist metal flow. This is common practice in industry, except that the conical or dish-shaped lead-in is incoporated in the die-backer with the die itself being a small insert (section

FIGURE 3.2

THE EXTRUSION TOOLING

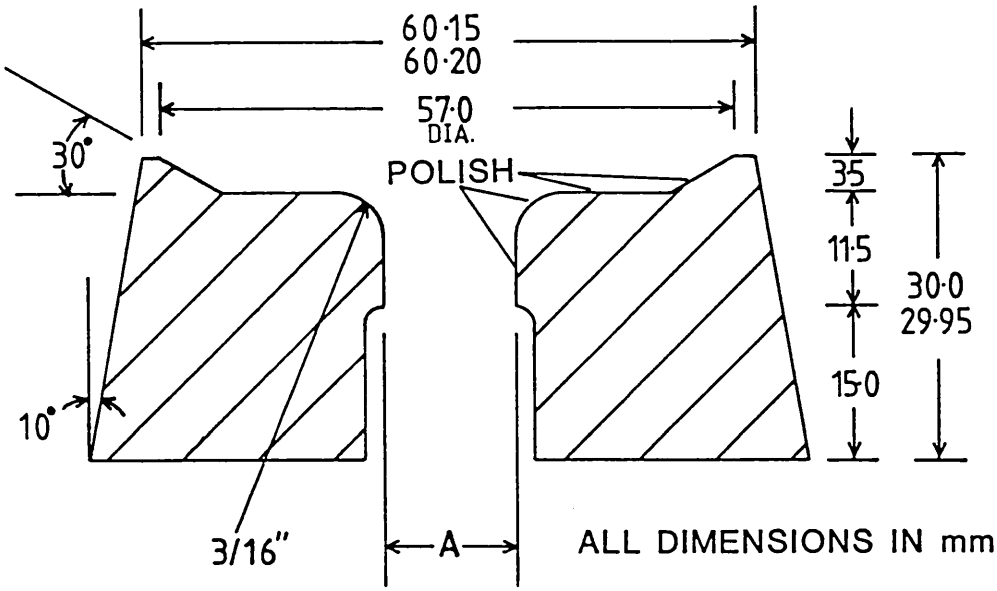

EXTRUSION RATIO	A
10:1	18·0
20:1	12·75
40:1	9·0
60:1	7·35

Figure 3.3 EXTRUSION DIE DESIGN AND EXTRUSION RATIOS EMPLOYED IN EXTRUSION PROGRAMME

1.3.3.7). The dies were machined with a $^{3}/_{16}$ " radiused entry to the orifice. The upper face of the die was polished to reduce billet/die friction.

The die material employed, H13, is commonly used in the extrusion of steel, and combines very high toughness with a high resistance to softening and a medium resistance to wear at in-service temperatures (Table 1.3).

The die temperature employed throughout the extrusion programme was 350°C.

3.1.2.2.3 THRUST ROD

An important consideration when using smaller diameter liners and thrust rods is that the maximum pressure that can be exerted may be limited by the strength of the thrust rod rather than by the press capacity. H13 can be heat treated to give a maximum U.T.S. of approximately 1800 MNm^{-2}. To ensure an adequate margin of safety, the load employed was limited to a value which gave a pressure of 1350 MNm^{-2} on the thrust rod. The maximum load that could be safely employed was calculated to be 3.44 MN, which is well below the press capacity of 5 MN.

3.1.2.2.4 PRESSURE PADS

The pressure pads were machined to be a close fit with the liner to reduce the possibility of any back extrusion. The diameter of the pressure pads was 0.2 mm less than the liner diameter. The pads were 20 mm thick which gave a discard thickness of approximately 10 mm.

3.1.3 BILLET HEATING

The billets were heated in a Gallenkamp FR-741 size 2 electric muffle furnace of dimensions 38 cm long x 22 cm wide x 17 cm deep. Heating was provided by eight silicon carbide elements at the roof of the furnace. The furnace temperature was monitored by two platinum: 13% rhodium-platinum thermocouples inserted into the back of the furnace, the temperature being controlled by a simple on/off indicating controller. An energy regulator permitted fine control of the heating rate and the temperature fluctuation of the furnace.

An inert atmosphere was maintained in the furnace by feeding argon through an inlet at the front. This was to minimise scale formation during heating.

The furnace was calibrated using a billet with an inconel-sheathed chromel-alumel thermocouple inserted into the centre.

The billets took approximately $\frac{1}{2}$ an hour to achieve the desired temperature, and were then allowed to soak for a further $\frac{1}{2}$ an hour prior to extrusion.

3.1.3.1 BILLET TRANSFER

The total time from the removal of the billet from the furnace to the application of the extrusion pressure was 15 seconds $\pm$ 1 second, made up of 4 seconds for transfer through the air and 11 seconds for positioning of the pressure pad and bringing down the ram. The heat losses from the billet during transfer were established as follows :-

Three 1.5 mm inconel sheathed chromel-alumel thermocouples were inserted radially into the billet centre at the centre, 14 mm from the surface and 2 mm from the surface. The billet was heated up and then transferred to the container following the usual procedure, the temperature of the three thermocouples being monitored during transfer.

Cooling curves were obtained at 850°C, 950°C, 1050°C and 1150°C, the results being shown in Table 3.2. The cooling curves obtained at

TIME	850°C			950°C			1050°C			1150°C		
S	O	M	I	O	M	I	O	M	I	O	M	I
0	850	850	853	950	950	950	1050	1050	1050	1150	1150	1150
10	777	837	851	864	-	-	915	1020	1046	995	1113	1145
15	770	831	848	843	919	940	912	1005	1038	980	1099	1135
20	770	825	842	837	913	935	906	993	1026	971	1084	1125
25	770	820	840	826	905	929	901	984	1018	962	1071	1110
30	767	815	835	821	899	923	894	973	1007	951	1056	1096

TABLE 3.2 COOLING CALIBRATION RESULTS

Furnace Temperature °C	Actual Temperature °C
850	810
900	851
950	893
1000	934
1050	974
1100	1016
1150	1058

TABLE 3.3 AVERAGE BILLET TEMPERATURES AT COMMENCEMENT OF EXTRUSION

850°C and 1150°C are plotted in Figure 3.4. A line has been drawn in at a time of 15 seconds to indicate the temperature distribution within the billet at the commencement of extrusion. The temperature distributions are plotted in Figure 3.5. It is apparent that dramatic heat losses have occurred from the billet surface during transfer, ranging from 80°C at 850°C to 170°C at 1150°C, with the result that large temperature gradients exist in the billet at the start of extrusion.

The method of calculating the average billet temperature at the start of extrusion is shown in Figure 3.6. The temperature 2 mm from the billet surface is assumed to be the surface temperature. The average billet temperatures at the start of extrusion are shown in Table 3.3 and plotted in Figure 3.7. A linear relationship exists and enables the billet temperature at the start of extrusion to be evaluated for any initial heating temperatures, providing the transfer conditions are similar.

3.1.4 LUBRICATION

Lubrication was provided by a glass pad at the die/billet interface and a graphite-molybdenum disulphide grease (Gredag 1559)[85] at the billet/liner interface.

3.1.4.1 GLASS LUBRICATION

The glasses employed in the extrusion programme are shown in Table 3.4. The two definitions of the softening point are given, i.e. the temperature at which the viscosity of the glass is $10^{7.6}$ poise, and the temperature at which the glass just adheres to a biscuit tile (section 1.3.3.2.4). These values are sufficiently similar for the purposes of glass selection. The data was supplied by Bayer U.K.. Also given in the table is the ideal extrusion temperature defined as 1.5 x softening point, which is a rough guide to the temperature at which the glass will soften adequately during extrusion.

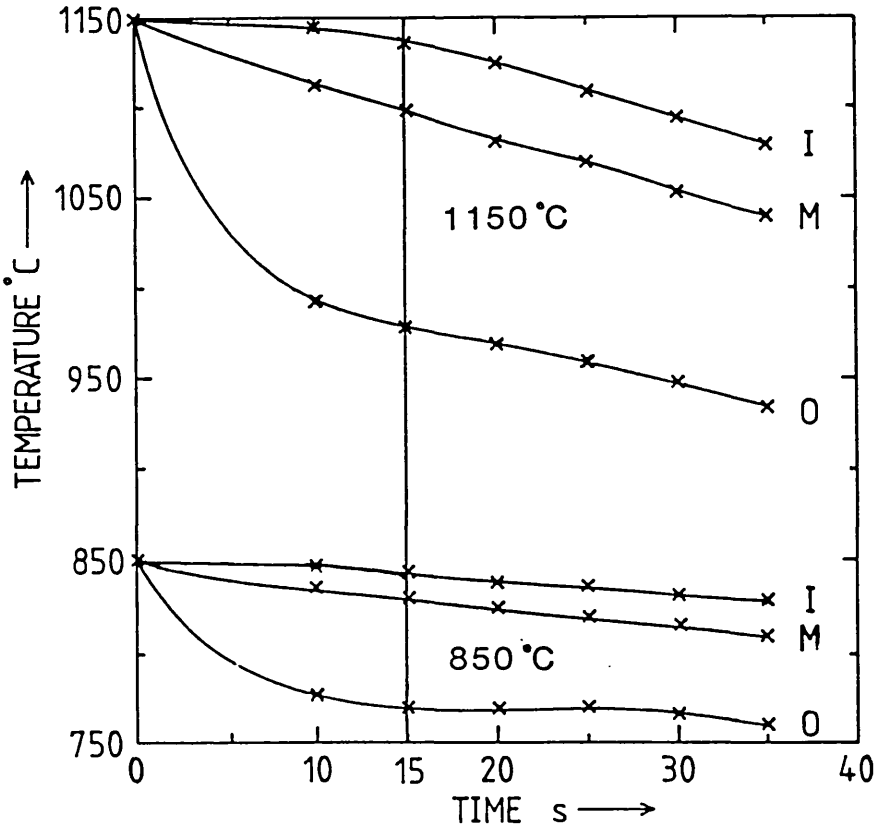

Figure 3.4 TYPICAL COOLING CURVES

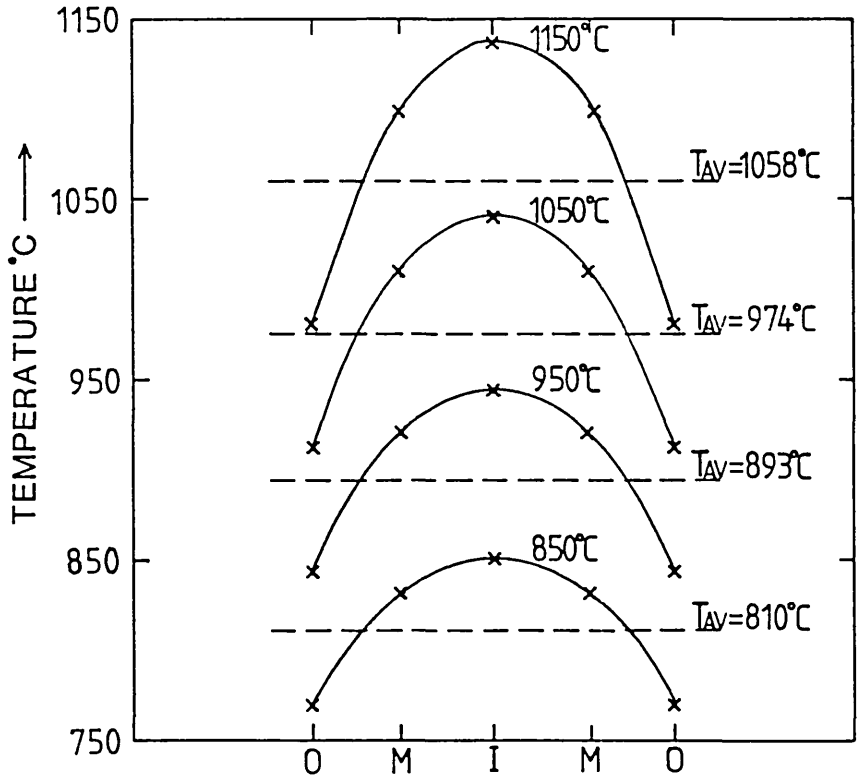

Figure 3.5 TEMPERATURE PROFILES IN THE BILLET AT COMMENCEMENT OF EXTRUSION

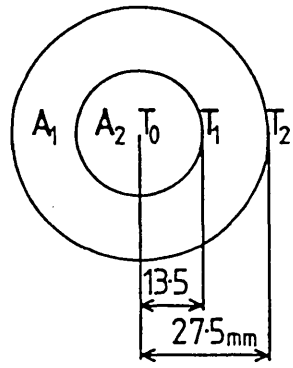

$$\text{AVERAGE TEMPERATURE °C} = \frac{A_1(T_0+T_1)/2 + A_2(T_1+T_2)/2}{A_1 + A_2}$$

Figure 3.6 CALCULATION OF THE AVERAGE BILLET TEMPERATURE AT THE COMMENCEMENT OF EXTRUSION

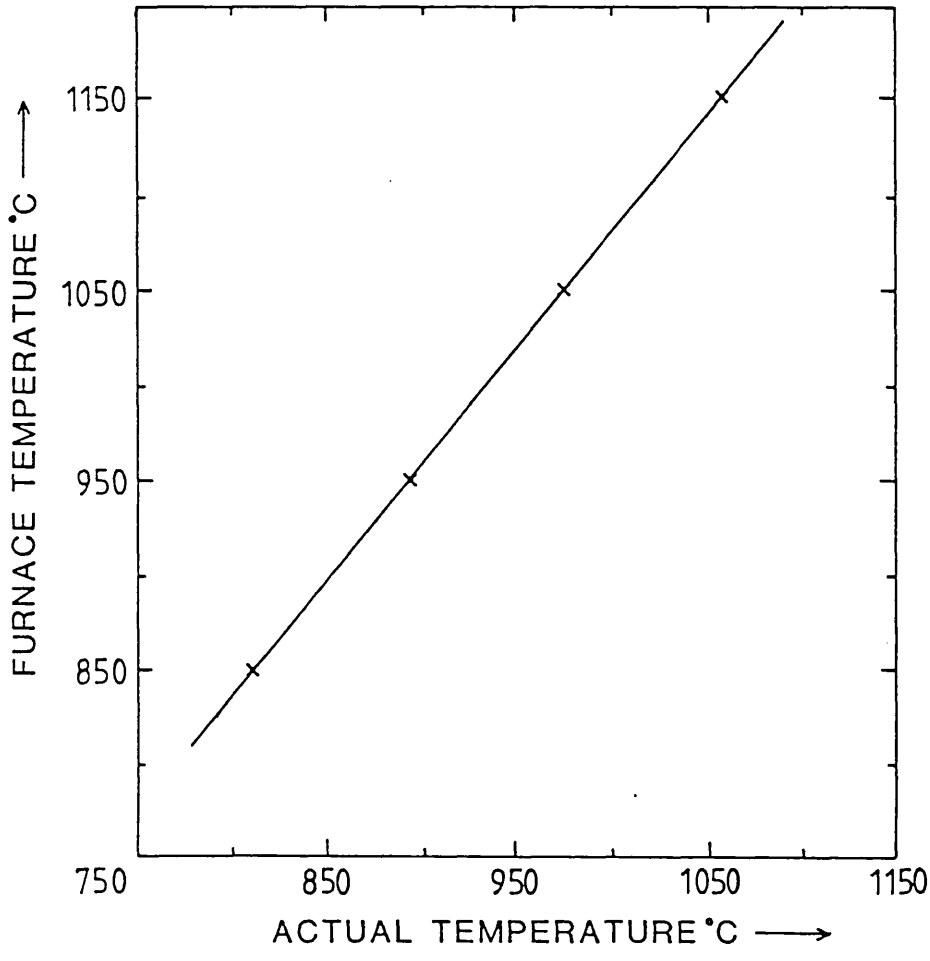

Figure 3.7 FURNACE TEMPERATURE VS. AVERAGE BILLET TEMPERATURE AT COMMENCEMENT OF EXTRUSION

Glass Type	Softening Point $10^{7.6}$ °C	Ideal Ext. Temp. °C	Softening Point Biscuit Tile °C	Ideal Ext. Temp. °C	Approximate Composition wt %					
					SiO_2	Na_2O	CaO	B_2O_3	Al_2O_3	K_2O
K7072	-	-	570	855	-	-	-	-	-	-
C6496	657	986	670	1006	43	21	15	20	-	-
C7216	795	1193	750	1125	84	5	9	-	1	1

TABLE 3.4 COMPOSITIONS AND SOFTENING POINTS OF GLASSES EMPLOYED IN EXTRUSION PROGRAMME

Temperature °C	LOG_{10} Viscosity C6496 S.P. = 657°C	LOG_{10} Viscosity C7216 S.P. = 795°C
900	2.647	6.133
950	2.176	5.587
1000	1.783	5.112
1050	1.451	4.696
1100	1.167	4.328
1150	0.921	4.000
1200	-	3.705

TABLE 3.5 TEMPERATURE - VISCOSITY RELATIONSHIPS FOR C6496 AND C7216 GLASSES

C6496 glass of intermediate softening point was used for the majority of the extrusions with the K7072 glass used for some extrusions at the lower temperature end of the extrusion range and the C7216 glass at the higher temperature end.

The second method of assessing the suitability of a glass as an extrusion lubricant involves measurement of the viscosity variation with temperature (section 1.3.3.2.4). The data employed was provided by Bayer U.K. and is shown in Table 3.5 for the C6496 and C7216 glasses. This data was not available for the K7072 glass.

3.1.4.2 MANUFACTURE OF GLASS PADS

The glass pads were made by mixing 40 g of 30-80 mesh powdered glass with 5 ml of sodium silicate solution. The mixture should just hold together when pressed between the fingers. The mixture was pressed using a ram into a slightly tapered mould of diameter 57 mm and then pushed out onto a steel tray and baked at 250°C for 2 hours. A central hole was then formed in the pad, of the same diameter as the extrude and one end of the pad profiled to match the conical lead-in to the die. A typical pad is shown in Figure 3.8.

3.1.5 EXTRUSION DATA RECORDING

The data for all the extrusions was recorded on a datalab DL2800 transient recorder. A detailed description of the recorder is given by Vierod[72]. The sample rate used was 2 ms which gave a recording time of 8 seconds.

The load was measured by a Mayes load cell situated directly above the ram. The ram displacement was measured by a rectilinear potentiometer fixed between the main ram and the base of the press. The hydraulic pressure was measured with a pressure transducer situated at the inlet to the main cylinder.

FIGURE 3.8

GLASS PAD

FIGURE 3.9

TORSION TEST PIECE

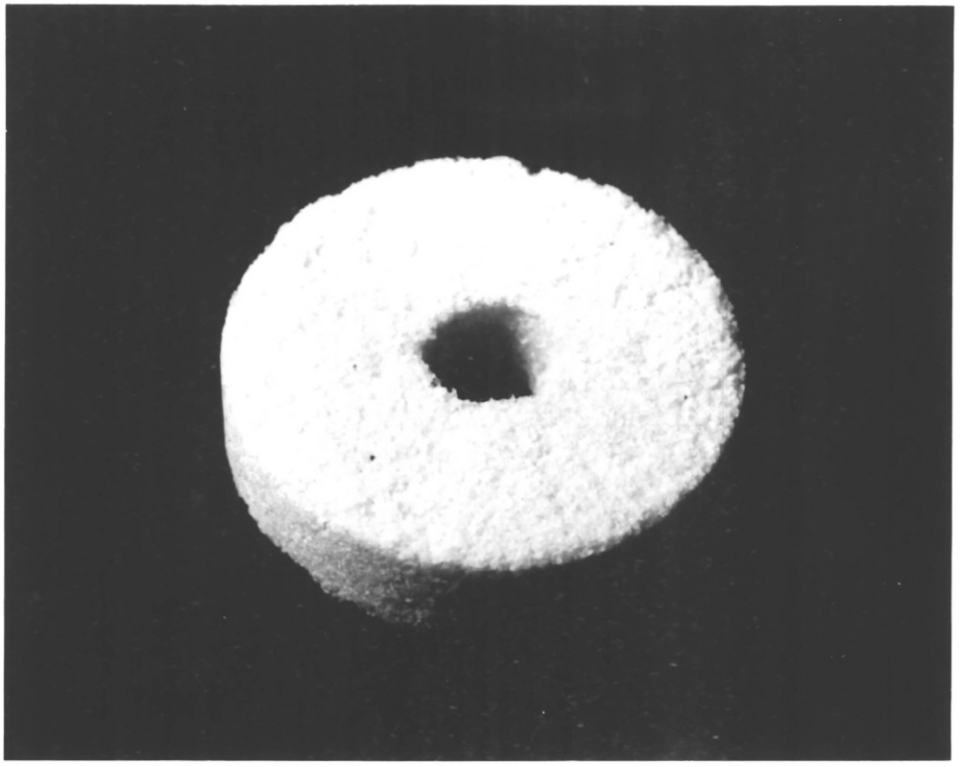

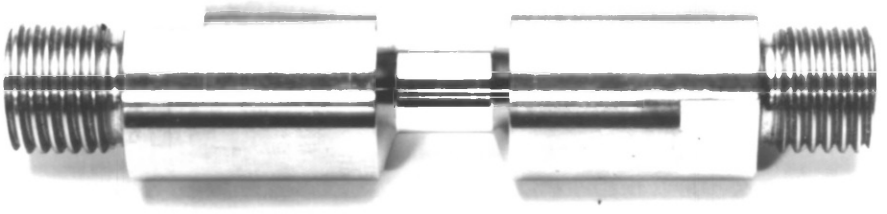

The transient recorder was linked to an x-y recorder from which a permanent record of the extrusion could be obtained. From this record the ram speed, hydraulic pressure and load-cell pressure were calculated.

3.1.6 COOLING RATE

To investigate the effect of cooling rate on the structure and properties of the extrude, some of the extrusions were water quenched and others air cooled after extrusion.

The first quench jet is situated 41 cm from the die exit, and therefore this amount of extrude will not be quenched. This only creates a problem at an extrusion ratio of 10:1 where the total length of extrude is only 85 cm.

3.1.7 EXPERIMENTAL PROCEDURE

The container was left at a temperature of 525°C for at least an hour before extrusion. This gave a liner temperature of 466°C and a die temperature of 350°C at the commencement of extrusion. The pressure pad was left on the container for at least an hour and attained a temperature of 300°C.

The billet was placed in the furnace at the required temperature and heated for 1 hour under argon.

A few minutes prior to extrusion the liner and die were swabbed with Gredag 1559 and the glass pad inserted in the liner and positioned on top of the die. Two semi-circular rings were placed on top of the container to prevent any damage to the main ram.

The accumulator was charged up, the furnace door opened and the billet transferred to the container using tongs. The pressure pad was dropped onto the billet using a magnetic holder and the fast ram approach activated. The transient recorder was switched on just before

the thrust rod hit the pressure pad. Extrusion was continued until the thrust rod touched the rings, whereupon the pumps were reversed and the ram raised. The container was then raised and the extrude cut with an abrasive wheel power saw, before being punched through the die to the pit below. The discard was removed by placing three circular rings between the bottom of the container and the die assembly and using the thrust rod to push a tightly fitting scraper pad through the container. The ejection of the discard was invariably smooth with no jarring. The pressure pad separated easily from the discard and could be used repeatedly after slight dressing. Occasionally, if only a thin disc of discard was produced, it would not be retracted with the container and would have to be prised out of the die. After each extrusion the die was removed and examined, and the liner checked for any skull or glass pick-up.

In order to assess the heat losses from the billet the extrusion cycle was timed from when the furnace door was opened until the ram hit the pressure pad.

3.1.8 PARTIAL EXTRUSIONS

In order to examine the flow patterns produced during glass-lubricated extrusion, three billets were only partially extruded. This was achieved by placing two 50 mm thick semi-circular rings on the container as opposed to the normal 25 mm thick rings. The discard thickness obtained was approximately 38 mm. The billets were sectioned along the longitudinal axis and then ground, polished and overetched to reveal the grain structure and flow pattern.

Three extrusion temperatures were chosen:- 900°C, 1000°C and 1100°C, the extrusion ratio employed being 10:1.

3.1.9 GLASS REMOVAL

Two techniques are available for removing the glass from the surface of the extrude (section 1.3.3.8), namely pickling and grit-blasting.

Grit blasting is much more convenient and was the technique employed throughout the extrusion programme. The extrude was blasted in a Guyson Blast Cleaning Cabinet using 24-30 Al_2O_3 grit. The diameter of the extrude before and after blasting was measured to obtain an estimate of the glass coating thickness. This was performed at 0.25, 0.5 and 0.75 of the extrude length, to observe the variation in glass thickness along the extrude length.

3.1.10 MEASUREMENT OF DIE WEAR

The major problem encountered throughout the course of the extrusion programmes was that of die wear, with only one extrusion per die being possible at higher temperatures and extrusion ratios.

A rough estimate of the die wear was obtained by measuring the diameter of the extrude at 0.25 and 0.75 of its length. The die wear was defined as:-

$$\text{DIE WEAR (mm)} = d_{0.75} - d_{0.25}$$

or, for comparison to be made between different reduction ratios,

$$\% \text{ DIE WEAR} = \frac{d_{0.75} - d_{0.25}}{d_{0.25}}$$

3.1.11 MODIFICATIONS TO EXTRUSION PROCEDURE

This section is to be read as part of the Results and Discussion section 4.1.2 - Elimination of Die Wear. The modified extrusion practice was performed on a few billets of Ti-4Al-4Mo-2Sn-0.5Si (I.M.I. 550) as the supply of Ti-6Al-4V billets had been exhausted. I.M.I. 550[86] is an alpha+beta alloy and has similar hot-working characteristics to Ti-6Al-4V, and so the results are equally applicable

to the latter. The results were viewed purely from a surface quality/ die wear aspect and no structural or property studies were carried out.

The material was provided in the form of 50.8 mm diameter as-rolled bar. This was machined into 49 mm diameter x 100 mm long billets with a $\frac{1}{4}$" radius at the leading end. The liner employed was 52 mm in diameter, and the thrust rod and pressure pads were scaled accordingly. The die design was modified slightly by eliminating the conical entry to the die. The use of flat-faced dies is common practice for experimental purposes, from the point of view of ease of machining and produces discard profiles similar to those produced using a conical lead-in.

The following major modifications were made to the extrusion procedure, all having the same aim of eliminating the oxide scale.

3.1.11.1 BILLET HEATING

A newly acquired Banyard Metal heat medium frequency induction heater was employed to heat up the billets. The billets could be heated up to 1150°C in under 10 minutes, thereby dramatically reducing heating times and hence the time for oxidation. In addition, argon was flushed through the induction chamber during heating, thereby further minimising scale formation.

The temperature of the billets was monitored by three nisil-nichromel thermocouples drilled 12.5 mm into the top of the billet, one drilled at the centre, and the other two on a line with the centre at 5 mm from the periphery. The billet temperature was controlled by one of the peripheral thermocouples, with the other two employed to measure the temperature gradient between the centre and the periphery of the billet. By careful selection of the heating rate and cycling time at temperature, the billet could be rapidly brought up to temperature, and at the same time the temperature gradient minimised.

The induction heater was attached to the left hand side of the extrusion press (Figure 3.1) and could be moved over the container by means of a pneumatic system operated by controls on the main press control panel. When the heater was above the container the hot billet was transferred manually by removing a rod that supported the billet in the coil. Extrusion could be started as soon as the heater had returned to its initial position. The extrusion cycle was timed from when the induction heater was switched off until the thrust rod hit the pressure pad.

3.1.11.2 GLASS COATINGS

As a further barrier to oxidation during heating a glass coating was applied to the cold billet. On heating the glass fuses to form a fluid protective barrier. The glass coating has the added advantage of providing additional lubrication at the liner/billet interface during extrusion.

The glass coating employed was Deltaglaze 12 produced by Acheson Colloids[87]. This is a dispersion of glass in isopropanol. On application of the coating the isopropanol vaporizes leaving behind a glass layer. The Deltaglaze 12 was applied as follows:-

The billet was first cleaned thoroughly with trichloroethylene to remove any contamination. The Deltaglaze was then diluted with a 6 parts ethanol/1 part water solution in the ratio 1 part Deltaglaze to 1 part diluent. The diluted Deltaglaze was then poured into a shallow tray and the billet rolled in the solution. The billet was then allowed to dry in air. A glass coating of approximately 1.5 g was obtained by rolling the billet twice through the solution.

3.1.11.3 MANUFACTURE OF GLASS PADS

A few minor amendments were made in the manufacture of the glass pads (c.f. section 3.1.4.2), it being felt that the pads being made were slightly too hard. The amount of sodium silicate solution used was

reduced from 5 ml to 3 ml per 40 g of powdered glass. After pressing and ejection from the mould the pad was simply allowed to air-harden rather than being baked. The resulting pad was softer, while still being hard enough to be handled.

3.1.11.4 TOOLING TEMPERATURE

Although the elimination of the oxide scale should afford better thermal insulation between the billet and die, as a further precaution the container temperature was reduced from 525°C to 350°C. This should also significantly reduce the chances of the die becoming overheated. This will obviously have the disadvantageous effect of increasing chilling of the billet surface, thereby increasing extrusion pressures.

It was hoped that these modifications would dramatically improve the die life. The results and discussion are given in section 4.12.

3.2 TORSION TESTING

The torsion test piece employed is shown in Figure 3.9. The specimens were machined from 25 mm Ti-6Al-4V bar purchased from I.M.I. Titanium. The material had been finished rolled well below the transus temperature and annealed for 2 hours at 700°C.

Testing was carried out on a machine built in the Metallurgy Department, details of which are given by Tweedale[88]. The machine twist rate variation from 0 to 1000 revolutions per minute permitted a maximum surface shear strain rate of 50.0 s^{-1} to be obtained with the specimen geometry employed.

The strain rates used in the testing programme were 0.05, 0.5, 5.0, 15.0 and 50.0 s^{-1} (surface equivalent strain rates of 0.0289, 0.289, 2.89, 8.67 and 28.9 s^{-1}). The temperatures employed ranged from 800°C to 1150°C in 50°C intervals. The torques obtained at 0.05 s^{-1} at temperatures above 1050°C were very small and subject to large error and were not included in the analysis.

Specimen heating was facilitated by an in-situ induction coil and temperature regulation was via a Eurotherm 211 programmer/controller connected to a 1.5 mm diameter inconel sheathed chromel-alumel thermocouple placed in the stationary end of the specimen to within 5 mm of the gauge length. Because of the poor thermal conductivity of titanium, the temperature monitored by this thermocouple did not represent the actual temperature in the gauge length. This was calibrated by drilling thermocouples into the gauge centre and ends to the depth of the specimen axis. Temperature gradients in the gauge length were carefully minimised by moving the position of the induction coil. The situation was further aided by using a coil which enclosed the specimen shoulders as well, thus reducing heat flow away from the gauge length.

Using the Eurotherm programmer the specimen was heated up to temperature in 5 minutes and then held at temperature for a further 5 minutes prior to twisting. Even with such rapid heating rates and short holding times, scaling was apparent at higher temperatures. Further tests were carried out with heating being conducted under argon. This eliminated the oxide scale and although the torque values were not significantly altered it is recommended that future testing programmes be carried out under an argon atmosphere, possibly even with a Deltaglaze glass coating to further minimise scaling.

During testing the stationary end was restrained from moving axially by clamping. Details of the torque and twist measurements are given by Tutcher[77]. Twisting was stopped either at failure or at some point after the maximum torque was obtained. Once the power to the induction coil had been switched off, the specimen was water quenched to retain the high temperature structure.

3.3 OPTICAL MICROSCOPY

The specimens for optical microscopy were sectioned on a Metaserv cut-off machine. These were then ground on 240, 400 and 800 grit papers. The specimens were then mounted in Metaserv D.A.P. moulding powder. They were then ground on 1200 grit paper and given a 15 micron

polish on a hard cloth. Finish polishing was carried out on a Buehler Vibromet vibratory polisher using microcloth with a slurry of 0.3 micron alumina.

Alternatively, the specimens were ground to 1200 grit, given a 15 micron polish, and then electropolished unmounted. A 10% Sulphuric-Methanol solution was employed for electropolishing using a voltage of 18V and a temperature of -30°C.

The specimens were then etched using the following solution :- 2% HF, 10% HNO_3, 88% H_2O. Etching times of up to 5 minutes were employed to ensure delineation of the transformed beta grain boundaries.

3.4 EVALUATION OF THE STARTING STRUCTURES FOR TORSION AND EXTRUSION

To evaluate the starting structures for torsion and extrusion, 1 cm sq. specimens were cut from the torsion and extrusion starting material. These were then heated for the appropriate times (5 minutes for torsion, $\frac{1}{2}$ hour for extrusion) at the temperatures employed in the torsion and extrusion programmes. The specimens were quenched immediately after removal from the furnace to retain the high temperature structure. They were then categorized in the usual manner.

The transition temperature for Ti-6Al-4V is quoted as 995°C $\pm$ 15°C[90]. Accurate evaluation of the transition temperature for both the torsion and extrusion material was obtained by heating speciments from 990°C to 1015°C at 5°C intervals following the procedure outlined above. These were then examined using an optical miscroscope at a magnification of x 400 for the presence of any primary α, and the transition temperature evaluated accordingly.

3.5 CATEGORIZATION OF STRUCTURES

In this section the techniques employed for categorizing the extrusion and torsion starting structures and the structures produced on extrusion, will be described.

3.5.1 STARTING STRUCTURES

The starting structures for extrusion and torsion were evaluated as described in section 3.4. The structures produced on heating in the two phase alpha+beta regime consist of equiaxed primary alpha + beta. Although water quenching results in the transformation of the beta phase to martensite, the relative properties of the two phases remain unaltered, and thus it is possible to determine the proportions of alpha and beta at the starting temperatures.

Measurement of the proportions of primary alpha+beta were made as follows. 4 photographs were taken for each structure at different locations, at a magnification of approximately 400 x. A gridded transparency, 10 cm x 10 cm, with lines at 1 cm intervals, was then placed over the photograph and the proportions of the two phases evaluated using the point-count technique.

The problem with this technique is that the alpha and martensite are very difficult to differentiate between at certain temperatures, thus making measurement prone to error. There would appear, however, to be no better technique for measuring the phase proportions.

The structures produced on heating in the single phase beta regime have a very coarse grain size. On quenching the beta phase transforms fully to martensite, however it is still possible to discern the original beta grain boundaries, so that categorization is possible by evaluating the grain size.

The best technique employed for evaluating the grain size was measurement off photographs. At least 4 photographs were taken for each structure, at various locations. A transparency with 10 horizontal lines scribed at 1 cm intervals was then placed over the photograph and the grain size evaluated using the linear intercept method.

3.5.2 EXTRUDED STRUCTURE

Only the structure at the centre of the extrude was employed for the purposes of categorization.

Approximately 75% of all the extrusion structures produced were fully recrystallised and hence could be categorized according to their grain size in the same manner as described for the beta starting structures. Transverse sections through the extrusions were examined in each case.

The remainder of the structures produced on extrusion can be divided into two categories :-

a) Two phase primary alpha + transformed beta structures. The best technique for categorizing these structures is to evaluate the proportions of primary alpha + transformed beta in the same manner as described for the starting structures. It is important that at least four areas should be examined to avoid erroneous results due to banding. Transverse sections through the extrusions were examined in each case.

b) Partially unrecrystallised fully transformed beta structures. Only three structures contained any unrecrystallised transformed beta. The coarse elongated unrecrystallised areas are readily discernible on low magnification longitudinal optical macrographs. Macrographs were taken at a magnification of x 6 and the structures graded visually according to the proportion of unrecrystallised structure.

3.6 ELECTRON MICROSCOPY

Specimens for transmission electron microscopy were ground down to 0.20 mm, with final grinding being carried out on 800 grit paper. 3 mm diameter discs were punched from these specimens and were electropolished in a Struers double-jet electropolishing device. The same electropolishing conditions were employed as for optical microscopy. The discs were examined using a Philips EM301 electron microscope operating at 100 kV.

3.7 HEAT TREATMENT

10 cm sections were cut from the middle of the extrude length. These were then grit blasted prior to heat treatment to remove the glass. The following heat treatments were carried out :-

a) The air cooled extrusions were annealed for 2 hours at 700°C

b) The water quenched extrusions were aged for 4 hours at 540°C

In addition, sections of both air cooled and water quenched 20:1 extrusions were solution treated for 1 hour at 950°C, followed by water quenching and ageing for 4 hours at 540°C.

Heating was carried out in air in each case. For solution treatment of thinner sections, a protective atmosphere is required.

8 cm is required for the tensile test piece, with the remainder being employed for optical and electron microscopy studies. Prior to machining the solution treated specimens should be pickled to remove the hard oxide scale. The pickling solution employed was 5% HF 20% HNO_3 and 75% H_2O at a temperature of 50°C.

3.8 TENSILE TESTING

Tensile testing was carried out at the Royal Aircraft Establishment, Farnborough, on a Zwick 1474 testing machine. A standard $\frac{1}{4}$" B.S.F. test piece was employed, with a gauge diameter of 3.99 mm and a parallel gauge length of 22 mm. A strain rate of 0.003 s^{-1} was employed for all the tests. The use of a Zwick dual-averaging extensometer permitted the accurate measurement of the Young's modulus. The 0.2% Proof Stress, Ultimate Tensile strength, % Elongation on 5.65 $\sqrt{S_o}$ and Reduction of Area were also measured for each specimen.

CHAPTER FOUR

RESULTS AND DISCUSSION

CHAPTER FOUR

RESULTS AND DISCUSSION

4.1 INTRODUCTION

The results and discussion section has been divided into four subsections.

SECTION ONE - TORSION ANALYSIS

In this section the hot working constants in the constitutive equation have been evaluated in the alpha+beta and beta regimes. Structural studies have been carried out to identify the dynamic restoration mechanisms operative in the two regimes. The hot working characteristics of the alloy in the two regimes has been investigated,in particular the flow stress dependence of temperature and strain rate and the hot ductility.

SECTION TWO - FACTORS INFLUENCING DIE WEAR AND THE VARIATION IN THE LUBRICATING BEHAVIOUR OF EXTRUSION GLASSES WITH THE EXTRUSION VARIABLES

In this section the factors influencing die wear have been discussed, and the effect of wear on the extrusion pressure, surface quality and the lubricating behaviour of the extrusion glasses. The technique developed for eliminating die wear is presented. The variation in the lubricating behaviour of the extrusion glasses with the extrusion variables is discussed and related to the viscosity of the glass at the extrusion temperature.

SECTION THREE - EXPERIMENTAL AND THEORETICAL EXTRUSION ANALYSIS

This section has been divided into three subsections. In the first section the variation in the extrusion pressure with the extrusion variables is discussed. Empirical relationships have been established between the pressure and the temperature compensated strain rate z and the flow stress σ, using the values of the hot working constants obtained from torsion testing.

In the second section an axisymmetric upper bound analysis is presented, and theoretical predictions of P/σ compared with the experimentally observed values. Information from the upper bound analysis has also been used for the mean strain rate and temperature rise calculations.

In the third section the temperature changes occurring during extrusion have been predicted using an integral profile technique. These values are compared with the experimentally observed temperature changes obtained from a structural analysis, and their influence on the peak pressure, z-parameter and flow stress discussed.

SECTION FOUR - STRUCTURE AND PROPERTIES OF EXTRUDED Ti-6Al-4V

In this section the relationship between the extrusion variables and the structure and tensile properties of extruded Ti-6Al-4V is discussed. The extrusion structures have been categorized using optical microscopy and related to the extrusion variables through the z-parameter. The tensile properties have also been related to the z-parameter. The dynamic restoration mechanisms operative in extrusion have been compared to those obtained in torsion, and the validity of employing the hot working constants obtained from torsion in the extrusion analysis discussed.

Summaries have been presented at the end of each section.

SECTION ONE

4.2 TORSION ANALYSIS

4.2.1 INTRODUCTION

Torsion testing was carried out over the temperature range of 800°C - 1150°C at surface strain rates of 0.05 s^{-1} to 50.0 s^{-1} as described in section 3.2. Using the values of torque obtained, the hot working constants in the constitutive equation were evaluated as described in section 2.2.2. Optical and electron microscopy studies were carried out on the torsion structures to identify the dynamic restoration mechanisms operative during deformation.

4.2.2 STARTING STRUCTURES

The structure of the as-received material and the starting structures for torsion, evaluated as described in section 3.4, are shown in Figure 4.1. The transition temperature was calculated to be 997.5 $\pm$ 2°C. Below this temperature the structure is two phase alpha+beta, the proportion of alpha phase (white) increasing with decreasing temperature (Table 4.1 and Figure 4.2). Above the transition temperature the structure is single phase beta, the beta grain size increasing with increasing temperatures (Table 4.2 and Figure 4.2).

A marked change in microstructure is apparent on moving from the alpha+beta to the beta regime. On heating in the single phase beta regime a very coarse recrystallised grain size is produced, however in the duplex alpha+beta regime, the presence of the primary alpha markedly inhibits beta grain growth, resulting in a very much finer structure.

The torsion data can therefore be conveniently divided into two regimes :- the alpha+beta regime below 1000°C, and the beta regime above and including 1000°C.

4.2.3 ANALYSIS OF TORSION DATA

The results from the torsion tests are shown in Table 4.3 for the alpha+beta regime and Table 4.4 for the beta regime. For the highest strain rate runs at 50.0 s^{-1}, the machine could not generate the twist rate rapidly enough, and an average twist rate to peak torque had to be taken.

Hot working is normally carried out at temperatures greater than approximately 0.6 Tm, where Tm is the melting temperature in °K[15]. The melting point of pure titanium is 1948°K, but vanadium and aluminium both serve to depress it giving a melting range for Ti-6Al-4V of 1813°K - 1923°K[7]. Taking an average value of 1868°K yields 0.6 Tm = 1120°K = 848°C. Hence at a temperature of 800°C (= 0.57 Tm) the

(a)

AS-RECEIVED

(b)

800°C

FIGURE 4.1

AS-RECEIVED AND STARTING STRUCTURES

FOR TORSION

(c)

850°C

(d)

900°C

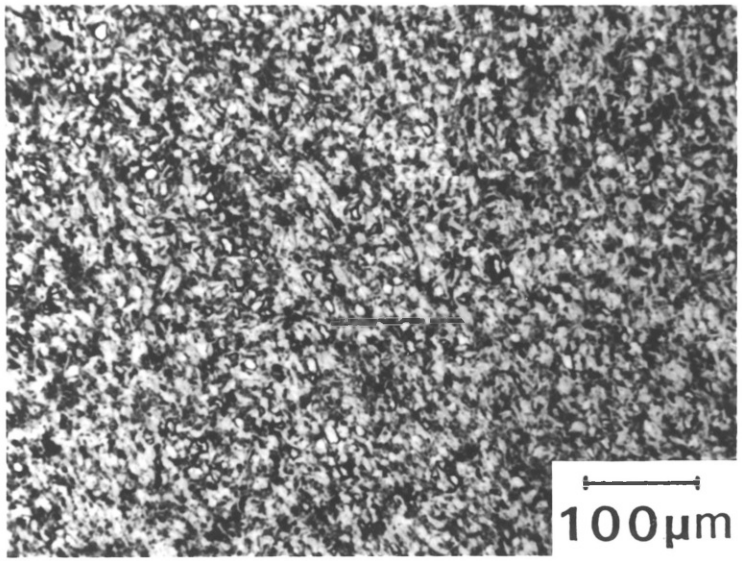
100μm

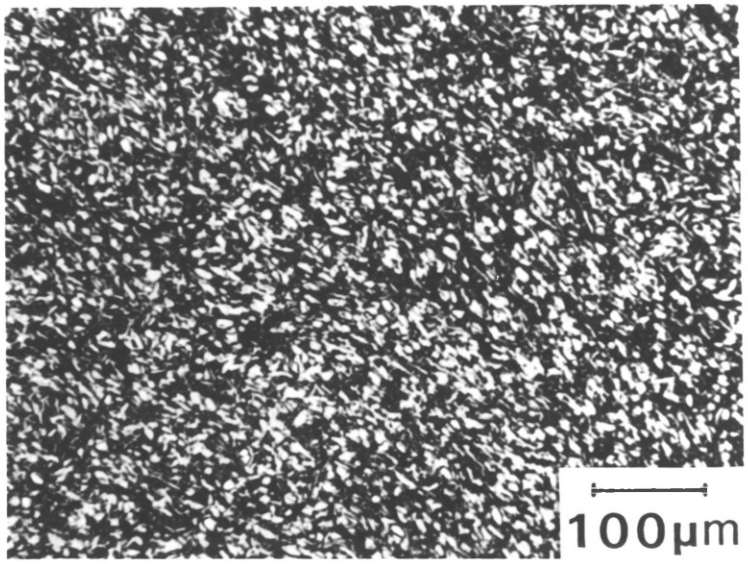
100μm

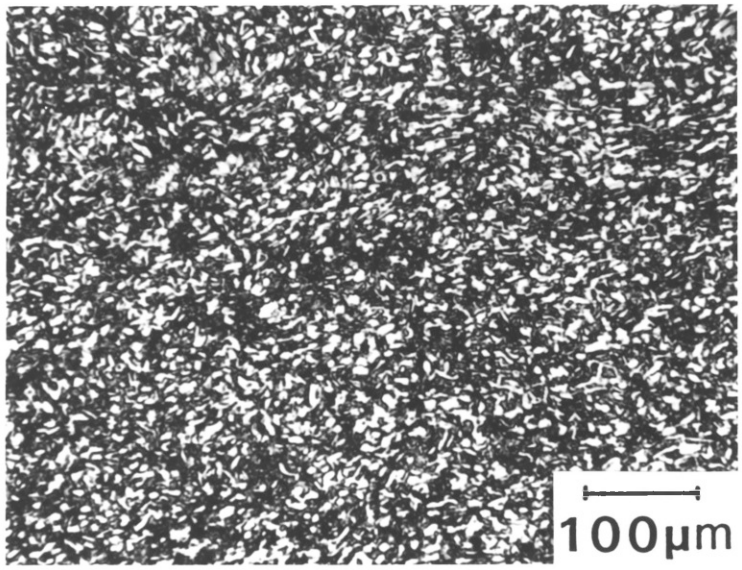
100μm

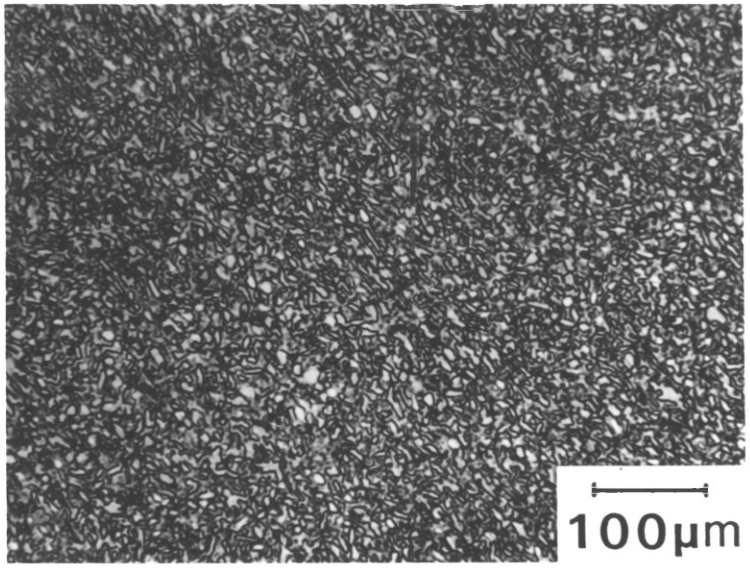
100μm

(e)

950°C

(f)

990°C

FIGURE 4.1 (CONTINUED)

(g)

1050°C

(h)

1150°C

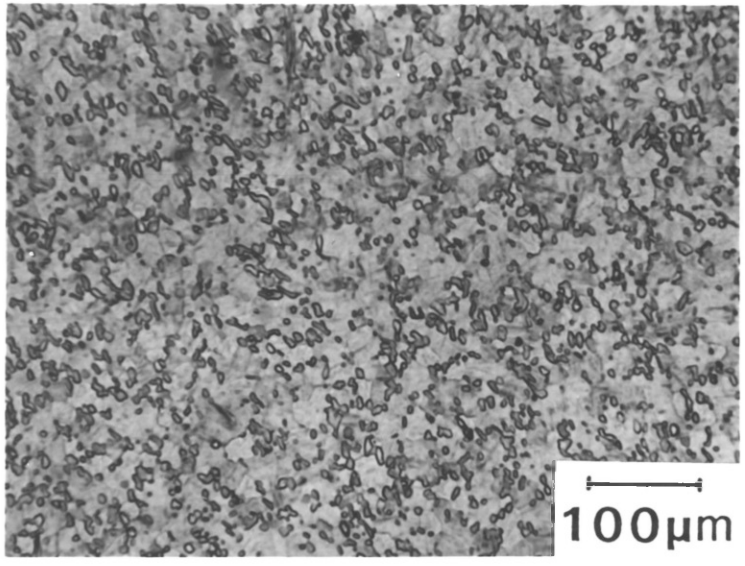
100μm

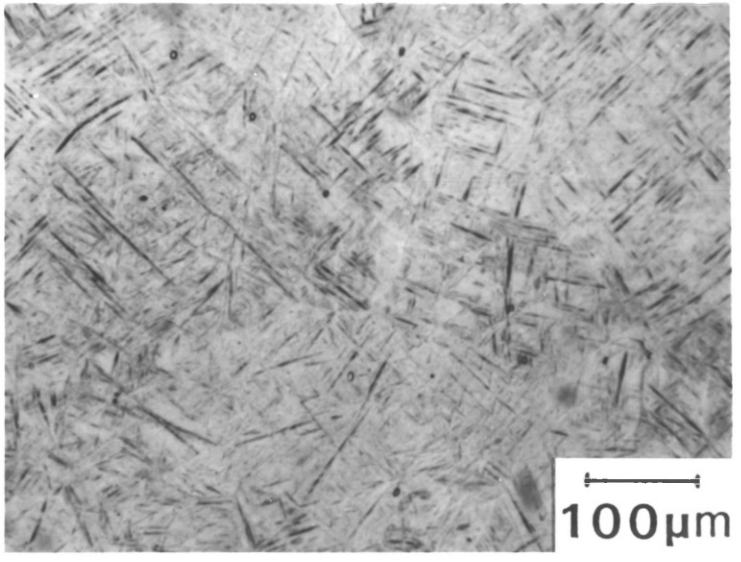
100μm

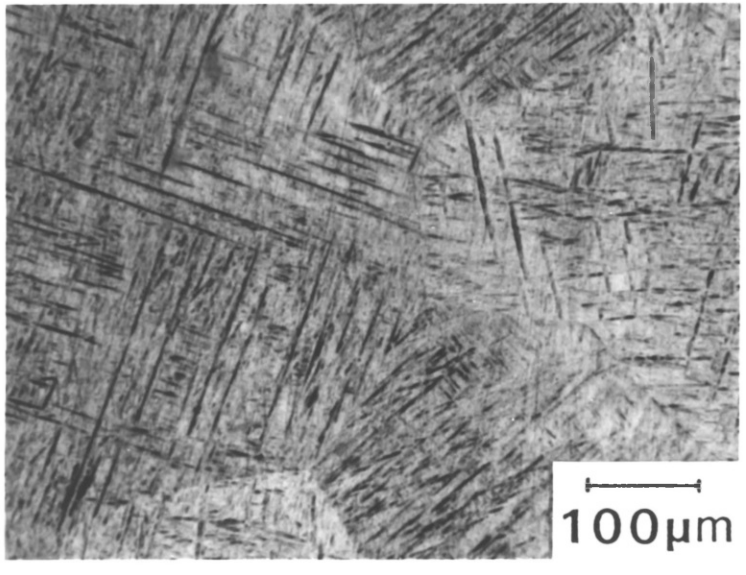
100μm

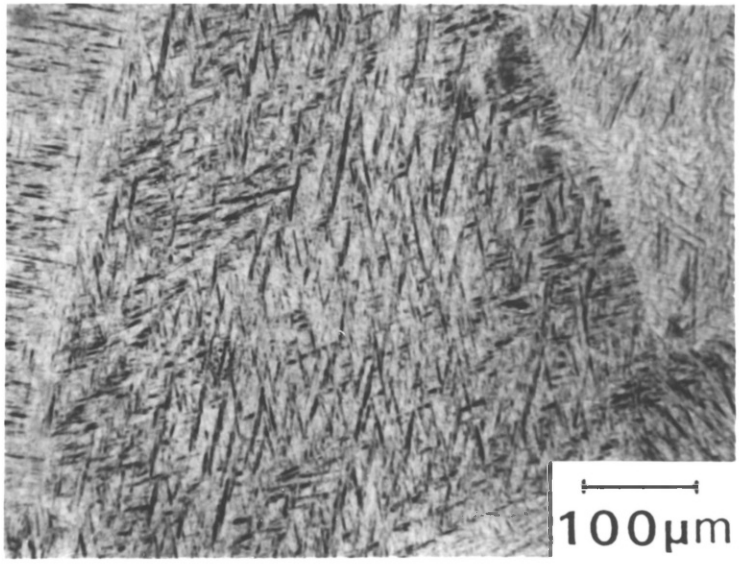
100μm

Temperature °C	% Alpha Phase	% Beta Phase
800	58.8	41.2
850	50.0	50.0
900	36.2	63.8
950	19.1	80.9

TABLE 4.1 VARIATION IN THE PERCENTAGE OF ALPHA AND BETA PHASES WITH TEMPERATURE FOR THE TORSION STARTING MATERIAL

Temperature °C	Beta Grain Size μm
1000	-
1050	301
1100	334
1150	381

TABLE 4.2 VARIATION IN BETA GRAIN SIZE WITH TEMPERATURE FOR THE TORSION STARTING MATERIAL

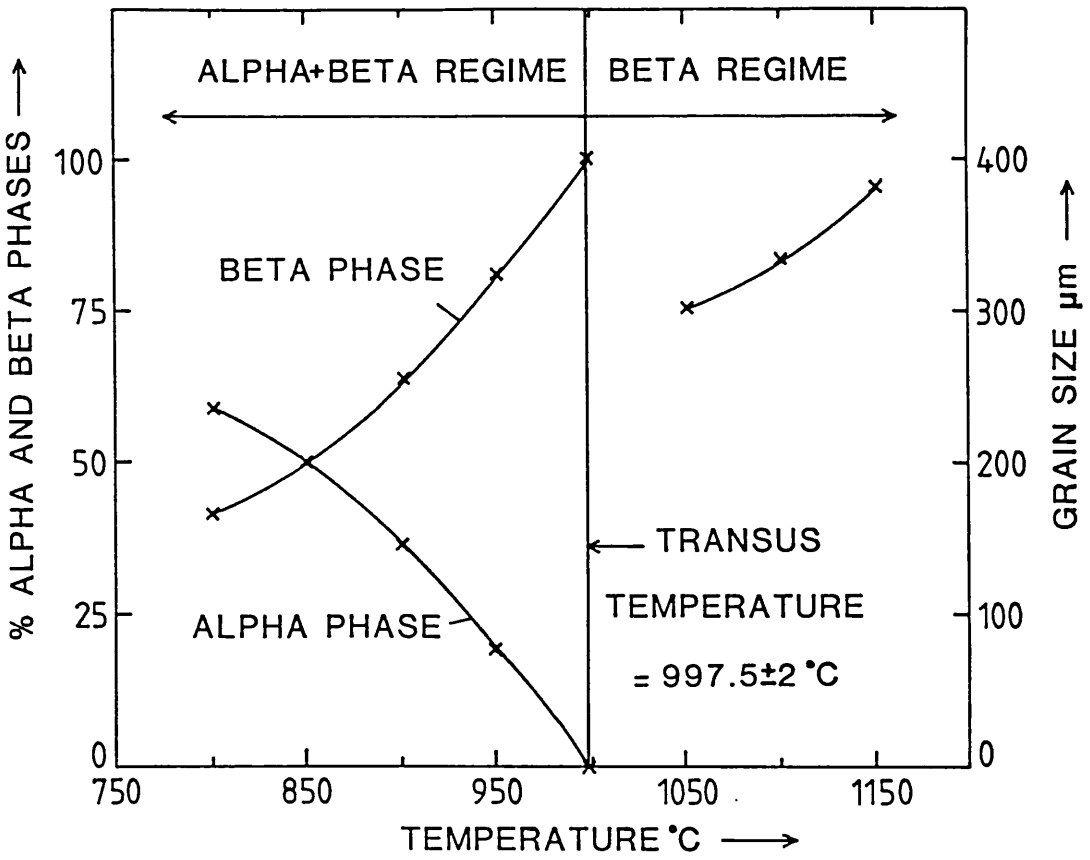

Figure 4.2 VARIATION IN THE PERCENTAGE OF ALPHA AND BETA PHASES AND BETA GRAIN SIZE WITH TEMPERATURE

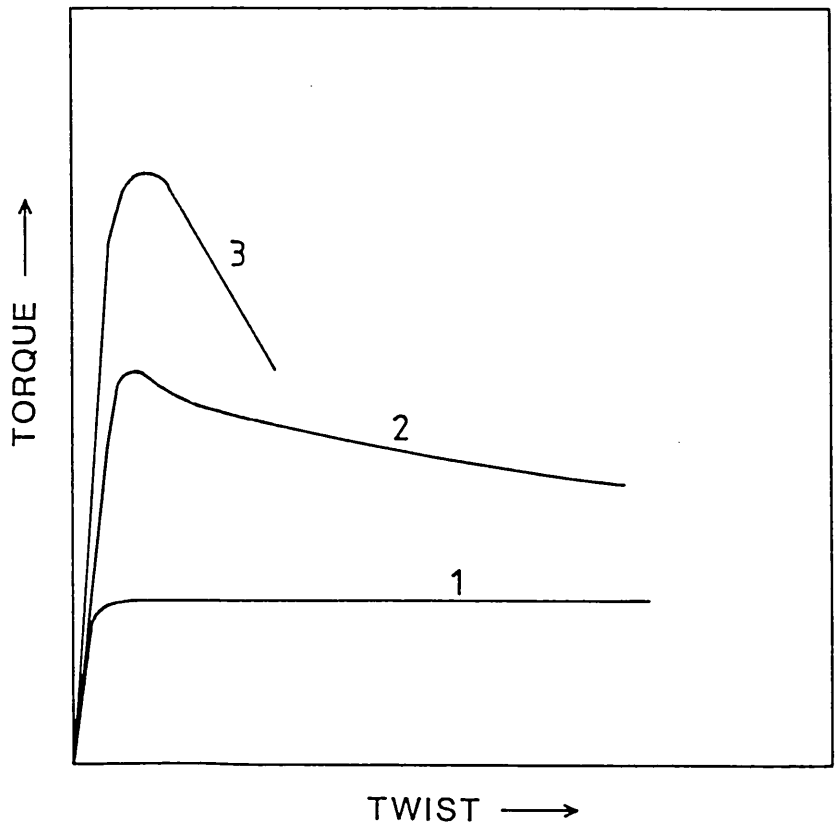

Figure 4.4 SCHEMATIC OF THE DIFFERENT TYPES OF TORQUE-TWIST CURVE PRODUCED ON TORSION TESTING.

Run Code	Initial Temperature °C	Twist Rate Rev/sec	LN Twist Rate	Peak Torque Nm	Strain To Peak	Torque E_H=0.75 Nm	Torque E_H=0.5 Nm
1	800	0.0125	-4.38	19.14	0.63	19.02	18.59
2	800	0.16	-1.83	34.83	0.69	34.58	34.33
3	800	1.30	0.26	44.57	0.94	43.7	43.14
4	800	4.46	1.49	49.18	0.96	48.89	47.74
5	800	7.44	2.01	51.19	1.16	50.90	49.75
6	850	0.0125	-4.38	11.68	0.52	11.60	11.42
7	850	0.16	-1.83	24.18	0.63	23.94	23.45
8	850	1.38	0.32	33.2	0.96	32.85	31.86
9	850	4.46	1.49	39.03	0.83	38.78	38.04
10	850	9.66	2.27	40.84	1.03	39.68	37.39
11	900	0.0125	-4.38	7.20	0.51	7.08	6.96
12	900	0.16	-1.83	14.82	0.59	14.46	14.10
13	900	1.45	0.37	21.75	0.90	21.57	21.26
14	900	4.61	1.53	27.05	0.96	26.68	25.81
15	900	8.27	2.11	29.76	0.98	28.90	26.43
16	950	0.0125	-4.38	3.74	0.82	3.67	3.56
17	950	0.16	-1.83	7.79	0.82	7.67	7.47
18	950	1.47	0.39	13.31	0.86	13.12	12.82
19	950	4.78	1.56	15.92	0.45	15.55	14.40
20	950	8.76	21.7	16.55	0.96	15.90	14.15

TABLE 4.3 TORSION RESULTS ALPHA+BETA REGIME

Run Code	Initial Temperature °C	Twist Rate Rev/sec	LN Twist Rate	Peak Torque Nm	Strain To Peak	Torque E_H=0.75	Torque E_H=0.5
21	1000	0.0125	-4.38	2.06	0.52	2.01	1.87
22	1000	0.16	-1.83	5.08	0.63	5.02	4.93
23	1000	1.50	0.41	8.70	0.57	8.62	8.44
24	1000	4.78	1.56	11.79	0.46	11.42	10.57
25	1000	9.24	2.22	13.73	0.685	13.06	11.30
26	1050	0.16	-1.83	4.19	0.45	4.15	3.93
27	1050	1.51	0.42	7.85	0.43	7.79	7.49
28	1050	4.74	1.56	9.56	0.48	9.18	8.73
29	1050	9.75	2.28	11.91	0.88	11.48	11.06
30	1100	0.16	-1.83	3.48	0.48	3.43	3.25
31	1100	1.54	0.43	6.11	0.44	5.96	5.75
32	1100	4.83	1.57	9.0	0.40	8.79	7.91
33	1100	8.67	2.16	10.27	0.61	9.96	8.75
34	1150	0.16	-1.83	3.02	0.42	2.98	2.88
35	1150	1.53	0.42	5.72	0.40	5.67	5.58
36	1150	4.87	1.54	7.85	0.38	7.79	7.47
37	1150	8.90	2.19	9.11	0.91	8.63	7.59

TABLE 4.4 TORSION RESULTS BETA REGIME

material is below the generally accepted hot working range, however since extrusions were carried out at this temperature it is included in the analysis.

4.2.3.1 NATURE OF TORQUE-TWIST CURVES

Typical torque-twist curves are shown in Figure 4.3.

Three general types of curve were produced as shown schematically in Figure 4.4.

1) At very low values of peak torque,i.e. high temperatures and low strain rates, a rapid rise to peak torque occurs, followed by a steady state regime in which the torque is essentially independent of the twist (curve 1). The initial rapid rise in torque corresponds to the interval of microstrain deformation. During this period the strain rate rises from zero to that applicable to the test. The decrease in slope of the loading curve indicates that this stage has been left and work hardening commences. As the rate of work hardening decreases, so the slope of the load curve decreases until the steady state is attained during which the rates of dislocation production and annihilation cancel out.

This type of curve is generally associated with high temperature restoration by dynamic recovery processes, and apart from very low strain rates at high temperatures in the alpha+beta regime, was confined to the beta regime.

2) At intermediate values of peak torque, i.e. all conditions in the beta regime except low strain rates, and intermediate strain rates at high temperatures in the alpha+beta regime, a gradual decrease in torque occurs after the peak (curve 2), the magnitude of the drop increasing with decreasing temperature and increasing strain rate. There are two possible explanations for this shape of curve.

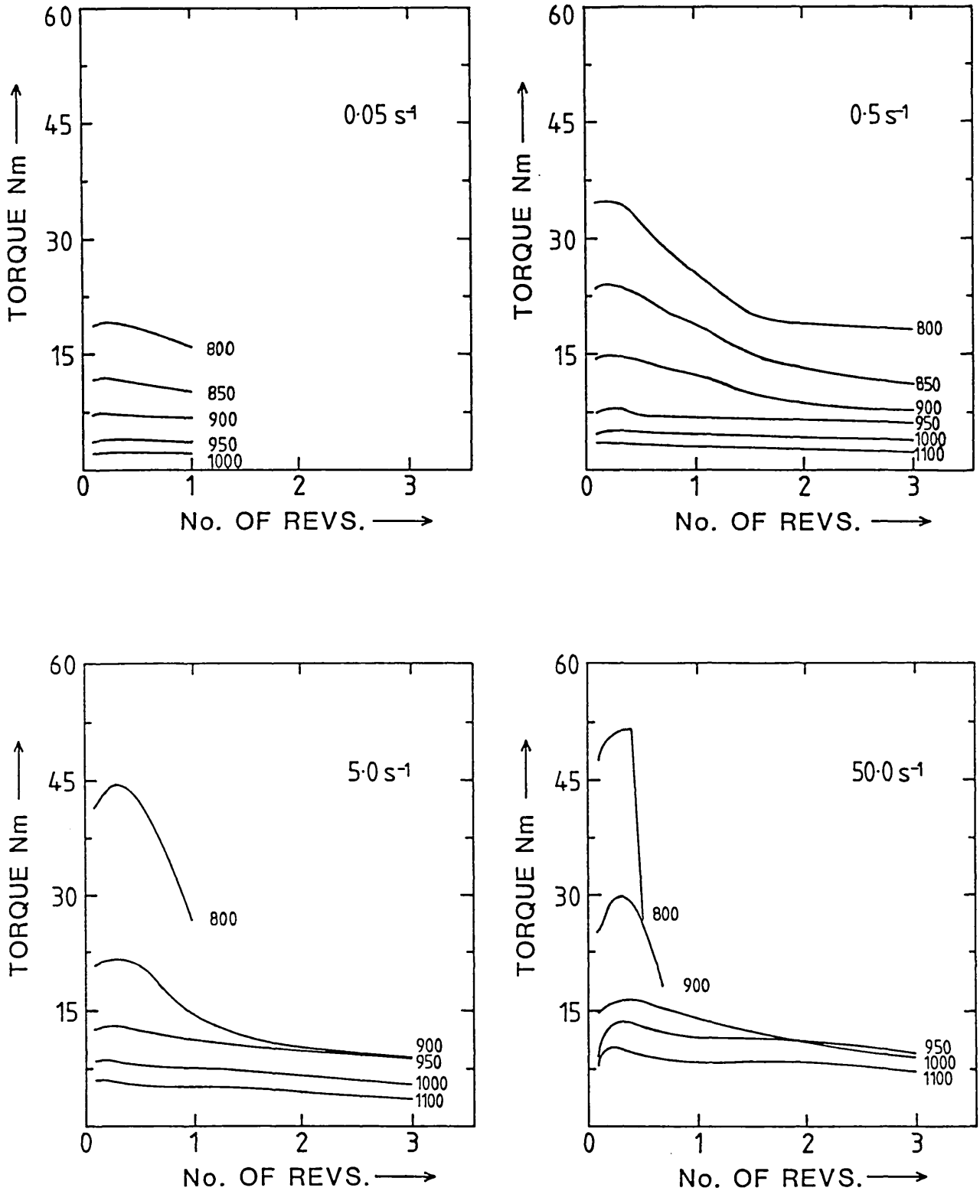

Figure 4.3 TYPICAL TORQUE-TWIST CURVES

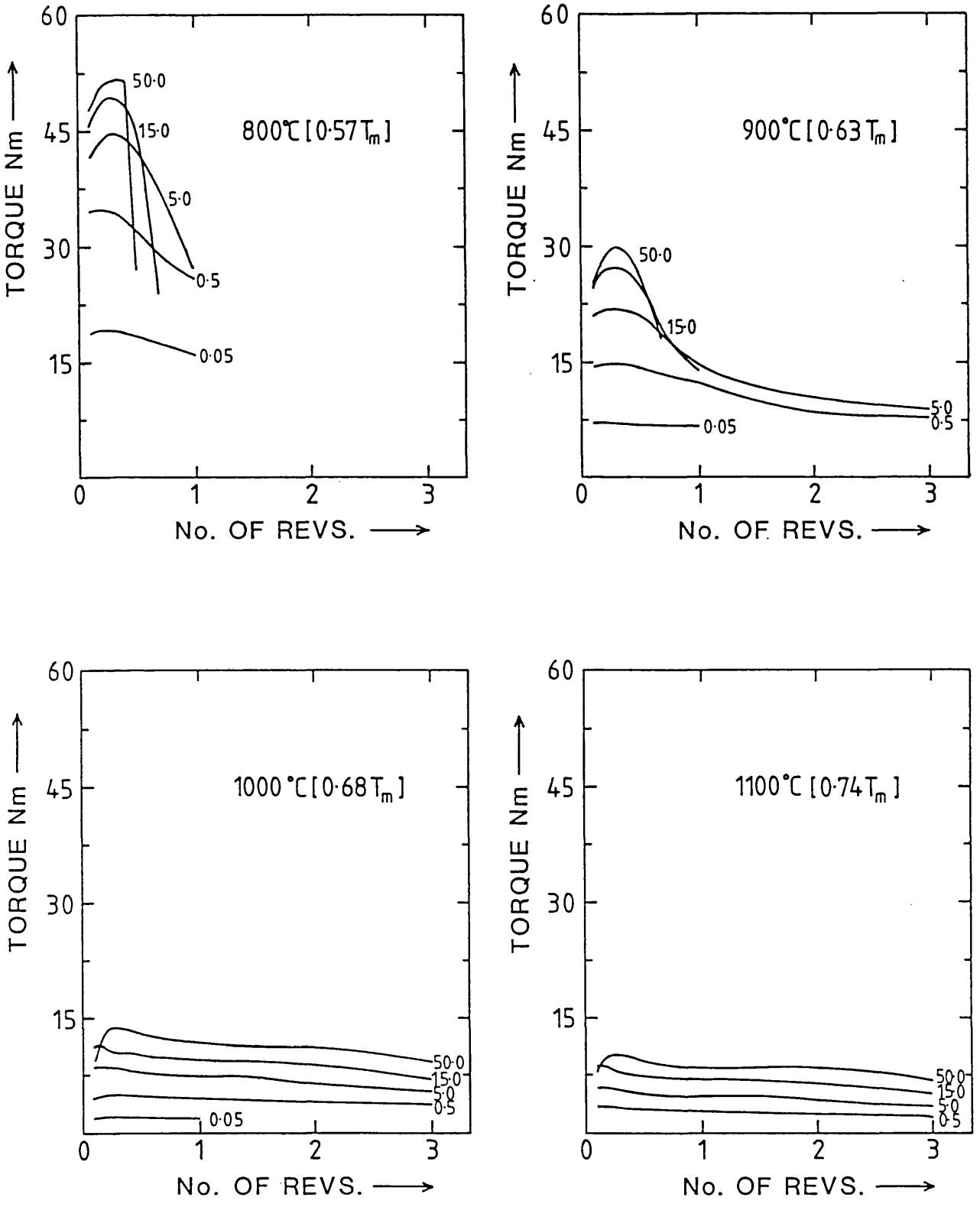

Figure 4.3 (Cont.) TYPICAL TORQUE-TWIST CURVES

(a) Dynamic recovery in the high temperature restoration mechanism, but the temperature rises occurring during testing cause a decrease in flow stress and an associated decrease in torque.

(b) Dynamic recrystallisation in the operative restoration mechanism, the recrystallisation resulting in softening and hence a decrease in torque after peak. Temperature rises may also contribute to the decrease in flow stress in this case also.

3) At high values of peak torque, exceeding approximately 20 Nm, i.e. low temperatures and high strain rates in the alpha+beta regime, there is a marked decrease in torque after the peak as a result of specimen fracture, the strain to fracture decreasing with decreasing temperature and increasing strain rate.

In terms of the starting microstructures it is apparent that the hot ductility of the alloy is substantially greater in the single phase beta regime compared to the two phase alpha+beta regime. This is because the alpha phase is h.c.p. and is relatively much less ductile than the b.c.c. beta phase at elevated temperatures. Decreasing the temperature in the alpha+beta regime results in an increase in the proportion of alpha phase and hence a decrease in hot ductility.

4.2.3.2 VARIATION OF PEAK TORQUE WITH TEMPERATURE

A plot of peak torque versus initial temperature is shown in Figure 4.5, for all twist rates. The temperature dependence of torque is much greater in the alpha+beta regime compared to the beta regime. Taking the relationship between the peak torque and temperature to be of the form $m = a + bT$ in both regimes, the results for a and b are given in Table 4.5, together with the ratio of the torque - temperature gradients in the two regimes.

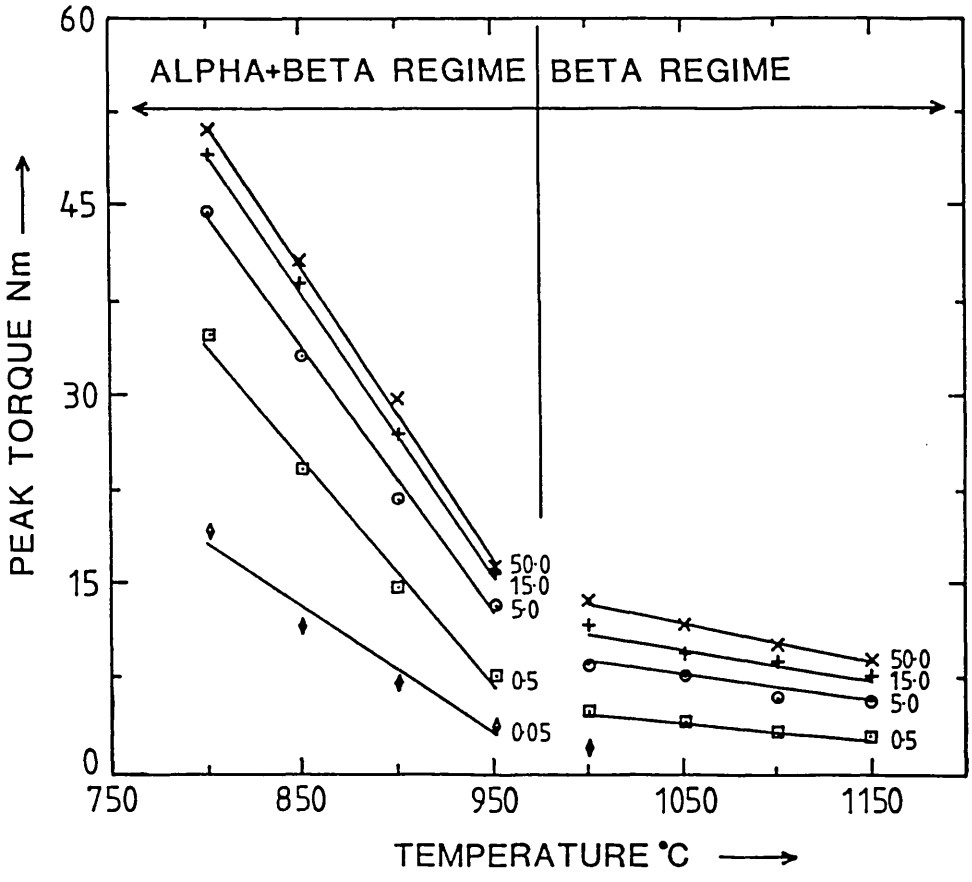

Figure 4.5 PEAK TORQUE VS. TEMPERATURE

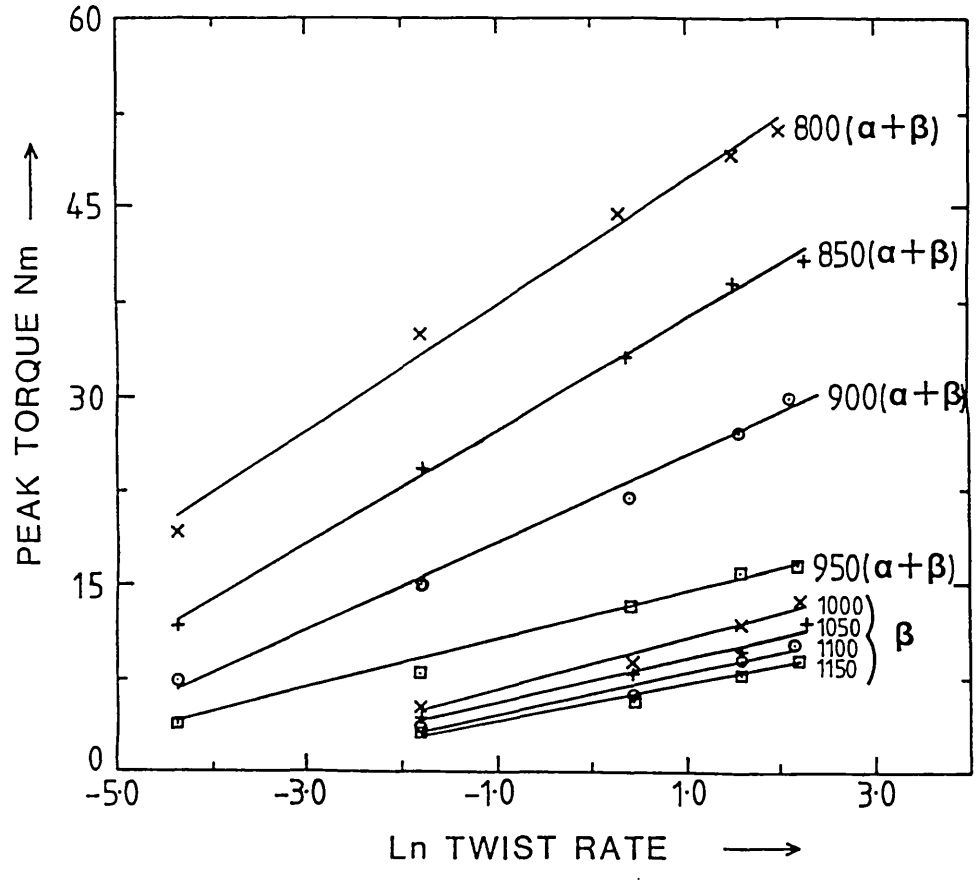

Figure 4.6 PEAK TORQUE VS. LN TWIST RATE

Twist Rate s^{-1}	Alpha+Beta Regime			Beta Regime			Ratio Of Slopes
	b	a	cc	b	a	cc	
0.05	-0.101	99.13	0.984	-	-	-	-
0.5	-0.181	178.75	0.996	-0.014	18.76	0.990	12.93
5.0	-0.210	212.36	0.998	-0.021	30.06	0.974	10.0
15.0	-0.224	228.38	0.999	-0.025	36.17	0.966	8.96
50.0	-0.23	235.84	0.998	-0.031	44.58	0.995	7.42

TABLE 4.5 PEAK TORQUE-TEMPERATURE RELATIONSHIPS

Temperature °C	a	b	cc
800	42.22	4.976	0.995
850	31.68	4.451	0.998
900	21.63	3.433	0.995
950	12.48	1.926	0.988

TABLE 4.6 PEAK TORQUE-ln TWIST RATE RELATIONSHIPS IN THE ALPHA+BETA REGIME

Temperature °C	a	b	cc
1000	8.58	2.10	0.989
1050	7.29	1.791	0.990
1100	6.23	1.693	0.981
1150	5.56	1.499	0.992

TABLE 4.7 PEAK TORQUE-ln TWIST RATE RELATIONSHIPS IN THE BETA REGIME

Except at the lowest strain rate, an excellent linear fit occurs between the temperature and torque in the alpha+beta regime, the slopes being approximately constant for different strain rates. In the beta regime a poorer correlation exists for a linear fit to the data.

There is a marked decrease in peak torque with increasing temperature in the alpha+beta regime, but only a small decrease with increasing temperature in the beta regime, as indicated by the ratio of the torque temperature gradients in the two regimes. A decrease in slope of an approximate order of magnitude occurs on moving from the alpha+beta to the beta regime. Thus increasing the proportion of alpha phase in the alpha+beta regime results in a marked increase in flow stress, while increasing the beta grain size in the beta regime leads to only a relatively small decrease in flow stress.

These results highlight two important features of Ti-6Al-4V fabrication. Working in the alpha+beta regime results in very much higher flow stresses, and only a small benefit with regard to flow stress can be obtained by increasing the temperature within the beta phase field.

4.2.3.3 VARIATION IN PEAK TORQUE WITH TWIST RATE

A plot of peak torque versus ln twist rate is shown in Figure 4.6. Taking the relationship between the peak torque and twist rate to be of the form $m = a + b \ln \dot{\theta}$, the results are shown in Tables 4.6 and 4.7.

A marked increase in torque with increasing strain rate occurs in the alpha+beta regime, the strain rate sensitivity decreasing with increasing temperature as the proportion of alpha phase decreases. In the beta regime the strain rate sensitivity is lower and decreases with increasing temperature as the beta grain size increases.

This highlights another important feature of Ti-6Al-4V fabrication. For a similar increase in strain rate, a larger proportionate increase in flow stress occurs when working in the alpha+beta regime compared to the beta regime.

Thus the torsion test has revealed very useful information on the hot working behaviour of Ti-6Al-4V, particularly in relation to the relative merits of working in the alpha+beta and beta regimes.

4.2.3.4 DERIVATION OF THE CONSTANTS IN THE HOT WORKING EQUATION

It is apparent from the previous section that the alloy exhibits markedly different behaviour depending on whether it is worked in the two phase alpha+beta regime or the single phase beta regime. Thus the splitting up of the data into these two regimes would appear to be justified for the purposes of evaluation of the hot working constants, as it is likely that the operative high temperature restoration mechanisms are markedly different in the two regimes.

Following the analysis described in section 2.2.2, the hot working constants were obtained for the alloy, in the alpha+beta regime over the temperature range of 800°C - 950°C and in the beta regime over the temperature range of 1000°C - 1150°C, at homologous strains of 0.5, 0.75 and 1.0. The results are given in Table 4.8, with no allowance having been made for temperature rises during testing.

4.2.3.4.1 EVALUATION OF THE TEMPERATURE RISE DURING TESTING

The temperature rise during testing was evaluated using the analysis described in section 2.2.2, the results being given in Table 4.9 and 4.10. The predicted temperature rises occurring in the beta regime are less than 1% of the test temperature and can be neglected. In the alpha+beta regime, however, the temperature rises are substantial, the temperature rise increasing with decreasing temperature and increasing twist rate. The new values of temperature were substituted back into

	Alpha+Beta Regime			Beta Regime		
	$E_H = 0.5$	$E_H = 0.75$	$E_H = 1.0$	$E_H = 0.5$	$E_H = 0.75$	$E_H = 1.0$
Q J/mole	556,306	530,263	521,697	195,924	176,022	169,962
n	3.73	3.64	3.52	2.58	3.05	3.25
α (m^2/MN)	8.64×10^{-3}	8.44×10^{-3}	8.63×10^{-3}	3.32×10^{-2}	1.918×10^{-2}	1.41×10^{-2}
A (s^{-1})	3.313×10^{24}	2.015×10^{23}	7.487×10^{22}	1.188×10^{7}	1.352×10^{7}	3.982×10^{7}
cc	0.986	0.989	0.990	0.987	0.993	0.995

TABLE 4.8 THE HOT WORKING CONSTANTS IN THE ALPHA+BETA AND BETA REGIMES AT HOMOLOGOUS STRAINS OF 0.5, 0.75 and 1.0 - NO TEMPERATURE RISE

Run Code	Initial Temperature °C	Twist Rate Rev/sec	Strain To Peak	Temperature Rise °C			Temperature At Peak Torque °C
				$\frac{\sigma}{\sigma_H}$ =0.5	$\frac{\sigma}{\sigma_H}$ =0.75	$\frac{\sigma}{\sigma_H}$ =1.0	
1	800	0.0125	0.63	0	0	0	800.0
2	800	0.16	0.69	8.9	10.9	12.2	812.2
3	800	1.3	0.94	22.8	31.0	38.0	838.0
4	800	4.46	0.96	29.7	41.2	52.0	852.0
5	800	7.44	1.16	38.0	52.6	65.6	865.6
6	850	0.0125	0.52	0	0	0	850.0
7	850	0.16	0.63	5.2	6.6	7.5	857.5
8	850	1.38	0.96	16.4	22.4	28.1	878.1
9	850	4.46	0.83	18.7	26.8	33.9	883.9
10	850	9.66	1.03	26.1	36.9	46.9	896.9
11	900	0.0125	0.82	0	0	0	900.0
12	900	0.16	0.82	2.9	3.7	4.3	904.3
13	900	1.45	0.86	10.3	14.3	18.0	918.0
14	900	4.61	0.45	14.8	21.1	27.1	927.1
15	900	8.27	0.96	17.6	24.6	31.7	931.7
16	950	0.0125	0.82	0	0	0	950.0
17	950	0.16	0.82	2.0	2.4	2.7	952.7
18	950	1.47	0.86	6.0	8.6	10.9	960.9
19	950	4.61	0.45	4.8	7.0	9.2	959.2
20	950	8.76	0.96	11.5	16.5	21.3	971.3

TABLE 4.9 TORSION TEMPERATURE RISES IN ALPHA+BETA REGIME

Run Code	Initial Temperature °C	Twist Rate Rev/sec	Strain To Peak	Temperature Rise °C			Temperature At Peak Torque
				$\frac{\sigma}{\sigma_H} = 0.5$	$\frac{\sigma}{\sigma_H} = 0.75$	$\frac{\sigma}{\sigma_H} = 1.0$	
21	1000	0.0125	0.52	0	0	0	1000.0
22	1000	0.16	0.63	1.0	1.3	1.5	1001.5
23	1000	1.5	0.57	2.7	3.9	5.1	1005.1
24	1000	4.78	0.46	3.1	4.6	6.2	1006.2
25	1000	9.24	0.69	5.1	7.8	10.6	1010.6
26	1050	0.16	0.45	0.7	0.9	1.0	1051.0
27	1050	1.51	0.43	1.8	2.7	3.4	1053.4
28	1050	4.74	0.48	2.7	4.1	5.5	1055.5
29	1050	9.75	0.88	5.8	8.8	11.9	1061.9
30	1100	0.16	0.48	0.5	0.7	0.8	1100.8
31	1100	1.54	0.44	1.6	2.3	3.0	1103.0
32	1100	4.83	0.4	2.0	3.0	4.1	1104.1
33	1100	8.67	0.61	3.5	5.3	7.1	1107.1
34	1150	0.16	0.42	0.4	0.5	0.6	1151.0
35	1150	1.53	0.4	1.2	1.8	2.3	1152.0
36	1150	4.87	0.38	1.7	2.6	3.4	1153.0
37	1150	8.9	0.91	4.5	6.8	9.1	1159.0

TABLE 4.10 TORSION TEMPERATURE RISES IN BETA REGIME

the minimisation routine to reevaluate the hot working constants. The data, however, failed to reminimise, suggesting that the predicted temperature rises are unreasonable. The model has been used successfully in the prediction of temperature rises occurring during the torsion testing of aluminium alloys[72,73,76-78], however the torques produced in these cases are substantially lower (approximately half at 0.6 Tm). The problem with the generation of such high torques is that the torsion machine cannot produce the desired test twist rate rapidly enough, and there is an acceleration in the initial stages of the test. This precludes accurate measurement of the strain rate and strain to peak, so that the predicted temperature rises are unreliable, and is the most likely cause for the failure of the data to reminimise. For future torsion programmes it would be sensible to employ a smaller test piece in the alpha+beta regime, thus reducing the values of torque required.

Thus, while the values of the hot working constants in the beta regime are accurate, in the alpha+beta regime they are subject to error. It is considered unlikely, however, that correction of the alpha+beta regime constants for temperature rise will substantially alter the values, and certainly for the purposes of comparison of the behaviour of the alloy in the two regimes they provide sensible results.

4.2.3.5 SIGNIFICANCE OF THE HOT WORKING CONSTANTS - STRUCTURAL CHANGES DURING TORSION TESTING

The markedly different behaviour exhibited by Ti-6Al-4V in the alpha+beta and beta regimes is reflected in the markedly different values of the hot working constants (Table 4.8). The value of Q represents the activation energy of the high temperature restoration mechanism and is a factor of three times greater in the alpha+beta regime, indicating the probability of different dynamic softening processes operating in the two regimes.

Both optical and electron microscopy studies of the torsion structures were carried out in an effort to establish the dynamic restoration mechanisms responsible for these values of activation energy.

The torsion tests were normally continued for several revolutions, producing surface strains of the order of 10-20, except for very low strain rates and occasions where fracture of the specimen occurred. Hence the structures produced, particularly at low temperatures and high strain rates in the alpha+beta regime, will be markedly influenced by the temperature rises occurring during torsion. This makes structural interpretation difficult, and clearly for a more meaningful structural analysis the structure at the peak torque will have to be looked at.

Nevertheless, a substantial amount of useful information was obtained from the structural studies, which gave good indications of the dynamic restoration mechanisms operative in the two regimes.

Longitudinal sections were taken through the test piece. The peripheral structure was concentrated on, the strain and strain rate being a maximum here.

Considering first the beta regime. The starting structure consists of coarse grained single phase b.c.c. beta, with the beta grain size increasing with increasing temperature (section 4.2.2). Typical torsion structures produced at both ends of the temperature and strain rate range are shown in Figure 4.7.

The specimens were water quenched immediately upon cessation of the test, with the result that in all cases the beta transformed martensitically (Figure 4.7(e) and (f)). The martensite is in the form of acicular plates interspersed with very much finer secondary plates. The martensite transformation wipes out any deformation substructure, however the boundaries of the deformed beta grains are retained by quenching, so that it is possible to discern in the optical micrographs the extent to

(a)

1000°C 0.05 s^{-1}

(b)

1150°C 0.05 s^{-1}

FIGURE 4.7

TORSION STRUCTURES PRODUCED ON TESTING

IN THE BETA REGIME

(c)

1000°C 50.0 s^{-1}

(d)

1150°C 50.0 s^{-1}

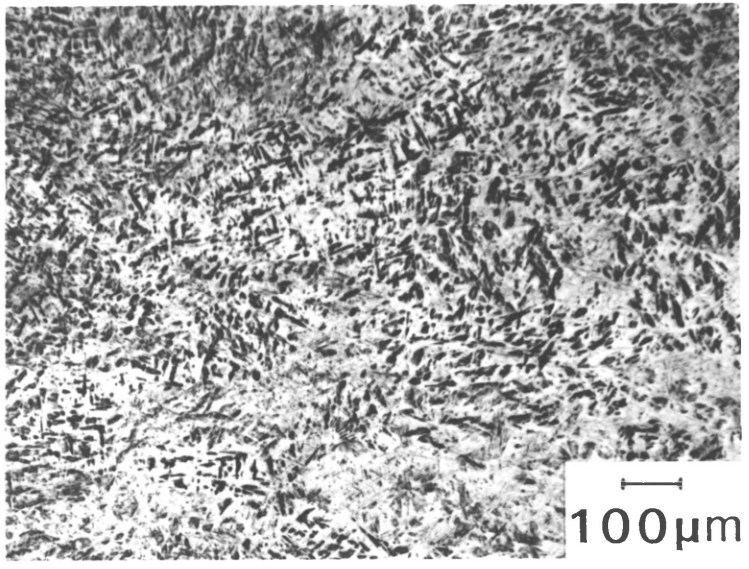
100μm

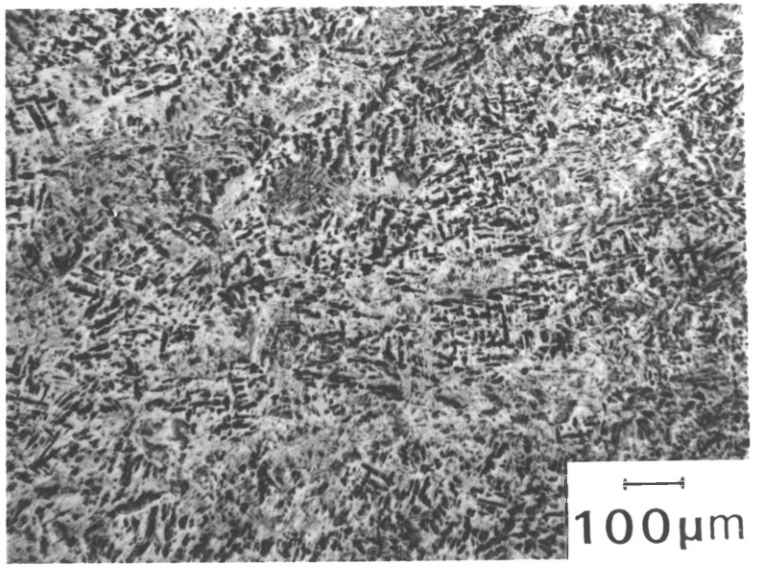
100μm

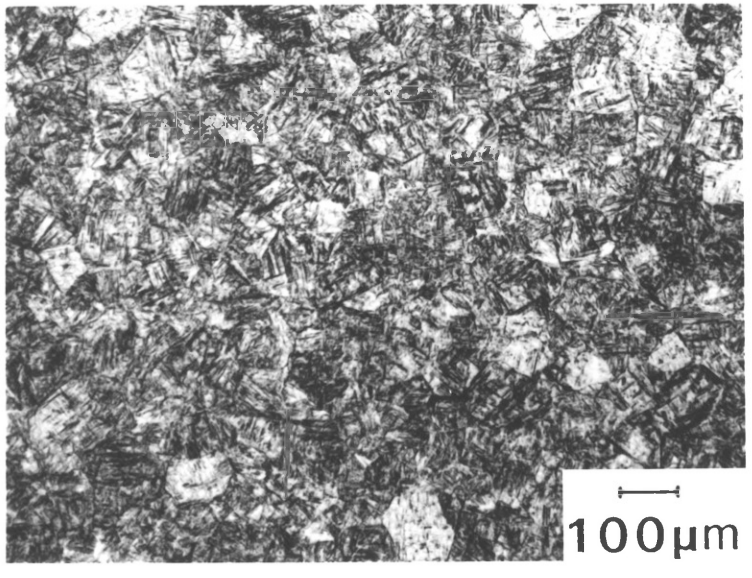
100μm

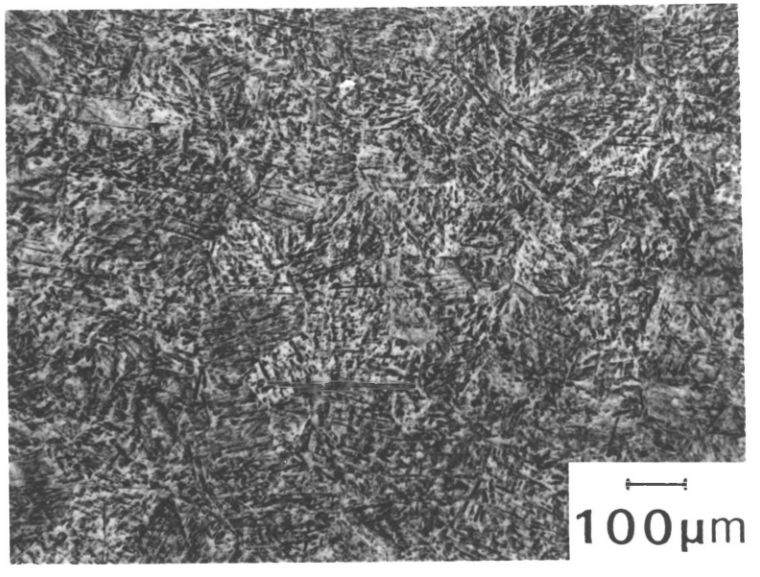
100μm

(e)

ACICULAR MARTENSITE PLATES FORMED

ON QUENCHING FROM THE BETA REGIME

FIGURE 4.7 (CONTINUED)

(f)

HIGHER MAGNIFICATION OF (e)

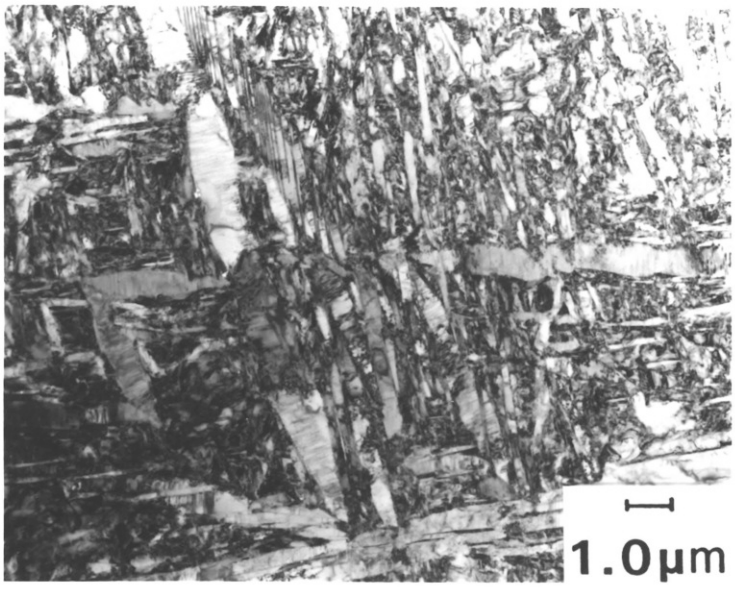
1.0μm

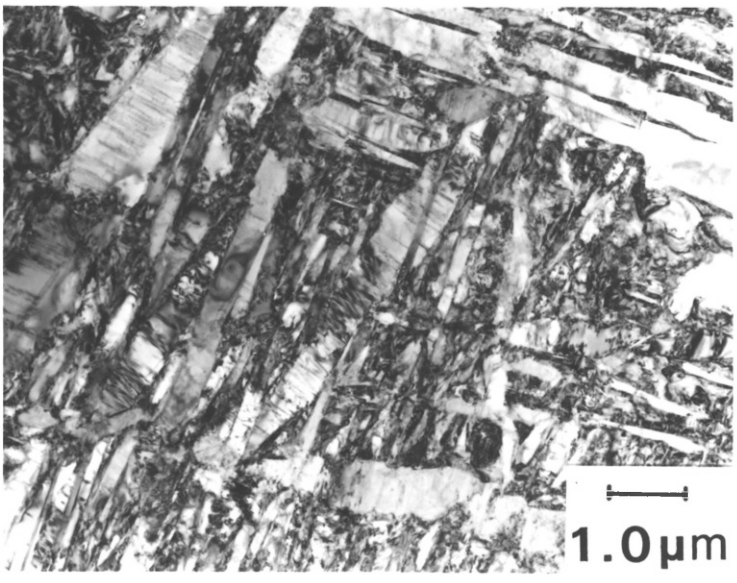
1.0μm

which the structure has recrystallised. At high strain rates the structure is fully recrystallised (Figures 4.7(c) and (d)), however at low strain rates, the periphery is completely unrecrystallised (Figures 4.7(a) and (b)). Comparison with Figure 4.1 highlights the extent to which the structure has been refined by deformation.

The value of activation energy for hot working in the beta regime at peak torque is 169,962 J/mole. This is not too dissimilar to the activation energy for self-diffusion in the beta phase of super-purity titanium of 152,818 (section 1.2.4.3). The difference in values may well be due to the presence of aluminium and vanadium in solid solution in the beta phase of Ti-6Al-4V. The similarity of the values suggests that dynamic recovery is the operative dynamic restoration mechanism in the beta phase. This is certainly the case at low strain rates, however at high strain rates a fully recrystallised structure is produced at the periphery, which may well have occurred as a result of dynamic recrystallisation. Equally, however, increasing the strain rate increases the driving force for static recrystallisation, so that dynamic recovery followed by rapid static recrystallisation may have occurred.

The torque-twist curves at high strain rate exhibited a reduction in torque after peak (curve 2, Figure 4.4). The predicted temperature rises in the beta regime are very small (Table 4.10), so that it is feasible that the softening is due to dynamic recrystallisation. The phase transformations occurring during cooling preclude the conclusive determination of this argument.

Coyne[27] in his work on the beta forging of Ti-6Al-4V observed an unrecrystallised structure on finish forging in the beta regime, which is further evidence that in relatively low strain rate operations dynamic recovery is the only operative high temperature restoration mechanism.

Considering now the alpha+beta regime. The starting structures for torsion consist of two phase primary alpha+beta, with the proportion of alpha phase decreasing with increasing temperature (section 4.2.2).

The activation energy obtained from torsion testing is 521,697 J/mole, which is approximately 3 x greater than the activation energy for self-diffusion in the alpha and beta phases of super purity titanium. This would suggest that an alternative mechanism to dynamic recovery is operational in the alpha+beta regime, possibly dynamic recrystallisation.

Sastry et al in their work on the hot compression testing of Ti-6Al-4V in the alpha+beta regime obtained values of 470,000 J/mole and 572,000 J/mole at flow stresses of 200 MPa and 100 MPa respectively (section 1.2.4.3). The average of these values is 521,000 which is in excellent agreement with the values obtained in this work. Their electron microscopy studies revealed both dynamic recovery and dynamic recrystallisation as evidenced by hexagonal networks of dislocations within the alpha phase and the formation of small equiaxed alpha.

Correlating all the data, on the hot deformation of Ti-6Al-4V, Bryant also observed high values of activation energy (section 1.2.4.3). He was able to split the data into two regimes, described as "low temperature" mechanism and "high temperature" mechanism, for which the former had an activation energy of 355,878 and the latter 711,756 J/mole. He was not able to identify a mechanism for the low temperature deformation activation energy, but suggested that the high temperature mechanism might be dynamic recrystallisation. No structural studies were carried out to verify these claims, and there would not appear to be any explanation for this change in activation energy. The average of these values in the two regimes is 533,817 J/mole which again is in good agreement with the value obtained in this work.

Typical optical structures are shown in Figure 4.8, the micrographs being taken at the specimen periphery. It is apparent that the structures are effectively recrystallised at all temperatures and strain rates. Substantial temperature rises occurred during testing, particularly at high strain rates, as was evidenced by a reduction in the proportion of alpha phase compared to the starting structure. Comparison of the deformed structures with the starting structures revealed that the deformation had produced a reduction in the alpha and beta grain sizes, the refinement increasing with increasing strain rate.

(a)

800°C 0.05 s^{-1}

(b)

800°C 50.0 s^{-1}

FIGURE 4.8

TORSION STRUCTURES PRODUCED ON TESTING IN THE

ALPHA+BETA REGIME - OPTICAL MICROSCOPY

(c)

900°C 0.05 s^{-1}

(d)

900°C 50.0 s^{-1}

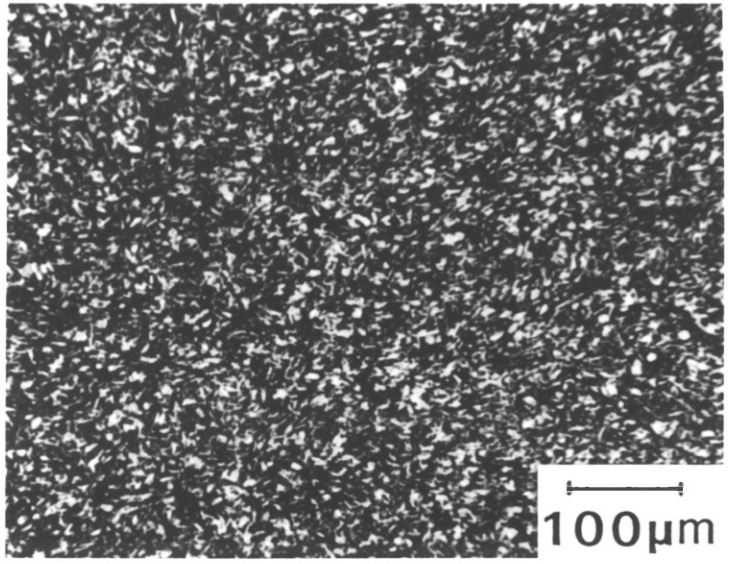
100μm

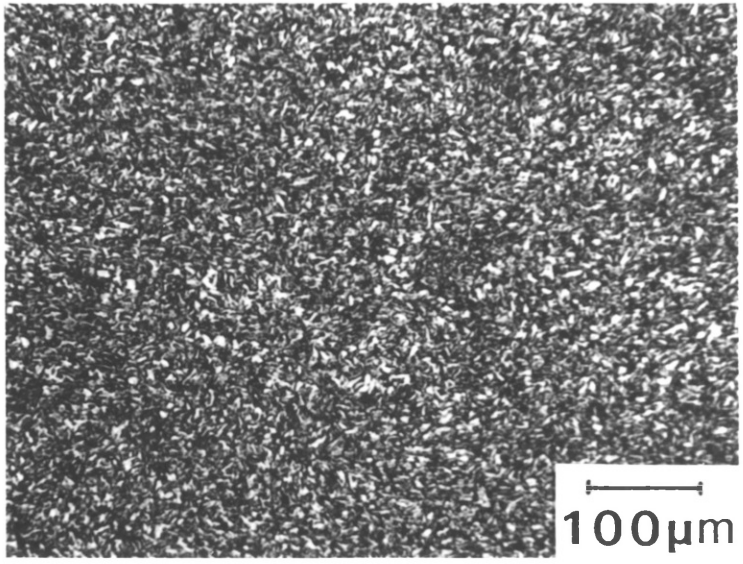
100μm

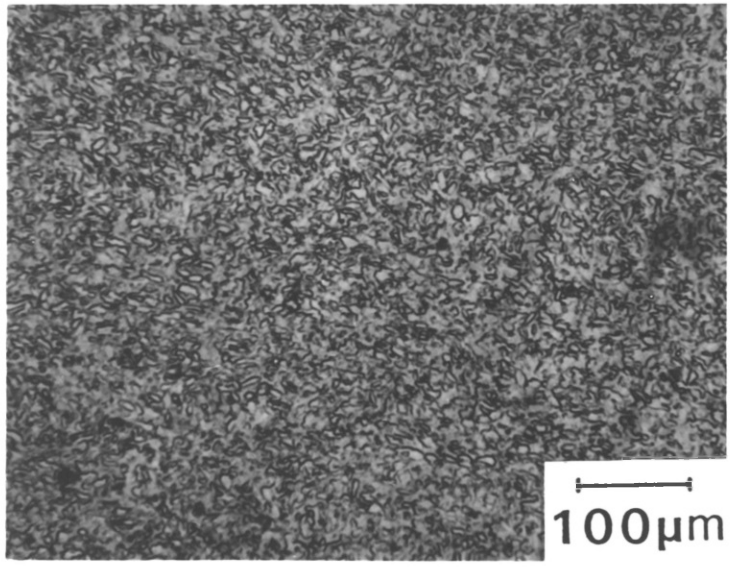
100μm

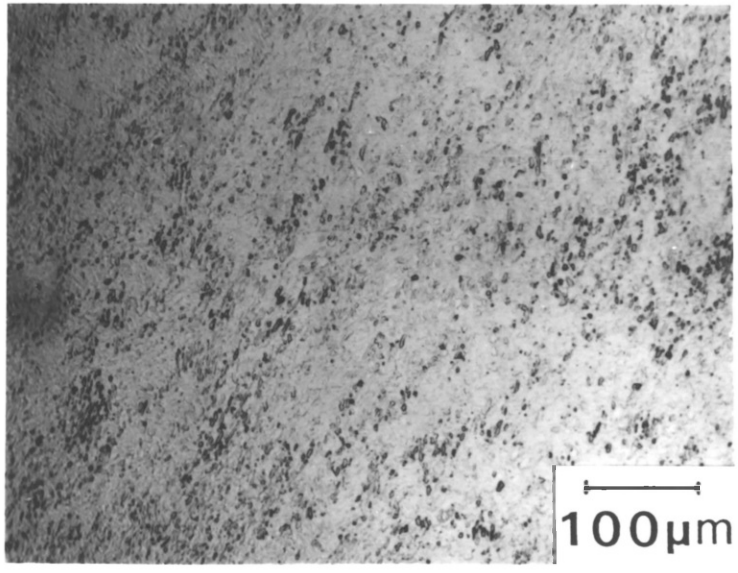
100μm

The recrystallised structure produced on torsion testing could have arisen from either dynamic recovery followed by static recrystallisation or dynamic recrystallisation followed by static or metadynamic recrystallisation. As will be discussed in a later section, water quenching of the alpha+beta extruded structures resulted in the retainment of a dynamically recovered structure, so equally if dynamic recovery had occurred during torsion, it would be expected that the recovered structure would be retained by quenching.

Thus the occurrence of a recrystallised structure is conclusive evidence that dynamic recrystallisation has occurred during torsion, which is in agreement with the high value of activation energy obtained and the limited observations of other workers.

Moving on now to a discussion of the electron microscopy structures (Figure 4.9). Since straining of the material continues during nucleation and growth of the dynamically recrystallised grains, the grains deform as they grow, and hence if post-deformation structural changes could be avoided the centre of the dynamically recrystallised grains would contain a dislocation substructure, with different grains being at different stages of deformation.

However, dynamically recrystallised structures are unstable and the dynamically recrystallised nuclei will continue to grow immediately upon cessation of the test, with the grain boundaries sweeping regions free of dislocations. This process is known as metadynamic recrystallisation and although its progress will be limited by water quenching, significant modification of the dynamically recrystallised structure will occur.

These structural modifications have to be borne in mind when interpreting the electron micrographs.

The beta phase, as was observed above the transus, undergoes a martensitic transformation on quenching which wipes out any deformation substructure, and hence evidence of the operative dynamic restoration mechanism can only be obtained from the alpha phase.

(a) 850°C 0.05 s^{-1}

(c) 900°C 50.0 s^{-1}

(e) 950°C 0.05 s^{-1}

FIGURE 4.9

TORSION STRUCTURES PRODUCED ON TESTING IN THE ALPHA+BETA REGIME - ELECTRON MICROSCOPY

(b) 850°C 50.0 s^{-1}

(d) 900°C 50.0 s^{-1}

(f) 950°C 0.05 s^{-1}

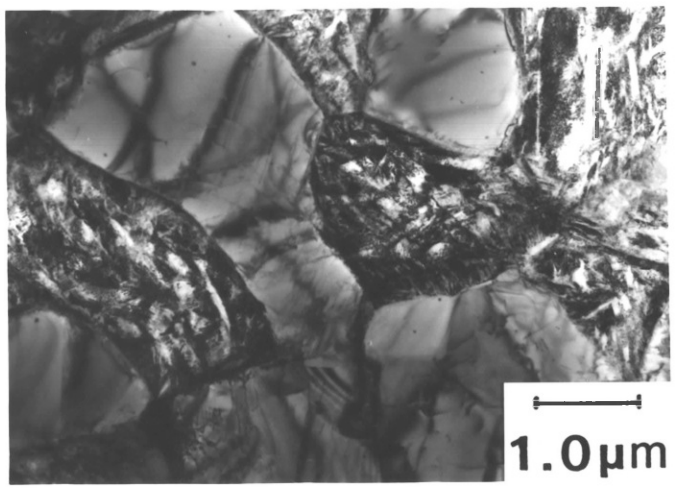
1.0μm

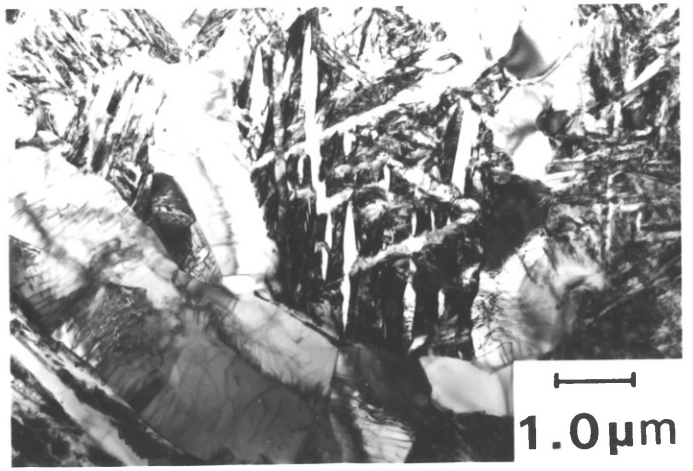
1.0μm

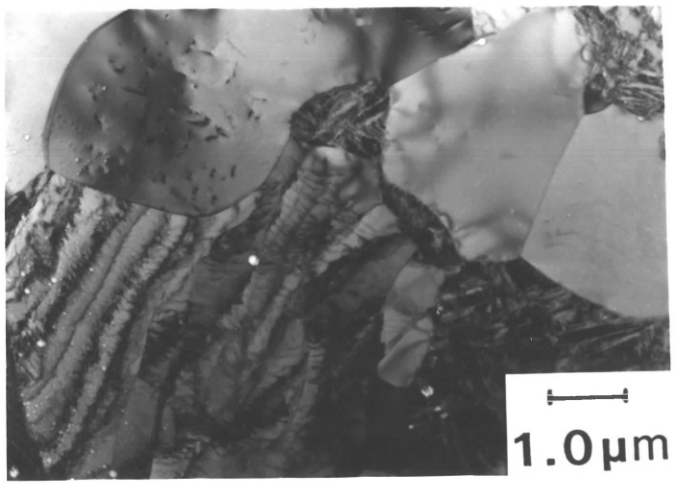
1.0μm

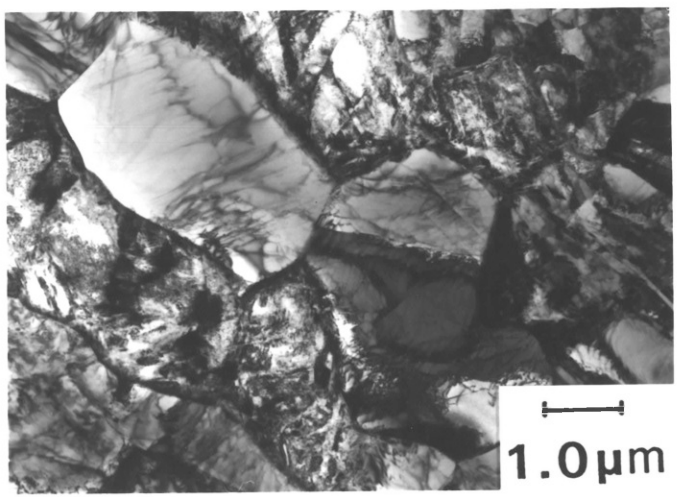
1.0μm

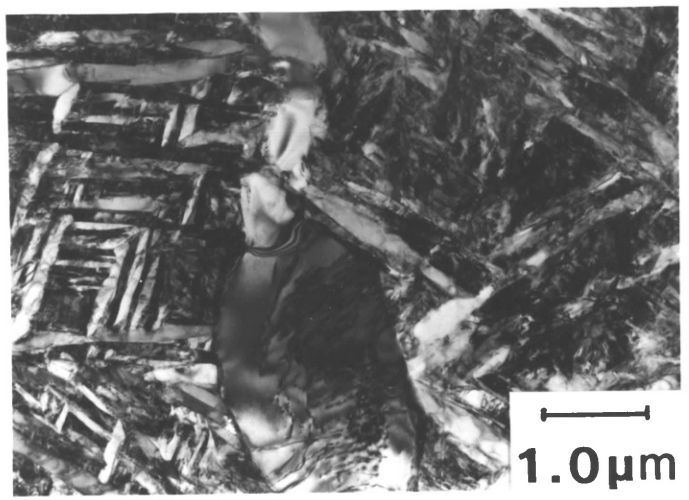
1.0μm

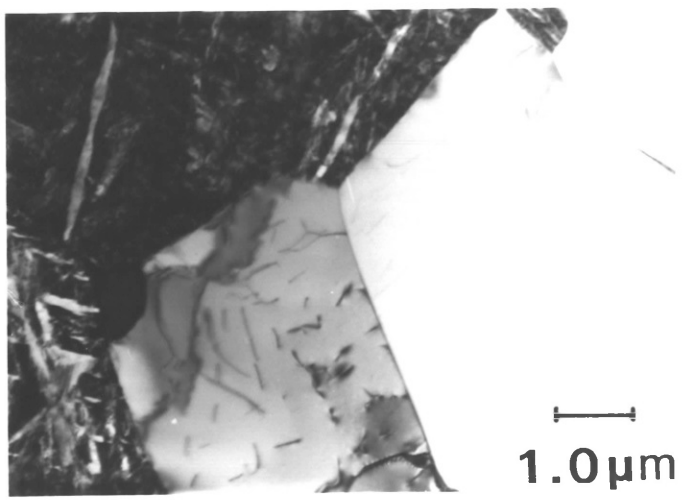
1.0μm

(g)

800°C 5.0 s^{-1}

(i)

900°C 50.0 s^{-1}

(k)

800°C 50.0 s^{-1}

FIGURE 4.9 (CONTINUED)

(h)

850°C 0.05 s^{-1}

(j)

850°C 0.05 s^{-1}

(l)

800°C 50.0 s^{-1}

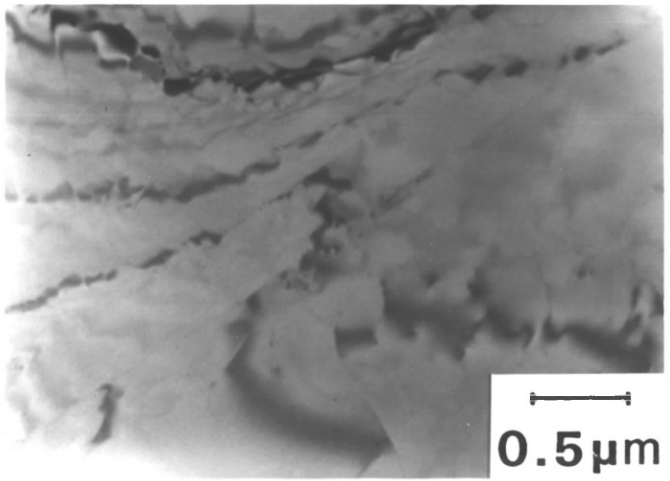
0.5μm

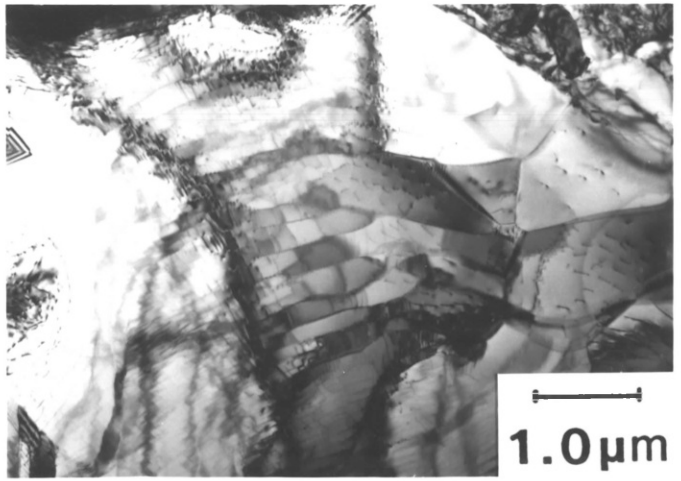
1.0μm

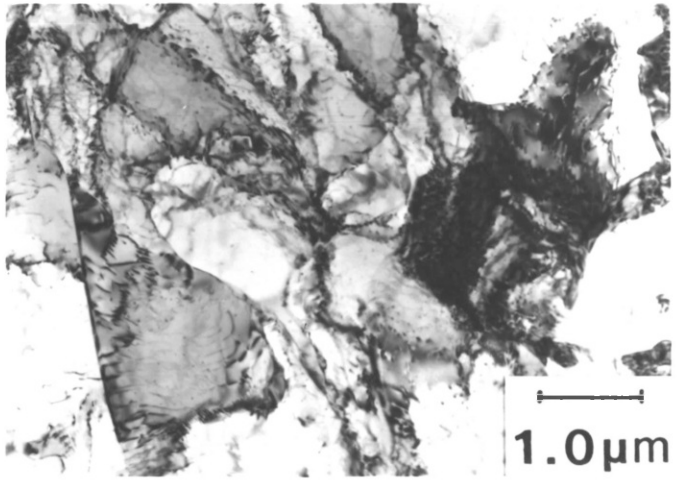
1.0μm

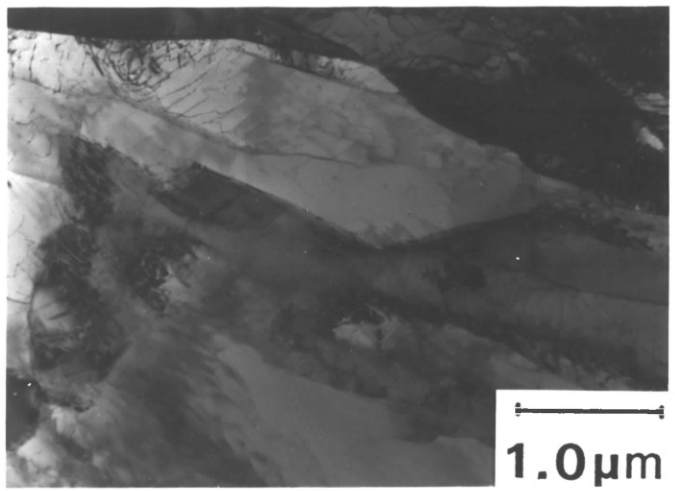
1.0μm

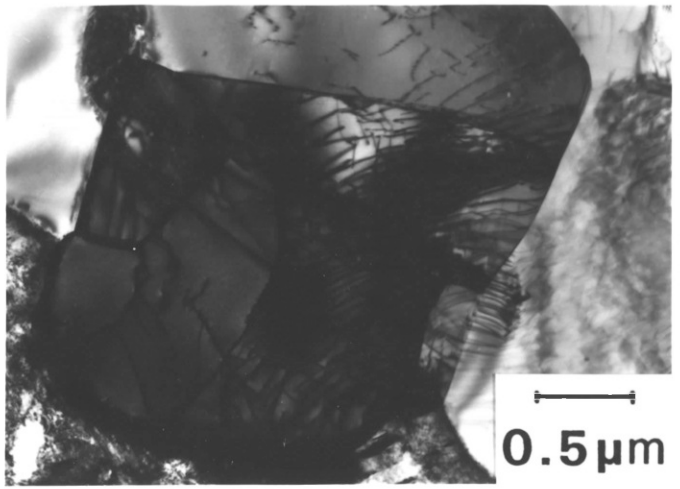
0.5μm

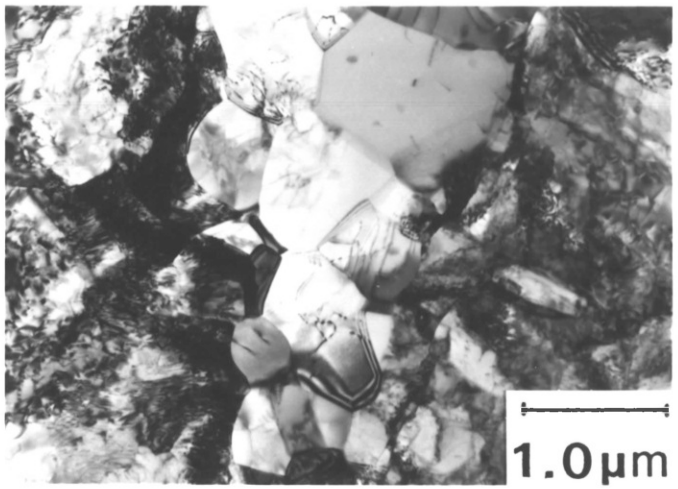
1.0μm

Electron microscopy studies revealed a large gradation in alpha grain size and dislocation substructure within the alpha phase for each test condition. This is illustrated in the micrographs (Figure 4.9) by comparison of Figures (a), (h) and (j), all for T = 850°C, $\dot{\gamma} = 0.05\ s^{-1}$. Figure (a) shows an area of very small equiaxed alpha grains, while Figure (h) shows a very large alpha grain and Figure (j) an alpha grain containing a dislocation substructure. Other examples of the variation in structure observed for the same test condition are illustrated by comparison of Figures (c), (d) and (i) for T = 900°C $\dot{\gamma} = 50.0\ s^{-1}$ and Figures (e) and (f) for T = 950°C $\dot{\gamma} = 0.05\ s^{-1}$.

This variation in structure for a given test condition is to be expected as metadynamic recrystallisation will have proceeded to different extents depending on what stage dynamic recrystallisation had reached in a particular area.

A large number of the alpha grains contained a dislocation substructure, with particularly impressive examples being shown in Figures (i) and (j). In Figure (i) a subgrain network has formed in the interior of the grain while in (j) a tangled dislocation network is apparent. At first sight this would appear to be classical evidence of dynamic recrystallisation with the dislocation substructure having formed as a result of deformation of a dynamically recrystallised grain during growth. Figure (i) could represent a relatively early stage of deformation of a dynamically recrystallised grain with the dislocations having rearranged themselves into a subgrain network as a result of dynamic recovery. Figure (j) could represent a relatively advanced stage of deformation with a high density of dislocations having built up, and the grain may well be on the point of renucleating a dynamically recrystallised grain. It would therefore appear that metadynamic recrystallisation has not served to remove all the evidence of dynamic recrystallisation.

Care must be taken, however, in the interpretation of dislocation substructures within alpha grains, as substructure is sometimes observed even in undeformed specimens of Ti-6Al-4V[89]. Obviously, however, the evidence presented of a dislocation substructure within the alpha phase fits in well with the overall picture of dynamic recrystallisation observed during torsion testing.

Specimens tested at 800°C at high strain rates fractured at very low strains (Figure 4.3). This is not unexpected as 800°C (= 0.57 Tm) is below the generally accepted hot working range (= 0.6 Tm). The electron micrographs were characterized by a high dislocation density within the alpha phase which is generally poorly recovered (Figure (k)), although in some areas a subgrain network has formed (Figure (l)).

4.2.3.5.1 SIGNIFICANCE OF THE OTHER CONSTANTS IN THE HOT WORKING EQUATION

The physical interpretation of the other constants in the hot working equation has not been clearly established, but it is interesting to note which constants are most markedly different when comparing the two regimes (Table 4.8) and hence are most influenced by the variation in the starting structures.

There is a huge variation (approximately 10^{15}) in the value of A in the two regimes, illustrating the marked influence of starting structure on this constant. The value of α is also significantly different in the two regimes, although not to the same extent as A, being approximately 68% greater in the beta regime.

The difference in n values is only 8.3% between the two regimes and hence n is relatively insensitive to structure. Some workers[72,76,77] have suggested that n is a measure of the stress sensitivity of the strain rate. However, as discussed in section 4.2.3.3 the flow stress dependence of strain rate in the alpha+beta regime is markedly greater than in the beta regime (Figure 4.6), so that the value of n is clearly not a measure of the strain rate sensitivity.

4.2.4 SUMMARY OF TORSION ANALYSIS

1) The starting structures for torsion in the alpha+beta regimes consist of two phase alpha+beta, the proportion of alpha phase increasing with decreasing temperature. In the single phase beta regime, the starting structure consists of coarse recrystallised grains, the grain size increasing with increasing temperature. The starting structure has a profound influence on the deformation behaviour of the alloy:-

(a) The hot ductility of the alloy is much greater in the beta regime, with the hot ductility decreasing markedly with decreasing temperature in the alpha+beta regime as the proportion of alpha phase increases.

(b) There is a marked reduction in flow stress with increasing temperature in the alpha+beta regime, but only a small decrease in the beta regime.

(c) There is a marked increase in flow stress with increasing strain rate in the alpha+beta regime, the strain rate sensitivity decreasing with increasing temperature. In the beta regime the strain rate sensitivity is lower and decreases with increasing temperature.

2) The markedly different deformation behaviour exhibited by Ti-6Al-4V in the alpha+beta and beta regimes is reflected in the markedly different values of the hot working constants.

(a) In the beta regime the activation energy of 169,962 J/mole is similar to that for self-diffusion in the beta phase of super-purity titanium. This suggests that dynamic recovery is the operative restoration mechanism in the beta regime. This was proven at low strain rates where an unrecrystallised structure was apparent, however at high strain rates, a recrystallised

structure was produced which may have occurred as a result of either dynamic recovery followed by static recrystallisation or dynamic recrystallisation. The phase transformations occurring on cooling from the beta regime wipe out any deformation substructure and hence this argument cannot be conclusively resolved.

(b) In the alpha+beta regime, the activation energy of 521,697 J/mole is substantially greater than the activation energy for self-diffusion in the alpha and beta phases of super-purity titanium. This high value of activation energy, allied with the optical microscopy evidence of a recrystallised structure and electron microscopy evidence of a dislocation substructure within the alpha phase, indicates that dynamic recrystallisation is the predominant high temperature restoration mechanism in the alpha+ beta regime.

SECTION TWO

4.3 FACTORS INFLUENCING DIE WEAR AND THE VARIATION IN THE LUBRICATING BEHAVIOUR OF EXTRUSION GLASSES WITH THE EXTRUSION VARIABLES

4.3.1 DIE WEAR

The major problem encountered throughout the course of the extrusion programmes was that of die wear, with "wash-in" occurring at the radiused entry to the die orifice (Figure 4.10) resulting in a product with a poor surface quality.

The severity of the die wear increased with increasing temperature and extrusion ratio as shown in Table 4.11 and Figure 4.11. At low temperatures and extrusion ratios the wear on the die is small, but as the temperature exceeds 1000°C the wear increases substantially. C6496 was the glass employed for the majority of the extrusions, but at higher extrusion temperatures the higher softening point glass C7216 was used and this significantly reduced the die wear. The use of the C6496 glass at T = 1050°C, R = 40:1 resulted in die wear of 9.2%, whereas the C7216 glass at T = 1100°C, R = 40:1 resulted in wear of only 3.7%.

Only the results for new dies are shown in Figure 4.11. Subsequent extrusions through these worn dies resulted in further deterioration of the die. This is shown in Table 4.12 where 2 extrusions have been carried out through the same die under identical conditions. The wear has increased substantially and, as would be expected, the pressure required for the second extrusion is significantly lower.

Examination of the extrudes revealed a discontinuous cracked oxide scale at the surface (Figure 4.12),the thickness of the oxide "case" increasing with temperature. Titanium has a very high reactivity with oxygen forming a very hard brittle oxide scale on heating in air (section 1.3.3.6). Although heating was conducted under argon in an electric muffle furnace (section 3.1.3) the heating times were

FIGURE 4.10

EXAMPLE OF DIE WEAR

FIGURE 4.13

UNWORN DIE

Run Code	Furnace Temp. °C	Extrusion Ratio	Glass Type	Wear mm	% Wear
1	850	20	C6496	0.045	0.36
6	900	20	K7072	0.081	0.64
8	900	40	C6496	0.146	1.65
10	900	60	C6496	0.103	1.43
11	950	20	C6496	0.094	0.75
13	950	40	C6496	01076	0.86
15	950	60	C6496	0.150	2.06
17	1000	20	C6496	0.205	1.62
19	1000	40	C6496	0.202	2.29
21	1000	60	C6496	0.452	6.09
23	1050	40	C6496	0.830	9.20
24	1050	60	C6496	0.742	9.10
26	1100	20	C6496	0.476	3.82
28	1100	40	C7216	0.329	3.71
29	1100	60	C7216	1.050	14.4
32	1150	40	C7216	0.266	3.0

TABLE 4.11 EFFECT OF THE EXTRUSION PARAMETERS ON DIE WEAR

Temp. °C	Ext. Ratio	Extrusion 1		Extrusion 2		% Reduction in Pressure
		% Die Wear	Peak Pressure MNm-2	% Die Wear	Peak Pressure MNm-2	
900	40	1.65	932	5.65	873	6.3
950	20	0.75	683	6.67	645	5.6
950	40	0.86	808	8.22	784	3.0
1000	20	1.62	560	11.65	486	13.2
1000	40	1.37	674	15.43	620	8.0

TABLE 4.12 EFFECT ON DIE WEAR AND PEAK PRESSURE OF SUBSEQUENT EXTRUSIONS THROUGH WORN DIES

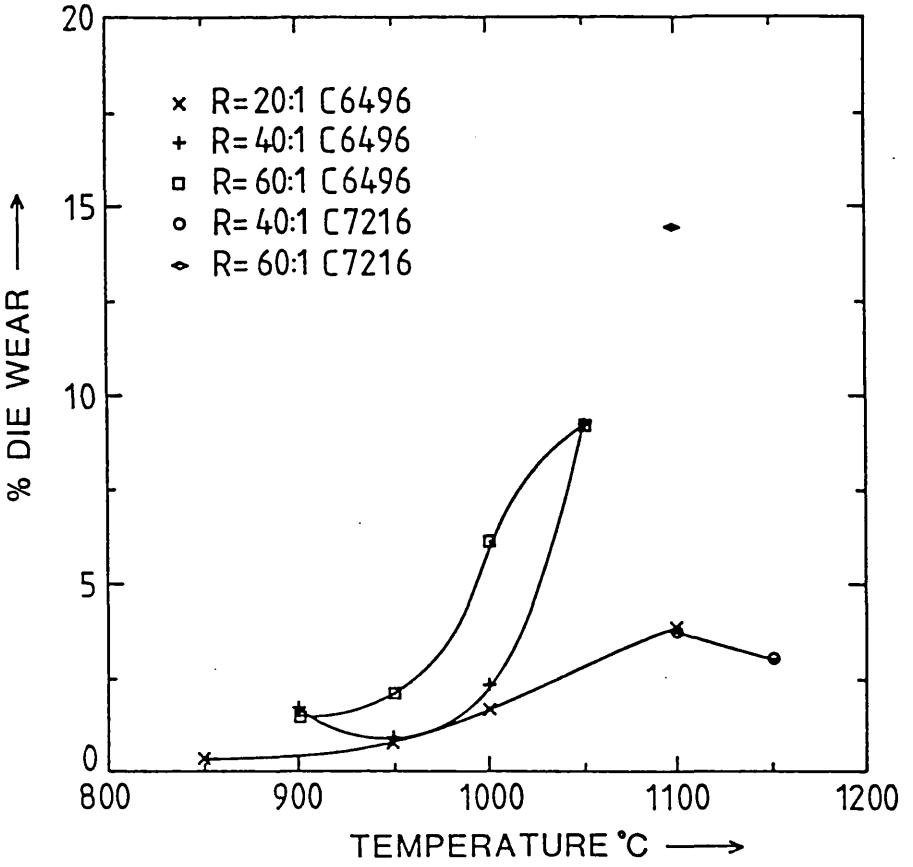

Figure 4.11 EFFECT OF TEMPERATURE, EXTRUSION RATIO AND GLASS TYPE ON DIE WEAR

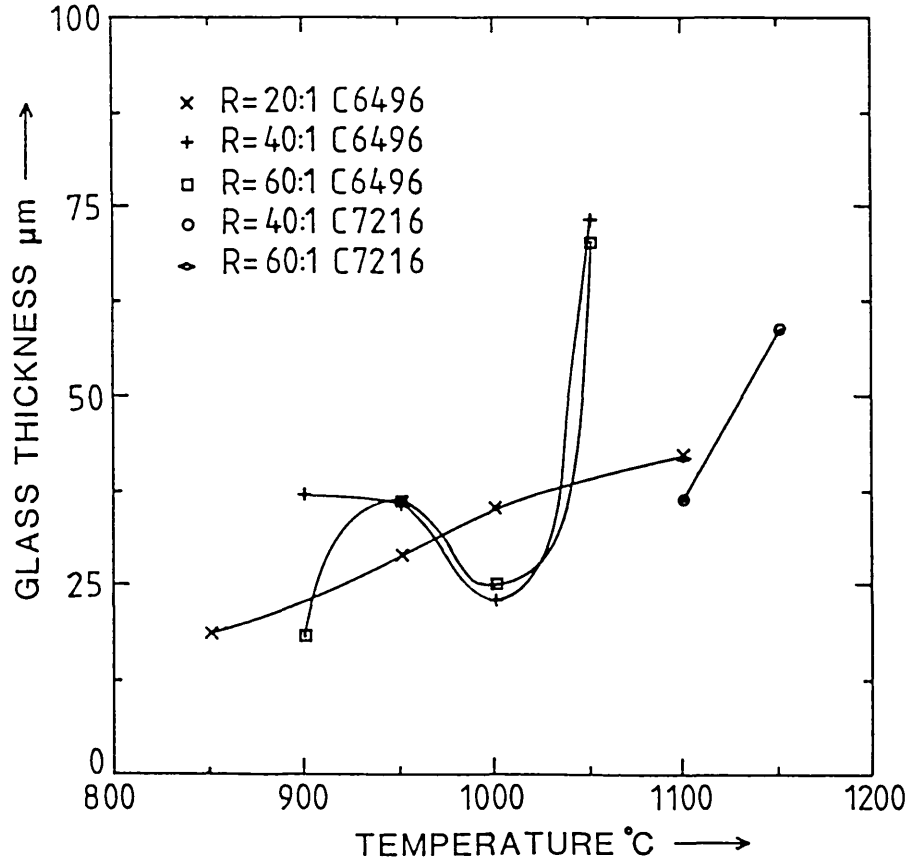

Figure 4.14 VARIATION IN GLASS THICKNESS WITH THE EXTRUSION VARIABLES

FIGURE 4.12

OXIDE SCALE

ON SURFACE OF EXTRUDE

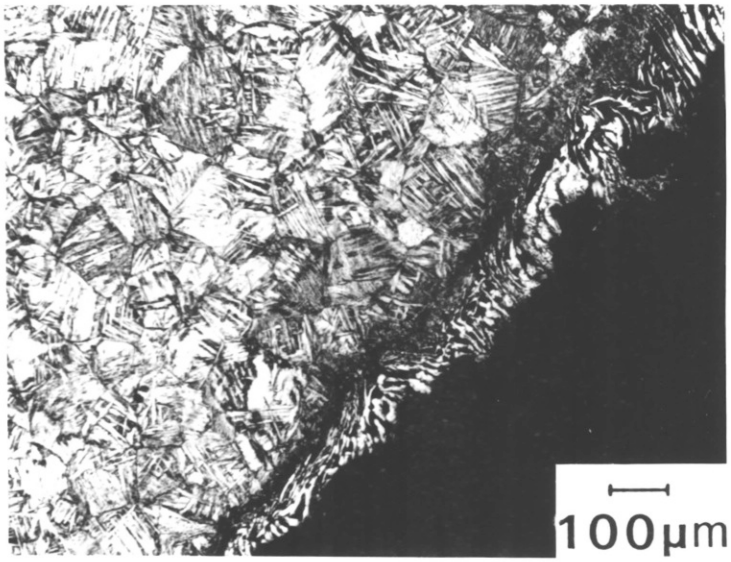
100μm

prolonged (1 hour) and some reaction with traces of oxygen in the furnace must have occurred. In addition, transfer of the billet through air to the container, although achieved in around 15 seconds, must have resulted in further oxidation. Hence the surface of the billet at commencement of the extrusion stroke had a thin very hard brittle oxide scale on it, the thickness of the scale increasing with increasing extrusion temperature.

In glass-lubricated extrusion the metal flow is such that the surface of the billet becomes the surface of the extrude and therefore the oxide scale comes into contact with the glass pad. During extrusion the brittle oxide layer cracks under pressure, and as it comes into contact with the glass pad, entrains the glass and inhibits proper lubrication at the die/billet interface. The die is therefore not adequately insulated from the heat of the billet and becomes overheated. This results in softening of the die material and "wash-in". In addition, any hard oxide scale that comes into contact with the die will cause further erosion.

Obviously, the higher the extrusion temperature the thicker will be the oxide scale, and the greater will be the heat transfer from the billet to the die, resulting in greater die wear.

4.3.2 ELIMINATION OF DIE WEAR

For die wear to be substantially reduced the oxide layer must be prevented from forming during heating and transfer. The modifications made to the experimental procedure are given in section 3.1.11.

Only two extrusions were carried out using these modified conditions, but these were sufficient to establish the dramatic improvement in die life that can be obtained by eliminating the oxide scale.

The extrusion conditions employed are shown in Table 4.13, extrusion 2 representing particularly severe extrusion conditions.

Run Code	Temperature °C	Extrusion Ratio	Cooling Medium	Glass Type
1	950	20	W.Q.	C6496
2	1100	40	W.Q.	C7216

TABLE 4.13 CONDITIONS EMPLOYED FOR MODIFIED EXTRUSION PRACTICE USING I.M.I. 550

The dies employed showed no evidence of any die wear as is shown in Figure 4.4 for the higher temperature run. Table 4.14 shows the variation in diameter along the extrude lengths, measurements being taken at 0.25, 0.5 and 0.75 of the extrude length before and after deglassing. A slight reduction in extrude diameter has occurred in both cases, rather than the increase in diameter observed when die wear was apparent.

The combination of a rapid heating rate and the use of an argon atmosphere and a protective glass coating have produced a scale-free billet surface. In the absence of the scale, the glass is able to lubricate and insulate the die properly, thereby preventing overheating and hence wear. The use of lower tooling temperatures has also probably contributed to reducing the possibility of overheating of the dies.

4.3.3. THE EFFECT OF THE EXTRUSION VARIABLES ON METAL FLOW AND THE LUBRICATING BEHAVIOUR OF GLASS

As discussed in the previous section the presence of an oxide scale has a profound effect on the performance of the glass and hence metal flow.

Nevertheless, some valid observations can still be made which indicate how the glass behaviour and metal flow vary with temperature

Run Code	0.25			0.5			0.75			Average
	Dav Glassed mm	Dav De-Glassed mm	Glass Thickness µm	Dav Glassed mm	Dav De-Glassed mm	Glass Thickness µm	Dav Glassed mm	Dav De-Glassed mm	Glass Thickness µm	Glass Thickness µm
1	11.489	11.424	32.5	11.474	11.412	31.0	11.448	11.413	17.5	27.0
2	8.231	8.101	65.0	8.121	8.039	41.0	8.111	8.058	26.5	44.2

TABLE 4.14 VARIATION IN EXTRUDE DIAMETER AND GLASS THICKNESS ALONG THE EXTRUDE LENGTH USING MODIFIED EXTRUSION PRACTICE

and extrusion ratio. The following techniques have been employed.

1) VISUAL EXAMINATION

The distribution of glass along the extrude length and the "dryness" or "wetness" of the extrude surface give a good indication of the suitability of the glass for the extrusion conditions employed. The extrudes were examined before and after blasting, typical surfaces being shown in the following Figures, the right hand side of the extrude having been deglassed.

2) MEASUREMENT OF "GLASS" THICKNESS

The variation in "glass" thickness was measured as described in 3.1.9. The results for new dies are shown in Table 4.15 and Figure 4.14. These results must be treated with caution as the "glass" layer is in fact a mixture of glass and oxide. The exceptions are the extrusions performed using the improved technique as here the oxide scale has been eliminated.

3) EXAMINATION OF THE DISCARD SURFACE

The discards were approximately 10 cm in length. A large amount of information can be gleaned from the discard profile and the distribution of glass on the discard face.

4) PARTIAL EXTRUSIONS

Three partial extrusions were carried out as described in 3.1.8. The type of metal flow obtaining can be established from the etched-up sectioned discards.

4.3.3.1 VARIATION IN THE LUBRICATING BEHAVIOUR OF THE GLASSES WITH THE EXTRUSION VARIABLES

The glasses employed in the extrusion programme are given in Table 3.4. The performance of the glass C6496 was evaluated over the whole of the extrusion range with the lower softening point glass

Run Code	Temp. °C	Ext. Ratio	Glass Type	"Glass" Thickness µm			Average Glass Thickness
				0.25	0.5	0.75	
1	850	20	C6496	20.5	-	17.5	19.0
6	900	20	K7072	15.0	-	7.0	11.0
8	900	40	C6496	44.5	-	29.5	37.0
10	900	60	C6496	15.5	-	21.0	18.3
11	950	20	C6496	31.0	-	26.5	28.8
13	950	40	C6496	30.5	29.0	47.0	35.5
15	950	60	C6496	49.0	43.0	16.0	36.0
17	1000	20	C6496	29.0	-	41.5	35.3
19	1000	40	C6496	18.0	33.0	18.0	23.0
21	1000	60	C6496	7.5	37.0	31.0	25.2
23	1050	40	C6496	55.0	79.0	86.0	73.3
24	1050	60	C6496	47.0	62.5	101.5	70.3
26	1100	20	C6496	40.5	-	44.0	42.3
28	1100	40	C7216	35.5	38.0	35.5	36.3
29	1100	60	C7216	38.5	50.0	37.0	41.8
32	1150	40	C7216	64.0	55.5	57.5	59.0

TABLE 4.15 VARIATION OF GLASS THICKNESS WITH EXTRUSION PARAMETERS

Furnace Temperature °C	Surface Temperature °C	Log_{10} Viscosity C6496	Log_{10} Viscosity C7216
850	770	5.25	-
900	805	4.53	7.43
950	843	3.73	6.90
1000	875	3.10	6.47
1050	912	2.50	6.00
1100	945	2.20	5.67
1150	980	1.90	5.30

TABLE 4.16 VISCOSITIES OF GLASSES AT TEMPERATURES EMPLOYED IN EXTRUSION PROGRAMME

K7072 employed at low temperatures and the higher softening point glass C7216 employed at high temperatures.

As discussed in section 1.3.3.2.4 there are two methods of assessing the suitability of a glass as an extrusion lubricant; measurement of its softening point, and measurement of its temperature-viscosity variation. This data was available for the C6496 and C7216 glasses and is shown in Table 3.5 and plotted in Figure 4.15. No viscosity data was available below 900°C and so a straight line was drawn for each glass from the value at 900°C to the softening temperature (dashed line). Only the softening point was available for the K7072 glass. The horizontal lines at 10^2 and 10^4 poise viscosity correspond to the reported desired viscosity range for extrusion glasses at the extrusion temperature (section 1.3.3.2.4). The softening point of the glass was defined as the temperature at which the viscosity of the glass is $10^{7.6}$ poise.

From this data the viscosity of the glasses can be evaluated at the extrusion temperatures. Since it will be the billet surface temperature at the commencement of extrusion that governs the performance of the glass, the viscosity is given at this temperature (Table 4.16). The viscosity values read off below 900°C are obviously only approximations because of the linear fit assumed between viscosity and temperature.

The billet surface temperature will obviously change during the extrusion stroke as a result of chilling when it upsets to contact the liner, and heat generated due to deformation work. Nevertheless, some understanding of the lubricating behaviour of the glass can be obtained from the use of the initial billet surface temperature.

The results will be discussed temperature by temperature over the range 850°C - 1150°C. The influence of temperature, extrusion ratio and glass type on the lubricating behaviour of extrusion glasses will be considered.

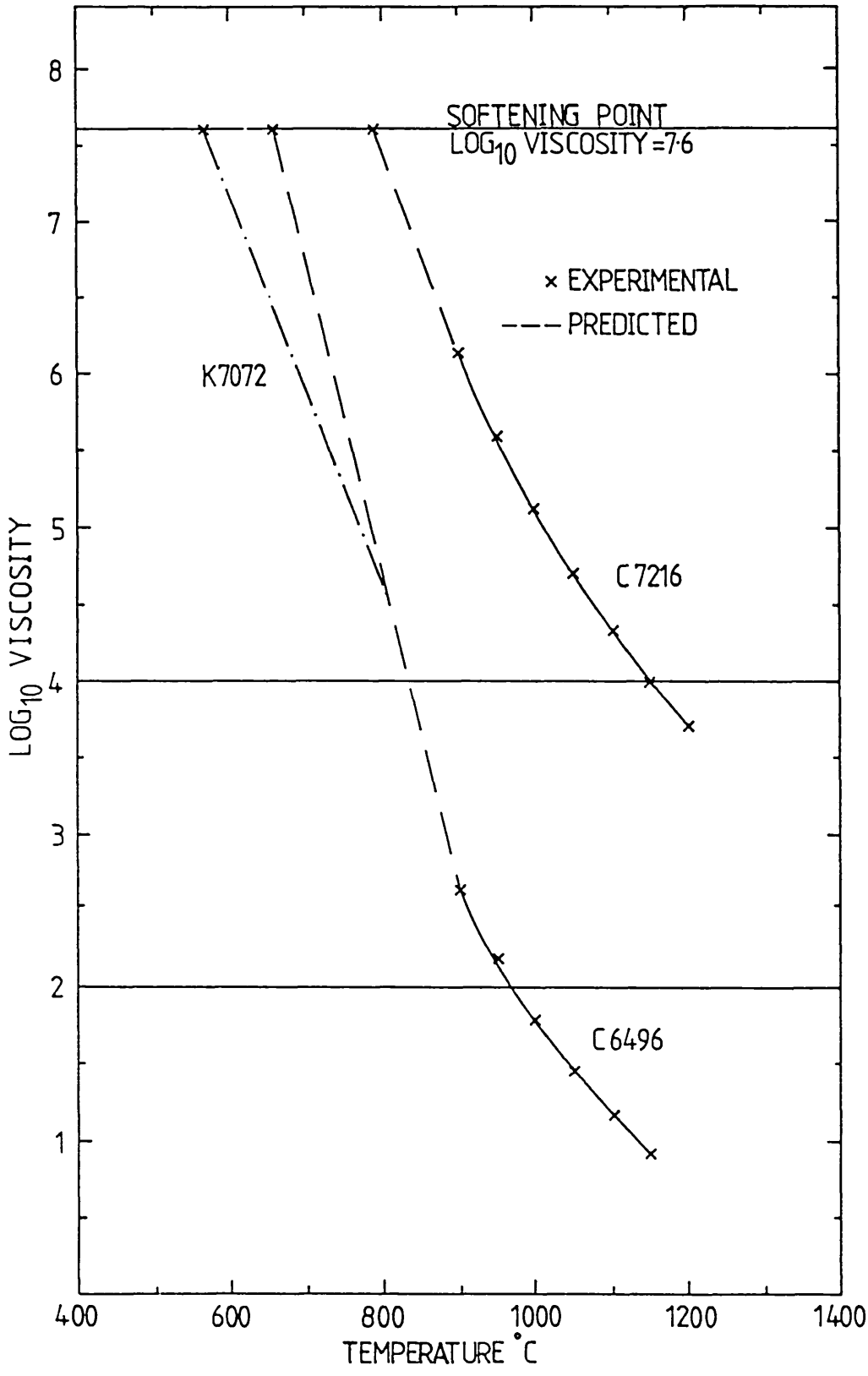

Figure 4.15 TEMPERATURE-VISCOSITY RELATIONSHIPS FOR THE EXTRUSION GLASSES

1) EXTRUSION TEMPERATURE = 850°C

Only one extrusion ratio, R = 20:1, was used at this temperature.

The surface temperature of the billet at the commencement of extrusion (Table 4.16) falls below the minimum temperature at which the glass acts as a lubricant. The result is that the glass does not soften adequately and some of the pad is extruded before the metal (Figure 4.16a). The remainder of the glass coats predominantly the front portion of the extrude, leading to gross overglassing at the front end (Figure 4.16b) and a very thin coating over the remainder of the extrude (Figure 4.16c).

There is no evidence of glass on the discard face (Figure 4.17a) indicating almost complete exhaustion of the glass pad. However, the discard profile is rounded at the edges, showing that during extrusion some glass became entrapped between the billet and the corner of the conical lead-in, serving to smooth out the metal flow.

Removal of the glass at the front end (Figure 4.16b) revealed a divoted surface as a result of chunks of unsoftened glass having become embedded in the metal. The remainder of the extrude, however, has a reasonable surface finish with only light longitudinal scoring apparent (Figure 4.16c). The scoring is probably due to a small amount of metal pick up on the die, due to failure of the glass to completely lubricate the die/billet interface. Despite the apparent inadequacy of the glass, the die wear is very small (Table 4.11). This is because the low temperature involved has substantially reduced the tendency for scaling and seizing between the billet and die.

For glass lubricated extrusion to be successful at low temperature a lower softe ning point glass will have to be employed. However, the minimal wear encountered, even when the glass has not provided proper lubrication, would suggest that glass is not required at these temperatures. An alternative method at low temperatures would be to use conical dies with molybdenum disulphide grease as the sole lubricant (section 1.3.3.10). The conical dies would allow streamlined flow to occur (Figure 1.8) in a similar manner to that obtaining during glass

FIGURE 4.16

EXTRUDED SECTIONS AT 850°C

(a) T = 850°C R = 20:1 W.Q. (EXT 1)
UNSOFTENED GLASS PAD EXTRUDED BEFORE METAL

(b) AS ABOVE OVERGLASSED AT FRONT END
GLASS THICKNESS ≃ 150 μm

(c) AS ABOVE UNDERGLASSED SECTION
GLASS THICKNESS = 17 μm

(d) T = 850°C R = 20:1 A.C. (EXT 3)
NO GLASS PAD EMPLOYED - DRY SCORED EXTRUDE

FIGURE 4.17

DISCARDS AT 850°C

L.H.S. (a) T = 850°C R = 20:1 W.Q. (EXT 1)
NO GLASS ON DISCARD FACE

R.H.S. (b) T = 850°C R = 20:1 A.C. (EXT 3)
NO GLASS PAD EMPLOYED

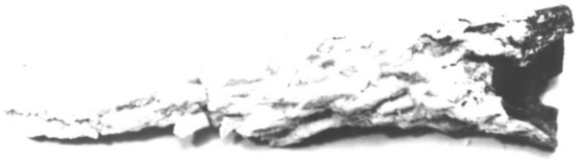

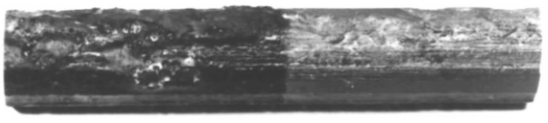

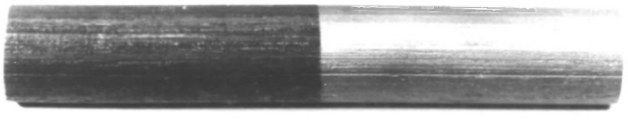

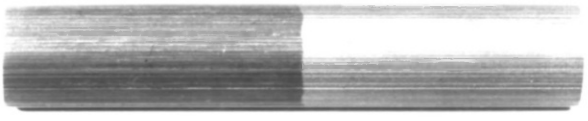

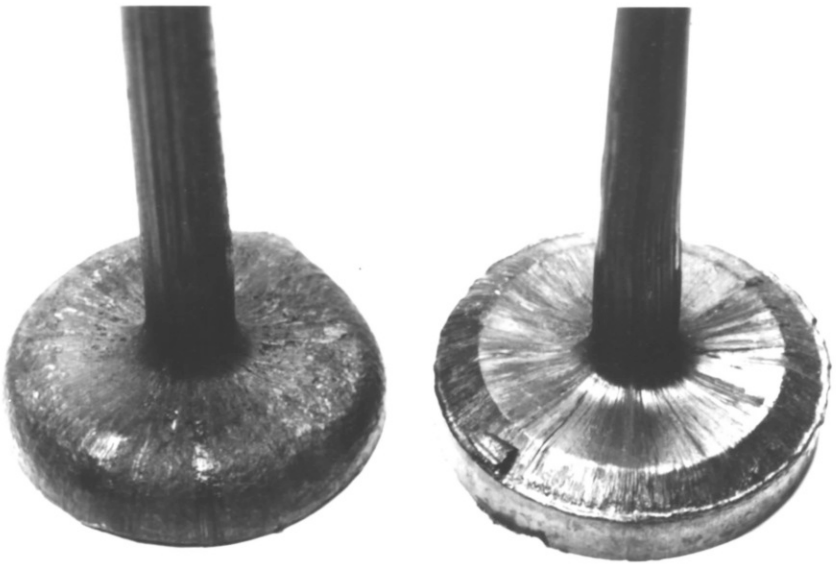

lubricated extrusion. This technique has been successfully used for the extrusion of steel at temperatures down to 600°C, with the advantage of improved surface quality compared to bars extruded at 'high' temperature.

An extrusion was mistakenly performed at T = 850°C, R = 20:1 (EXT. 3) without a glass pad. An increase in pressure of 149 MNm^{-2} (14.9%) was observed. The discard is shown in Figure 4.17b and it is apparent that the front end of the billet has taken up the same shape as the die face. Some metal shear has occurred at the die face as a result of friction between the billet and die, and this is responsible for the increase in pressure. The die design is obviously totally inappropriate for non-glass lubricated extrusion. A typical section of the extrude is shown in Figure 4.16d. The surface is completely dry and scored as a result of metal pick-up on the die face.

During transfer of the billet from the furnace to the liner the surface of the billet loses temperature far more rapidly than the interior (Figure 3.5). Also, after upsetting, the billet will be in intimate contact with the liner wall, maintained at 466°C and therefore further chilling of the billet surface will occur relative to the centre. This is reflected in the microstructural differences between the extrude periphery and centre as shown in Figures 4.18 and 4.19 for extrusion 1. A much greater volume fraction of the heavily elongated, low temperature primary alpha phase is present at the billet periphery as a result of severe chilling.

However, when any metal shearing occurs at the die face, as was the case in extrusion 3, when no glass lubricant was employed, very substantial temperature rises occur at the billet periphery as is shown in Figure 4.20. A fully transformed beta structure is apparent at the periphery, indicating that the alpha+beta/beta transus temperature of approximately 1000°C has been exceeded.

FIGURE 4.18

T = 850°C R = 20:1 (EXT 1)

EXTRUDE CENTRE

FIGURE 4.19

AS ABOVE

EXTRUDE PERIPHERY

FIGURE 4.20

T = 850°C R = 20:1 (EXT 3)

NO GLASS PAD EMPLOYED

EXTRUDE PERIPHERY

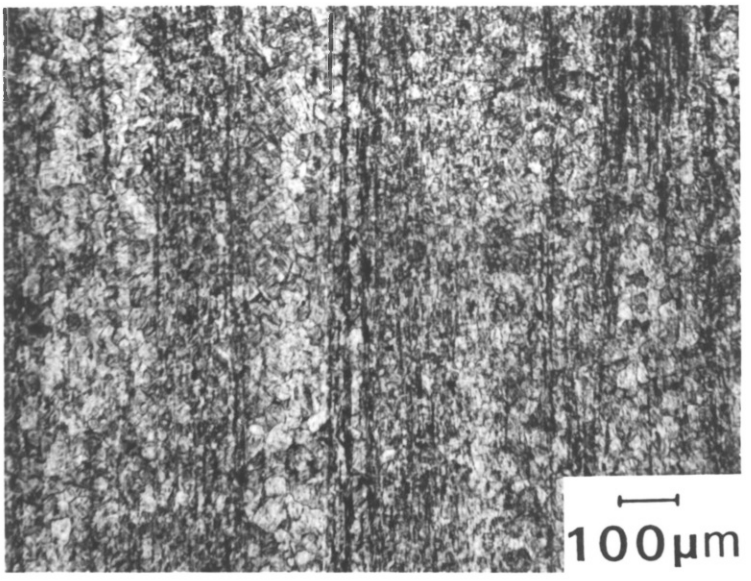
100μm

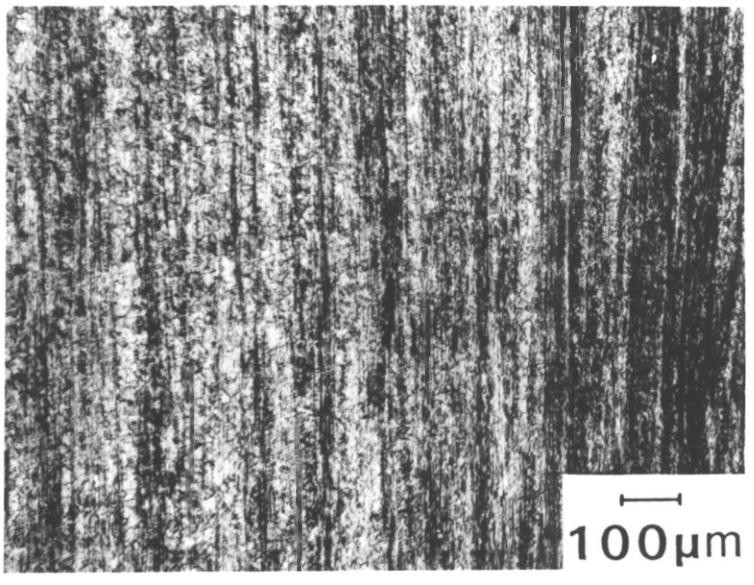
100μm

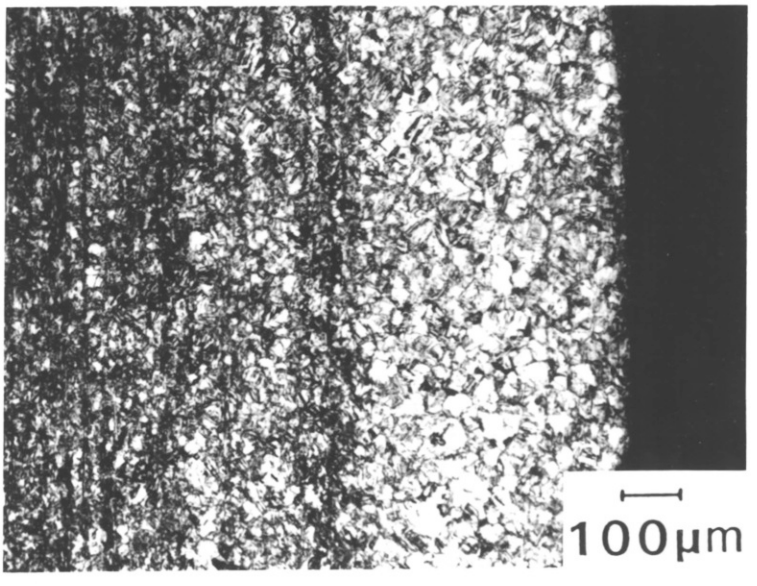
100μm

2) EXTRUSION TEMPERATURE = 900°C

A partial extrusion was carried out at an extrusion ratio of 10:1 (Run Code 4). Again the glass did not soften adequately, with a large proportion of the pad being extruded in front of the billet. The remainder of the glass coated the front portion of the extrude (Figure 4.21b), however the pad soon became exhausted. The billet then stuck to the die face and a dead metal zone was formed. The remainder of the billet then sheared past this dead metal zone, which became detached from the main body of the billet, forming a conical skull (Figure 4.21a). The majority of the extrude was therefore unlubricated (as shown in Figure 4.21c). The surface quality is excellent, the oxidised skin of the billet having been sheared off, with virgin metal forming the extrude surface. This type of unlubricated flow is similar to that produced during aluminium extrusion (section 1.3.3.1). Although it produces an excellent surface quality at low temperatures, much higher extrusion pressures are required to produce metal shearing, compared to fully lubricated flow.

Large temperature rises again occurred at the periphery of the extrude as a result of metal shearing, the structure consisting of fully transformed beta.

The etched up partial discard is shown in Figure 4.22. A schematic diagram of the discard was also constructed incorporating the die (Figure 4.23). This shows clearly the formation of the dead metal zone, represented by the cross-hatch section. Little or no die wear was observed, because of the low temperatures involved.

Increasing the extrusion ratio to 20:1 resulted in elimination of the metal skull. The front end of the extrude was still overglassed, however, and the remainder of the extrude had only a very thin coating of glass. In this respect, there was only a small improvement compared to an extrusion temperature of 850°C. The discard profiles were also similar.

FIGURE 4.21

PARTIAL EXTRUSION AT

T = 900°C R = 10:1 (EXT 4)

(a) METAL SKULL

(b) FRONT END
GLASS THICKNESS = 54 μm

(c) MIDDLE SECTION
UNLUBRICATED

FIGURE 4.24

EXTRUDED SECTIONS AT

T = 900°C R = 40:1, 60:1

(a) T = 900°C R = 40:1 (EXT 8) FRONT END
UNSOFTENED GLASS GLASS THICKNESS = 17 μm

(b) AS ABOVE WELL LUBRICATED SECTION
GLASS THICKNESS = 45 μm

(c) AS ABOVE DIVOTED SURFACE

(d) T = 900°C R = 60:1 (EXT 10)
WELL LUBRICATED SECTION

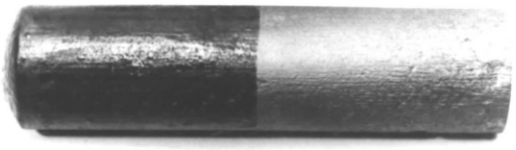

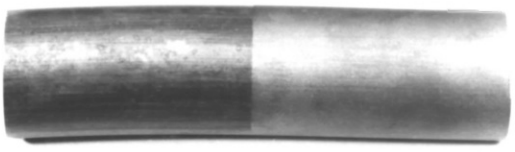

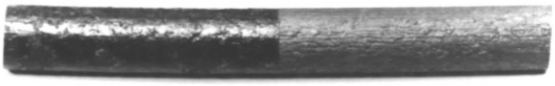

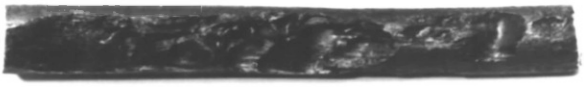

FIGURE 4.22

MACROGRAPH OF PARTIAL EXTRUSION

AT T = 900°C R = 10:1 (EXT 4)

FIGURE 4.23

SCHEMATIC OF ABOVE

INCORPORATING DIE

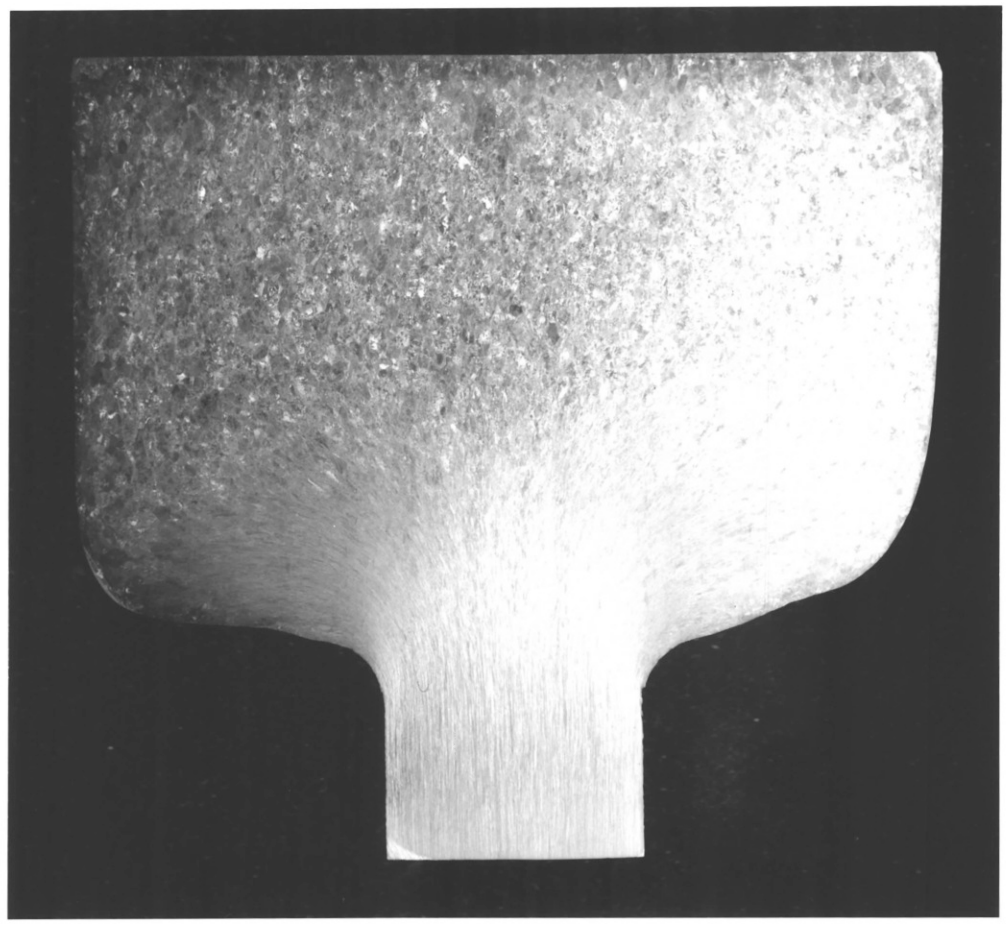

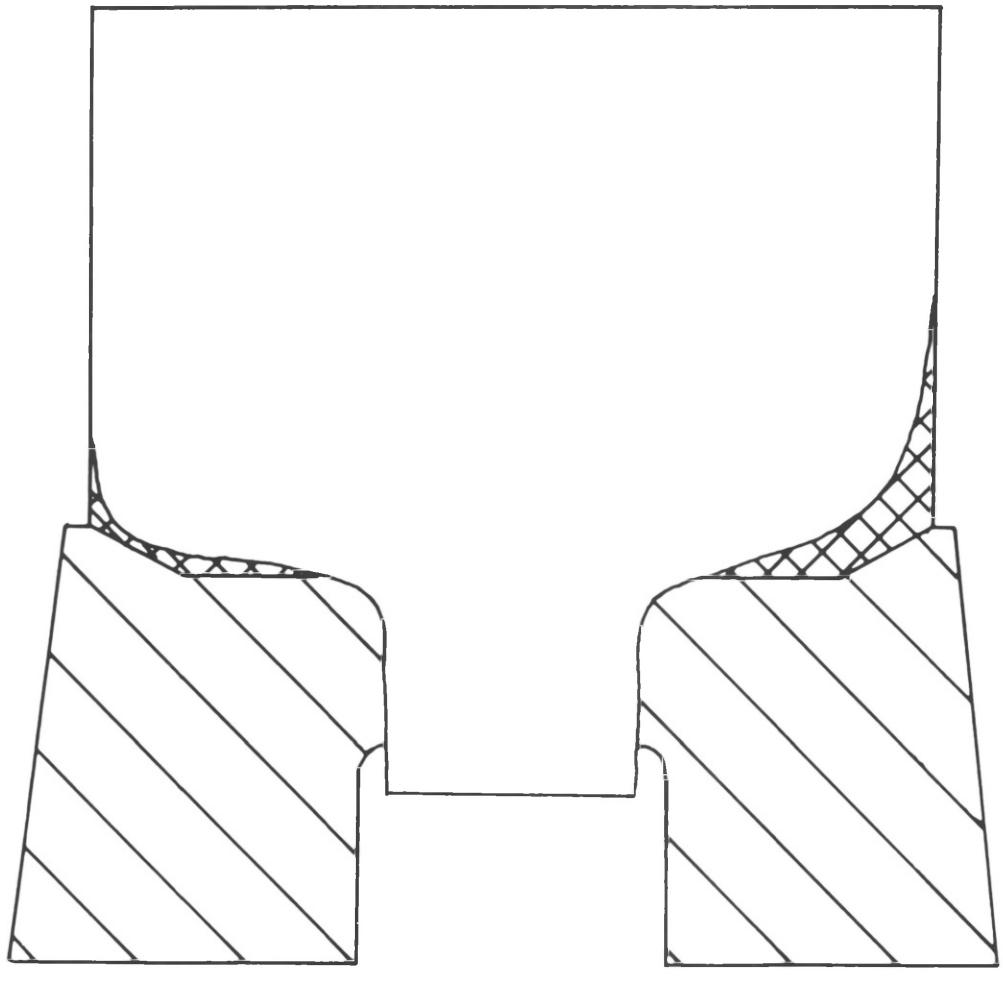

To observe whether the glass K7072 provided better lubricating properties at low temperatures, two extrusions were carried out at an extrusion ratio of 20:1, one using K7072 and the other C6496. Little or no improvement was observed when using the K7072 which is surprising in view of the much lower softening point of the glass, 570°C as opposed to 670°C. This would suggest that the viscosities of the two glasses are similar at the extrusion temperature. This would be possible if the temperature-viscosity behaviour of the K7072 glass followed the dot-dash line shown in Figure 4.15. This shows up the big limitation in using only the softening point to assess the suitability of a glass; glasses of differing softening points may well have similar viscosities over the extrusion temperature range, so that they exhibit similar lubricating behaviour, while glasses of similar softening points may well have markedly different temperature-viscosity characteristics and perform completely differently over the extrusion temperature range.

Increasing the extrusion ratio to 40:1 resulted in some improvement in the performance of the glass. There was none of the overglassing at the front end observed at lower extrusion ratios. At the very front end of the extrude the glass had still not softened completely, giving a roughened appearance to the extrude (Figure 4.24a). This effect soon disappeared, with the extrude taking on a well-lubricated "wet" look (Figure 4.24b). The glass had become more fluid and flowed much better with the metal, yielding much better lubrication. However, approximately a third of the way along the extrude length large divots were apparent (Figure 4.24c). These were caused by a rush of unsoftened glass through the die, which spalled off on quenching, leaving large divots in the extrude surface. This effect was only apparent for a short distance, but after this section the lubrication was patchy.

Some glass was apparent on the discard face (Figure 4.25a) indicating a more uniform melting of the glass pad compared to lower temperatures and extrusion ratios. In addition, a thicker glass coating was produced on the extrude.

Similar behaviour was observed at an extrusion ratio of 60:1. A

FIGURE 4.25

DISCARDS AT T = 900°C R = 40:1

AND T = 950°C R = 20:1

L.H.S. (a) T = 900°C R = 40:1 EXT 8
SOME EVIDENCE OF GLASS ON DISCARD FACE

R.H.S. (b) T = 950°C R = 20:1 EXT 11
DISCARD FACE UNIFORMLY COVERED WITH GLASS

FIGURE 4.26

EXTRUDED SECTIONS AT

950°C AND 1050°C

(a) T = 950°C R = 20:1 EXT 11 FRONT END
UNSOFTENED GLASS GLASS THICKNESS = 76 μm

(b) AS ABOVE WELL LUBRICATED SECTION
GLASS THICKNESS = 31 μm

(c) T = 1050°C R = 40:1 EXT 23
WELL LUBRICATED FRONT END
GLASS THICKNESS = 68 μm

(d) AS ABOVE DRY BACK END
GLASS THICKNESS = 79 μm

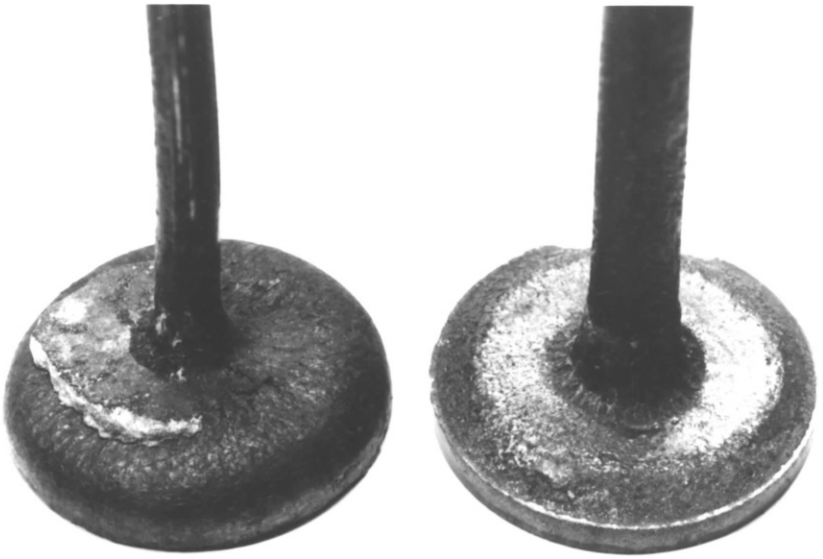

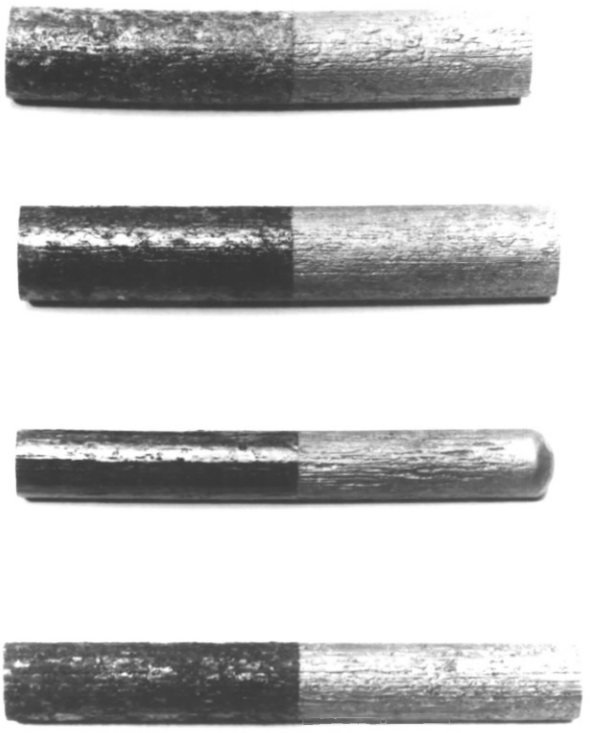

well-lubricated extrude was produced for the first half of the extrusion (Figure 4.24d) but then a divoted surface was apparent as a result of unsoftened glass being forced through the die.

3) EXTRUSION TEMPERATURE = 950°C

A marked improvement in the performance of the glass occurred at this temperature for all extrusion ratios. Apart from a short section at the front end where the glass has not softened completely (Figure 4.26a) the extrudes were all well glassed with no evidence of any divoting (Figure 4.26b). The discard faces were fully and uniformly covered with glass (Figure 4.25b). These features indicate that the glass pad has melted down uniformly throughout the extrusion stroke with a plentiful supply of glass being available at all stages to lubricate and insulate the die. This represents classical glass lubricated extrusion with the surface of the billet forming the surface of the extrude.

Figure 4.27 shows an extrusion where the glass pad remained intact and actually separated from the billet discard. The front face of the glass pad has taken up the shape of the die face with the back face taking up the shape of the radiused billet. The glass pad has therefore served to smooth out the contours of the die preventing the formation of a dead metal zone and allowing streamlined metal flow to occur.

Hence the glass C6496 starts to provide effective lubrication somewhere between 805°C and 843°C, with the corresponding viscosities being $10^{4.53}$ and $10^{3.73}$ poise (Table 4.10 and Figure 4.15). This is in good agreement with the reported viscosity maximum for extrusion glasses of 10^{4} poise at the extrusion temperature (section 1.3.3.2.4). The values of viscosity for the C7216 glass, approximately 10^{7}, make it totally unsuitable for use at these low temperatures.

With regard to the softening point criterion the glass starts to provide effective lubrication when the billet surface temperature exceeds 1.25 x softening temperature. This is well below the generally accepted

FIGURE 4.27

GLASS PAD DETACHED FROM DISCARD

T = 950°C R = 40:1 (EXT 13)

FIGURE 4.30

DISCARDS AT 1050°C USING C6496 GLASS

AND 1100°C USING C7216 GLASS

L.H.S. (a) T = 1050°C R = 40:1 (EXT 23) C6496 GLASS

REDUCED AMOUNT OF GLASS ON DISCARD FACE

R.H.S. (b) T = 1100°C R = 40:1 (EXT 28) C7216 GLASS

DISCARD FACE UNFORMLY COVERED WITH GLASS

value of 1.5 x softening temperature, however the initial billet temperature is employed in this case rather than the surface temperature at the commencement of extrusion. Using the initial billet temperature in the present case, the C6496 glass starts to provide effective lubrication at approximately 925°C which is 1.41 x softening temperature.

Despite the well lubricated appearance of the extrude, after removal of the glass the underlying surface quality is always poor. This, as discussed in section 4.3.1, is due to the presence of an oxide scale on the surface of the billet which cracks during extrusion, preventing proper lubrication and resulting in die wear and poor surface quality. These effects are accentuated by increasing extrusion ratio and temperature.

4) EXTRUSION TEMPERATURE = 1000°C

Similar behaviour was observed to that obtained at 950°C, except for a deterioration in surface quality as a result of die wear.

A 10:1 partial extrusion was carried out (Ext. 16),the etched up discard being shown in Figure 4.28,with a schematic in Figure 4.29. The cross hatched section represents the glass pad. The rear of the billet is undeformed with all the deformation occurring in a conical zone of intense shear at the mouth of the die as is obviated by the marked change in microstructure. No dead metal zone is formed in the billet. The layers of glass in contact with the hot billet melt down forming a thin film of viscous glass which lubricates the passage of the metal through the die. During the course of the extrusion the glass pad becomes smaller and smaller as more and more glass melts down. Thus a sufficiently thick glass pad must be provided to avoid premature exhaustion of the glass reservoir.

FIGURE 4.28

MACROGRAPH OF PARTIAL EXTRUSION

AT T = 1000°C R = 10:1 (EXT 16)

OVERLAY SHOWS THE PREDICTED DEFORMATION ZONE

DIMENSIONS FROM UPPER BOUND ANALYSIS

———————— FULLY LUBRICATED m = 0

- - - - - - - - - - - - - - - - - - STICKING FRICTION m = 1

FIGURE 4.29

SCHEMATIC OF ABOVE

INCORPORATING DIE

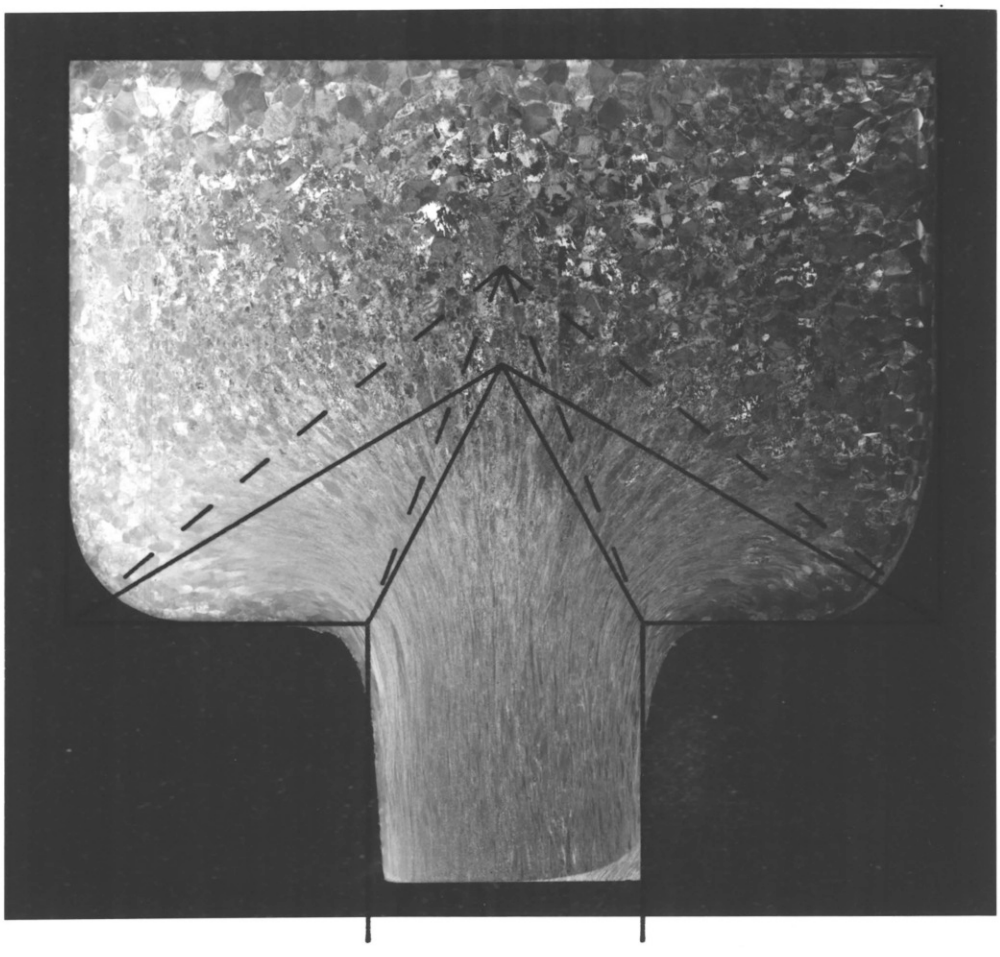

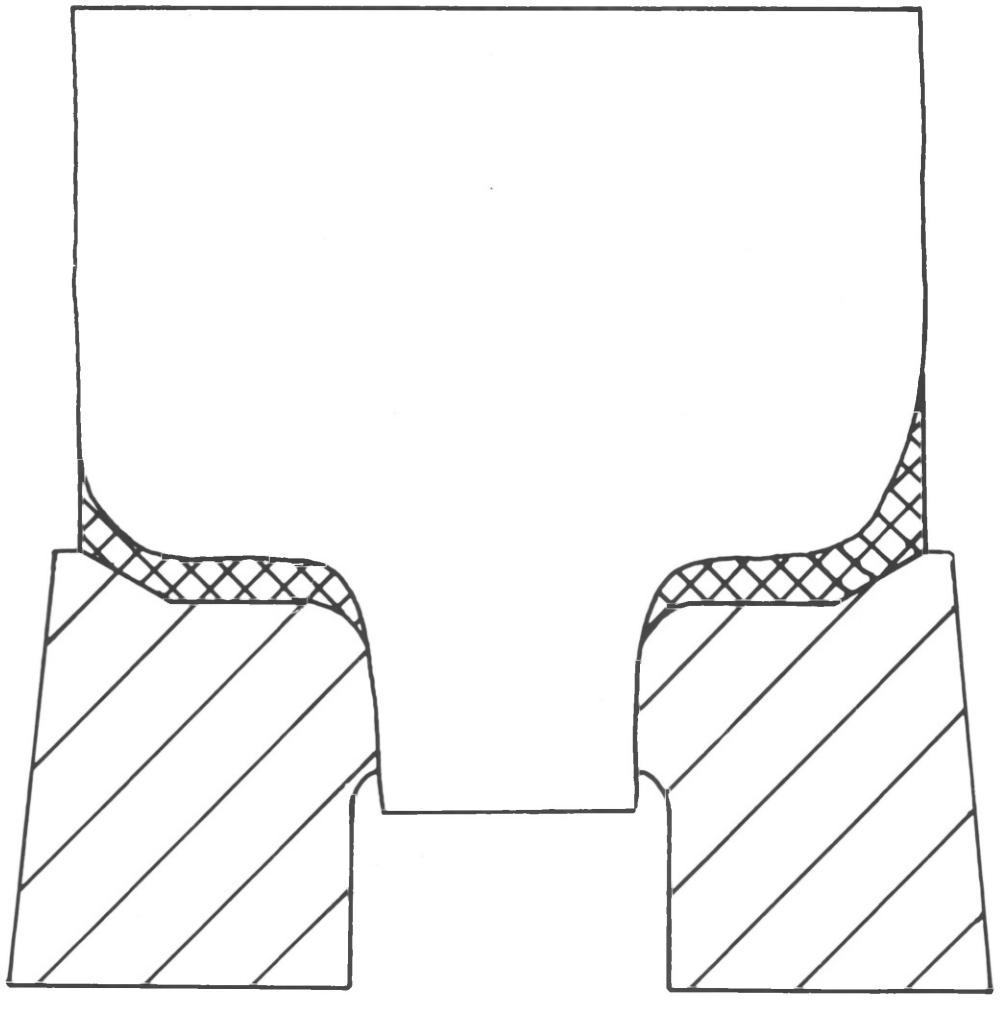

Thus a marked improvement in metal flow has occurred compared to that obtaining in the partial extrusion carried out at 900°C. No metal skull was formed, and a well lubricated extrude was produced.

Comparison of the average "glass" thicknesses at 950°C and 1000°C for the various extrusion ratios (Table 4.15 and Figure 4.14) indicate no trend of glass thickness with temperature or extrusion ratio. Any trend however is likely to be masked by the additional factors of die wear and scale formation both of which will markedly influence the "glass" thickness.

5) EXTRUSION TEMPERATURE = 1050°C

Increasing the extrusion temperature to 1050°C resulted in a marked increase in die wear (Figure 4.11) with a resultant deterioration in surface quality.

The extrudes were well glassed over most of their length, even at the very front end (Figure 4.26c), however towards the back end as the wear became very severe the surface took on a much drier appearance (Figure 4.26d).

The increased die wear, thicker oxide scale and reduction in viscosity of the glass have contributed to almost trebling the "glass" thickness compared to 1000°C (Table 4.15). As a result of the thicker "glass" coating on the extrudes the amount of glass remaining on the discard face is reduced (Figure 4.30a).

The upper limit of usefulness of the C6496 glass cannot be determined because of die wear problems, but it will obviously correspond to a temperature at which the glass pad melts too rapidly and becomes exhausted before the end of the extrusion stroke. The viscosity of the glass falls below the reported desired minimum of 10^2 poise at a temperature of 975°C, so it would not be expected that the glass could be used much above this temperature.

6) EXTRUSION TEMPERATURE = 1100°C

A 10:1 partial extrusion was carried out (Ext. 25),the etched up discard being shown in Figure 4.31, with a schematic Figure 4.32. The shaded area represents the wear on the die. This is the "wash-in" discussed earlier with the die metal being overheated and hence softening as a result of the inadequate insulation afforded by the glass, the properties of which have been markedly altered by the oxide scale on the billet.

The higher softening point glass C7216 was employed at extrusion ratios of 40:1 and 60:1. The viscosity of the glass (Figure 4.15 and Table 4.16) is $10^{5.67}$ which is well above the 10^{4} poise maximum reported for optimum lubrication, and at the front end of the extrude the glass has not softened adequately (Figure 4.33a). However, this effect soon disappears and the remainder of the extrude is reasonably well lubricated, although the glass has clearly not softened completely (Figure 4.33b). Thus, despite the high viscosity of the glass, some lubrication has been afforded. The discard is fully and uniformly glassed (Figure 4.30b) as opposed to the near exhausted pad observed with the C6496 glass. In addition, the glass coating is much thinner (Figure 4.14). These two factors indicate that the C7216 glass does not soften as rapidly as the C6496 glass at similar temperatures as a result of the much higher viscosity of the C7216 glass.

The die wear was substantially reduced using the C7216 glass (Figure 4.11) the higher viscosity glass providing much more effective insulation between the billet and die.

7) EXTRUSION TEMPERATURE = 1150°C

An extrusion was carried out at an extrusion ratio of 10:1 using C7216 glass (Ext. 30). The glass did not soften adequately producing a grossly overglassed surface at the front end (Figure 4.33c) and a dry worn back end. This highlights the marked influence of extrusion ratio on glass performance, the glass having been quite successfully used at a higher extrusion ratio even at a lower temperature.

FIGURE 4.31

MACROGRAPH OF PARTIAL EXTRUSION

AT T = 1100°C R = 10:1 (EXT 25)

OVERLAY SHOWS THE PREDICTED DEFORMATION ZONE

DIMENSIONS FROM UPPER BOUND ANALYSIS

———————— FULLY LUBRICATED m = 0

---------- STICKING FRICTION m = 1

FIGURE 4.32

SCHEMATIC OF ABOVE

INCORPORATING DIE

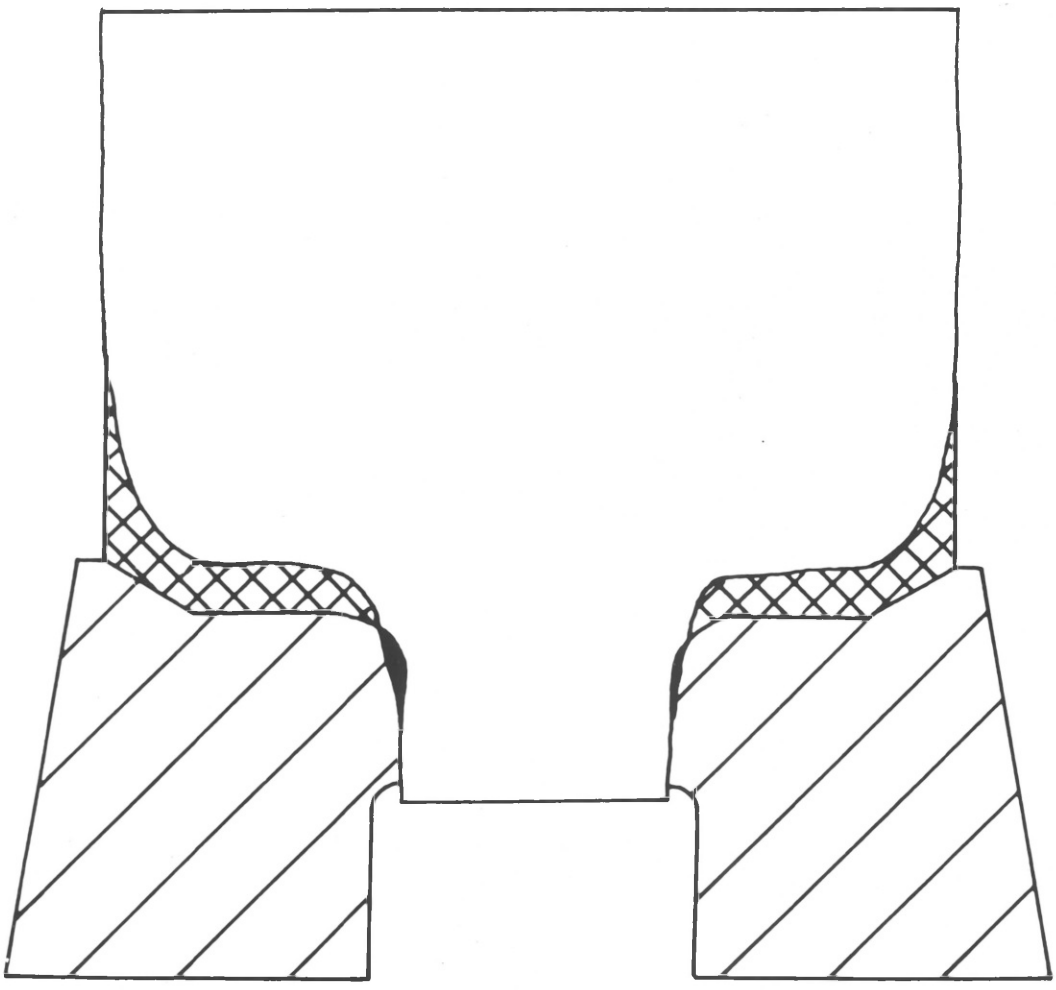

FIGURE 4.33

EXTRUDED SECTIONS AT 1100°C AND

1150°C USING C7216 GLASS

(a) T = 1100°C R = 40:1 (EXT 28)
UNSOFTENED GLASS AT FRONT END
GLASS THICKNESS = 68 μm

(b) AS ABOVE LUBRICATED SECTION
GLASS THICKNESS = 36 μm

(c) T = 1150°C R = 10:1 (EXT 30)
GROSSLY OVERGLASSED AT FRONT END
GLASS THICKNESS ≃ 770 μm

(d) T = 1150°C R = 40:1 (EXT 32)
TYPICAL SECTION GLASS THICKNESS = 64 μm

FIGURE 4.34

EXTRUDED SECTIONS PRODUCED

USING MODIFIED EXTRUSION PRACTICE

(a) T = 950°C R = 20:1 C6496 GLASS
TYPICAL SECTION GLASS THICKNESS = 27 μm

(b) T = 1100°C R = 40:1 C7216 GLASS
TYPICAL SECTION GLASS THICKNESS = 44 μm

Further extrusions were carried out at ratios of 40:1 and 60:1, producing a much better distribution of glass (Figure 4.33d). Increasing the extrusion ratio results in an increase in extrusion pressure, which in turn results in a larger temperature rise during extrusion. These factors serve to decrease the viscosity of the glass and hence improve its lubricating behaviour.

4.3.4 EFFECT OF MODIFIED EXTRUSION PRACTICE ON SURFACE QUALITY

As would be expected, elimination of the oxide scale and hence die wear resulted in a marked improvement in surface quality. The first extrusion was carried out at T = 950°C, R = 20:1 using C6496 glass. The extrude was well lubricated along its length (Figure 4.34a) the surface quality on removal of the glass being excellent.

The second extrusion was carried out at T = 1100°C, R = 40:1 using C7216 glass. As was observed with previous extrusions, this temperature is probably slightly below the ideal softening range of the C7216 glass, but nevertheless a reasonably well glassed extrude was produced (Figure 4.34b). Deglassing revealed the extrude surface to be slightly scored, but this was due to unsoftened glass rather than any die wear.

Only a very thin disc of discard was left at the end of the extrusion, thicker pressure pads having been employed, thus preventing any observation of the discard profiles produced using flat dies. The use of a flat die, however, would not appear to have any deleterious effect with regard to glass lubrication.

The glass thickness in both cases decreased from the front to the back of the extrude (Table 4.14).

4.3.5 SUMMARY OF THE FACTORS INFLUENCING DIE WEAR AND THE VARIATION IN THE LUBRICATING BEHAVIOUR OF GLASS WITH THE EXTRUSION VARIABLES

1) The die wear encountered in the extrusion programme was due to the presence of a very hard, brittle oxide scale on the billet surface, formed by reaction of the alloy with oxygen during heating and transfer. The oxide scale cracked during extrusion, thereby preventing effective lubrication and insulation by the glass at the billet/die interface. The prevention of the formation of this oxide scale virtually eliminated any die wear and resulted in a marked improvement in the surface quality.

2) The lubricating behaviour of glass varies considerably with the extrusion temperature and can be related to the viscosity of the glass at the extrusion temperature.

3) The C6496 glass starts to provide effective lubrication at a temperature somewhere between 805°C and 843°C with the corresponding viscosities being $10^{4.53}$ and $10^{3.73}$ poise. Below this temperature range the viscosity of the glass is too high and the glass does not soften adequately during extrusion, producing an erratic distribution of glass along the extrude length. To extrude below this temperature range a lower viscosity glass will have to be employed. Alternatively, a conical die could be employed, with molybdenum disulphide grease as the lubricant.

4) The much higher viscosity of the C7216 glass at the lower extrusion temperatures make it totally unsuitable as a lubricant. It begins to afford reasonable lubrication at 945°C, corresponding to a viscosity of $10^{5.67}$, although only at higher extrusion ratios.

5) The softening point should not be used as the sole criterion in the comparison of extrusion glasses. The temperature-viscosity characteristics of the glass must also be known.

6) The extrusion ratio has a profound effect on the performance of the glass. A glass that provides effective lubrication at high extrusion ratios may well be inadequate for low extrusion ratios. This is attributed to the increased pressure and hence temperature rises produced at higher extrusion ratios.

SECTION THREE

EXPERIMENTAL AND THEORETICAL EXTRUSION ANALYSIS

4.4 EFFECT OF THE EXTRUSION VARIABLES ON THE PEAK PRESSURE

4.4.1 STARTING STRUCTURES FOR EXTRUSION

The material was provided either in the form of smooth turned billet 75 mm diameter x 100 mm long or as blocks 75 mm square x 200 mm long (section 3.1.1). Although the exact processing conditions were not known for the starting material it will typically have been forged and rolled from approximately 750 mm diameter ingot in several stages to the final product[6,7].

The microstructure was similar in both as-received products and is shown in Figure 4.35. The microstructure is well worked and it is apparent from the large volume fraction of alpha phase and its relatively equiaxed morphology that the material was finish worked well below the transus temperature. Compared to the as-received bar used for the torsion test pieces (Figure 4.1) the structure is not as well refined. This is due to the greater amount of deformation given to the torsion stock in rolling to 25 mm diameter bar.

The starting structures for extrusion were evaluated as described in section 3.4. The transition temperature was evaluated to be 1012.5 $\pm$ 2°C. This is approximately 15°C above the transition temperature for the torsion material. Although no chemical analysis was available for the torsion material, it will presumably contain lesser amounts of the alpha stabilising element aluminium or greater amounts of the beta stabilising vanadium than the extrusion material.

The proportions of alpha and beta at the extrusion temperatures employed are shown in Table 4.17. As would be expected from the higher transition temperature the extrusion starting structures contain a larger proportion of alpha phase for a given temperature than the

FIGURE 4.35

AS RECEIVED

BILLET MICROSTRUCTURE

FIGURE 4.36

TYPICAL STARTING STRUCTURE FOR EXTRUSION

IN THE ALPHA+BETA REGIME

FIGURE 4.37

TYPICAL STARTING STRUCTURE FOR EXTRUSION

IN THE BETA REGIME

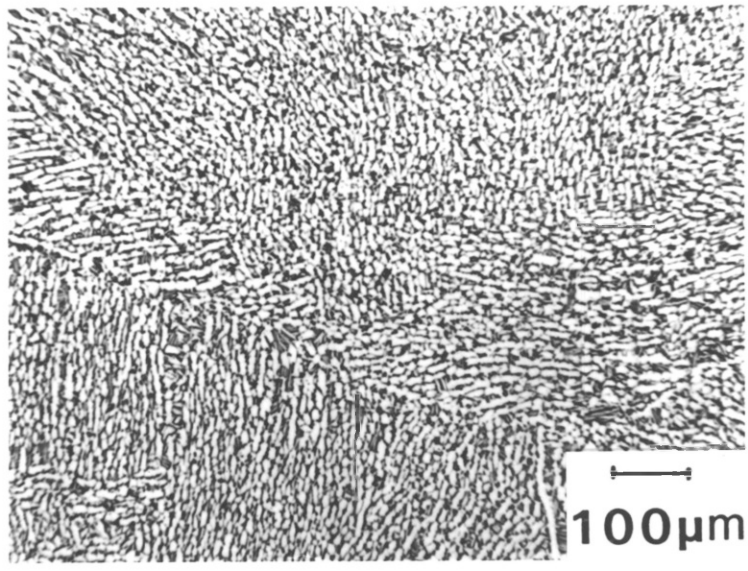
100μm

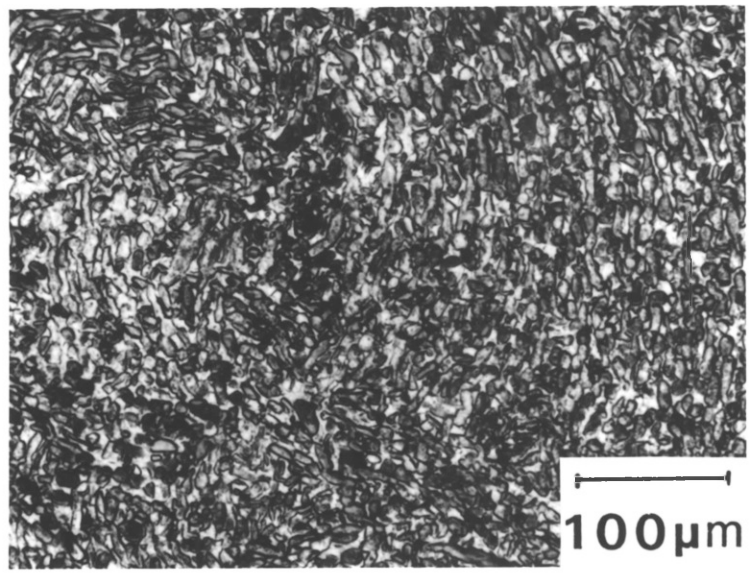
100μm

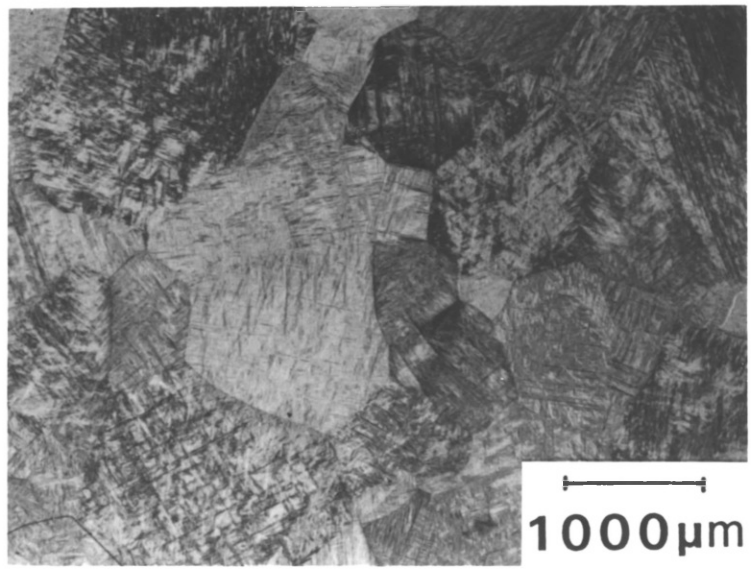
1000μm

Temperature °C	% Alpha	% Beta
850	54	46
900	41	59
950	25	75
1000	6	94

TABLE 4.17 VARIATION IN THE PERCENTAGE OF ALPHA AND BETA PHASES WITH TEMPERATURE FOR THE EXTRUSION STARTING MATERIAL

Temperature °C	Beta Grain Size µm
1050	851
1100	932
1150	991

TABLE 4.18 VARIATION IN BETA GRAIN SIZE WITH TEMPERATURE FOR THE EXTRUSION STARTING MATERIAL

torsion starting structures (Table 4.1). It should be noted that 1000°C is in the alpha+beta regime for the extrusion material and in the beta regime for the torsion material.

In the beta regime the grain size increases with increasing temperature (Table 4.18), however the grain sizes are substantially coarser (by a factor of 3 times) than the torsion starting structures (Table 4.2). This is because the torsion material was heated using induction heating, while the extrusion billets were heated in an electric furnace, the former having a total heating time of 10 minutes and the latter 1 hour. As a result the grain growth in the extrusion material was much greater. With the acquisition of a new induction heater, similar heating and holding times will be possible for extrusion and torsion, so that the starting structures will be more similar.

Similar variations in structures with temperature were observed in extrusion to those obtained in torsion. Typical starting structures in the alpha+beta and beta regimes are shown in Figures 4.36 and 4.37. The huge variation in microstructure on moving from the alpha+beta to the beta regime is again apparent.

4.4.2 EFFECT OF THE EXTRUSION VARIABLES ON THE PRESSURE REQUIRED FOR EXTRUSION

4.4.2.1. EXTRUSION DATA RECORDING

The extrusion data was recorded as described in section 3.1.5. The extrusion stroke can be essentially described by plotting the ram speed, ram travel, hydraulic pressure and load cell pressure versus time, as shown in Figures 4.38 and 4.39 which are typical traces for low and high temperature runs respectively. The main features of the two traces are plotted together for comparison in Figure 4.40.

An auxiliary pump enabled a fast ram approach prior to the commencement of extrusion. When the ram hit the pressure pad and the pressure in the main cylinder exceeded 0.69 MNm^{-2}, the pump was

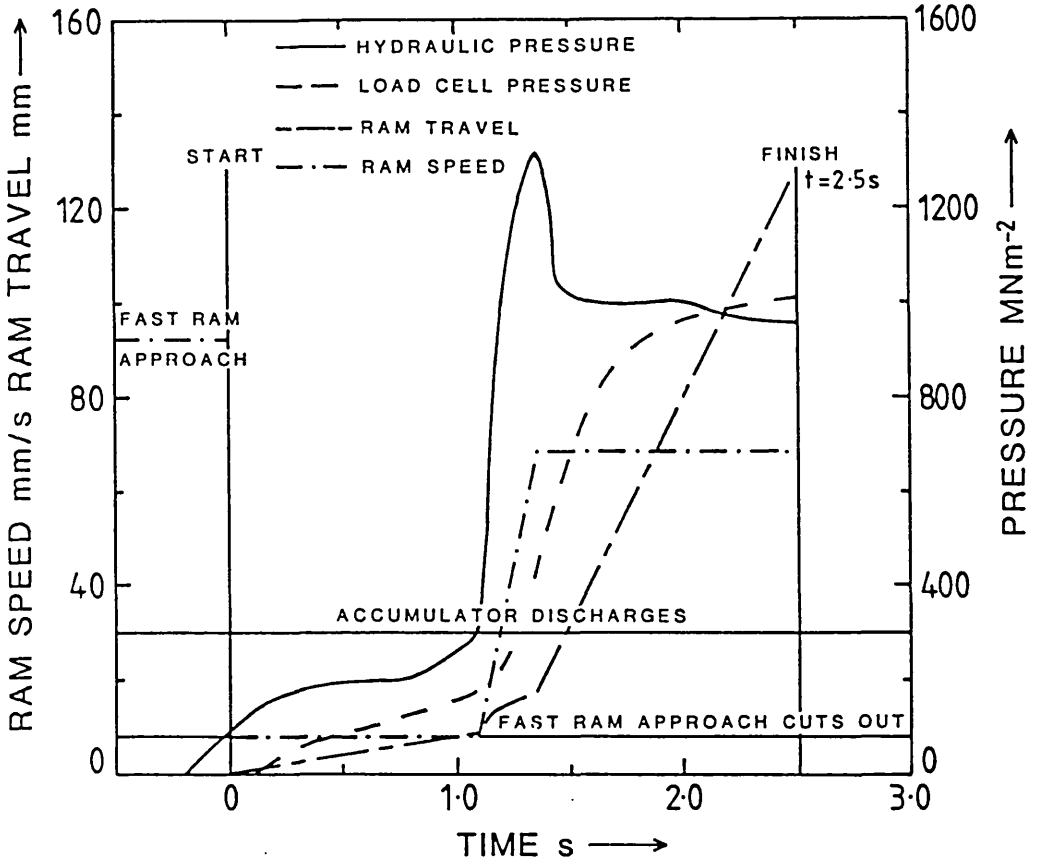

Figure 4.38 HYDRAULIC PRESSURE, LOAD CELL PRESSURE, RAM TRAVEL AND RAM SPEED VARIATION DURING THE EXTRUSION STROKE FOR A TYPICAL LOW TEMPERATURE RUN (T=850°C,R=20:1)

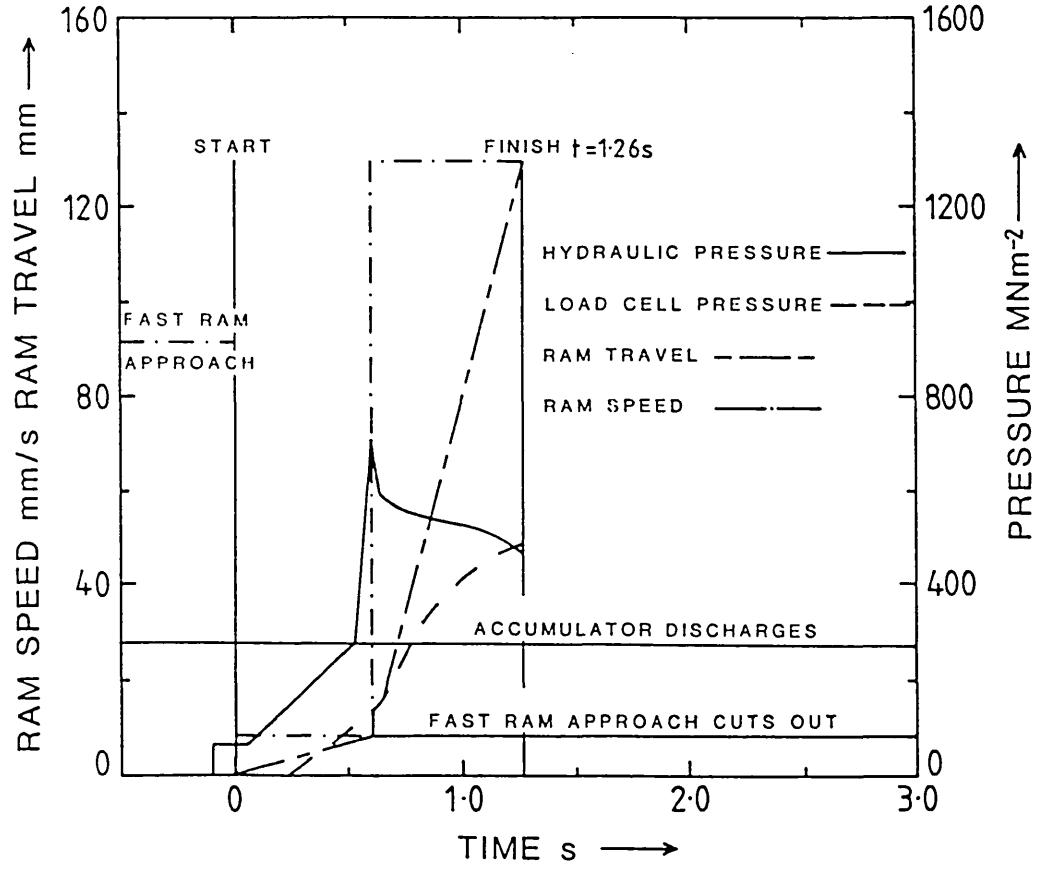

Figure 4.39 HYDRAULIC PRESSURE, LOAD CELL PRESSURE, RAM TRAVEL AND RAM SPEED VARIATION DURING THE EXTRUSION STROKE FOR A TYPICAL HIGH TEMPERATURE RUN (T=1100°C,R=20:1)

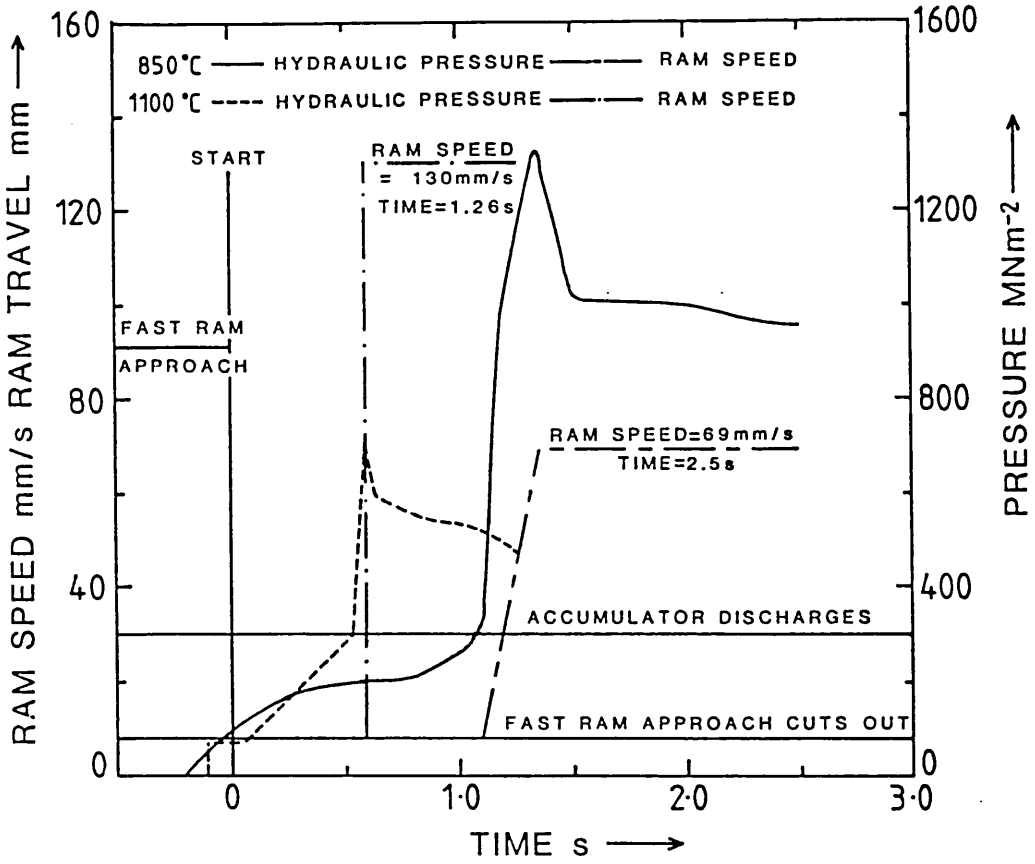

Figure 4.40 COMPARISON OF TYPICAL HIGH AND LOW TEMPERATURE EXTRUSIONS

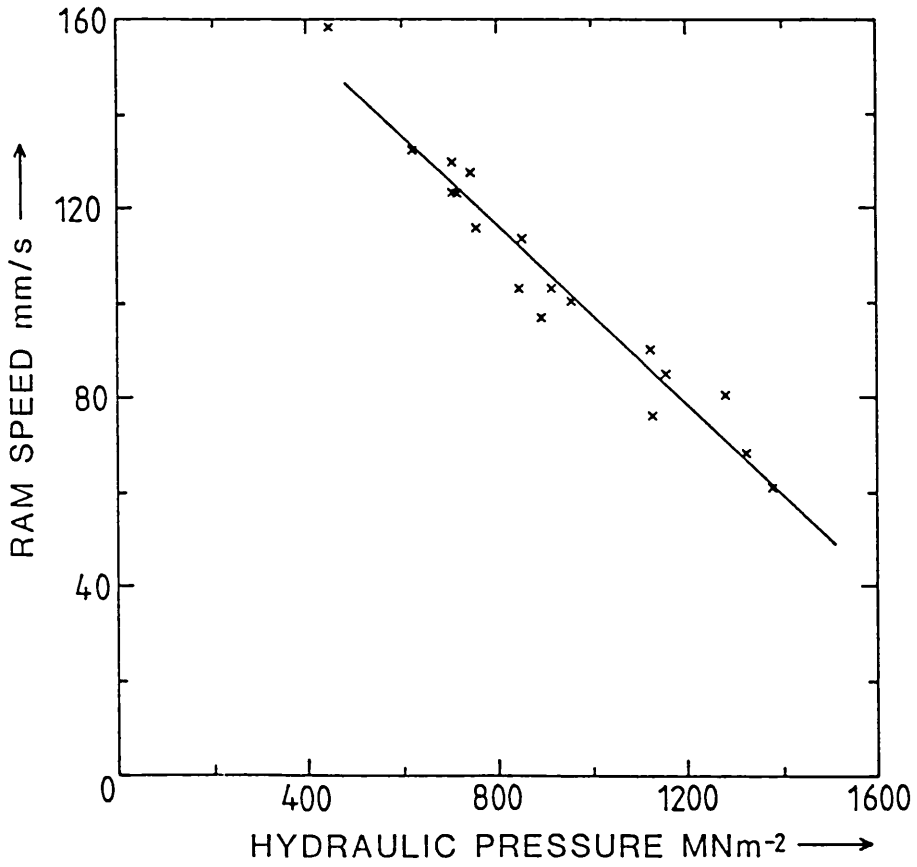

Figure 4.41 RAM SPEED VS. HYDRAULIC PRESSURE

automatically bypassed, and the ram slowed down. When the pressure reached 3.45 MNm^{-2} in the main cylinder, the accumulator drive was activated, with four nitrogen filled cylinders discharging, resulting in a very high rate of oil delivery to the main ram. The hydraulic pressure rises very rapidly to a peak, and the ram speed increases dramatically. A constant ram speed was maintained until the ram hit the rings, whereupon the pumps were reversed and the ram raised.

The following points should be noted:-

1) A time delay exists between the fast ram approach cutting out and the accumulator discharging. This is because the pressure has to build up to a value of 3.45 MNm^{-2} before the accumulator drive is activated. The length of this time interval increases with decreasing temperature (Appendix III).

2) The ram speed cannot be preset, but varies inversely with the hydraulic pressure (Figure 4.41). A linear relationship exists, given by :-

   RAM SPEED (mm/sec) = 192.8 - 0.0948 [HYDRAULIC PRESSURE MNm^{-2}]

   Hence decreasing the temperature and increasing the extrusion ratio results in a reduced ram speed.

   Hence at lower temperatures, the longer time intervals before the accumulator is discharged in combination with the lower ram speeds results in longer times for extrusion (Appendix III).

3) The hydraulic pressure does not truly represent the extrusion pressure due to turbulence and friction losses. The load cell pressure measured by a transducer situated behind the ram gives a much more accurate reading, the peak load cell pressure being approximately 73% of the peak hydraulic pressure. The peak load cell pressure is the extrusion pressure used throughout the thesis. The load cell pressure increases continuously throughout the stroke, reaching a peak at the end of extrusion. This type of trace is untypical of that normally observed for glass lubricated extrusion

in which a rapid rise to peak pressure occurs followed by a fall to a steady state pressure (section 1.3.3.5). This can be explained in terms of the different temperature charges occurring during extrusion and is discussed in a later section.

The pressure employed in the extrusion analysis is the peak load cell pressure which is that obtaining at the end of extrusion. The value of the pressure is governed more by the temperature at the end of extrusion rather than that at the start. However, the temperature changes occurring during extrusion are extremely difficult to predict. Consideration of this subject is given in a later section, however for the purposes of highlighting trends, the temperature employed will be that obtaining at the commencement of extrusion.

4.4.2.2 EXTRUSION PARAMETER MEASUREMENT

The following parameters were recorded for each extrusion run. The results are given in Appendix III.

1) Run Code (P) indicates a partial extrusion
2) Furnace Temperature
3) Initial Temperature at Commencement of Extrusion
4) Extrusion Ratio
5) Glass Type
6) Cooling Medium - Water quenched or Air cooled
7) Die Number (n) indicates nth extrusion through die
8) Peak Load Cell Pressure
9) Peak Hydraulic Pressure
10) Ram Speed
11) Time until Accumulator is Activated
12) Total Time to Extrude Billet

4.4.2.3 VARIATION OF PEAK PRESSURE WITH TEMPERATURE

Although for an initial temperature of 1050°C, the cooling that occurs during transfer takes the average billet temperature into the alpha+beta regime (Table 3.3), the overall behaviour of the material at this temperature is more typical of beta extruded, rather than alpha+beta extruded material, and so this temperature will be included in the beta regime results.

The relationship between the peak pressure and temperature is shown in Figure 4.42, only the results for new dies being given. A linear relationship exists between the peak pressure and temperature in the alpha+beta regime for all extrusion ratios,the pressure increasing markedly with decreasing temperature as the proportion of alpha phase increases. This confirms the observations made in torsion that the flow stress is markedly dependent on temperature in the alpha+beta regime. Assuming a relationship of the form $P = a + bT$, the values of a and b are given in Table 4.19.

It should be noted, however, that the ram speed approximately doubles on moving from 850°C to 1000°C in the alpha+beta regime as a result of the reduced pressure requirements, which will obviously influence the slope of the lines. This change of ram speed can be accommodated in the temperature compensated strain rate (see section 4.4.2.5).

In the beta regime, as discussed in section 4.3.1, the die wear is particularly severe and the peak pressures obtained will be significantly altered compared to the condition of no die wear. In addition, the type of glass employed significantly alters the severity of the die wear and hence the peak pressure, and accounts for the erratic distribution of points in the beta regime. This prevents any satisfactory correlation between temperature and pressure in the beta regime, however, to obtain some idea of the general trend, a best straight line can be drawn through the points. A marked change in slope is apparent compared to the alpha+beta regime, as was predicted from torsion theory. Hence in the single phase beta regime, the

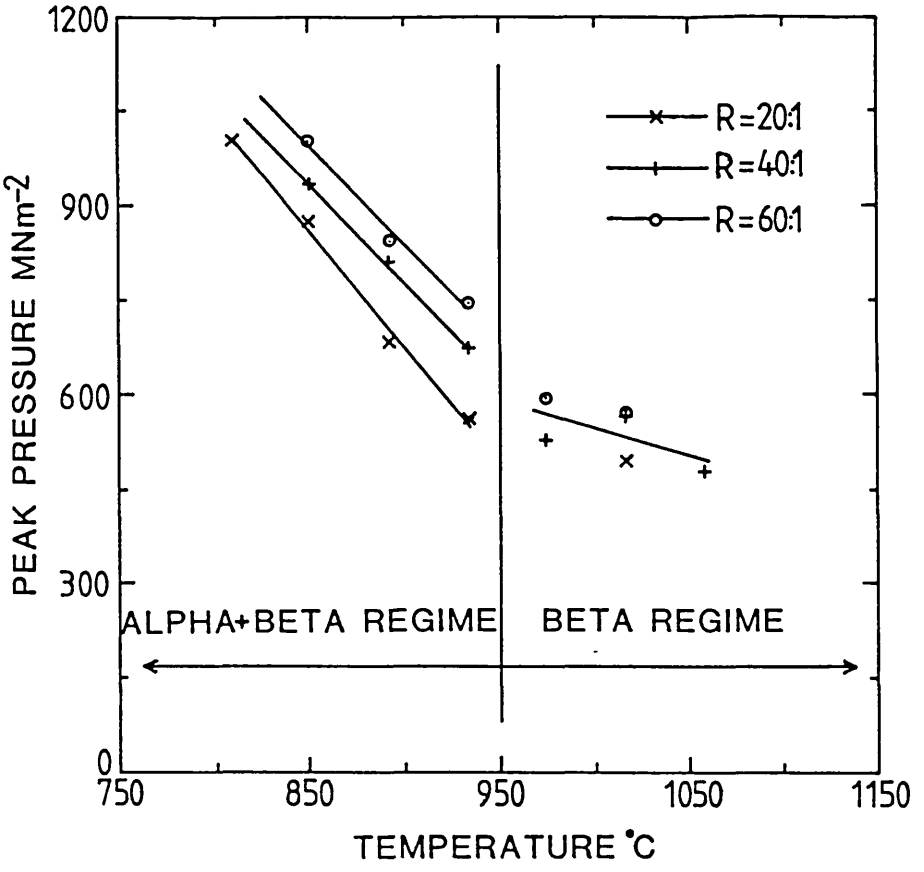

Figure 4.42 PEAK PRESSURE VS. TEMPERATURE

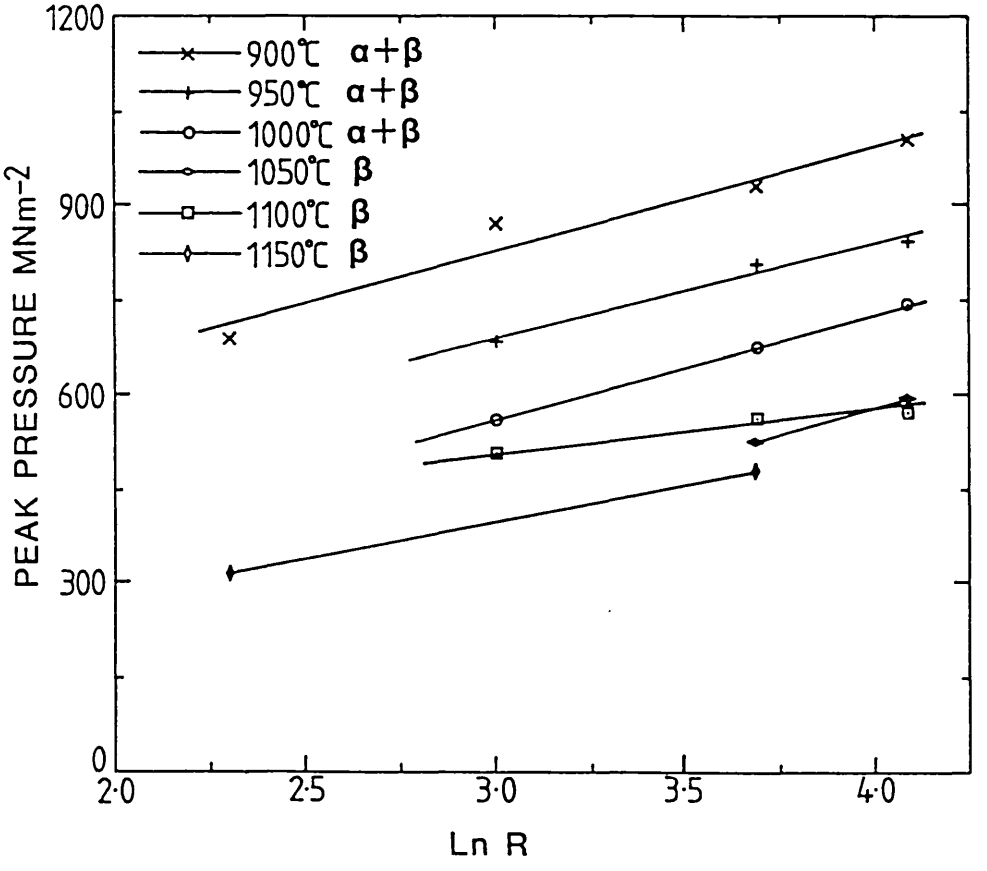

Figure 4.43 PEAK PRESSURE VS. LN EXTRUSION RATIO

Extrusion Ratio	P = a + bT		Correlation Coefficient
	a	b	
20	3973.8	- 3.663	0.997
40	3578.9	- 3.108	0.999
60	3640.3	- 3.111	0.992

TABLE 4.19 PEAK PRESSURE-TEMPERATURE RELATIONSHIPS IN THE ALPHA+BETA REGIME

Temperature °C	P = a + b ln R		Correlation Coefficient
	a	b	
900	331.4	165.9	0.975
950	237.0	150.6	0.987
1000	54.17	168.4	0.999

TABLE 4.20 PEAK PRESSURE-LN EXTRUSION RATIO RELATIONSHIPS IN THE ALPHA+BETA REGIME

Extrusion Ratio	P = a + b ln Z		Correlation Coefficient
	a	b	
20	- 4281.8	85.10	0.997
40	- 3582.1	74.75	0.999
60	- 3636.5	76.59	0.996

TABLE 4.21 PEAK PRESSURE-LN Z RELATIONSHIPS IN THE ALPHA+BETA REGIME

temperature dependence of pressure is markedly reduced, highlighting the small influence of beta grain size on the extrusion pressure.

Similar temperature-pressure trends were also observed by Gurney and Male in their work on the extrusion of Ti-6Al-4V[30].

4.4.2.4 VARIATION OF PEAK PRESSURE WITH EXTRUSION RATIO

The effect of the extrusion ratio on the peak pressure is shown in Figure 4.43, only the results for new dies being employed. As would be expected an increase in extrusion ratio results in an increase in pressure. A linear relationship exists between peak pressure and ln R for each temperature in the alpha+beta regime, the slopes being approximately constant. Assuming a relationship of the form $P = a + b \ln R$, the results for a and b are given in Table 4.20.

In the beta regime, although an increase in pressure with extrusion ratio is apparent at each temperature, the die wear has again confused the issue, preventing satisfactory correlation.

4.4.2.5 VARIATION OF PEAK PRESSURE WITH THE Z-PARAMETER

The z-parameters (equation 1.2) combines the elements of temperature and strain rate and hence the variability of ram speed with extrusion pressure can be allowed for. The equations for z in the two regimes are :-

$$z = \dot{\varepsilon} \exp\left(\frac{521,697}{RT}\right) \quad \text{in the alpha+beta regime} \qquad 4.1$$

$$z = \dot{\varepsilon} \exp\left(\frac{169,962}{RT}\right) \quad \text{in the beta regime} \qquad 4.2$$

The strain rate was evaluated as described in section 2.4 and the temperature was that obtaining at the commencement of extrusion. The values of z are given in Appendix III.

The variation of peak pressure with ln z in the alpha+beta regime is shown in Figure 4.44. A linear relationship is apparent for each extrusion ratio, the statistical data being given in Table 4.21.

In the beta regime no satisfactory correlation was obtained between the peak pressure and ln z because of the problems of die wear. The results are shown in Figure 4.45 for new dies.

4.4.2.6 VARIATION OF P/σ WITH ln R

It has been shown in the previous section that separate relationships exist between the peak pressure and ln z for each extrusion ratio. The next step therefore is to relate the pressure to all the extrusion variables by a single relationship. It has been shown from axisymmetric upper bound analysis that a linear relationship exists between P/σ and ln R (section 4.5.1) given by

$$P/\sigma = a + b \ln R \qquad 4.3$$

where σ is the flow stress and (a + b ln R) takes into account the work for homogeneous deformation and redundant work.

Verification of the relationship can be obtained by evaluating σ from the hot working equation[72]:-

$$\sigma = \frac{1}{\alpha} \ln \left| \left(\frac{z}{A}\right)^{\frac{1}{n}} + \left\{ \left(\frac{z}{A}\right)^{\frac{2}{n}} + 1 \right\}^{\frac{1}{2}} \right| \qquad 4.4$$

where A, α and n and Q in the z-parameter are obtained from torsion testing. The values of σ and P/σ are given in Appendix III and plotted in Figures 4.46 and 4.47 for the alpha+beta and beta regimes respectively. The temperatures employed were those obtaining at the commencement of extrusion.

A reasonably good linear fit exists in the alpha+beta regime, the equation being

$$\frac{P}{\sigma_I} = 0.945 + 0.527 \ln R \qquad \text{c.c.} = 0.957 \qquad 4.5$$

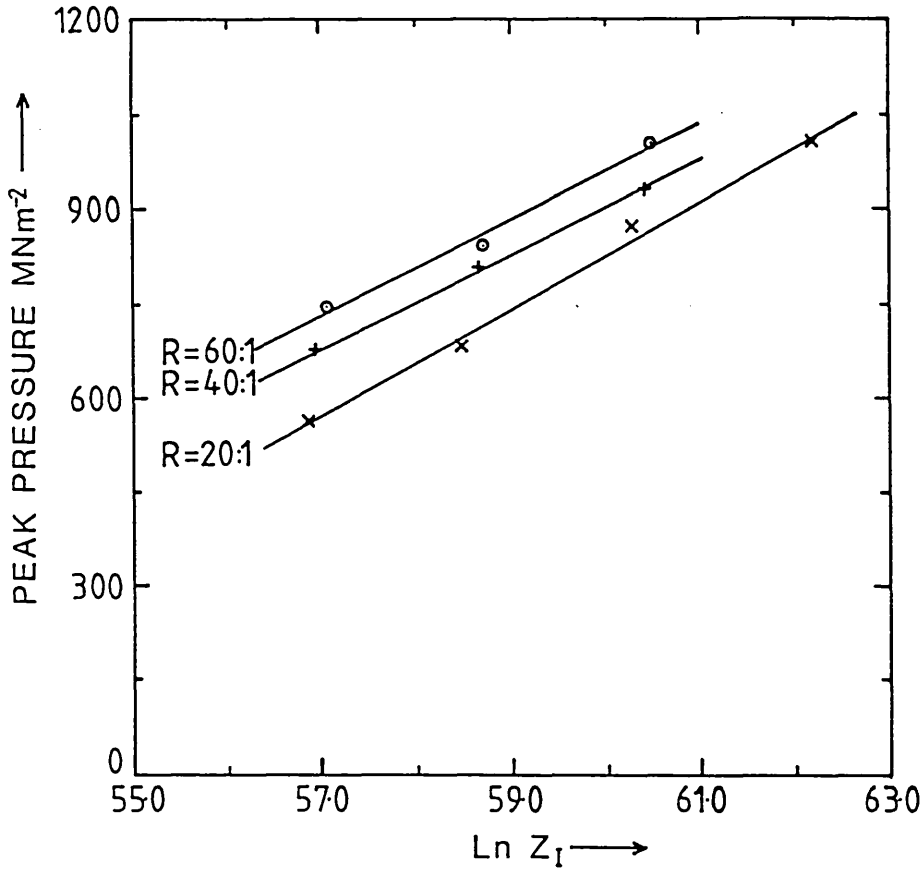

Figure 4.44 PEAK PRESSURE VS. LN Z_I IN THE ALPHA+BETA REGIME

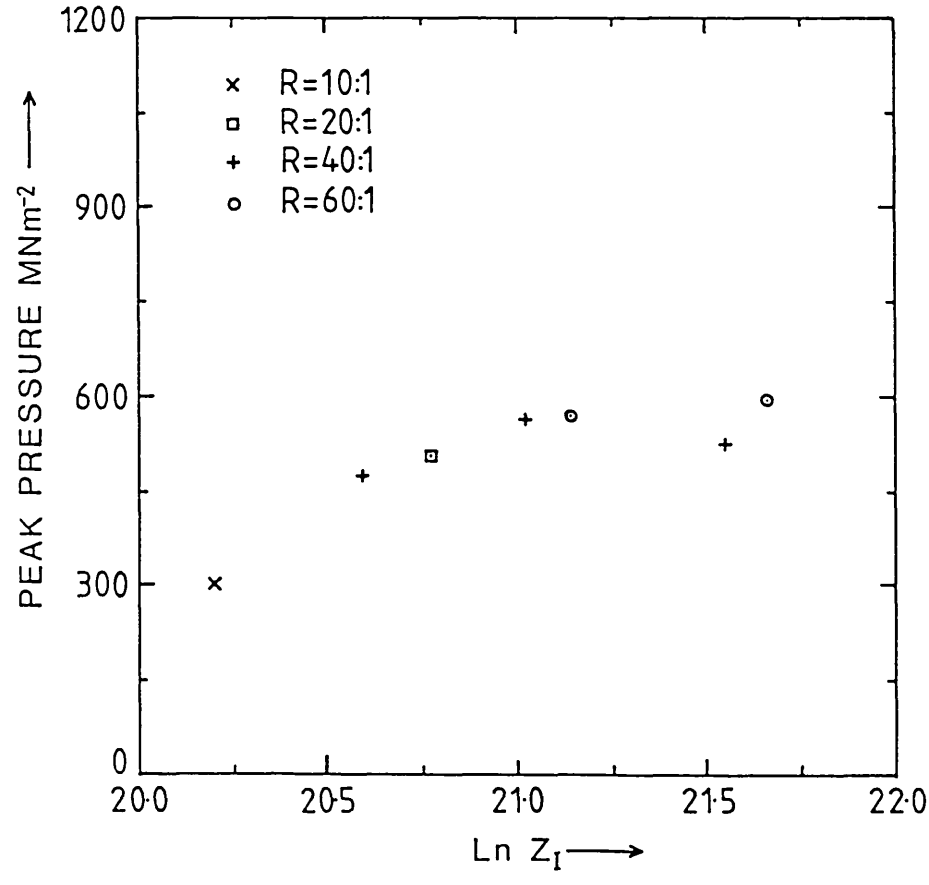

Figure 4.45 PEAK PRESSURE VS. LN Z_I IN THE BETA REGIME

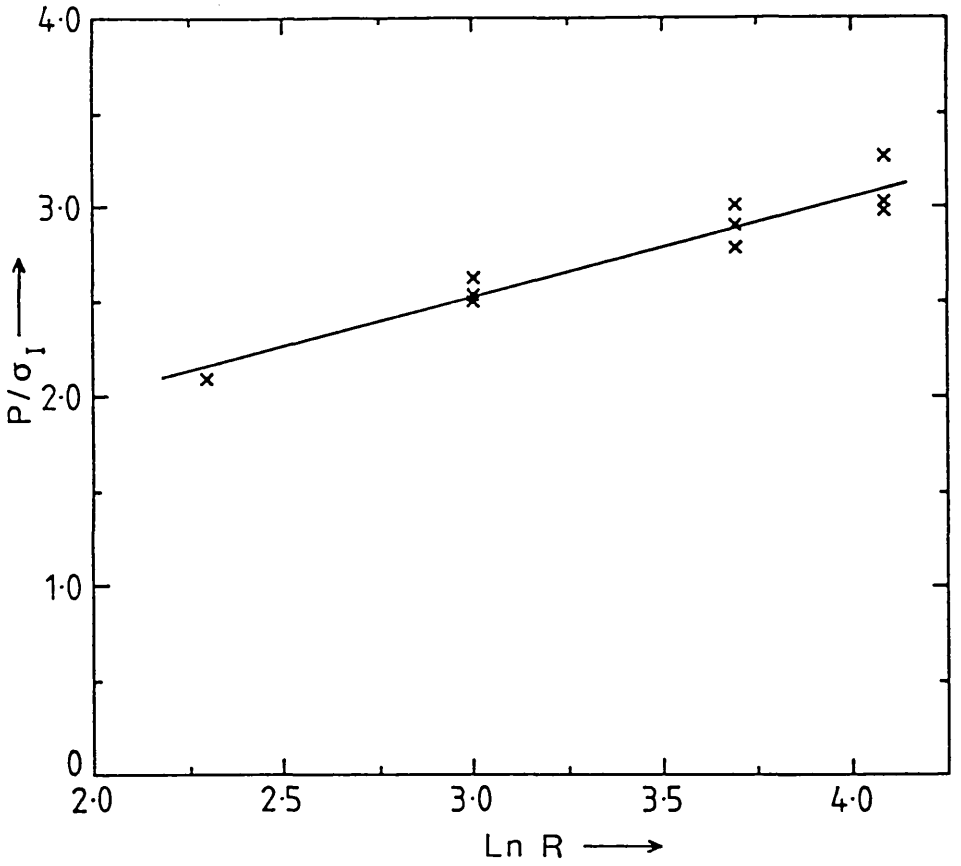

Figure 4.46 P/σ_I VS. LN R IN THE ALPHA+BETA REGIME

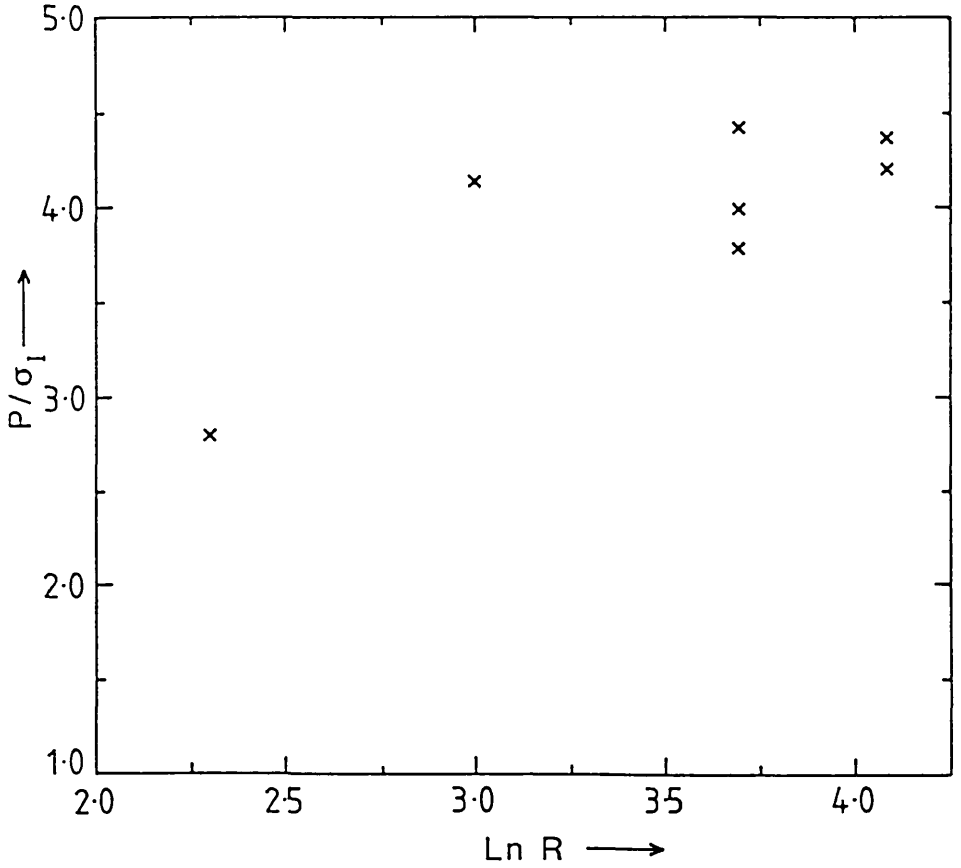

Figure 4.47 P/σ_I VS. LN R IN THE BETA REGIME

It should be remembered, however, that no allowance has been made in σ for temperature changes occurring during extrusion. This is discussed in a later section.

In the beta regime as would be expected a very large scatter of results occurs due to the influence of die wear on the extrusion pressure.

Thus a single line relationship has been obtained in the alpha+ beta regime to relate the extrusion pressure to the extrusion variables of temperature, strain rate and extrusion ratio through the temperature compensated strain rate z and the hot working constants obtained from torsion testing.

4.5 AXISYMMETRIC UPPER BOUND ANALYSIS

An axisymmetric upper bound analysis has been employed in the theoretical prediction of the extrusion pressure and the mean strain rate, details of which are given in section 2.3. An indirect extrusion model was modified to allow for frictionless conditions at the billet/die interface. A single triangle velocity field was chosen to describe the deformation zone.

4.5.1 PREDICTION OF P/σ

The analysis used to predict values of P/σ for glass lubricated extrusion has been outlined in section 2.3. The theory obtained a minimized upper bound solution by varying the dimensions of the deformation zone, which implies that a reasonable representation of the deformation zone is required for an accurate result.

In order to check that the theoretical deformation zone proposed in Figure 2.1 was representative, billets were partially extruded at 900°C, 1000°C and 1100°C at an extrusion ratio of 10:1 and then sectioned and macroetched as described in section 3.1.8. The resulting macrographs are shown in Figures 4.21, 4.28 and 4.31. Figure 4.21, as

discussed earlier, is unrepresentative of glass lubricated extrusion the glass not softening adequately at this temperature.

The overlays (Figure 4.28 and 4.31) show the predicted deformation zones for fully lubricated flow (m = 0 in equation 2.11) and for sticking friction at the die face, i.e. indirect extrusion (m = 1 in equation 2.11). The dimensions of the deformation zone as defined by x_1, the depth of the deformation zone, θ, the deformation zone semi angle and the deformation zone volume are given in Table 4.22.

The closer representation to the experimentally observed deformation field is given by the fully lubricated condition which predicts a smaller deformation field compared to the sticking friction condition. For sticking friction at the die face the model predicts that the deformation zone should extend further back into the billet, which does not appear to be the case.

The deformation zone predicted for fully lubricating conditions does appear to give a reasonable representation of the observed experimental field. A more accurate prediction could be obtained by allowing for a short conical lead in and a radiused entry to the die orifice, but this would substantially increase the complexity of the problem.

The values of P/k obtained from the analysis were converted into P/σ values by application of Von Mises criterion, these being shown in Table 4.22 for fully lubricated and sticking friction conditions.

Plots of P/σ versus ln R are given in Figure 4.48 for m = 0 and m = 1. As would be expected, the values of P/σ are higher in the indirect extrusion case due to shearing at the billet/die interface. A linear relationship exists in both cases the equations of the best straight lines being

$$m = 0 \qquad P/\sigma = 1.486 + 1.091 \ln R \qquad \text{c.c.} = 0.999 \qquad 4.6$$

$$m = 1 \qquad P/\sigma = 1.321 + 1.639 \ln R \qquad \text{c.c.} = 0.999 \qquad 4.7$$

Extrusion Ratio	Fully Lubricated Extrusion m = 0				Sticking Friction m = 1			
	P/σ	x_1 mm	θ	Volume mm^3	P/σ	x_1 mm	θ	Volume mm^3
10	4.03	16.83	59.4	1.29×10^4	5.14	23.19	50.9	1.77×10^4
20	4.71	14.26	63.4	1.53×10^4	6.17	20.48	54.3	1.65×10^4
40	5.49	12.02	67.1	1.00×10^4	7.33	17.81	58.0	1.48×10^4
60	5.99	10.80	69.2	9.1×10^3	8.08	16.55	59.9	1.38×10^4

TABLE 4.22 PREDICTED VALUES OF P/σ AND DEFORMATION ZONE DIMENSIONS FROM UPPER BOUND FOR FULLY LUBRICATED AND STICKING FRICTION CONDITIONS

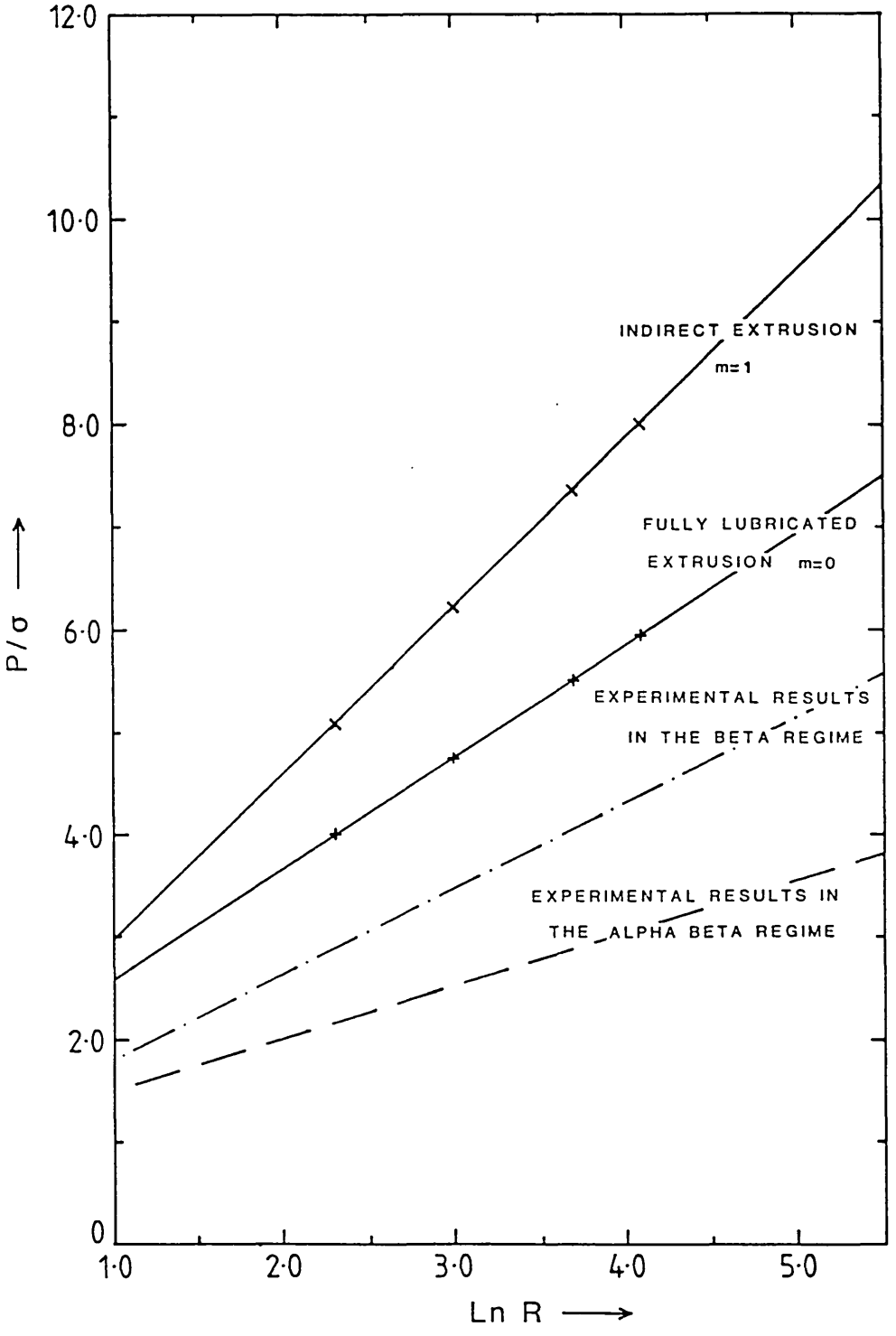

Figure 4.48 P/σ VS. LN R - THEORETICAL PREDICTIONS FROM UPPER BOUND ANALYSIS AND EXPERIMENTAL RESULTS

Also included in the Figure are the corresponding experimental values of P/σ_I, obtained as described in section 4.4.2.6, in the alpha+beta and beta regimes. Although a large scatter was observed in the beta regime, a best straight line has been drawn through the points to indicate their relative positions to the theoretical lines.

The experimental values in the alpha+beta regime are approximately half the predicted values for fully lubricated extrusion. Substantial temperature rises occurred during extrusion, however, as will be discussed in a later section, and these will tend to decrease σ and hence increase the P/σ values, taking them closer to the theoretical, fully lubricated line. The values in the beta regime lie closer to the theoretical lines, however the temperature rises are much less in this case, and hence the values of P/σ more closely represent their true values.

4.5.2 EVALUATION OF THE STRAIN RATE DURING EXTRUSION

The average strain rate during extrusion was evaluated using the modified Feltham equation as described in section 2.4. The values of $(a + b \ln R)$ and the deformation zone semi-angle θ were obtained from the upper bound analysis (Table 4.22). Hence a linear relationship exists between strain rate and ram speed for each extrusion ratio as shown in Figure 4.49 for conditions of full lubrication and sticking friction at the die face. The multiplying factors for conversion of ram speed in mm/sec to strain rate are given in Table 4.23.

Extrusion Ratio	Multiplying Factor	
	m = 0	m = 1
10	0.797	0.740
20	1.043	0.951
40	1.402	1.266
60	1.691	1.492

TABLE 4.23 MULTIPLYING FACTORS FOR CONVERSION OF RAM SPEED IN MM/SEC INTO FELTHAM'S STRAIN RATE FOR m = 0 AND m = 1

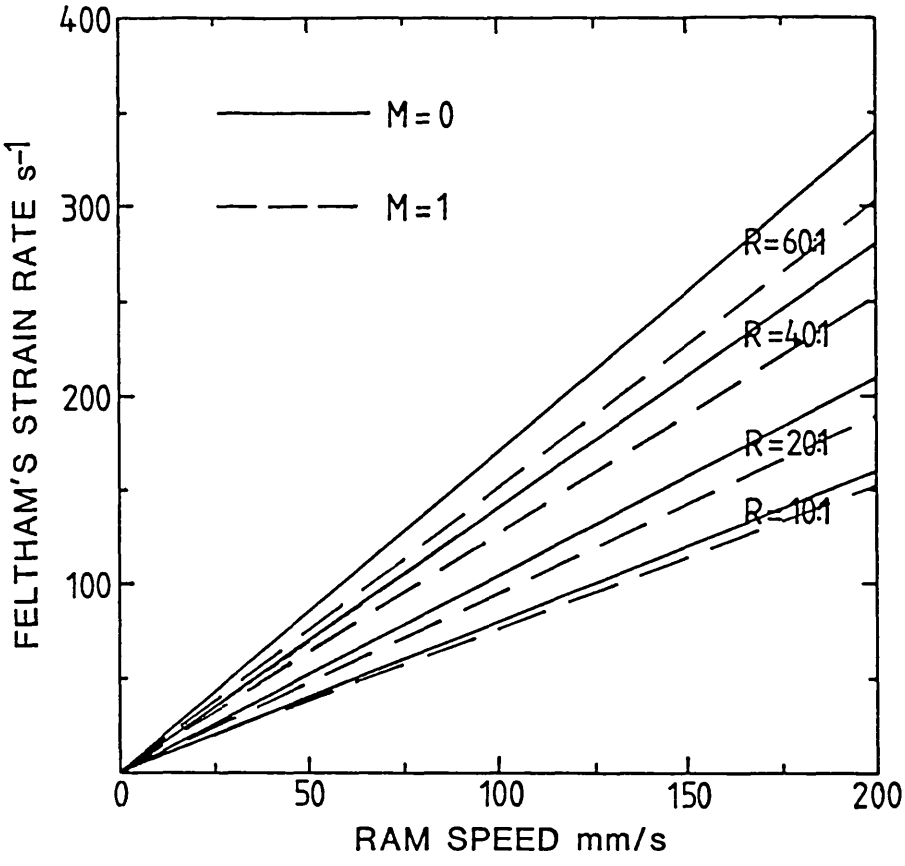

Figure 4.49 FELTHAM'S STRAIN RATE VS. RAM SPEED FOR VARYING EXTRUSION RATIO AT m = 0 AND m = 1

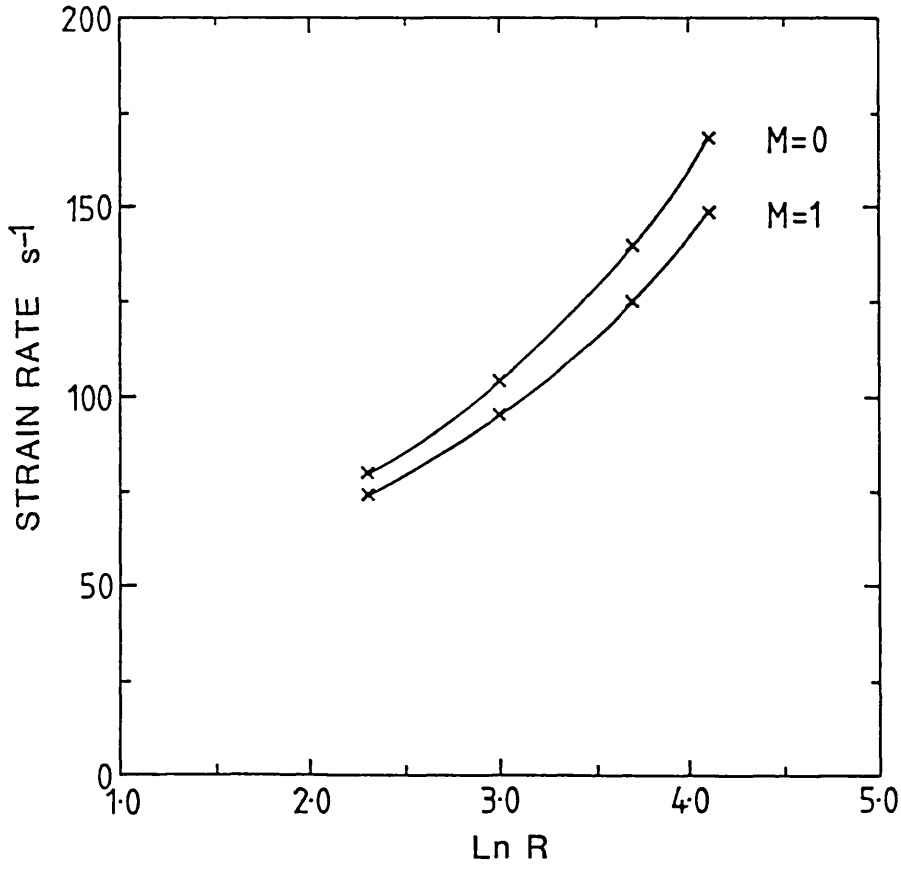

Figure 4.50 FELTHAM'S STRAIN RATE VS. LN R FOR m = 0 AND m = 1 AT A RAM SPEED OF 100 mm/sec

The predicted strain rates are lower in the sticking friction case as a result of the larger deformation zone volume (Table 4.22) outweighing the increased strain contribution. The variation of strain rate with extrusion ratio is shown in Figure 4.50 at a ram speed of 100 mm/s, which is typical of the values obtained in the extrusion programme. A non-linear increase in strain rate with extrusion ratio is apparent, the increase being associated with a decrease in the deformation zone volume.

Because the theoretical deformation field for fully lubricated extrusion gave a closer approximation to the experimentally observed deformation zone, the value of the strain rate for fully lubricated extrusion was employed in the extrusion analysis. The values of strain rate for each run are given in Appendix III, varying from 68.6 s^{-1} at low ram speeds and low extrusion ratios, to 200 s^{-1} at high ram speed and high extrusion ratio.

4.6 TEMPERATURE CHANGES OCCURRING DURING EXTRUSION

4.6.1 INTRODUCTION

All the relationships presented in the previous sections have taken no account of temperature changes during extrusion. The temperature compensated strain rate z and the flow stress σ are both strongly dependent on temperature and hence any substantial temperature changes occurring during extrusion will markedly alter their values. In addition, the pressure required for extrusion and the structure and properties of the alloy will be altered by temperature changes occurring during the stroke.

Unfortunately, accurate prediction of the temperature changes occurring during extrusion in extremely difficult because of the large number of variables involved and the difficulty of definition of some of the parameters. Only a limited success has been achieved in predicting the temperature changes occurring during extrusion using the analysis described in section 2.5. These results are presented in the following discussion, and the problems with the analysis outlined.

4.6.2 THE LOAD-DISPLACEMENT CURVE

In evaluating the heat generated during extrusion the area under the load-displacement curve has to be evaluated as discussed in section 2.5.2.

Typical load-displacement curves for high and low temperatures are shown in Figure 4.51 to illustrate the selection of data from the traces. The data presented is for initial temperatures of 850°C and 1100°C at an extrusion ratio of 20:1. Figures 4.38 to 4.40 also refer to the same extrusion conditions and these should also be referred to in the following discussion.

As discussed in section 4.4.2.1 a finite time exists between the ram impacting the pressure pad and the accumulator discharging and represents typically 50% of the total extrusion time. Hence the heat changes occurring during this interval have to be considered.

During this time interval the ram moves very slowly, the glass pad is compacted and the billet is upset to fill the container. Only a small increase in load and displacement occurs, particularly at high temperatures (Figure 4.47) and hence the heat generated is small. The heat losses that occur in this time interval have also been assumed to be small as the billet is not in direct contact with the container until the billet is upset. Thus the temperature changes occurring in the time prior to the accumulator discharging are assumed to be negligible which considerably simplifies the analysis. When the accumulator is discharged the ram speed accelerates very rapidly and a constant ram speed is maintained throughout the remainder of the extrusion.

Hence in the analysis employed, extrusion was assumed to start when the accumulator discharged (dotted lines in Figure 4.51). The remainder of the load-displacement curve was split into 10 increments of equal time and the area under the load-displacement curve evaluated in each increment as discussed in section 2.5.2.

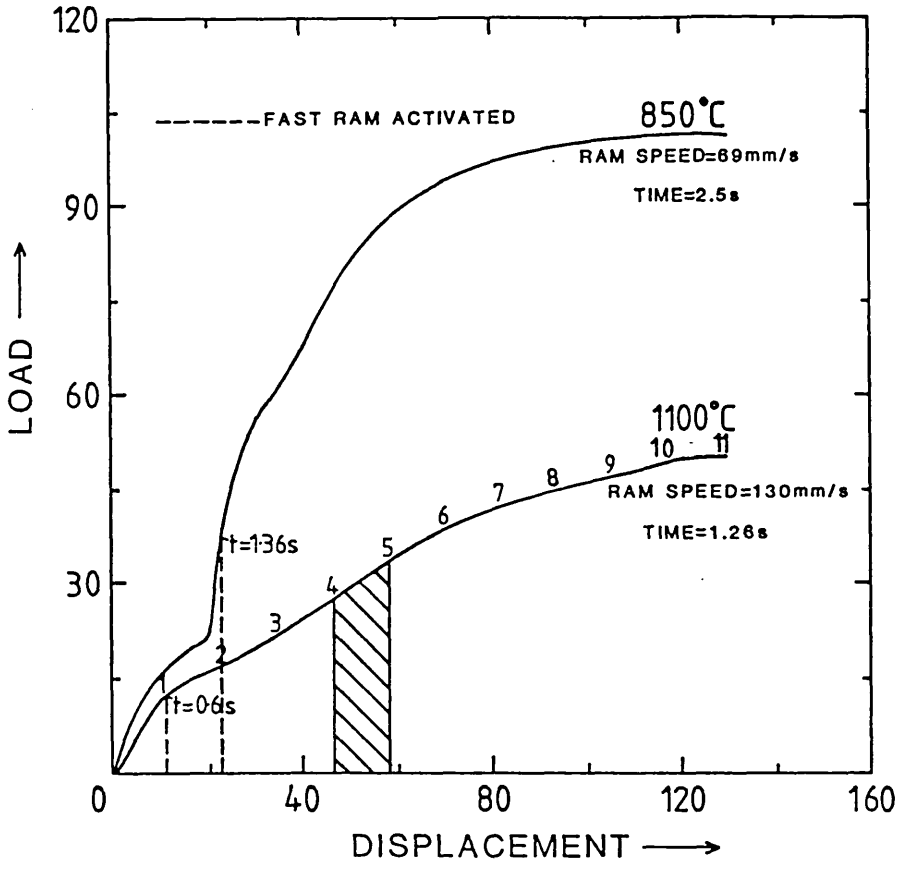

Figure 4.51 COMPARISON OF LOAD VS. DISPLACEMENT CURVES FOR TYPICAL HIGH AND LOW TEMPERATURE EXTRUSIONS TO ILLUSTRATE SELECTION OF DATA FOR TEMPERATURE RISE MODEL

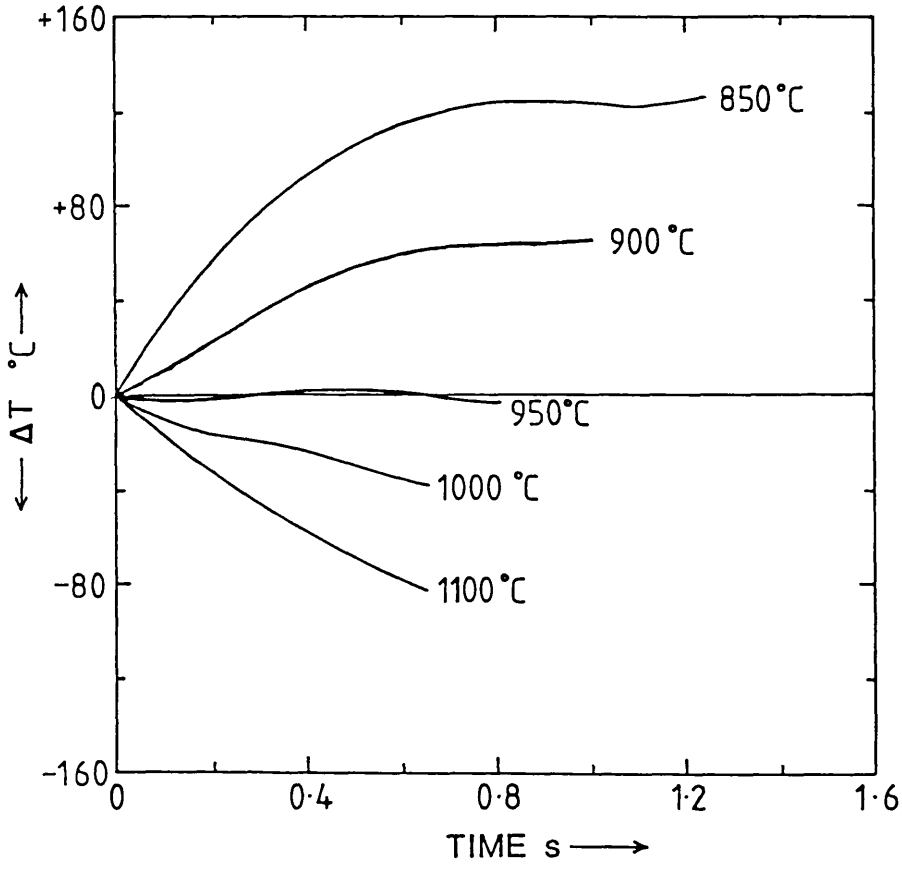

Figure 4.52 PREDICTED TEMPERATURE CHANGES OCCURRING DURING THE EXTRUSION STROKE FOR DIFFERENT INITIAL TEMPERATURES

Two points are immediately obvious from the load-displacement curves. The area under the load-displacement curve is much greater at lower temperatures and hence the heat generated will be much greater. Balanced against this the slower speeds encountered at lower temperatures will increase the time for heat losses to occur.

The predicted temperature changes during extrusion will now be discussed.

4.6.3 TEMPERATURE RISE PREDICTIONS

The temperature rise predictions for new dies are given in Appendix III and summarised in Table 4.24. Two conditions were considered :-

(a) A glass pad at the billet/die interface. The glass thermal constants were therefore employed in the equations for Q_1 and Q_3 (equations 2.23 and 2.28). The glass pad was assumed to be at the temperature of the die (= 350°C).

(b) No glass pad at the billet/die interface, i.e. direct contact occurs between the billet and die. This is allowed for by replacing the glass thermal constants with those for the die steel in the equations for Q_1 and Q_3. This condition is assumed to be approached when the glass does not soften adequately during extrusion and is pushed out of the die before the extruding metal (section 4.3.3.1).

These two conditions should therefore provide an upper and lower limit to the temperature rises occurring during extrusion.

Considering first the trends predicted by the temperature rise model. The change in temperature in the deformation zone throughout the extrusion stroke, and hence the resultant variation in temperature along the extrude length, for different initial temperatures is shown in Figure 4.52. The results are for an extrusion ratio of 20:1, with a glass pad at the die face. The extrusion times are longer at lower temperatures because of the lower ram speeds obtained.

Run Code	Extrusion Ratio	Furnace Temperature °C	Initial Temperature °C	Glass Pad		No Glass Pad	
				Final Temp.	Temp. Rise	Final Temp.	Temp. Rise
1	20	850	810	937	+ 127	868	+ 58
5	10	900	851	856	+ 5	804	- 47
6	20	900	851	918	+ 67	856	+ 5
8	40	900	851	942	+ 91	872	+ 21
10	60	900	851	972	+ 121	894	+ 43
11	20	950	893	889	- 4	833	- 60
13	40	950	893	930	+ 37	867	- 26
15	60	950	893	936	+ 43	868	- 25
17	20	1000	934	896	- 38	842	- 92
19	40	1000	934	921	- 13	861	- 74
21	60	1000	934	957	+ 23	890	- 44
23	40	1050	974	908	- 66	851	- 124
24	60	1050	974	938	- 36	876	- 98
26	20	1100	1016	933	- 83	874	- 142
28	40	1100	1016	949	- 67	887	- 129
29	60	1100	1016	955	- 61	891	- 125
30	10	1150	1058	909	- 149	856	- 203
32	40	1150	1058	965	- 93	902	- 156

TABLE 4.24 PREDICTED TEMPERATURE RISES OCCURRING DURING EXTRUSION WITH AND WITHOUT A GLASS PAD AT THE DIE FACE

At low temperatures an increase in temperature is predicted during extrusion, the heat generated due to deformation work outweighing the heat losses to the tooling. The temperature rise is rapid initially, but remains essentially constant over the latter part of the extrusion. This explains the shape of the load-displacement curve obtained at low temperatures (Figure 4.51), the load flattening off towards the end of the extrusion.

At high initial temperatures a continuous temperature fall is predicted during extrusion, the lower extrusion pressures resulting in a smaller heat generation term, this being outweighed by the heat losses to the tooling. This explains the continuous increase in load with displacement at high extrusion temperatures (Figure 4.51).

At intermediate temperatures, a balance occurs between the heat generated and the heat lost so that an essentially isothermal extrusion is achieved.

The variation in the predicted temperature rise with extrusion ratio, with a glass pad at the die face, is shown in Figure 4.53. The higher pressures required at higher extrusion ratios result in an increased heat generation term, so that larger temperature rises are predicted for higher extrusion ratios. The predicted variation in temperature rise with extrusion ratio is substantial with a temperature difference of 120°C between R = 10:1 and R = 60:1 at an initial temperature of 900°C.

The influence of the glass pad on the temperature rises occurring during extrusion is shown in Figure 4.54. As would be expected, the glass pad substantially reduces the heat lost to the die resulting in an increased temperature rise (or reduced temperature fall) during extrusion of approximately 60°C.

The total individual heat losses $Q_1 - Q_7$ are shown in Table 4.25 for typical high and low temperature runs, with and without the glass pad. The individual heat losses are expressed as percentages of the total heat loss. Also shown, in Tables 4.26 and 4.27, and plotted in

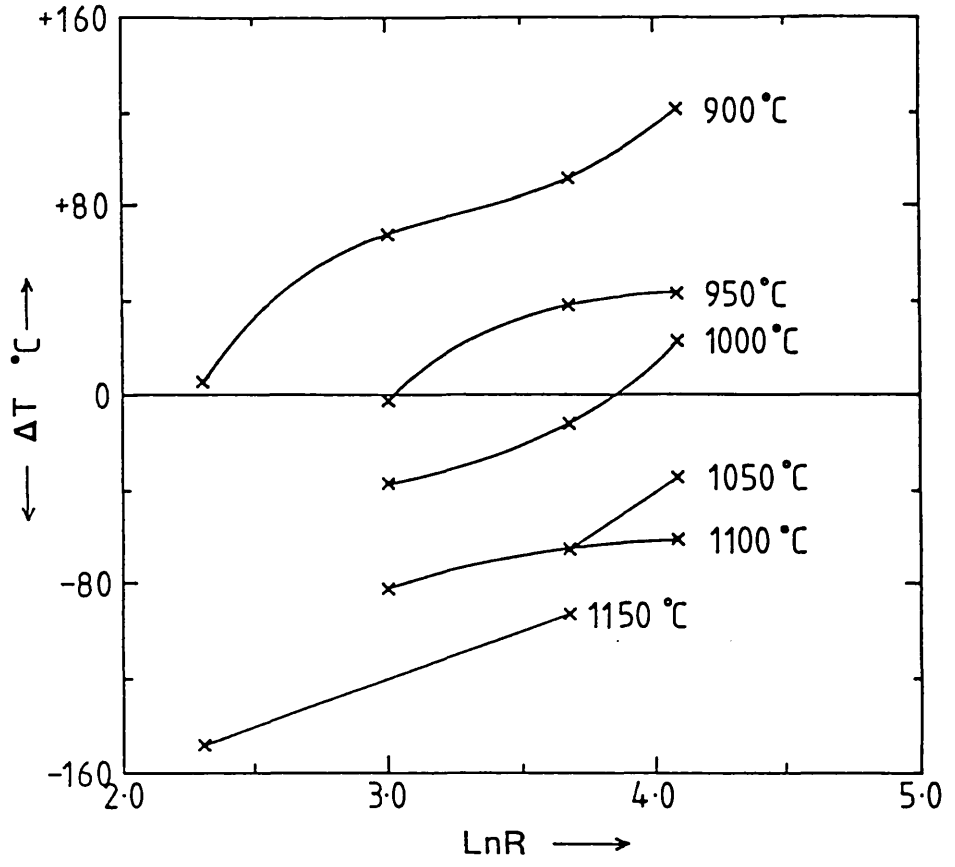

Figure 4.53 VARIATION OF PREDICTED TEMPERATURE RISE WITH EXTRUSION RATIO FOR DIFFERENT INITIAL TEMPERATURES

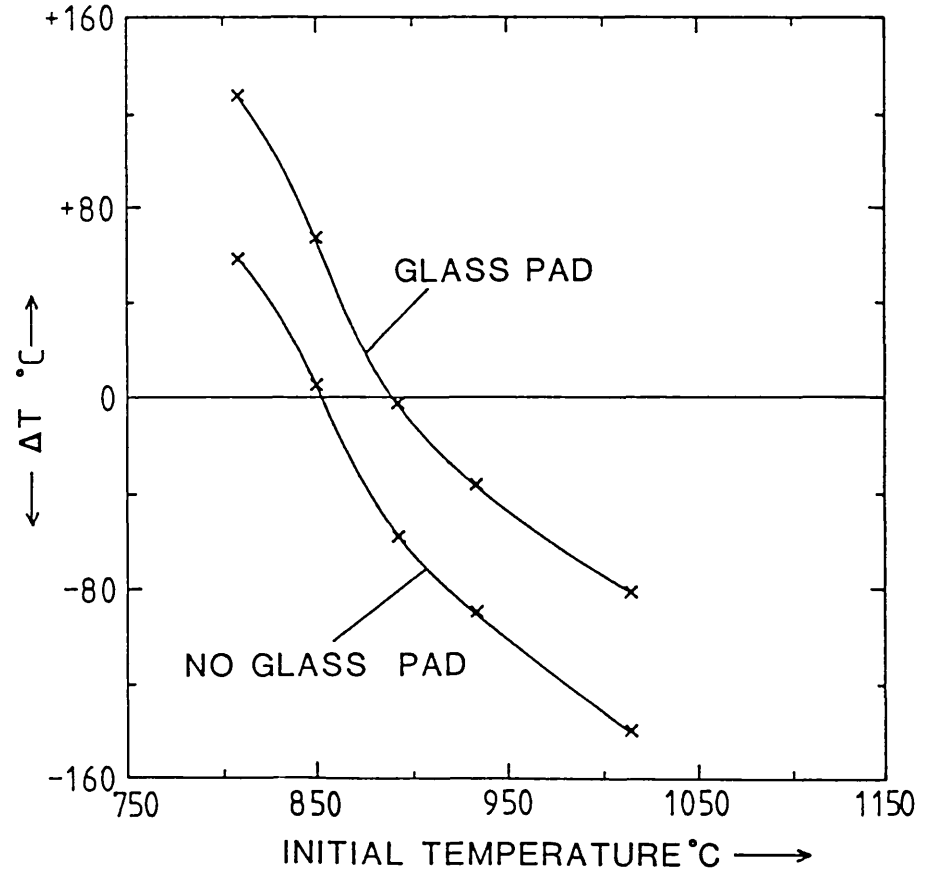

Figure 4.54 VARIATION OF PREDICTED TEMPERATURE RISE WITH INITIAL TEMPERATURE WITH AND WITHOUT THE GLASS PAD

Individual Heat Losses	Low Temperature T = 850°C R = 20:1		High Temperature T = 1100°C R = 20:1	
	With Glass Pad %	No Glass Pad %	With Glass Pad %	No Glass Pad %
Q_1	7.6	19.95	7.7	19.9
Q_2	28.3	24.25	30.0	26.2
Q_3	2.6	6.1	2.8	6.2
Q_4	13.4	10.9	9.0	7.0
Q_5	27.1	25.7	47.1	45.6
Q_6	13.0	12.1	15.5	14.6
Q_7	8.0	1.0	-12.1	-19.5

TABLE 4.25 INDIVIDUAL HEAT LOSSES FOR TYPICAL HIGH AND LOW TEMPERATURE EXTRUSIONS WITH AND WITHOUT THE GLASS PAD

Time S	Glass Pad				No Glass Pad			
	Deformation Zone Temperature Rise °C	Undeforming Zone Temperature Rise °C	Temperature In Deformation Zone °C T_I = 810°C	Temperature In Undeforming Zone °C T_I = 810°C	Deformation Zone Temperature Rise °C	Undeforming Zone Temperature Rise °C	Temperature In Deformation Zone °C T_I = 810°C	Temperature In Undeforming Zone °C T_I = 810°C
0.12	37.1	- 27.8	847.1	782.4	25.9	- 27.6	836.0	782.4
0.25	67.1	- 59.1	877.1	750.9	45.4	- 59.3	855.4	750.7
0.37	89.7	- 90.7	899.7	719.3	59.0	- 91.5	869.0	718.5
0.49	105.6	- 120.5	915.7	689.6	67.1	- 122.2	877.1	687.8
0.62	116.0	- 147.1	926.0	662.9	70.8	- 150.2	880.8	659.8
0.74	121.7	- 169.7	931.7	640.3	70.9	- 174.8	880.9	635.2
0.87	124.2	- 187.6	934.2	622.4	68.5	- 195.5	878.5	614.5
0.99	124.2	- 200.2	934.2	609.9	64.2	- 211.7	874.2	598.3
1.11	122.3	- 205.6	932.3	604.4	58.6	- 222.3	868.6	587.7
1.24	126.6	-	936.6	-	57.7	-	867.7	-

TABLE 4.26 VARIATION IN TEMPERATURE IN THE DEFORMING AND NON-DEFORMING ZONES DURING THE EXTRUSION STROKE FOR A TYPICAL LOW TEMPERATURE RUN (T = 850°C R = 20:1)

Time S	Glass Pad				No Glass Pad			
	Deformation Zone Temperature Rise °C	Undeforming Zone Temperature Rise °C	Temperature In Deformation Zone °C T_I = 1016°C	Temperature In Undeforming Zone °C T_I = 1016°C	Deformation Zone Temperature Rise °C	Undeforming Zone Temperature Rise °C	Temperature In Deformation Zone °C T_I = 1016°C	Temperature In Undeforming Zone °C T_I = 1016°C
0.07	- 11.6	- 36.7	1004.4	979.3	- 21.4	- 36.7	994.6	979.3
0.13	- 22.6	- 80.8	993.4	935.2	- 41.3	- 80.9	974.7	935.1
0.20	- 32.4	- 127.7	983.6	888.3	- 58.8	- 128.2	957.2	887.8
0.26	- 40.6	- 175.1	975.4	840.9	- 73.6	- 176.2	942.4	839.8
0.33	- 48.1	- 221.3	967.9	794.7	- 86.7	- 223.4	929.3	792.6
0.39	- 55.6	- 265.1	960.4	750.9	- 99.1	- 268.6	916.9	747.4
0.46	- 63.2	- 305.8	952.8	710.2	- 110.9	- 311.3	905.0	704.7
0.52	- 71.2	- 342.7	944.8	673.3	- 122.6	- 351.1	893.4	665.0
0.59	- 79.4	- 375.1	936.7	640.9	- 134.1	- 387.7	882.0	628.3
0.65	- 83.4	-	932.6	-	- 142.1	-	873.9	-

TABLE 4.27 VARIATION IN TEMPERATURE IN THE DEFORMING AND NON-DEFORMING ZONES DURING THE EXTRUSION STROKE FOR A TYPICAL HIGH TEMPERATURE RUN (T = 1100°C R = 20:1)

Figures 4.55 and 4.56, are the predicted temperature changes occurring in the deforming and non-deforming zones during the extrusion stroke for the same runs.

The values of Q_1 and Q_3, the heat losses to the die, are substantially reduced by the use of the glass pad (Table 4.25) as is reflected by the increased temperature rise in the deformation zone. The major heat losses occur from the deformation zone to the container (Q_2) and from the non-deforming zone to the container (Q_5), the latter being responsible for almost 50% of the heat losses at higher extrusion temperatures. Material is thus chilled very substantially in the non-deforming zone (Figures 4.55 and 4.56) due to direct contact between the billet and tooling, the container being at 466°C and the pressure pad at 300°C. The heat loss from the non-deforming zone is slightly reduced by the glass pad at the die face, the increased temperature rise in the deformation zone resulting in a larger back conduction term Q_4.

The variation in the incremental heat losses throughout the extrusion stroke for the same runs are given in Tables 4.28 and 4.29, and plotted in Figures 4.57 and 4.58, for the condition of a glass pad at the die face. Considering first the deformation zone; the heat losses Q_1, Q_2 and Q_3 increase during the extrusion stroke, the rate of heat loss decreasing with increasing time. The heat loss Q_7 is negative at higher temperatures due to the material leaving the deformation zone being at a higher temperature than that of the deformation zone. The heat loss Q_4 from the deforming to the non-deforming zone increases sharply with increasing time as the temperature differential between the two zones increases. In the non-deforming zone the heat loss Q_5 decreases with increasing time as the zone decreases in size. The heat loss Q_6 increases with increasing time at lower temperatures, but at high temperatures levels off after an initial increase, and starts to fall towards the end of the stroke.

The major problem with the model is the magnitude of the temperature rises it predicts. Figure 4.59 shows the variation of predicted final temperature with initial temperature at an extrusion ratio of 20:1.

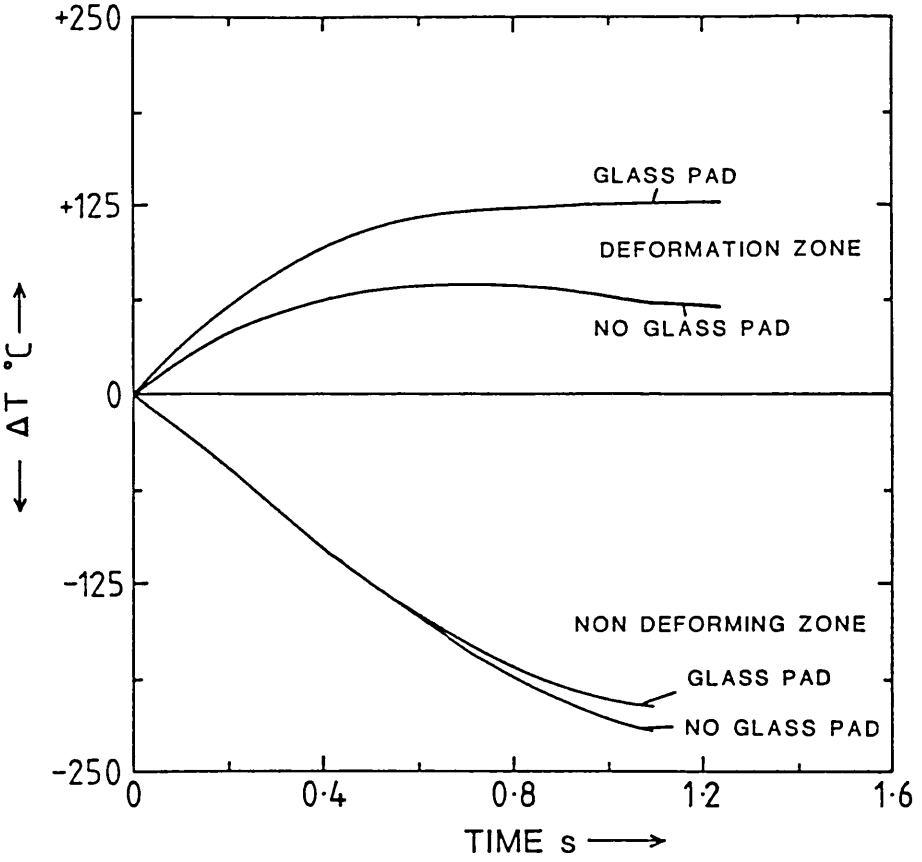

Figure 4.55 CHANGE IN TEMPERATURE IN THE DEFORMING AND NON-DEFORMING ZONES DURING THE EXTRUSION STROKE FOR A TYPICAL LOW TEMPERATURE RUN (T=850°C, R=20:1)

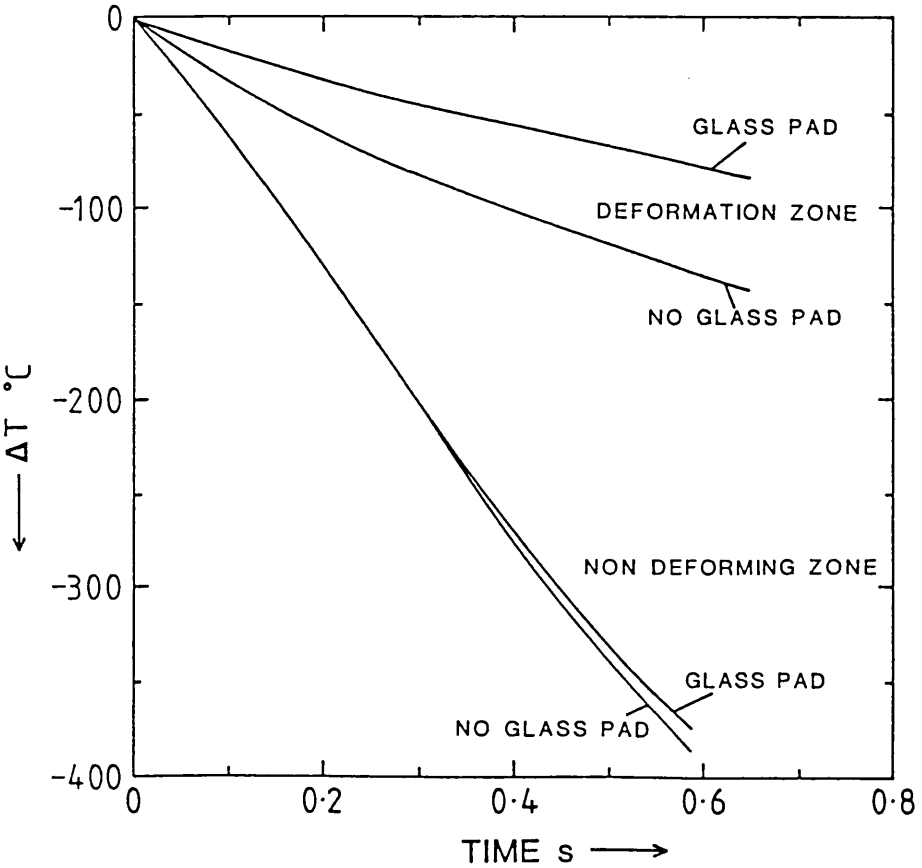

Figure 4.56 CHANGE IN TEMPERATURE IN THE DEFORMING AND NON-DEFORMING ZONES DURING THE EXTRUSION STROKE FOR A TYPICAL HIGH TEMPERATURE RUN (T=1100°C, R=20:1)

Time S	Q_1 x 10^3 J	Q_2 x 10^3 J	Q_3 x 10^3 J	Q_4 x 10^3 J	Q_5 x 10^3 J	Q_6 x 10^3 J	Q_7 x 10^3 J
0.12	0.770	3.557	0.308	0	11.40	1.985	2.119
0.25	1.154	4.893	0.430	0.684	11.57	2.530	3.450
0.37	1.474	5.931	0.529	1.663	10.47	2.804	3.934
0.49	1.749	6.778	0.613	2.784	9.009	2.953	3.704
0.62	1.990	7.480	0.685	3.937	7.566	3.044	3.003
0.74	2.200	8.063	0.746	5.046	6.312	3.124	2.015
0.87	2.384	8.562	0.800	6.058	5.313	3.225	1.021
0.99	2.547	8.982	0.847	6.941	4.588	3.384	-0.004
1.11	2.690	9.335	0.887	7.657	4.146	3.662	-1.019
1.24	2.864	10.04	0.938	0	0	7.168	2.518

TABLE 4.28 VARIATION OF INCREMENTAL HEAT LOSSES DURING THE EXTRUSION STROKE FOR A TYPICAL LOW TEMPERATURE RUN (T=850°C, R=20:1)

Time S	Q_1 x 10^3J	Q_2 x 10^3J	Q_3 x 10^3J	Q_4 x 10^3J	Q_5 x 10^3J	Q_6 x 10^3J	Q_7 x 10^3J
0.07	0.736	3.547	0.317	0	16.34	2.218	-0.688
0.13	1.022	4.495	0.407	0.211	16.88	2.823	-1.310
0.20	1.231	5.150	0.470	0.595	15.36	3.089	-1.734
0.26	1.403	5.672	0.520	1.120	13.06	3.169	-1.945
0.33	1.548	6.095	0.563	1.758	10.56	3.135	-2.205
0.39	1.674	6.434	0.598	2.469	8.173	3.035	-2.644
0.46	1.784	6.712	0.629	3.214	6.058	2.900	-3.159
0.52	1.880	6.937	0.656	3.961	4.303	2.757	-3.743
0.59	1.964	7.123	0.679	4.681	2.943	2.534	-4.304
0.65	2.058	7.448	0.705	0	0	5.028	-2.370

TABLE 4.29 VARIATION OF INCREMENTAL HEAT LOSSES DURING THE EXTRUSION STROKE FOR A TYPICAL HIGH TEMPERATURE RUN (T=1100°C, R=20:1)

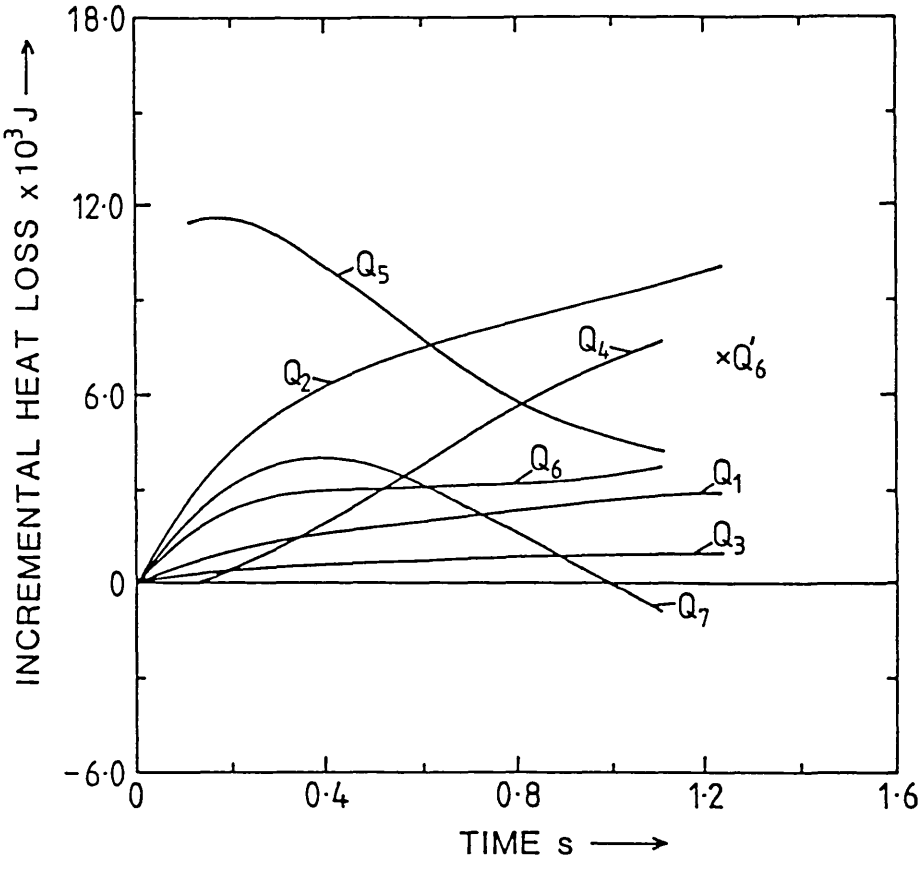

Figure 4.57 VARIATION IN THE INCREMENTAL HEAT LOSSES DURING THE EXTRUSION STROKE FOR A TYPICAL LOW TEMPERATURE RUN (T=850°C, R=20:1)

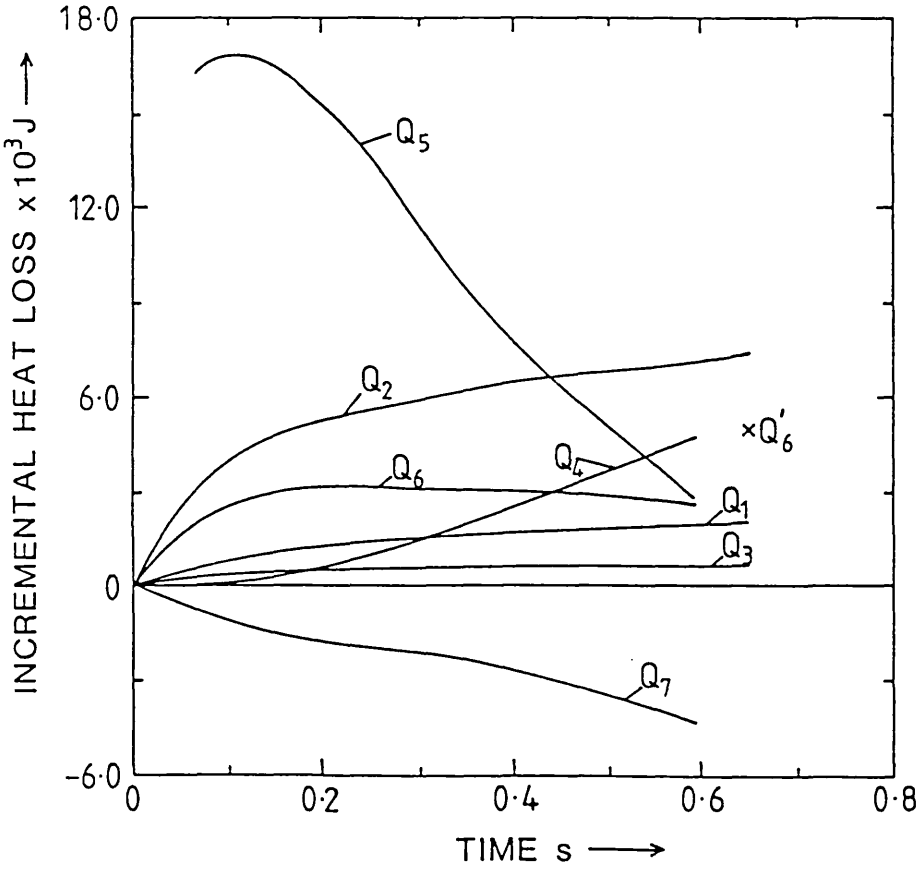

Figure 4.58 VARIATION IN THE INCREMENTAL HEAT LOSSES DURING THE EXTRUSION STROKE FOR A TYPICAL HIGH TEMPERATURE RUN (T=1100°C, R=20:1)

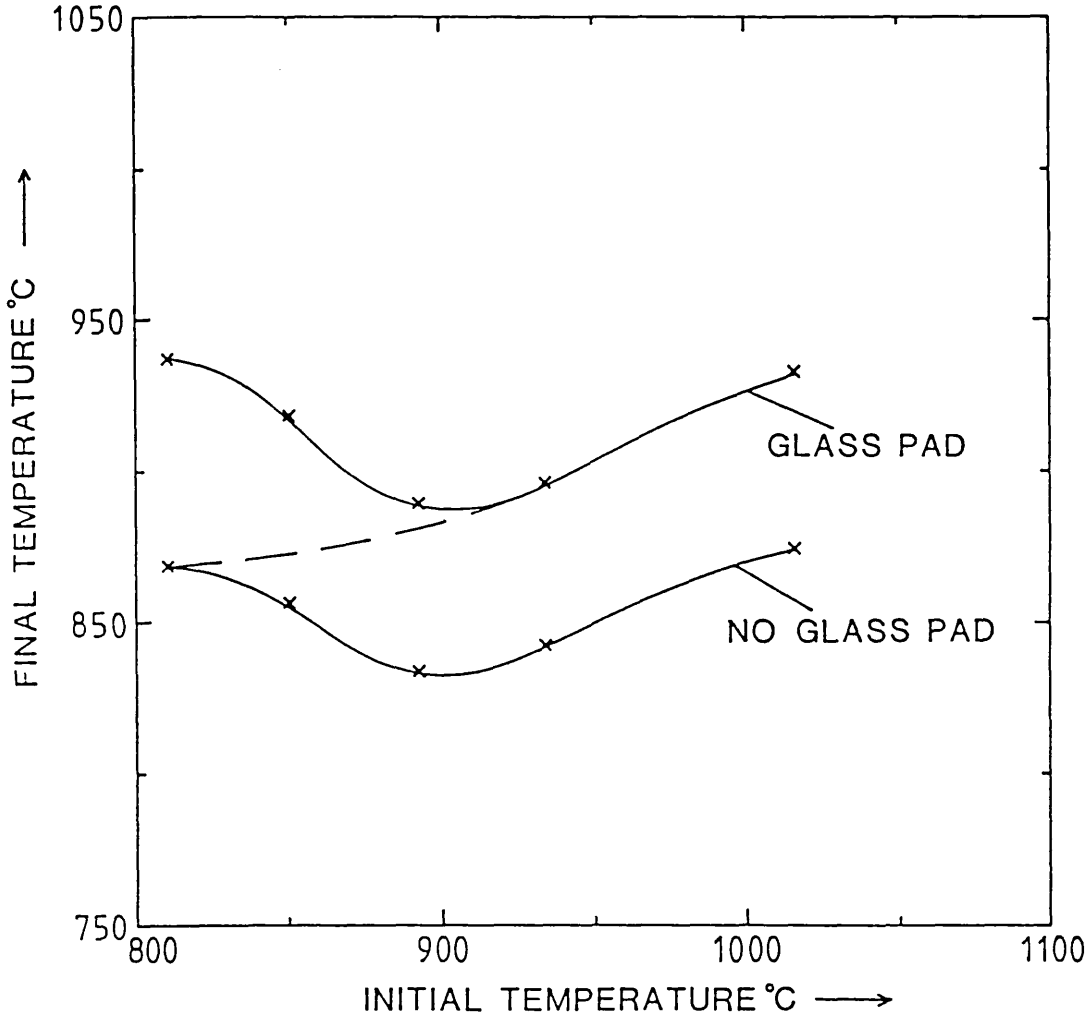

Figure 4.59 VARIATION OF FINAL TEMPERATURE WITH INITIAL TEMPERATURE AT R=20:1 WITH AND WITHOUT THE GLASS PAD

Similar trends were observed at other extrusion ratios. The model predicts that at low initial temperatures the final temperature decreases with increasing temperature. If this were the case the final pressure should be lower at lower temperatures, it being apparent from Figure 4.42 that this was not observed. At higher temperatures a more sensible trend of increasing final temperature with initial temperature is observed, which is in accord with the trend of decreasing pressure with increasing temperature.

At lower temperatures, however, the glass pad does not soften adequately during extrusion (section 4.3.3.1) with the result that the billet comes into direct contact with the die. Hence the actual final temperature should be closer to that predicted without the glass pad. The dotted line in Figure 4.59 is therefore probably a more reasonable representation of the true situation, and is in agreement with the trend of increasing pressure with decreasing initial temperature.

Even allowing for this adjustment, however, a difference in final temperatures of only 65°C is predicted between initial temperatures of 810°C and 1016°C, which is too low to account for the pressure variation.

Similar anomalies were observed in the predicted variation in temperature rise with extrusion ratio for a given initial temperature (figure 4.53). For example, at 900°C the difference in predicted temperature rise between an extrusion ratio of 10:1 and 60:1 is 116°C, which is obviously unreasonable.

4.6.4 EXPERIMENTALLY OBSERVED TEMPERATURE RISES

Some idea of the temperature changes occurring during alpha+beta extrusion can be obtained from structural studies. Since the proportions of alpha and beta depend on the temperature, any change in temperature that occurs during extrusion will be reflected in a change in proportion of these phases. In particular, if a fully transformed beta structure is produced from material extruded in the alpha+beta regime, then the temperature will have exceeded the transus (1012.5 $\pm$ 2°C) during extrusion, which enables a lower limit of the temperature rise to be obtained.

As will be apparent from the micrographs shown in the next section, very substantial temperature rises occurred during extrusion well in excess of those predicted from the model, even allowing for a glass pad at the die face. For example, at a furnace temperature of 900°C and an extrusion ratio of 40:1, the temperature at the commencement of extrusion was 851°C, with the predicted temperature midway through the stroke being 929°C, a rise of 78°C. Structural studies midway along the extrude length revealed that a fully transformed beta structure was produced, indicating that a rise of at least 160°C had occurred, approximately double the theoretical value. Thus the model, even allowing for a glass pad at the die face, which is certainly not the case at low temperatures produces an underestimate of the temperature rises occurring during extrusion.

4.6.5 THE INFLUENCE OF TEMPERATURE RISE ON THE Z-PARAMETER

The failure of the model to predict sensible values of temperature rise, means that the highly temperature dependent parameter, z, and hence the flow stress σ cannot be accurately determined as the temperature varies throughout the extrusion stroke. The marked influence of temperature on the z-parameter and flow stress in the alpha+beta regime can be illustrated from the example just used. For an initial temperature of 851°C and an extrusion ratio of 40:1, the initial z-parameter, flow stress and P/σ values are respectively 1.74×10^{26}, 335.7 MNm^{-2} and 2.78. Allowing for the observed temperature rises during extrusion of approximately 160°C, these values become 1.66×10^{23}, 121.7 MNm^{-2} and 7.66 respectively, which are very substantially different from their initial values. The P/σ value as is apparent from Figure 4.44, for $\ln R = 3.69$ is in much better agreement with the upper bound predictions, the value lying just above the sticking friction line. Obviously as the initial temperature increases the temperature rise will be reduced, so that the values of z, σ and P/σ will more nearly approach their initial values.

Thus, if accurate relationships are to be established between the extrusion pressure and the z-parameter and flow stress, a much more accurate temperature rise model is required.

4.7 SUMMARY OF THEORETICAL AND EXPERIMENTAL EXTRUSION RESULTS

1) A marked change in structure occurred on moving from the two phase alpha+beta regime to the single phase beta regime. In the two phase regime a very fine structure of alpha+beta was observed with the proportion of alpha phase increasing with decreasing temperature. In the single phase beta regime, grain growth is completely unimpeded and a very coarse grain size results, the grain size increasing with increasing temperature. The starting structure has a profound effect on the pressure required for extrusion, with markedly different behaviour being observed in the two regimes.

2) A linear relationship exists between the peak pressure and initial temperature in the alpha+beta regime for all extrusion ratios, the pressure increasing markedly with decreasing temperature as the proportion of alpha phase increases. This confirms the observations made in torsion that the flow stress is markedly dependent on temperature in the alpha+beta regime. Linear relatonships were also observed between peak pressure and ln R in the alpha+beta regime, the pressure increasing markedly with increasing extrusion ratio.

3) The die wear in the beta regime is very severe, the severity of the die wear varying with temperature, extrusion ratio and glass type. The die wear markedly influenced the values of pressure obtained, and hence a very erratic distribution of data was obtained in the beta regime which prevented the establishment of any satisfactory correlations between the peak pressure and the temperature, extrusion ratio and z-parameter. The indications were, however, that the pressure dependence of temperature was markedly reduced in the beta

regime, indicating the small influence of beta grain size on the preak pressure.

With the dramatic reduction in die wear obtained using the modified extrusion practice, any future study into titanium extrusion should allow for much more accurate relationships to to be established between the peak pressure and the extrusion variables in the beta regime.

4) Identical trends were observed in extrusion compared with those obtained in torsion and illustrates the usefulness of the simple laboratory torsion test on predicting behaviour during extrusion.

5) A linear relationship was observed between the peak pressure and ln of the temperature compensated strain rate for all extrusion ratios in the alpha+beta regime.

6) An empirical single line linear relationship was obtained in the alpha+beta regime between P/σ_I and ln R as predicted theoretically from the upper bound analysis. This enables the extrusion pressure to be predicted for any conditions of initial temperature, extrusion ratio and ram speed, using the values of the hot working constants obtained from torsion. The equation is given by :-

$$P/\sigma_I = 0.945 + 0.527 \ln R \qquad \text{c.c.} = 0.957$$

7) All the relationships established took no account of any temperature changes occurring during extrusion. This is because the temperature rise model employed failed to give reasonable predictions of the temperature rises occurring during extrusion and hence accurate temperature compensated relationships could not be established.

8) Some idea of the temperature rises occurring during extrusion was obtained from structural studies. These indicated that the actual temperature rises occurring during extrusion were well in excess of those predicted using the model. Using these experimentally determined estimates of the temperature rise, temperature compensated values of z, σ and P/σ were evaluated, and were found to be markedly different from their initial values, the deviation increasing with increasing temperature rise.

9) The temperature rise model does, however, give some insight into the factors influencing the temperature changes occurring during extrusion.

   (a) It highlights the effect of the glass pad on reducing heat losses to the die, this being reflected in an increased temperature rise in the deformation zone.

   (b) It gives some idea of the relative magnitude of the individual heat losses occurring during extrusion and how they vary throughout the extrusion stroke.

10) The theoretical deformation zone predicted from the upper bound analysis for fully lubricated extrusion, gives a reasonable representation of the experimentally observed deformation field.

11) A linear relationship exists between the theoretical values of P/σ and ln R for fully lubricated and sticking friction conditions. The latter values of P/σ are higher due to the additional term of energy dissipation due to shearing across the die face.

12) The strain rate was evaluated using the modified Feltham equation, with values of $(a + b \ln R)$ and $\tan \theta$ obtained from the upper bound solution for fully lubricated extrusion. The resultant values of strain rate varied from 68.6 s^{-1} at low ram speeds and low extrusion ratios to 200 s^{-1} at high ram speeds and high extrusion ratios.

SECTION FOUR

4.8 STRUCTURE AND PROPERTIES OF EXTRUDED Ti-6Al-4V

4.8.1 INTRODUCTION

In this section the relationship between the structure and properties of extruded Ti-6Al-4V and the extrusion variables will be discussed in both the alpha+beta and beta regimes. The extrudes were both water quenched and air cooled after extrusion to investigate the effect of cooling rate on the structure and properties.

Optical microscopy was employed to categorize the extrusion structures, with transmission electron microscopy being used predominantly to identify the dynamic restoration mechanisms operative during extrusion.

The properties were evaluated using a standard tensile test. The structure and properties were related to the extrusion variables through the z-parameter, using the values of temperature and strain rate obtaining at the commencement of extrusion.

4.8.2 OPTICAL MICROSCOPY

4.8.2.1 VARIATION OF STRUCTURE WITH THE EXTRUSION VARIABLES

4.8.2.1.1 VARIATION OF STRUCTURE WITH EXTRUSION TEMPERATURE

The variation in structure with the extrusion temperature at an extrusion ratio of 20:1 is shown in Figure 4.60 for both air-cooled and water quenched extrusions. Longitudinal sections are shown, the specimens being taken midway along the extrude length. The micrographs were taken at the centre of the extrude at a magnification of x 75. The temperatures employed throughout are the furnace temperatures, with the temperatures at the commencement of extrusion being given in Appendix III. Temperatures from 850°C to 1000°C represent alpha+ beta extrusion, while temperatures above this range represent beta extrusion.

(a)

850°C WATER QUENCHED

(b)

850°C AIR COOLED

FIGURE 4.60

VARIATION OF STRUCTURE WITH TEMPERATURE

AT R = 20:1

(c)

900°C WATER QUENCHED

(d)

900°C AIR COOLED

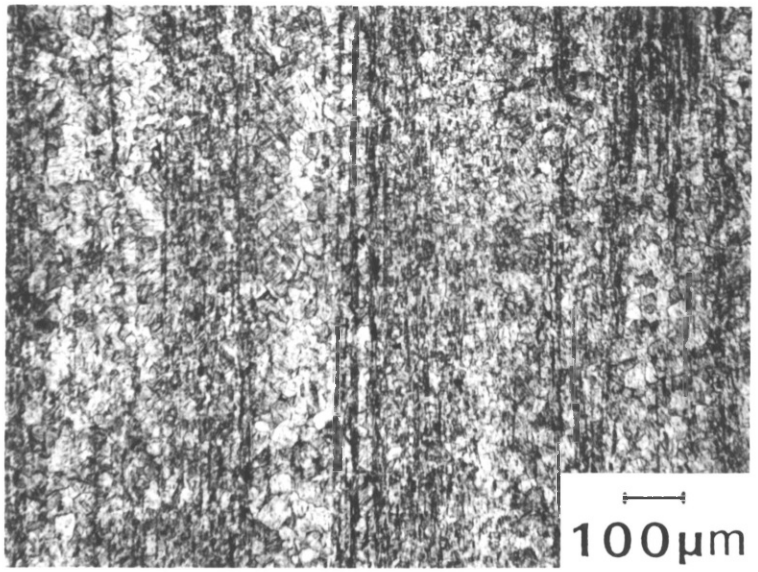
100μm

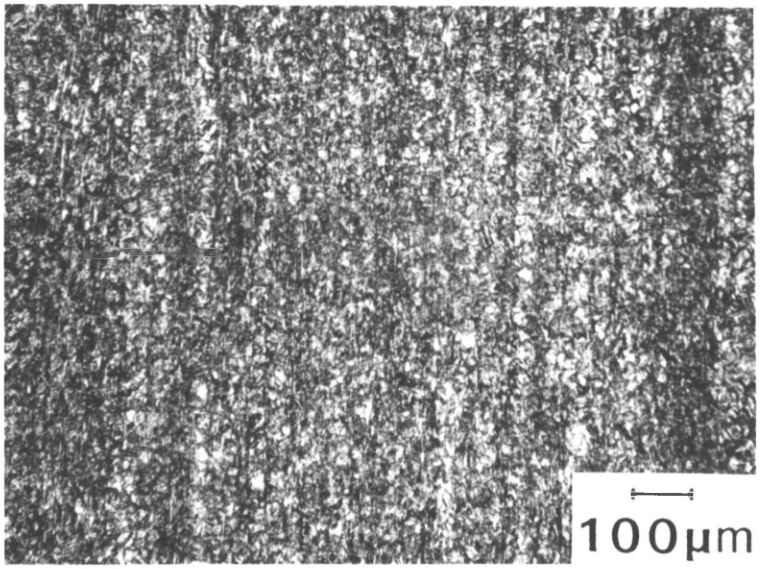
100μm

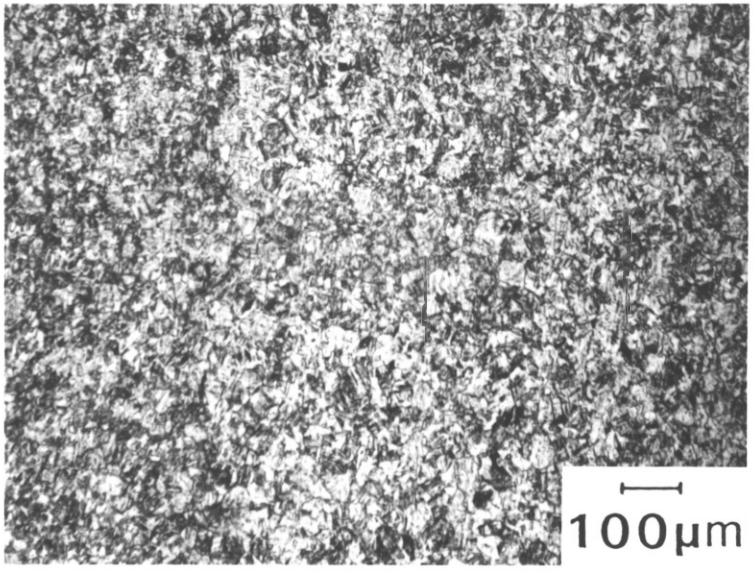
100μm

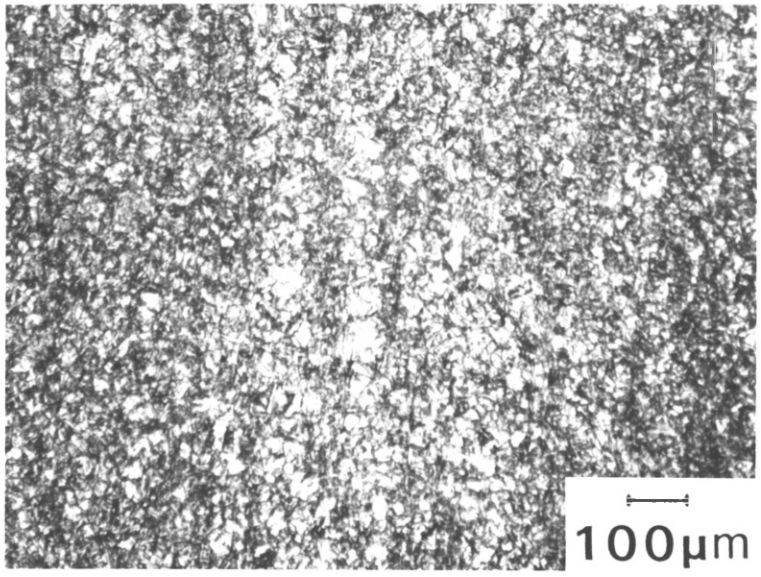
100μm

(e)

950°C WATER QUENCHED

GRAIN SIZE = 58.3 μm

(f)

950°C AIR COOLED

GRAIN SIZE = 72.2 μm

FIGURE 4.60 (CONTINUED)

(g)

1000°C WATER QUENCHED

GRAIN SIZE = 67.5 μm

(h)

1000°C AIR COOLED

GRAIN SIZE = 80.5 μm

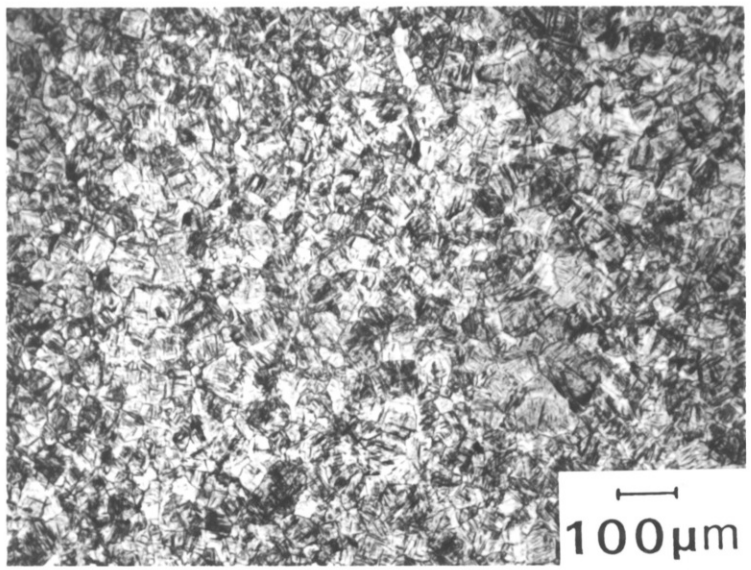
100μm

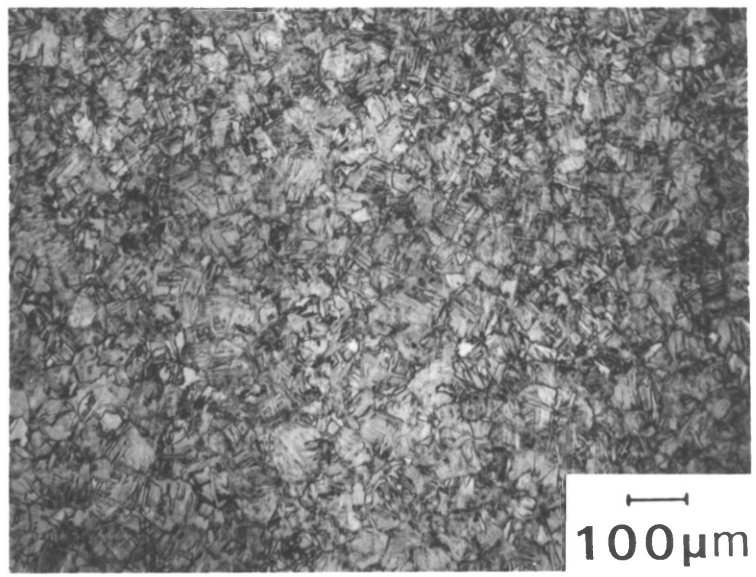
100μm

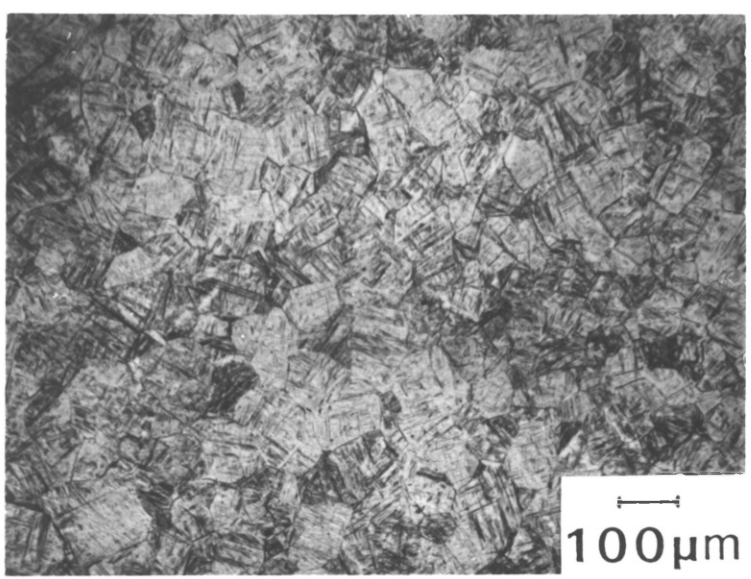
100μm

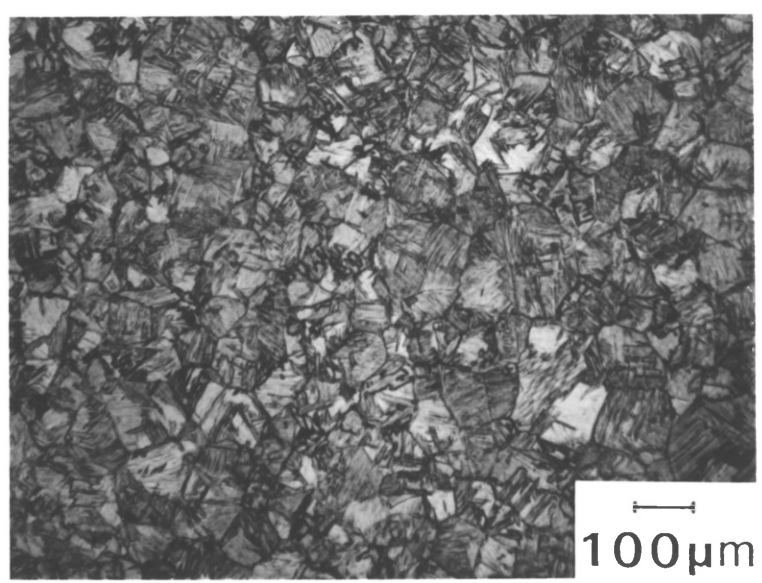
100μm

(i)

1050°C AIR COOLED

RECRYSTALLISED AREA

(j)

1050°C AIR COOLED

UNRECRYSTALLISED AREA

FIGURE 4.60 (CONTINUED)

(k)

1100°C AIR COOLED

RECRYSTALLISED AREA

(l)

1100°C AIR COOLED

UNRECRYSTALLISED AREA

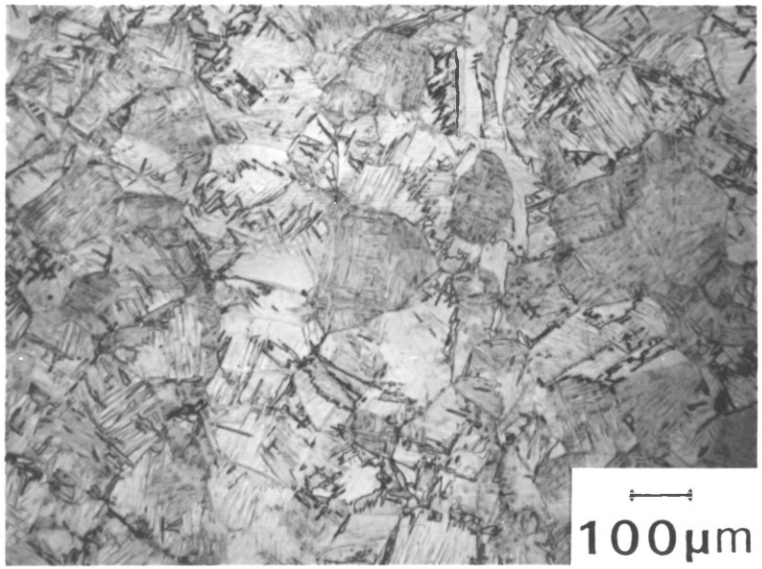
100μm

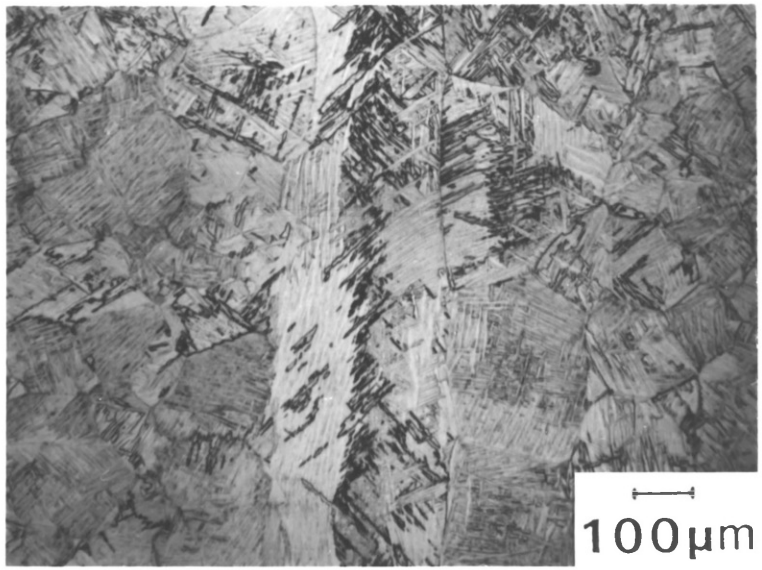
100μm

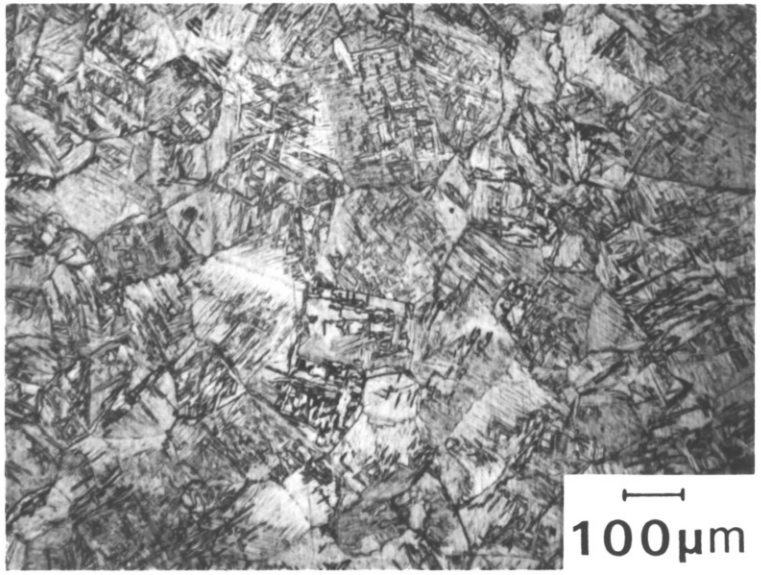
100μm

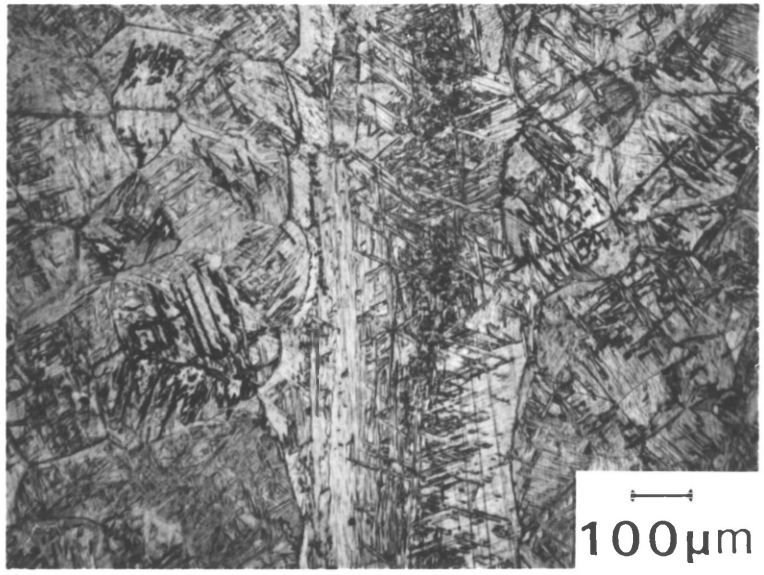
100μm

(m)

1100°C WATER QUENCHED

GRAIN SIZE = 89.9 μm

FIGURE 4.60 (CONTINUED)

(n)

1150°C AIR COOLED

GRAIN SIZE = 141.7 μm

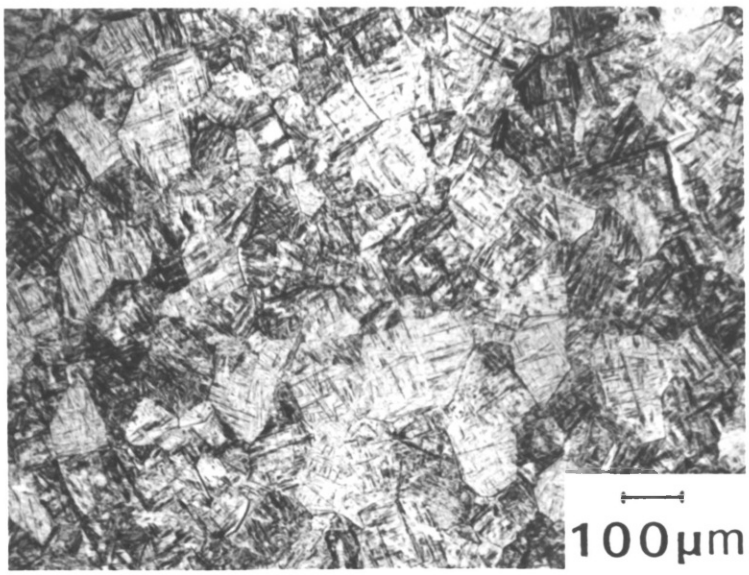
100μm

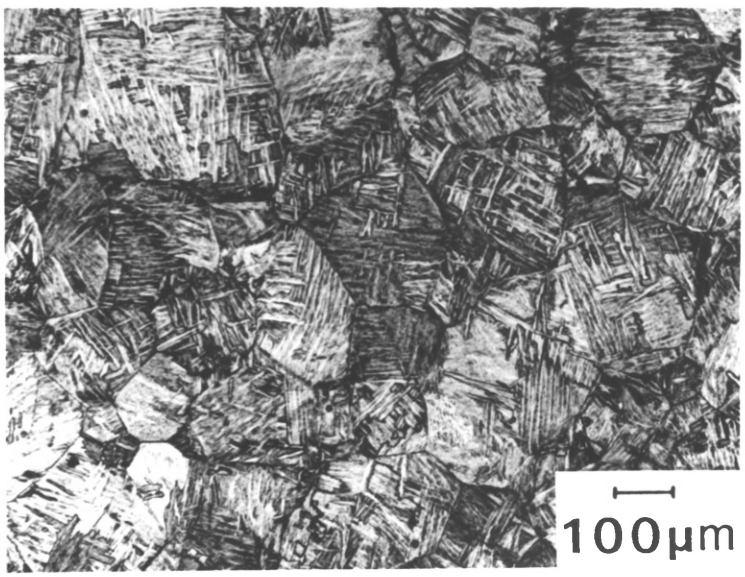
100μm

The alpha phase remains essentially untransformed during cooling, although some primary alpha regrowth may occur on air-cooling. The beta phase, however, as will be discussed in more detail in the electron microscopy section, undergoes a martensitic transformation on water quenching or transforms to a Widmanstatten structure of alpha+beta plates on air cooling, both transformations wiping out any high temperature substructure in the beta phase.

Similar trends were observed in both air cooled and water quenched extrusions in most cases, and hence they are discussed together.

Considering first the alpha+beta regime (Figure 4.60 (a) - (h)). The starting structures for extrusion consist of primary alpha+beta, the proportion of alpha phase decreasing with increasing temperature (section 4.4.1).

As discussed in the previous section, very substantial temperature rises occur during extrusion, the temperature rise increasing with decreasing temperature. At temperatures of 850°C and 900°C this is reflected in a marked reduction in the proportion of alpha phase compared to the starting structures, while at 950°C and 1000°C, the transus temperature is exceeded during extrusion so that a fully transformed beta structure is produced.

At an extrusion temperature of 850°C, the alpha and beta phases are elongated in the extrusion direction as is apparent from the fibrous structure. The elongated alpha phase contains an equiaxed subgrain structure (Figures 4.69 and 4.70), indicating that dynamic recovery is the predominant dynamic restoration mechanism during alpha+beta extrusion. This is a surprising result in view of the observation of dynamic recrystallisation during torsion testing in the alpha+beta regime. This will be discussed in more detail in a later section.

A distinct banding of the structure is apparent at this temperature, with some areas containing larger volume fractions of alpha phase than others. This is due to the heterogeneous nature of the deformation

occurring during extrusion, with some areas undergoing larger degrees of deformation than others, resulting in a gradation of temperature rise and hence structure across the extrude.

At the periphery of the extrude, the structure has been chilled by contact with the tooling, so that a larger volume fraction of alpha phase is present (Figure 4.61), thus accentuating the fibrous appearance of the structure.

If, however, substantial friction occurs between the periphery of the billet and the tooling, due to breakdown of the lubrication, a very substantial temperature rise occurs at the periphery, resulting in a fully transformed beta rim, as discussed in section 4.3.3.1 (Figure 4.20).

At a temperature of 900°C, the temperature rises occurring during extrusion have reduced the volume fraction of alpha phase at the extrude centre to only a few per cent, as is apparent from the virtual elimination of alpha stringers. The structure therefore consists predominantly of unrecrystallised transformed beta.

At 950°C and 1000°C no primary alpha phase was observed, indicating that the beta transus had been exceeded during extrusion. A fully recrystallised transformed beta structure was produced which indicates either that dynamic recrystallisation of the beta phase has occurred during extrusion, or that static recrystallisation of a dynamically recovered structure had proceeded very rapidly on cooling. The time above the beta transus is very short, and hence grain growth is limited so that a very fine grain size results. The higher temperatures obtaining during extrusion at 1000°C result in increased grain growth compared to 950°C and hence a coarser recrystallised grain size.

The increased strain and increased chilling at the billet periphery is reflected at these temperatures in a decrease in the recrystallised grain size at the extrude periphery (Figure 4.62).

Considering now the beta regime (Figures 4.60 (i) - (n)). The starting structures for extrusion consist of a very coarse recrystallised grain size, with the beta grain size increasing with increasing temperature (section 4.4.1).

FIGURE 4.61

T = 850°C R = 20:1 WATER QUENCHED

PERIPHERAL STRUCTURE

FIGURE 4.62

T = 1000°C R = 20:1 WATER QUENCHED

PERIPHERAL STRUCTURE

FIGURE 4.63

T = 1050°C R = 20:1 AIR COOLED

PERIPHERAL STRUCTURE

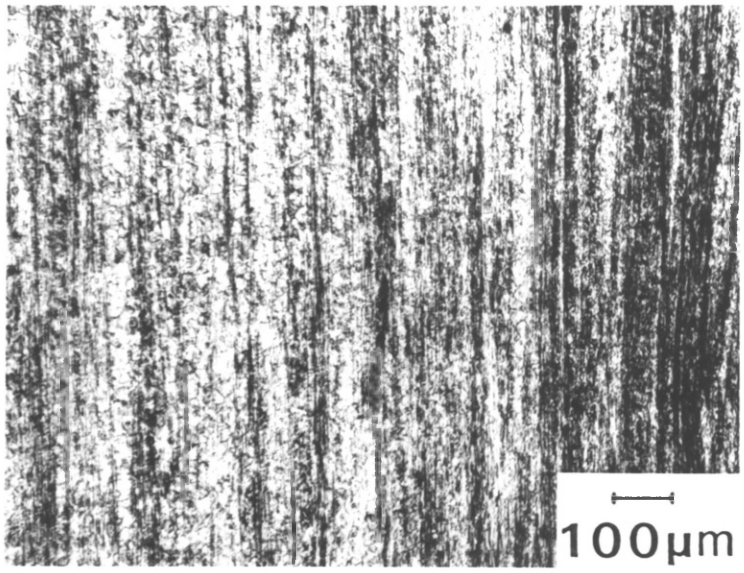
100μm

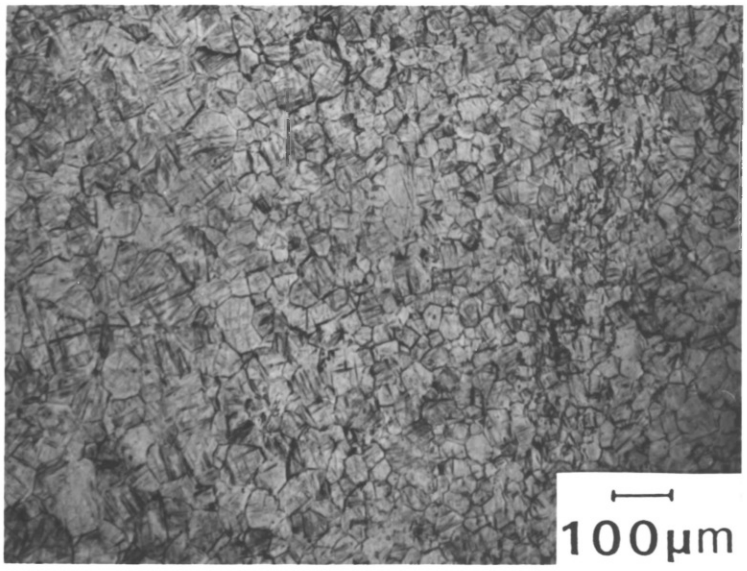
100μm

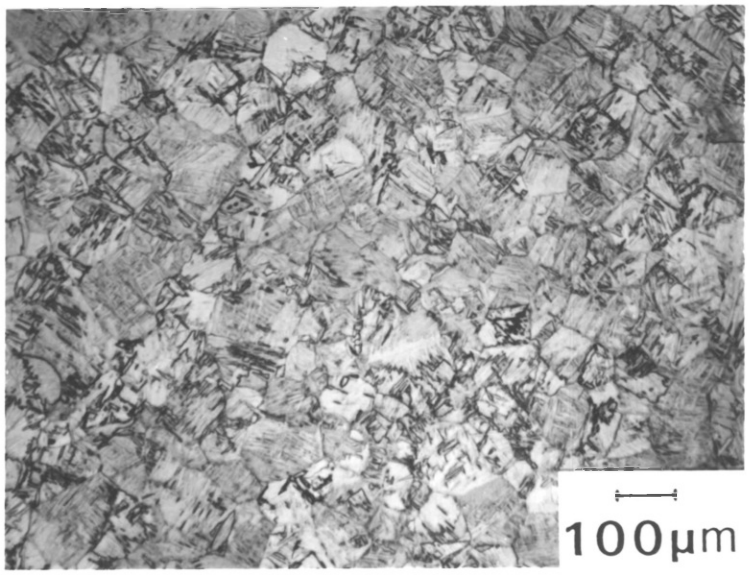
100μm

The air cooled structures produced at 1050°C and 1100°C consist predominantly of recrystallised transformed beta (Figures 4.60 (i) and (k)). However, some areas of extremely coarse unrecrystallised structure were observed (Figures 4.60 (j) and (l)). This indicates that dynamic recovery, at least in part, occurs during beta extrusion. The unrecrystallised areas were concentrated in the central regions of the extrude, with the periphery always being fully recrystallised (Figure 4.63). It would appear then that a critical strain has to be achieved during beta extrusion for recrystallisation, either dynamic or static, to occur. Similar behaviour was also observed in torsion, with unrecrystallised structures being produced at low strain rate, however fully recrystallised structures being produced at high strain rate (section 4.2.3.5).

The phase transformations occurring during cooling from the beta regime eliminate any high temperature substructure. Hence, while the observation of an unrecrystallised structure is conclusive evidence that dynamic recovery has occurred, the recrystallised structure could have arisen from either dynamic or static recrystallisation.

The presence of any unrecrystallised beta has a very profound effect on the reduction of area values of beta extruded material as will be discussed in section 4.8.4.2.

The water quenched extrusion at 1100°C was fully recrystallised (Figure 4.60 (m)). Since the influence of the increased quench rate would be to retard recrystallisation, the only explanation for this apparent anomaly can be found in the different pressures required to extrude the billets. The water quenched extrusion was carried out using a new die, with the air cooled extrusion being conducted with a worn die. The former required an increased pressure of approximately 28%, the higher pressure providing an increased driving force for recrystallisation.

At 1150°C, a fully recrystallised structure was produced (Figure 4.60 (n)) indicating that the critical strain for recrystallisation decreases with increasing temperature.

4.8.2.1.2 INFLUENCE OF EXTRUSION RATIO ON STRUCTURE

As was discussed in section 4.4.2.4, increasing the extrusion ratio produces an increase in pressure and hence an increased temperature rise during extrusion. This is reflected in the variation of structure with extrusion ratio.

The variation of structure with extrusion ratio at a temperature of 900°C is shown in Figure 4.64 for water quenched extrusions and it is apparent that a dramatic change of structure occurs on increasing the extrusion ratio. At R = 10:1, a large volume fraction of alpha phase is present as is apparent from the banded structure of elongated alpha+beta. At R = 20:1 only a very small volume fraction of alpha phase is present, and at R = 40:1 and R = 60:1 the temperature rises are such that the transus temperature is exceeded, resulting in a very fine fully recrystallised transformed beta grain size.

In the beta regime, the influence of increasing the extrusion ratio and hence the strain is to increase the driving force for recrystallisation. The variation of structure with extrusion ratio at a temperature of 1100°C is shown in Figure 4.65. At R = 10:1 the structure consists predominantly of elongated transformed beta (see also macrograph of partial extrusion, Figure 4.31). At R = 20:1, the proportion of unrecrystallised beta is substantially reduced, and at R = 40:1, a fully recrystallised structure is produced.

At 1150°C, where no unrecrystallised beta was produced even at R = 10:1, increasing the extrusion ratio produces a decrease in the recrystallised grain size. This refinement of the beta extruded structures by increasing the extrusion ratio has a very profound effect on the resultant properties of beta extruded material, as will be discussed in the mechanical properties section.

In their work on the extrusion of Ti-6Al-4V Gurney and Male also looked at the influence of the extrusion variables on the structure and properties of both air cooled and water quenched extrusions[30-33]. The following points are apparent on comparison of the results.

(a)

R = 10:1

(b)

R = 20:1

FIGURE 4.64

VARIATION OF STRUCTURE WITH EXTRUSION RATIO

AT T = 900°C

(c)

R = 40:1

(d)

R = 60:1

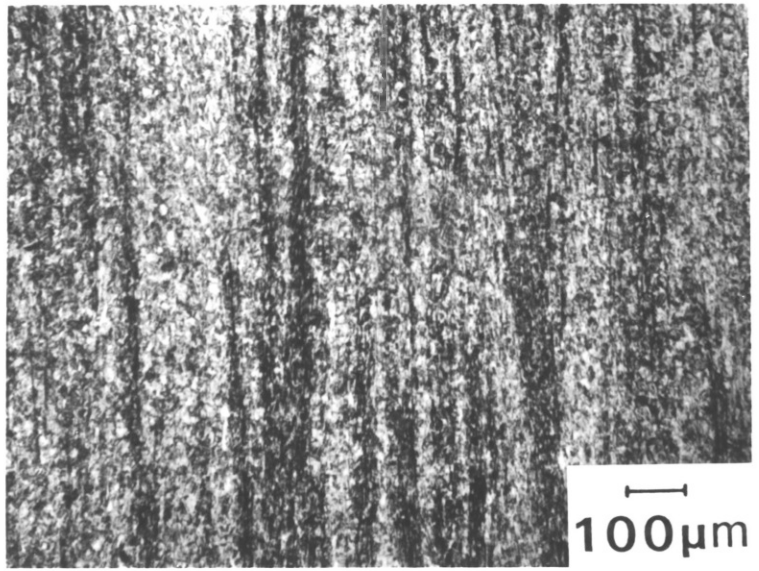
100μm

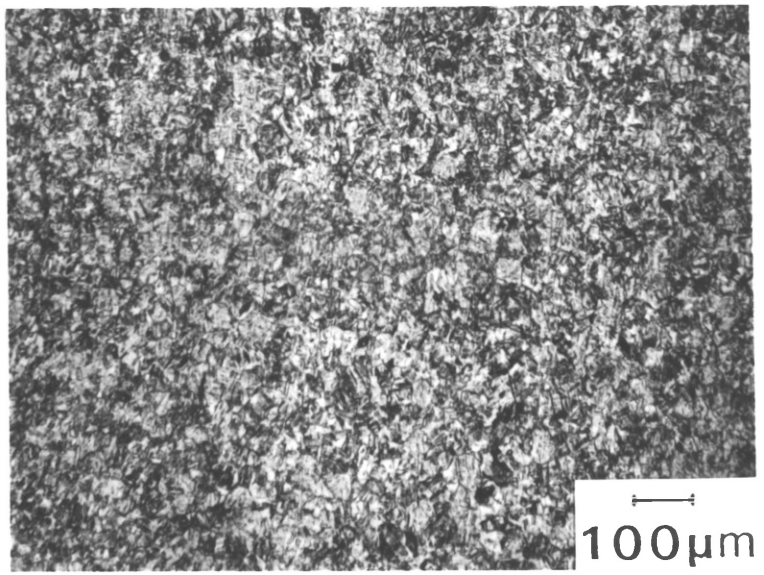
100μm

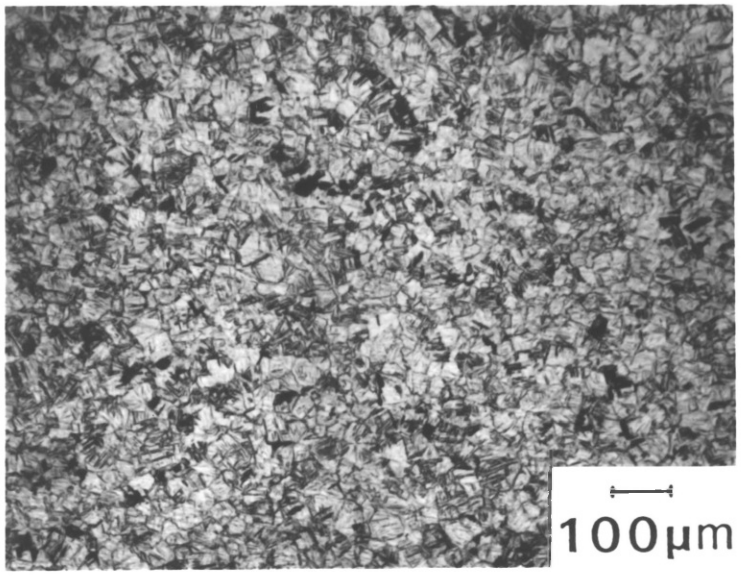
100μm

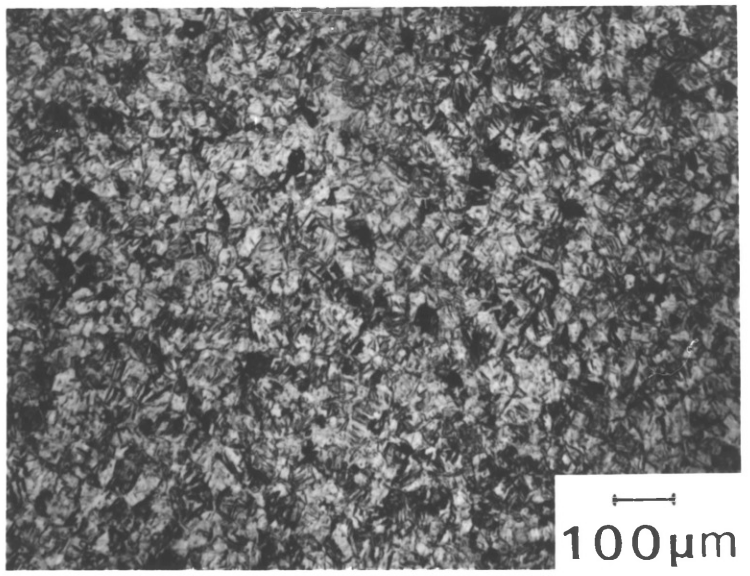
100μm

(a)

R = 10:1

(b)

R = 20:1

(c)

R = 40:1

FIGURE 4.65

VARIATION OF STRUCTURE WITH EXTRUSION RATIO

AT T = 1100°C

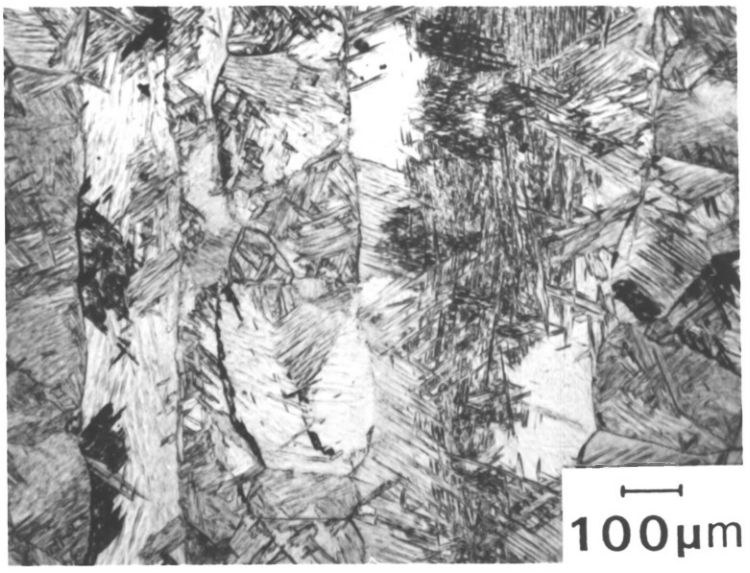
100μm

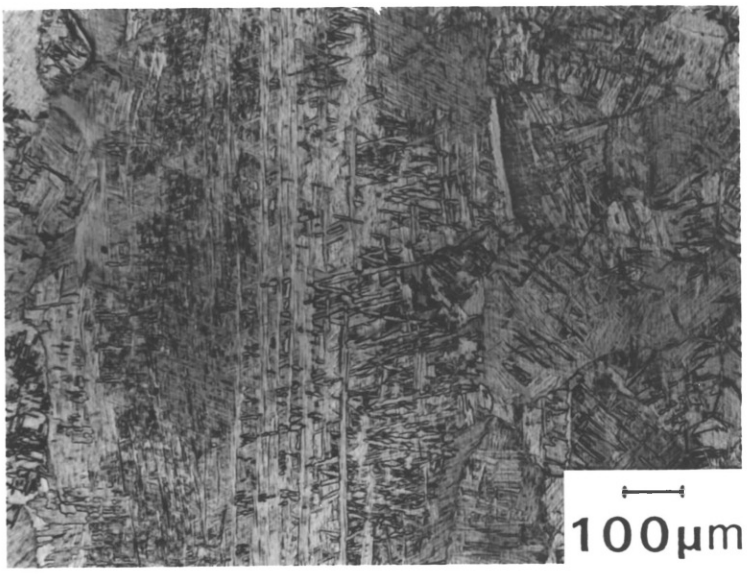
100μm

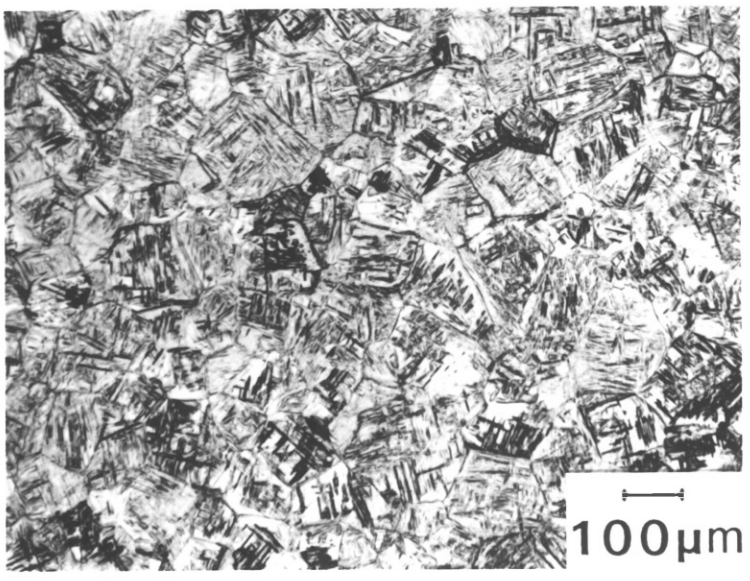
100μm

1) It is apparent from the structures that they present, that the temperature rises occurring during extrusion are not as large as those observed in this work. This can be attributed to the larger billets and in general lower extrusion ratios that they employed.

2) A similar trend of an increase in temperature rise with increasing extrusion ratio was observed in the alpha+beta regime. They have not investigated the criticalinfluence of extrusion ratio on structure in the beta regime.

3) Although they observed similar structures of elongated alpha+beta in the alpha+beta regime, the structures produced on beta extrusion were always fully recrystallised with no evidence of any unrecrystallised transformed beta. This can be attributed to the limited range of extrusion conditions that they investigated in the beta regime.

4) They have not attempted to categorize the structures produced on extrusion. This categorization is essential if any quantitative relationships between the structure and properties and the extrusion variables are to be established, and will be discussed in the following section.

4.8.2.2 CATEGORIZATION OF EXTRUSION STRUCTURES

4.8.2.2.1 FULLY RECRYSTALLISED STRUCTURES

Approximately 75% of all the extrusion structures produced were fully recrystallised. This occurred either as a result of the large temperature rises occurring during alpha+beta extrusion, resulting in the beta transus being exceeded, or as a result of recrystallisation during beta extrusion. These structures can be categorized according to the recrystallised grain size. This is relatively straight forward at high extrusion temperatures, where the grain boundaries are well defined

(example, Figure 4.60 (n)), however as the temperature decreases, it becomes increasingly more difficult,particularly for air-cooled material, to distinguish between the grain boundaries and the transformation products (example, Figure 4.60 (f)). Hence grain size determination is prone to greater error at lower temperatures. The grain sizes were evaluated as described in section 3.5.

The variation of grain size with temperature and extrusion ratio for fully recrystallised transformed beta structures is given in Tables 4.30 and 4.31, for air-cooled and water quenched extrusion respectively, and plotted in Figure 4.66.

The following points are apparent

1) Water quenching serves to reduce grain growth during cooling and hence a finer recrystallised grain size is produced compared to air cooling. The reduction in grain size is typically 17%.

2) There is an increase in grain size with increasing temperature in both alpha+beta and beta regimes. However, there is a jump in grain size on moving from the alpha+beta regime to the beta regime. This is because in the alpha+beta regime the structures are subjected to only a short exposure time above the beta transus and hence the time for grain growth is limited, while in the beta regime the starting structures are very coarse due to the long time exposure at temperature, and hence the extruded grain sizes are relatively coarse.

3) In general, increasing the extrusion ratio produces a decrease in the recrystallised grain size. Increasing the extrusion ratio results in an increased temperature rise during extrusion which will tend to increase the grain growth, however this trend is outweighed by the concomitant increase in strain and strain rate, which tend to refine the structure.

Run Code	Temperature °C	Extrusion Ratio	Grain Size μm	ln Z_I
9	900	40	55.2	60.49
12	950	20	72.2	58.53
14	950	40	64.0	58.69
16 (P)	1000	10	87.8	56.79
18	1000	20	80.5	56.98
20	1000	40	75.5	57.06
23	1050	40	107.5	21.55
24	1050	60	102.7	21.66
28	1100	40	114.7	21.02
29	1100	60	117.2	21.14
30	1150	10	154.6	20.2
31	1150	20	141.7	20.47
32	1150	40	135.7	20.59
33	1150	60	136.6	20.66

TABLE 4.30 VARIATION OF TRANSFORMED BETA GRAIN SIZE WITH TEMPERATURE AND EXTRUSION RATIO FOR AIR COOLED MATERIAL

Run Code	Temperature °C	Extrusion Ratio	Grain Size μm	ln Z_I
8	900	40	45.6	60.42
10	900	60	39.8	60.47
11	950	20	58.3	58.50
13	950	40	54.9	58.66
15	950	60	50.7	58.68
17	1000	20	67.5	56.88
19	1000	20	66.6	56.96
21	1000	60	61.8	57.09
26	1100	20	89.9	20.77

TABLE 4.31 VARIATION OF TRANSFORMED BETA GRAIN SIZE WITH TEMPERATURE AND EXTRUSION RATIO FOR WATER QUENCHED MATERIAL

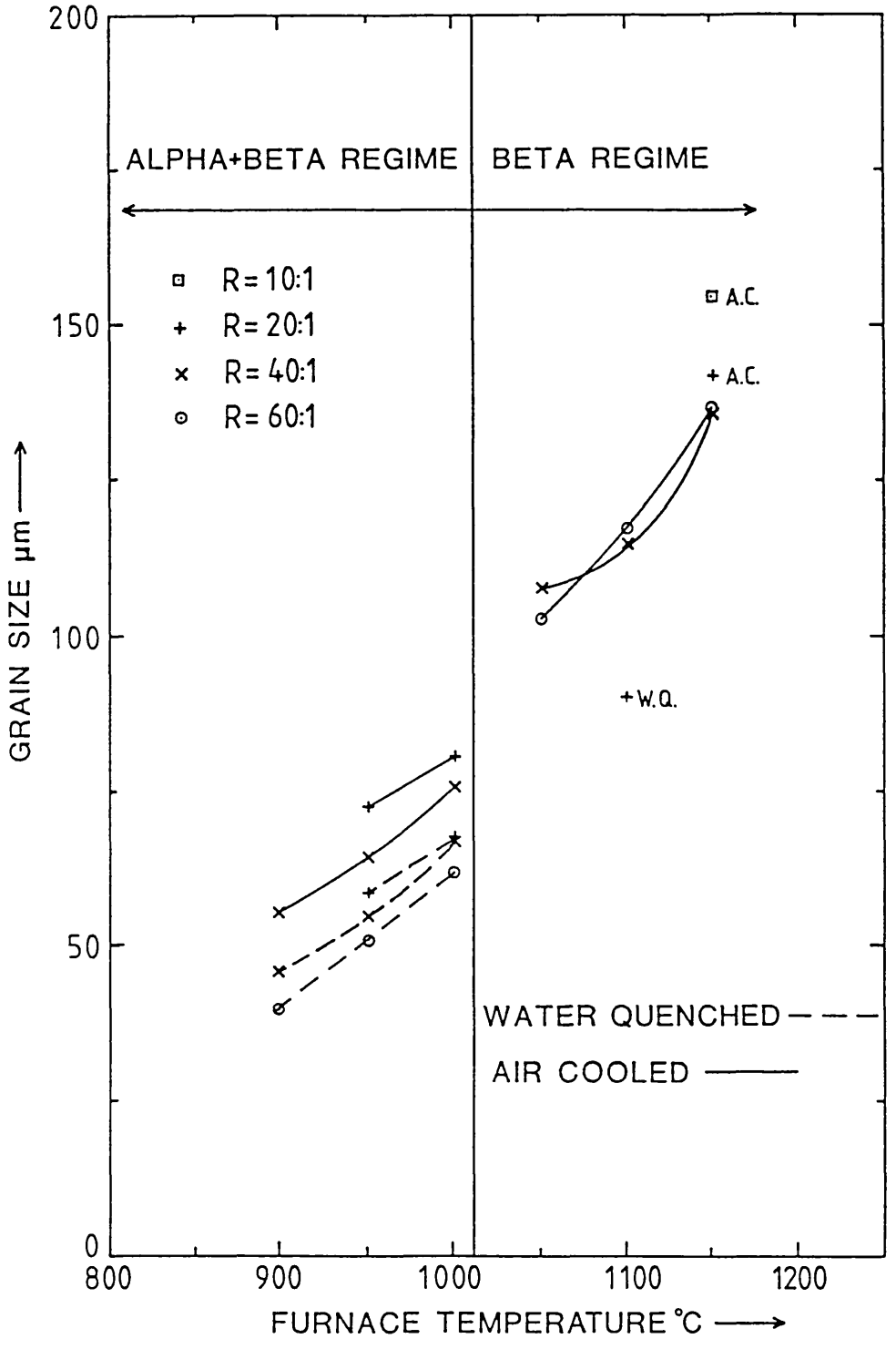

Figure 4.66 VARIATION OF TRANSFORMED BETA GRAIN SIZE WITH TEMPERATURE AND EXTRUSION RATIO FOR AIR-COOLED AND WATER QUENCHED EXTRUSIONS

4) Extrusion produces very substantial refinement of the beta starting structures. This is apparent by comparison of the extruded grain sizes with the starting structure grain sizes (Table 4.18). For example, at a temperature of 1150°C the grain size is reduced by a factor of x 6.4 at R = 10:1 and x 7.3 at R = 60:1. This dramatic structural refinement is the great advantage of extrusion over other metal working processes such as rolling and forging, where the deformation is not as severe, and hence the structural refinement possible is limited. The importance of this point will become apparent in the discussion of the influence of grain size on the properties of extruded Ti-6Al-4V.

4.8.2.2.2 VARIATION OF RECRYSTALLISED GRAIN SIZE WITH THE Z-PARAMETER

The variation in the recrystallised grain size with the z-parameter in the beta regime is shown in Figure 4.67 for air-cooled material. The grain size increases linearly with decreasing Z_I, i.e. increasing temperature and decreasing strain rate. The equation of the best straight line is given by :-

$$\text{GRAIN SIZE } (\mu m) = -34.5\ [\ln Z_I] + 847.9 \qquad \text{c.c.} = 0.979 \qquad 4.8$$

The variation in grain size with extrusion ratio is accommodated in the strain rate term of the z-parameter. This relationship only holds if full recrystallisation occurs during extrusion, i.e. for $Z_I < 20.66$ and extrusion ratios in excess of 40:1.

The variation in the recrystallised grain size with the z-parameter in the alpha+beta regime is shown in Figure 4.68 for both air-cooled and water quenched extrusions, the equations of the best straight lines being given by :-

$$\text{AIR COOLED} \quad \text{GRAIN SIZE } (\mu m) = -6.626[\ln Z_I] + 456.2 \qquad \text{c.c.}=0.954 \qquad 4.9$$

$$\text{WATER QUENCHED} \quad \text{GRAIN SIZE } (\mu m) = -6.595[\ln Z_I] + 441.2 \qquad \text{c.c.}=0.965 \qquad 4.10$$

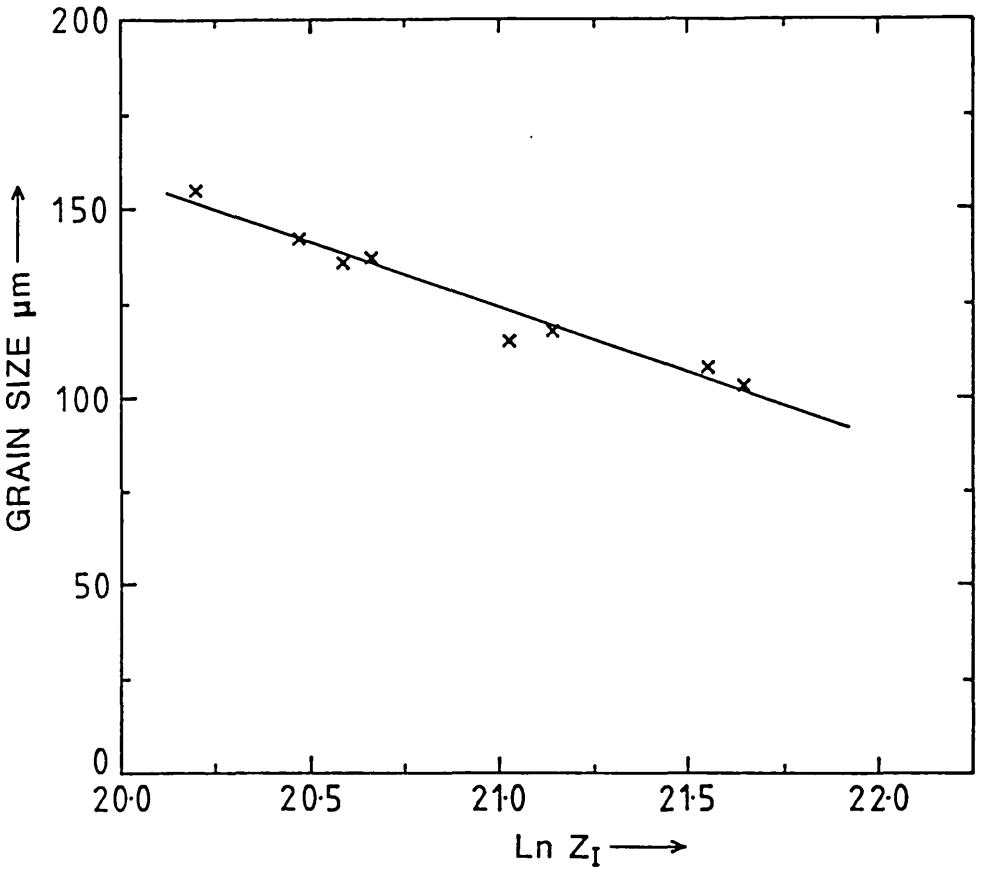

Figure 4.67 GRAIN SIZE VS. LN Z_I IN THE BETA REGIME FOR AIR COOLED MATERIAL

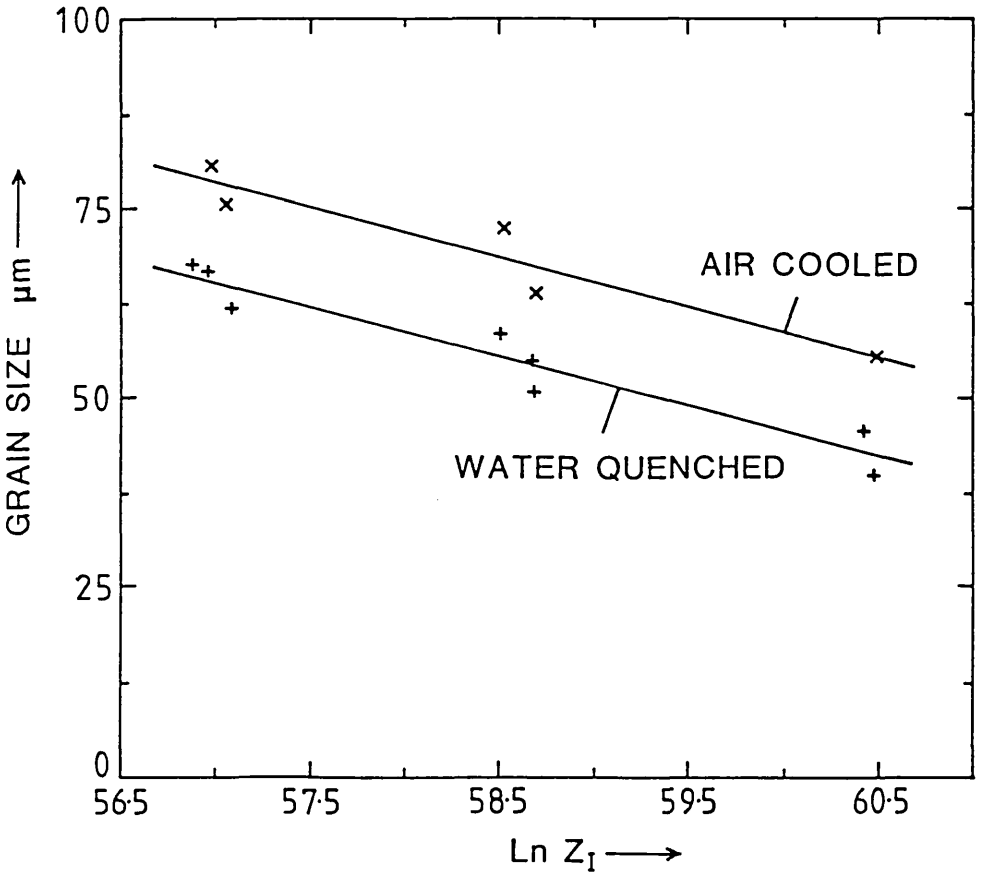

Figure 4.68 GRAIN SIZE VS. LN Z_I IN THE ALPHA+BETA REGIME FOR AIR COOLED AND WATER QUENCHED MATERIAL

These equations are only valid if the temperature rises are such that the transus temperature is exceeded during extrusion.

4.8.2.2.3 CATEGORIZATION OF PRIMARY ALPHA+TRANSFORMED BETA, AND PARTIALLY UNRECRYSTALLISED TRANSFORMED BETA STRUCTURES

The remainder of the structures produced on extrusion can be divided into two groups for the purposes of categorization :-

(a) Two phase primary alpha+transformed beta structures. The best technique for categorizing these structures is to evaluate the proportions of primary alpha+transformed beta as described in section 3.5. The problem with this technique is that it is difficult to differentiate between the primary alpha and the transformation products and hence only a rough approximation of the phase proportions can be obtained. The results for the water quenched extrusions are given in Table 4.32, these being slightly easier to categorize than the air-cooled extrusions. The air cooled extrusions for the same extrusion conditions will probably contain slightly more primary alpha as a result of alpha regrowth during cooling.

Run Code	Temperature °C	Extrusion Ratio	% Primary Alpha	% Transformed Beta
1	850	20	16	84
5	900	10	20	80
6	900	20	4	96

TABLE 4.32 PROPORTIONS OF PRIMARY ALPHA+TRANSFORMED BETA IN TWO PHASE EXTRUDED STRUCTURES

Comparison of these values with the phase proportions at the commencement of extrusion illustrate the substantial temperature rises occurring during extrusion, as is reflected by a marked reduction in the proportion of alpha phase.

At the extrude periphery the volume fraction of alpha phase is increased due to the chilling of the billet peripheral layers in contact with the container.

(b) Partially unrecrystallised fully transformed beta structures. Only three structures contained any unrecrystallised transformed beta. These were categorized visually according to the proportion of unrecrystallised structure, as described in section 3.5. The proportion of unrecrystallised transformed beta increased on moving from T = 1100°C R = 20:1 to T = 1050°C R = 20:1 to T = 1100°C R = 10:1.

4.8.3 ELECTRON MICROSCOPY

Electron microscopy studies were carried out on longitudinal sections of both air cooled and water quenched extrusions. Particular attention was given to the substructure present within the primary alpha phase to establish the dynamic restoration mechanism operative during alpha+beta extrusion. Only a limited study was possible because only a small number of the extrusions contained any primary alpha, due to the large temperature rises occurring during extrusion.

The elongated alpha phase produced on extrusion at low temperatures in the alpha+beta regime contained an equiaxed well-defined subgrain structure, typical examples being shown in Figures 4.69 and 4.70. Thus it is apparent that dynamic recovery is the predominant dynamic restoration mechanism in the alpha phase during extrusion. This is a surprising result in view of the observation of dynamic recrystallisation in the alpha+beta regime during torsion. The possible reasons for the different dynamic restoration mechanisms operating during extrusions and torsion are given in the next section.

FIGURE 4.69

T = 850°C R = 20:1 WATER QUENCHED
DYNAMIC RECOVERY WITHIN ALPHA PHASE

FIGURE 4.70

T = 850°C R = 20:1 WATER QUENCHED
DYNAMIC RECOVERY WITHIN ALPHA PHASE

FIGURE 4.71

T = 850°C R = 20:1
WATER QUENCHED AND DIRECT AGED
PRIMARY ALPHA+AGED MARTENSITE

FIGURE 4.72

T = 1000°C R = 20:1
WATER QUENCHED AND DIRECT AGED
AGED MARTENSITE

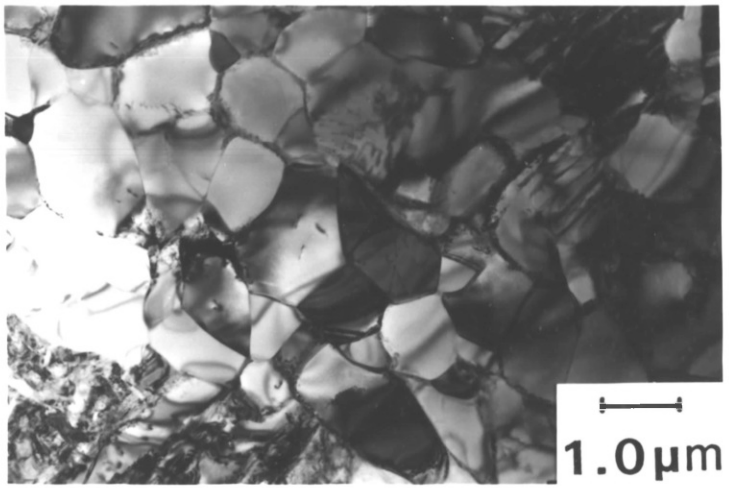
1.0μm

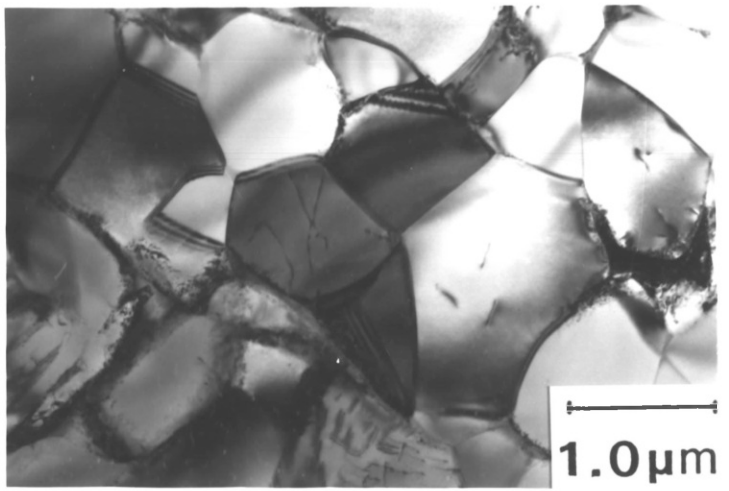
1.0μm

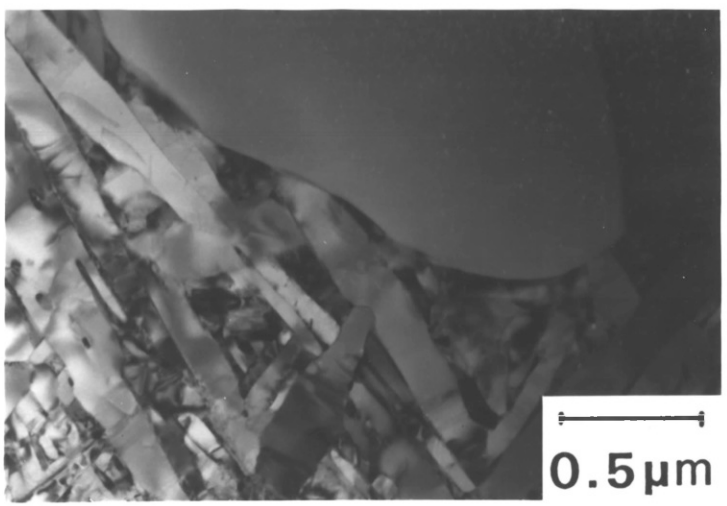
0.5μm

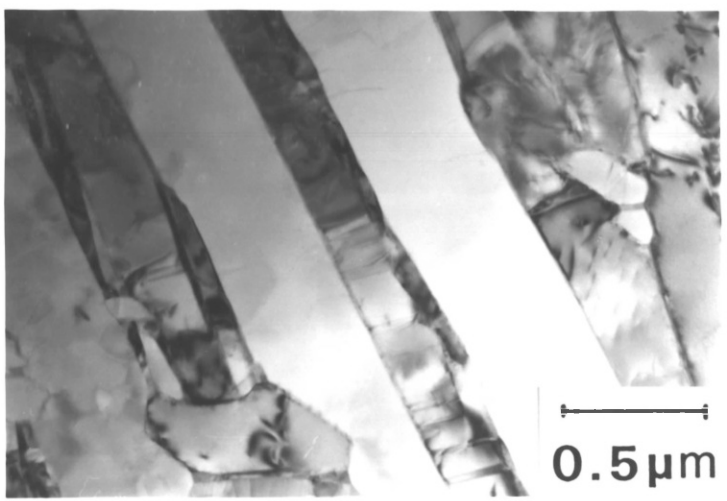
0.5μm

Considering now the phase transformations occurring in the beta phase during water quenching and air cooling. The structures produced on water quenching were similar to those produced on torsion with the beta phase undergoing a martensitic transformation forming plates of acicular morphology. The coarseness of the plates increases with increasing beta grain size. Thus, in cases where primary alpha was present in the structure, the plates were very fine, their growth being limited by the inter-alpha phase spacing, however in the case of fully beta structures, the plates were substantially coarser, the primary plates extending for large distances across the beta grains (compare Figures 4.7e and 4.9c).

All the water quenched extrusions were given a standard ageing treatment of 4 hours at 540°C. This ageing treatment, as will be discussed in section 4.8.5.3, produces a considerable strengthening response. The strengthening response obtained on solution treatment and ageing, as discussed in section 1.2.4.5, is a complex function of the solution treatment temperature (in this case the extrusion temperature) which governs the proportion and composition of the martensite, the ageing temperature and time, and the section size.

No structural analysis was carried out in this work to identify the influence of the extrusion variables on the ageing response of the martensite, the aim being only to obtain some idea of the strengthening potential of the alloy on water quenching and direct ageing. The generally accepted ageing mechanism, however, is[8] decomposition of the martensite to a fine equilibrium structure of acicular alpha+beta, the beta being formed directly by nucleation and growth. The beta is reportedly mostly nucleated heterogeneously at the martensite plate boundaries and at the internal martensitic substructure.

It would appear from the limited electron microscopy study carried out in this work that the beta nucleated predominantly at the martensite plate boundaries during ageing, typical examples being shown in Figures 4.71 and 4.72 for structures with and without primary alpha respectively.

On air cooling the beta phase transforms to plates of alpha and beta by a nucleation and growth process, typical structures being shown in Figures 4.73 and 4.74. A high resolution dark field image from a beta diffraction spot is shown in Figure 4.75. As would be expected the coarseness of the alpha/beta plates was observed to increase with increasing beta grain size.

No strengthening response is obtained on ageing of this structure. For property evaluation, as will be discussed in section 4.8.4, the air cooled structures were given the standard annealing treatment of 2 hours at 700°C. This had virtually no effect on the tensile properties. Structurally the treatment served to increase the volume fraction of alpha phase, as was evidenced in fully transformed beta structures by partial dissolution of the beta plates (Figure 4.76).

4.8.4 POSSIBLE REASONS FOR THE DIFFERENT DYNAMIC RESTORATION MECHANISMS OPERATIVE IN THE ALPHA+BETA REGIME DURING EXTRUSION AND TORSION

The optical and electron microscopy evidence has shown conclusively that different dynamic restoration mechanisms are operative in extrusion and torsion in the alpha+beta regime. During torsion dynamic recrystallisation was the predominant restoration mechanism and during extrusion, dynamic recovery. Possible reasons for the different dynamic restoration mechanisms occurring during extrusion and torsion will now be discussed.

For dynamic recrystallisation to occur then dynamic recovery processes alone cannot produce a high enough dislocation annihilation rate. A high dislocation density therefore builds up during deformation and when it exceeds a critical value, dynamic recrystallisation will occur. For a high dislocation density to build up during deformation, then extensive interaction between the operative slip systems must occur, resulting in extensive dislocation interaction at the intersecting slip systems. On the other hand, in the absence of such

FIGURE 4.73

ALPHA AND BETA PLATES FORMED ON

AIR COOLING FROM THE BETA REGIME

ALPHA-LIGHT BETA-DARK

FIGURE 4.74

ALPHA AND BETA PLATES FORMED ON

AIR COOLING FROM THE BETA REGIME

FIGURE 4.75

HIGH RESOLUTION DARK FIELD IMAGE

OF ALPHA AND BETA PLATES

ALPHA-DARK BETA-LIGHT

FIGURE 4.76

PARTIAL DISSOLUTION OF BETA PLATES

AS A RESULT OF ANNEALING

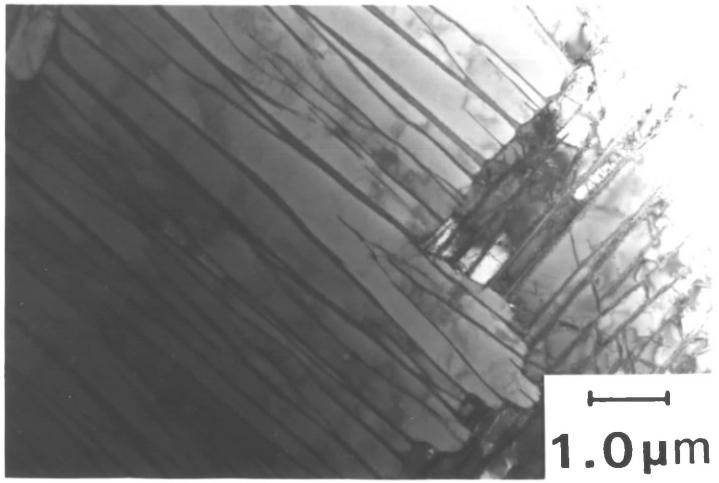
1.0μm

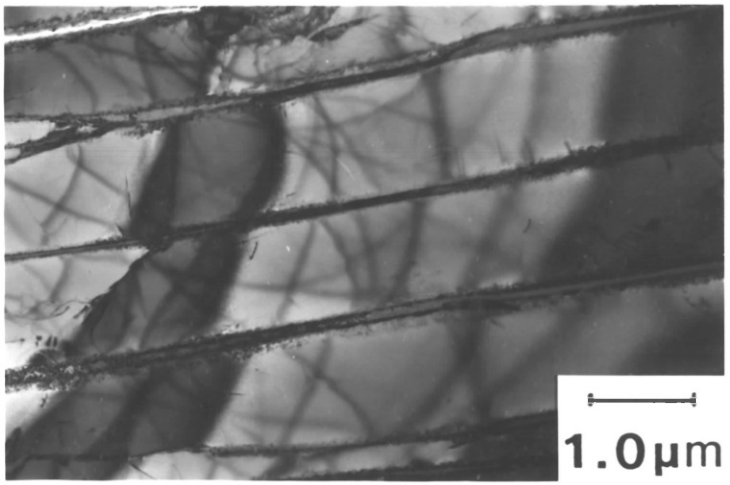
1.0μm

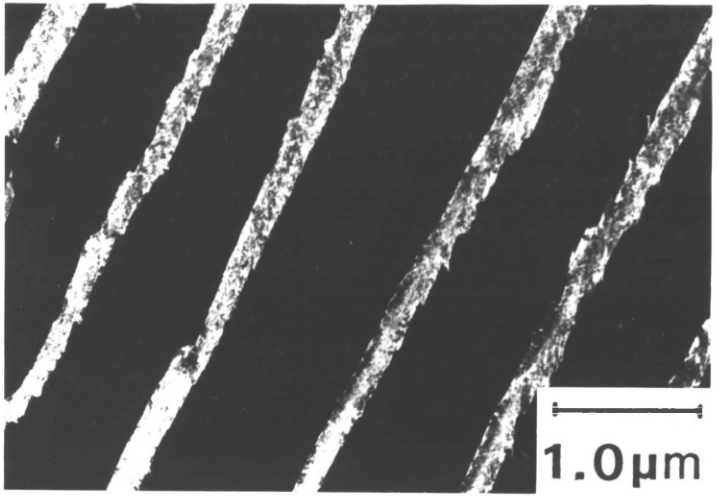
1.0μm

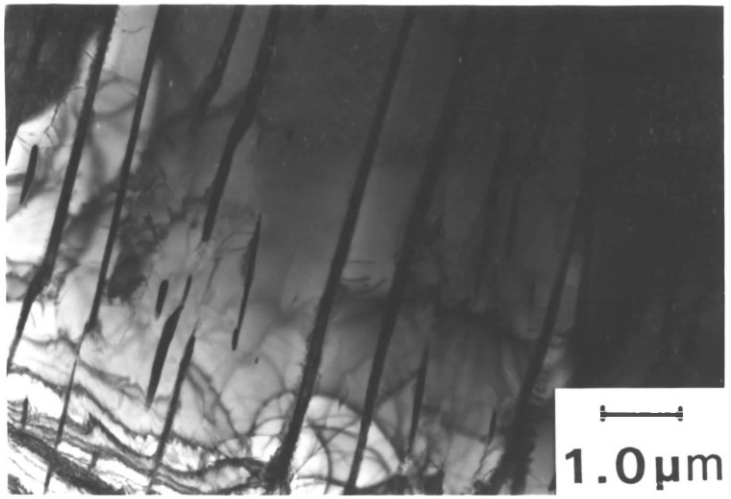
1.0μm

dislocation interaction, as may occur if only a limited number of slip systems are active, then high dislocation densities will not build up and hence dynamic recovery processes alone can annihilate sufficient dislocations to prevent dynamic recrystallisation from occurring.

Clearly then, different slip systems must be activated during extrusion and torsion to account for the different dynamic restoration mechanisms observed. There are two major factors which may contribute to activating different slip systems during extrusion and torsion.

(a) The texture in the starting material
(b) The deformation mode

Considering first the former point. No texture studies were carried out in the work and hence the following dicussion is based on the literature available on texture studies in Ti-6Al-4V[3,90-92].

The starting material for extrusion, as discussed in section 4.4.1, consisted either of smooth turned billet, 75 mm diameter x 100 mm long, or as blocks, 75 mm square x 200 mm long. Although the exact processing conditions were not available, the material will typically have been forged and rolled from approximately 750 mm diameter ingot in several stages to the final product. The microstructure of the starting material is given in Figure 4.35 from which it is apparent, from the absence of any marked directionality in the structure, that the billets will have been predominantly forged.

The starting material for torsion, however, consisted of 25 mm diameter bar, as discussed in section 4.2.2. The microstructure of the as-received bar is shown in transverse section in Figure 4.1 and in longitudinal section in Figure 4.77. It is apparent from Figure 4.77 that the bar has been finish rolled, with the alpha and beta phases elongated in the rolling direction.

FIGURE 4.77

LONGITUDINAL SECTION THROUGH

AS-RECEIVED TORSION BARSTOCK

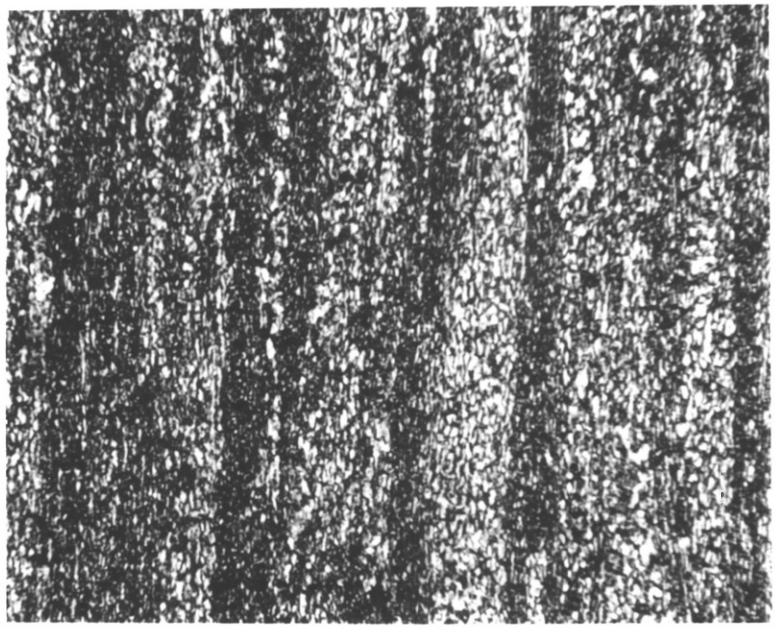

Thus, it is apparent that the starting structures for extrusion and torsion are significantly different, as a result of the latter having received a greater amount of deformation in rolling to 25 mm diameter bar. More importantly, however, the starting textures will be markedly different. Ti-6Al-4V can develop a very marked texture during hot deformation in the alpha+beta regime[3,90-92], due to the presence of the h.c.p. alpha phase, with the type of texture obviously depending on the deformation mode and the severity of deformation.

Thus, with the extrusion starting material having been predominantly forged, and the torsion starting material having been finish rolled and having received a larger amount of deformation, then the starting textures would be expected to be markedly different. Work by Bowen[90] has shown that the starting texture has a profound influence on the subsequent deformation of Ti-6Al-4V. It would therefore seem feasible that the different deformation textures present in the extrusion and torsion starting material could result in different slip systems being activated during torsion and extrusion and hence different dynamic restoration mechanisms being operative. It would appear that the deformation texture present in the torsion starting material results in considerable slip system and hence dislocation interaction during torsion, which promotes dynamic recrystallisation. The texture present in the extrusion billets, however, results in only limited slip system interaction during extrusion, with the result that dynamic recovery is the predominant restoration mechanism.

Clearly, more work requires to be done on identifying the textures present in the starting material and why these particular textures promote either dynamic recovery or dynamic recrystallisation.

The different deformation modes operative in extrusion and torsion may also be influencing the dynamic restoration mechanisms. This can be investigated by employing the same starting material for extrusion and torsion. This necessitates machining the torsion test pieces from the extrusion billet material, which will be extremely wasteful of material, but is nevertheless unavoidable.

Clearly then, the different dynamic restoration mechanisms obtained in extrusion and torsion calls into question the validity of employing the hot working constants obtained from torsion in the extrusion analysis. It would be expected that the different dynamic restoration mechanisms would have different activation energies, and hence the values of flow stress and temperature compensated strain rate should be affected. This can be checked in future work by employing the same starting material for extrusion and torsion, as discussed above, to observe whether the same dynamic restoration mechanisms are obtained and, if this is the case, whether the values of hot working constants obtained are significantly different from those evaluated in this work.

4.8.5 TENSILE PROPERTIES OF EXTRUDED Ti-6Al-4V

4.8.5.1 INTRODUCTION

The variation of mechanical properties with the structure and extrusion variables will be discussed in this section. The air cooled extrusions were given a standard annealing treatment of 2 hours at 700°C, and the water quenched extrusions were direct aged for 4 hours at 540°C, as described in section 3.7. In addition, sections from the 20:1 extrusions, both air cooled and water quenched, were solution treated at 950°C for 1 hour, water quenched and aged for 4 hours at 540°C.

The following properties were measured from a standard tensile test, as described in section 3.8 :- 0.2% Proof Stress, Ultimate Tensile Strength, Young's Modulus, % Elongation on $5.65\sqrt{So}$ and the Reduction of Area. The as annealed, direct aged and solution treated and aged tensile results are given in Tables 4.33 to 4.35, and plotted in Figures 4.78 to 4.81.

For comparison purposes, the property minima according to the I.M.I. specification[51] for alpha+beta extruded, air cooled and annealed material are plotted as horizontal dotted lines on the Figures, the values being given in Table 4.36.

Run Code	Extrusion Temperature °C	Extrusion Ratio	0.2% Proof Stress MNm^{-2}	U.T.S. MNm^{-2}	0.2%P.S. / U.T.S.	Youngs Modulus GNm^{-2}	% Elongation On $5.65\sqrt{So}$	Reduction of Area %
2	850	20	961	1046	0.92	114.2	16.0	45.0
4(P)	900	10	944	1032	0.91	115.2	16.0	42.5
7	900	20	947	1039	0.91	117.9	15.0	42.5
9	900	40	929	1048	0.89	114.8	15.0	36.0
12	950	20	922	1035	0.89	117.4	13.0	38.0
14	950	40	936	1040	0.90	117.6	15.0	37.0
16(P)	1000	10	896	1006	0.89	115.2	14.5	35.0
18	1000	20	908	1017	0.89	115.6	13.0	34.0
20	1000	40	923	1040	0.89	115.2	15.0	35.0
22	1050	20	934	1037	0.90	117.6	11.5	23.0
23	1050	40	933	1040	0.90	116.9	15.0	35.0
24	1050	60	937	1044	0.90	115.4	12.5	35.0
25(P)	1100	10	940	1030	0.91	118.6	11.5	22.0
27	1100	20	913	1010	0.90	115.8	10.0	29.0
28	1100	40	920	1033	0.89	115.1	14.0	32.0
29	1100	60	939	1048	0.90	115.9	13.0	35.0
30	1150	10	884	990	0.89	114.4	13.0	29.0
31	1150	20	904	1014	0.89	114.4	11.0	31.0
32	1150	40	Broke On Thread	-	-	-	-	-
33	1150	60	924	1038	0.89	115.2	14.5	33.0

TABLE 4.33 TENSILE PROPERTY RESULTS FOR AIR COOLED AND ANNEALED EXTRUSIONS

Run Code	Extrusion Temperature °C	Extrusion Ratio	0.2% Proof Stress MNm^{-2}	U.T.S. MNm^{-2}	0.2% P.S. / U.T.S.	Youngs Modulus GNm^{-2}	% Elongation On $5.65\sqrt{So}$	Reduction of Area %
1	850	20	1085	1178	0.92	116.9	11.5	43.0
5	900	10	1035	1136	0.91	116.5	14.5	42.5
6	900	20	1091	1188	0.92	117.3	11.0	40.0
8	900	40	1036	1153	0.90	118.6	16.5	42.5
10	900	60	1051	1175	0.89	117.3	10.0	37.0
11	950	20	999	1117	0.89	117.2	15.0	35.0
13	950	40	989	1102	0.90	118.2	15.0	35.0
15	950	60	1138	1243	0.92	116.4	14.0	42.5
17	1000	20	1058	1164	0.91	116.1	10.0	35.0
19	1000	40	987	1098	0.90	116.1	13.0	34.0
21	1000	60	1034	1152	0.90	115.6	12.5	32.0
26	1100	20	1081	1195	0.90	114.0	12.5	31.0

TABLE 4.34 TENSILE PROPERTY RESULTS FOR WATER QUENCHED AND DIRECT AGED EXTRUSIONS

Run Code	Extrusion Temperature °C	Extrusion Ratio	0.2% Proof Stress MNm^{-2}	U.T.S. MNm^{-2}	0.2% P.S. / U.T.S.	Youngs Modulus GNm^{-2}	% Elongation On $5.65\sqrt{So}$	Reduction Of Area %
1(W)	850	20	1133	1222	0.93	119.1	13.0	42.0
2(A)	850	20	1144	1231	0.93	116.8	13.5	44.0
6(W)	900	20	1130	1223	0.92	117.5	14.0	40.0
7(A)	900	20	1125	1220	0.92	117.7	12.5	40.0
11(W)	950	20	1107	1231	0.90	117.6	Broke Out of Gauge	-
12(A)	950	20	1113	1217	0.91	117.3	10.0	33.0
17(W)	1000	20	1089	1218	0.89	116.9	15.0	35.0
18(A)	1000	20	1098	1204	0.91	115.3	14.0	29.0
22(A)	1050	20	1085	1191	0.91	117.9	9.5	20.0
26(W)	1100	20	1077	1206	0.89	116.9	9.5	25.0
27(A)	1100	20	1085	1194	0.91	114.8	9.0	20.0
31	1150	20	1071	1176	0.91	116.3	10.0	25.0

(W) Water Quenched

(A) Air Cooled

TABLE 4.35 TENSILE PROPERTY RESULTS FOR SOLUTION TREATED AND AGED EXTRUSIONS AT R = 20:1

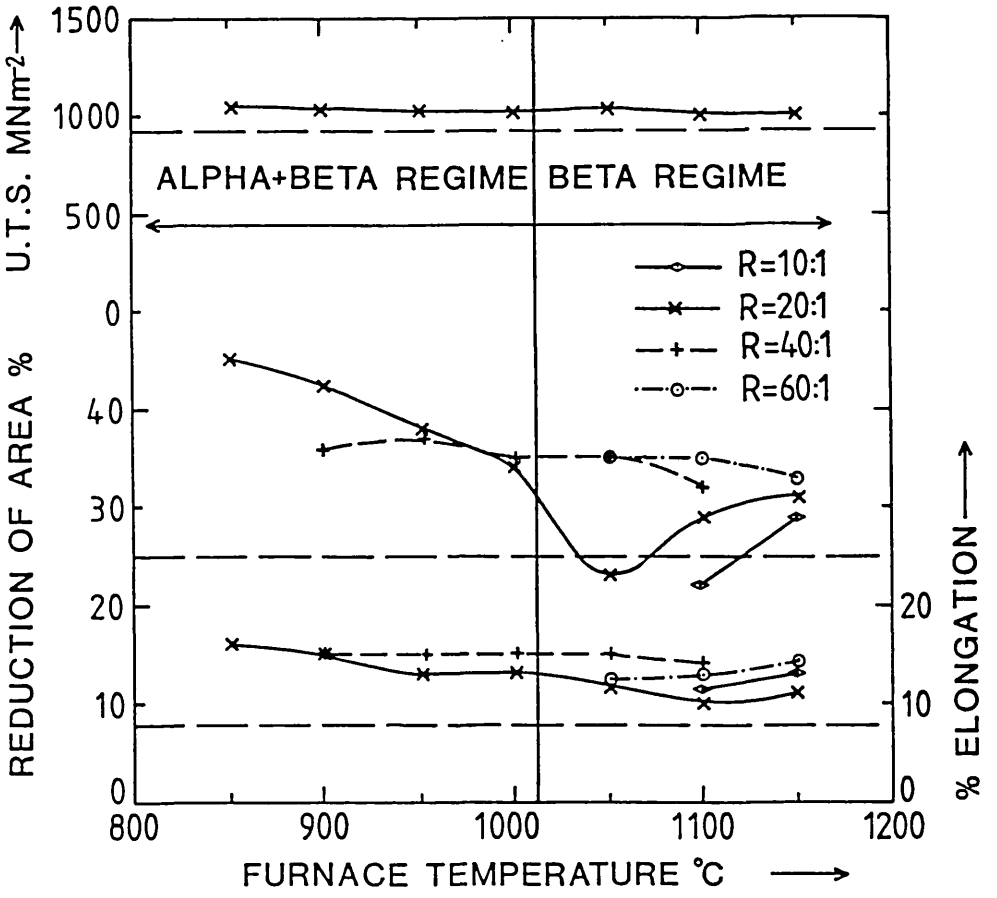

Figure 4.78 VARIATION OF AIR COOLED AND ANNEALED TENSILE PROPERTIES WITH TEMPERATURE AND EXTRUSION RATIO

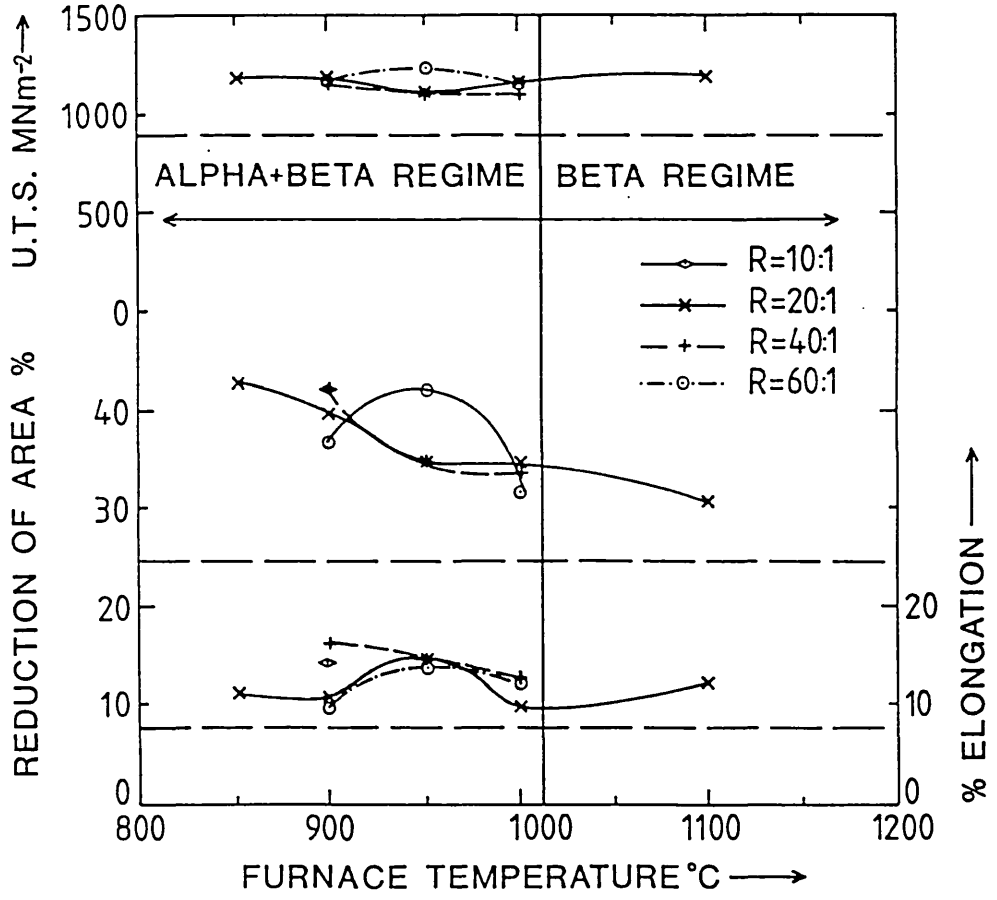

Figure 4.79 VARIATION OF WATER QUENCHED AND DIRECT AGED TENSILE PROPERTIES WITH TEMPERATURE AND EXTRUSION RATIO

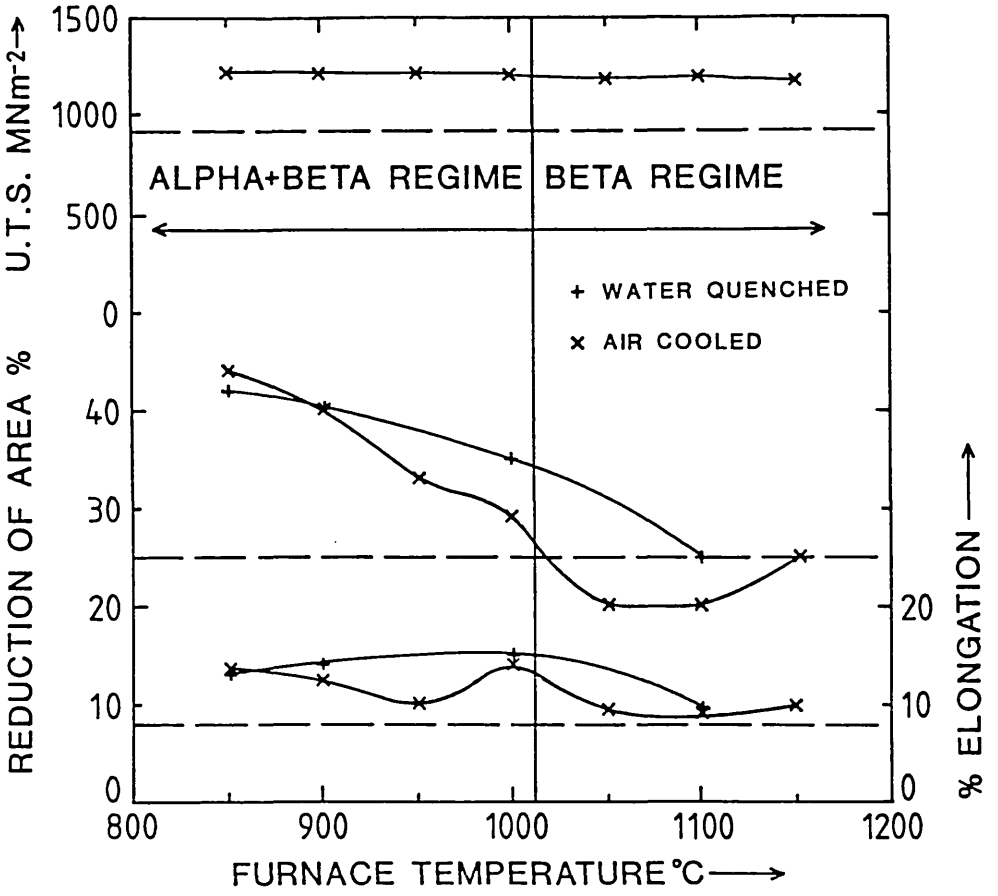

Figure 4.80 VARIATION OF SOLUTION TREATED AND AGED PROPERTIES WITH TEMPERATURE FOR AIR COOLED AND WATER QUENCHED EXTRUSIONS AT R = 20:1

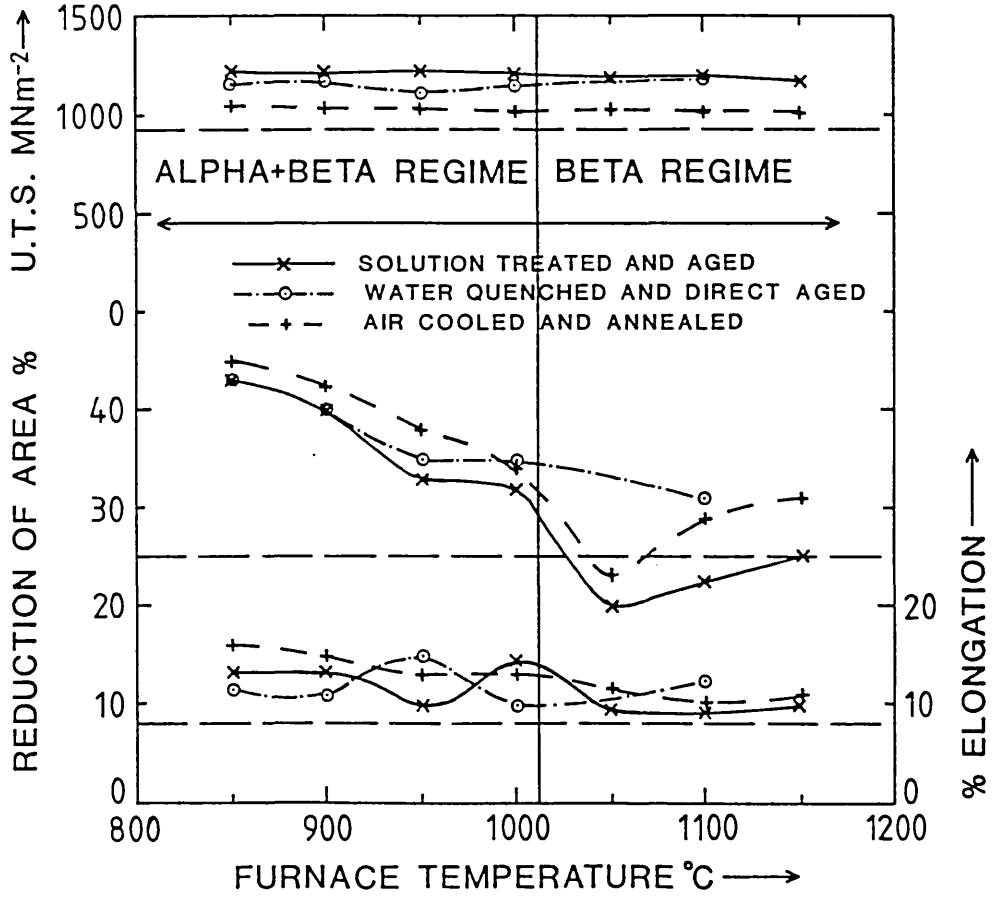

Figure 4.81 COMPARISON OF AS ANNEALED, DIRECT AGED AND SOLUTION TREATED AND AGED PROPERTIES AT R = 20:1

0.2% P.S. MNm^{-2}	U.T.S. MNm^{-2}	% Elongation	% Reduction of Area
830	930	8	25

TABLE 4.36 TENSILE PROPERTIES SPECIFICATION FOR ALPHA+BETA EXTRUDED SECTIONS OF I.M.I. Ti-6Al-4V, AIR COOLED AND ANNEALED 700°C[51]

4.8.5.2 AIR COOLED AND ANNEALED PROPERTIES

Considering first the air cooled and annealed properties. The U.T.S. and 0.2% P.S. do not vary significantly with temperature or extrusion ratio over the whole extrusion range, although there is a tendency for a small increase in these properties with increasing extrusion ratio and decreasing temperature. Representative values of U.T.S. for an extrusion ratio of 20:1 are given in Figure 4.78. The 0.2%P.S. follows an almost identical pattern, the 0.2% P.S./U.T.S. ratio remaining essentially constant at approximately 0.9. Average values of U.T.S. and Y.S. over the whole range are 1031 MNm^{-2} and 927 MNm^{-2} respectively which are well above the property minima.

There therefore appears to be little scope for improving the as annealed U.T.S. and 0.2% P.S. values by variation of the extrusion variables.

By contrast, a very substantial variation in reduction of area, and to a lesser extent % elongation occurs with temperature and extrusion ratio as is apparent from Figure 4.78. These variations can be directly attributable to changes in structure.

Considering first the variation in the reduction of area values with temperature at an extrusion ratio of 20:1, the corresponding structures being given in Figure 4.60. In the alpha+beta regime there is a reduction in the R. of A. values with increasing temperature, but the values are all relatively high. This is due initially to a reduction in the proportion of alpha phase, but as the alpha phase disappears the further reduction is due to an increase in the transformed beta grain size.

As the beta regime is entered, however, a marked drop in R. of A. occurs, before increasing again as the temperature increases. This trough in R. of A., which is below the specified minimum is clearly attributable to the presence of the very coarse unrecrystallised transformed beta. As the temperature is increased the proportion of unrecrystallised beta decreases, with an increase in the R. of A., until at 1150°C a fully recrystallised structure is produced, with its higher attendant R. of A. value.

A similar trough in R. of A. was observed in the case of the partial extrusion at 1100°C, R = 10:1, where again a very substantial proportion of unrecrystallised beta was present in the structure (Figure 4.65).

As was discussed in section 4.8.2.1.2, increasing the extrusion ratio in the beta regime serves to reduce the proportion of unrecrystallised beta, and also reduce the recrystallised grain size. This is reflected as an increase in the reduction of area values with increasing extrusion ratio as is apparent from Figure 4.78. For example, at 1100°C, increasing the extrusion ratio from 10:1 to 20:1 to 40:1 produces an increase in the R. of A. from 22% to 29% to 32%. The reason for this is apparent from Figure 4.65, where a predominantly unrecrystallised structure is present at R = 10:1, but as the extrusion ratio is increased the proportion of unrecrystallised beta decreases, until at R = 40:1 a fully recrystallised structure is produced.

The variation of reduction of area with grain size is shown in Figure 4.82 and it is apparent that there is a trend of a decrease in R. of A. with increasing grain size, although there is a large scatter in the results. The equation of the best straight line is given by :-

GRAIN SIZE (μm) = - 10.85 [R. of A.] + 472.20 c.c. = 0.848 4.11

The dependence of the R. of A. on grain size explains the low values obtained for the unrecrystallised structures. Transverse sections through unrecrystallised and recrystallised structures are shown in Figures 4.83 and 4.84 respectively. The number of grain boundaries is substantially greater in the recrystallised structure, with the unrecrystallised structure effectively behaving like a very coarse grained structure, with in consequence a low R. of A. value.

It is apparent from this discussion that the reduction of area values obtained in the beta regime are highly dependent on the extrusion parameters, with a substantial improvement being obtained by increasing the extrusion ratio. To a lesser extent, in so much as it increases the tendency for recrystallisation to occur, the extrusion temperature can be increased.

The average values of R. of A. in the alpha+beta and beta regimes are 38.3% and 30.4% respectively, highlighting an advantage of working in the two phase regime. By ensuring the elimination of the unrecrystallised structures, by careful extrusion parameter control, the latter value can be significantly improved.

The variation in the reduction of area with temperature and extrusion ratio can be combined into a single relationship using the z-parameter, the results in the alpha+beta and beta regimes being shown in Figures 4.85 and 4.86 respectively. The equations of the best straight lines are given by :-

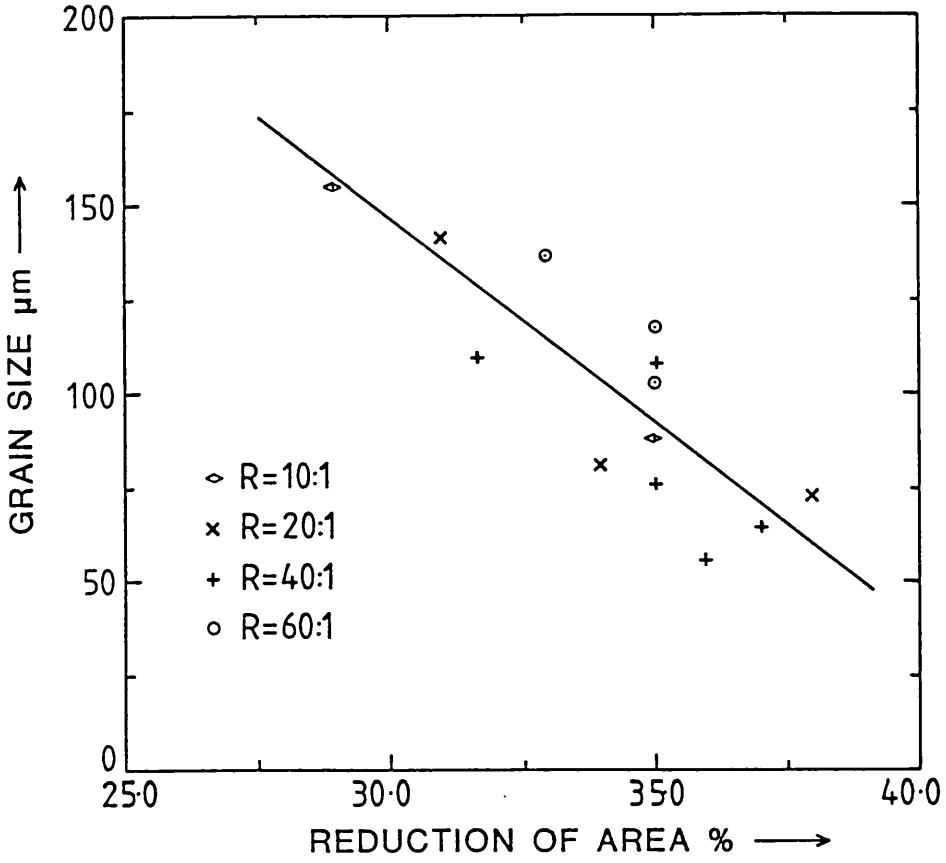

Figure 4.82 GRAIN SIZE VS. REDUCTION OF AREA FOR AIR COOLED AND ANNEALED MATERIAL

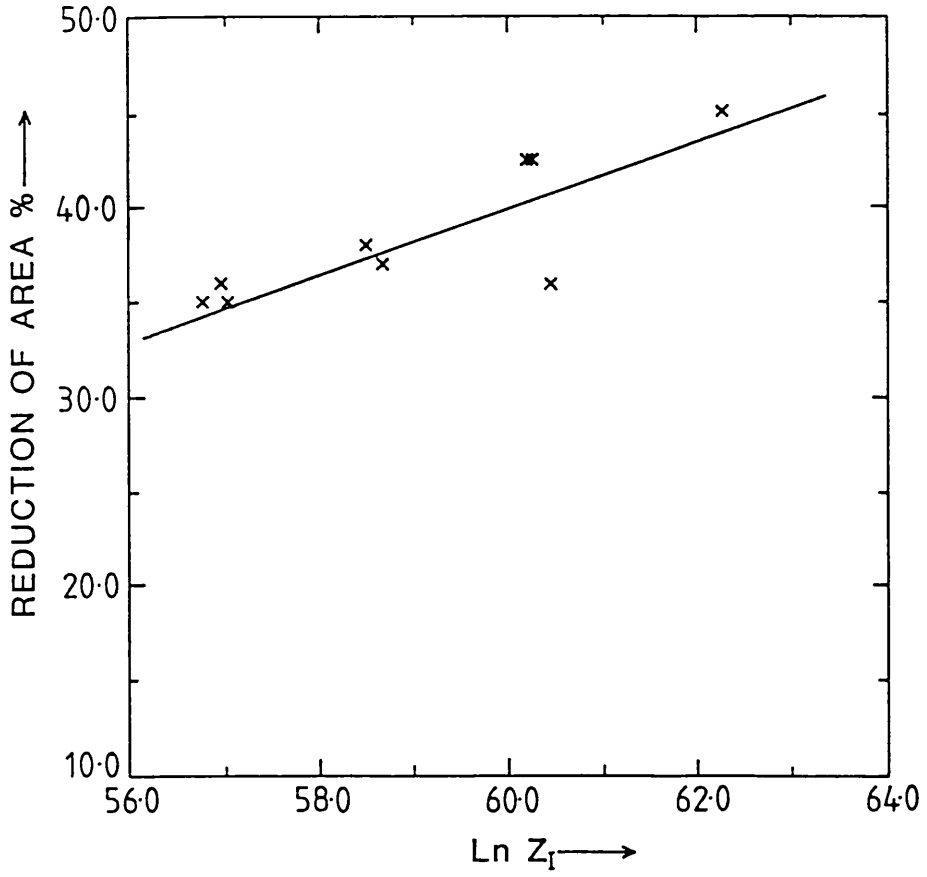

Figure 4.85 REDUCTION OF AREA VS. LN Z_I IN THE ALPHA+BETA REGIME FOR AIR COOLED AND ANNEALED MATERIAL

FIGURE 4.83

TRANSVERSE SECTION THROUGH

UNRECRYSTALLISED TRANSFORMED BETA

FIGURE 4.84

TRANSVERSE SECTION THROUGH

RECRYSTALLISED TRANSFORMED BETA

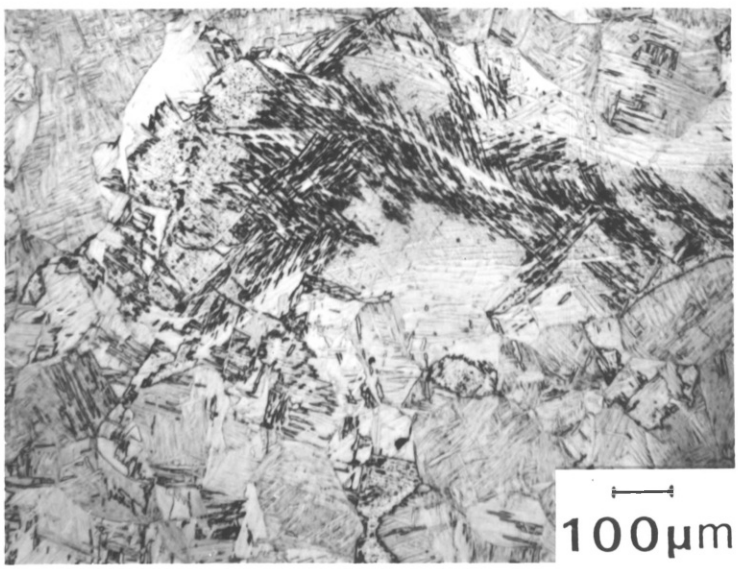
100μm

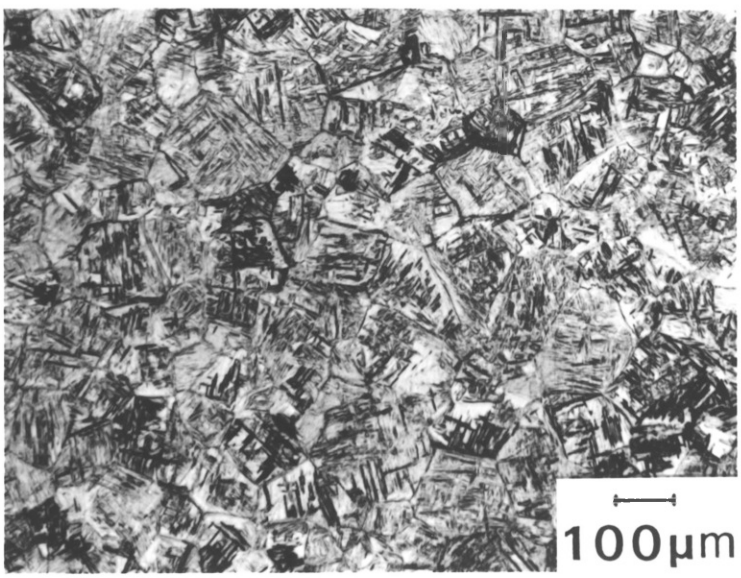
100μm

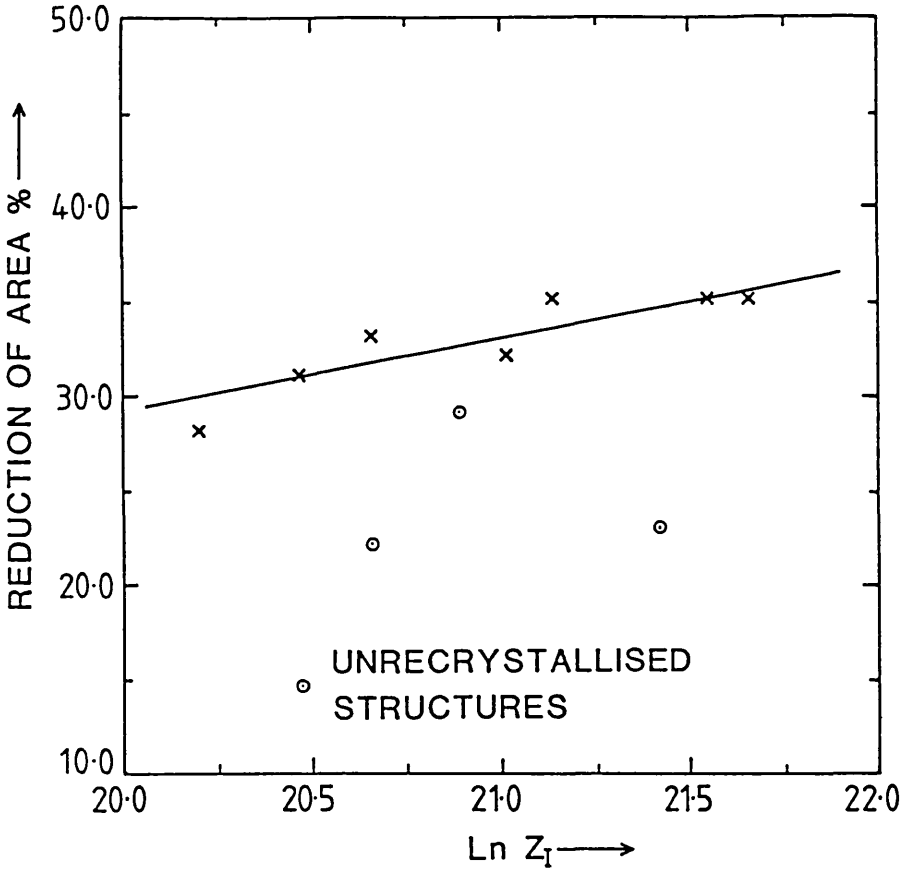

Figure 4.86 REDUCTION OF AREA VS. LN Z_I IN THE BETA REGIME FOR AIR COOLED AND ANNEALED MATERIAL

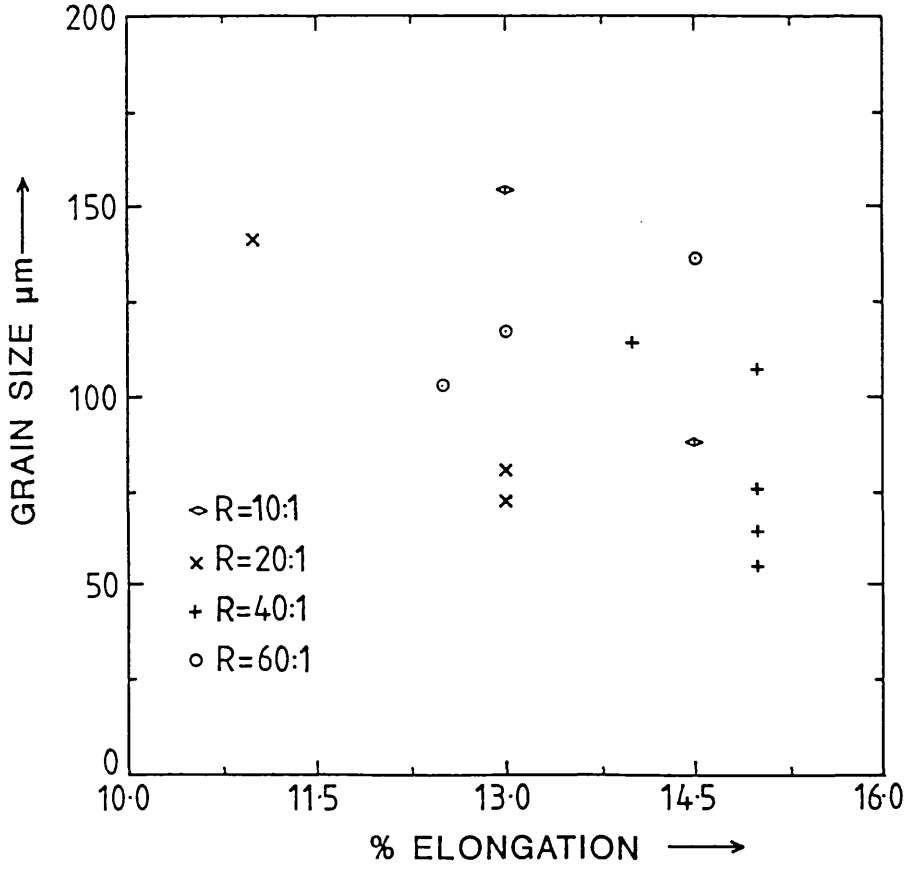

Figure 4.87 GRAIN SIZE VS. % ELONGATION FOR AIR COOLED AND ANNEALED MATERIAL

ALPHA+BETA
REGIME

$$\text{R. of A. (\%)} = 1.781\ [\ln Z_I] - 66.81 \qquad \text{c.c.} = 0.853 \qquad 4.12$$

BETA REGIME

$$\text{R. of A. (\%)} = 3.871\ [\ln Z_I] - 48.27 \qquad \text{c.c.} = 0.901 \qquad 4.13$$

The relationship in the beta regime is valid only for fully recrystallised structures, as is apparent if the results for the unrecrystallised structures are included in Figure 4.86.

The variation of % elongation with temperature and extrusion ratio was a lot more erratic compared to the R. of A. values, however there were general trends of a decrease in value with increasing temperature and decreasing extrusion ratio. The % elongation values were not as adversely affected by the presence of the unrecrystallised beta, with all the values being comfortably above the property minimum. In addition, there was clearly not the same grain size dependence of % elongation as was observed with the reduction of area values (Figure 4.87).

The average values of % elongation in the alpha+beta and beta regimes are 14.7% and 12.6% respectively, indicating a further advantage of alpha+beta extrusion. As was the case with the R. of A. values, however, the indications are that an improvement in the beta extrusion % elongation values can be obtained by correct selection of the processing conditions.

The Young's modulus was essentially independent of temperature and extrusion ratio, having an average value for air cooled and annealed material of 115.9 GNm^{-2}.

As was discussed in section 1.2.4.4, the structure of alpha and beta plates produced on air cooling from the beta phase field is reported to have substantially higher fracture toughness values compared to the primary alpha+beta structures. This is attributed to the

increased crack tortuosity occurring within the platelet structure. Although fracture toughness is not included in the I.M.I. standard, in certain applications high fracture toughness may be the dominant requirement and hence beta extrusion will be more attractive. It will be particularly interesting to investigate the influence of grain size and alpha and beta platelet width on the fracture toughness, as well as the presence of any unrecrystallised transformed beta.

4.8.5.3 WATER QUENCHED AND DIRECT AGED PROPERTIES

Considering now the water quenched and direct aged results. The results are given in Table 4.34 and plotted in Figure 4.79. Only one extrusion was water quenched from the beta regime.

Comparison of the U.T.S., reduction of area and % elongation values with those of air cooled and annealed material is given in Figure 4.81 for an extrusion ratio of 20:1.

A greater variation in the U.T.S. and 0.2% P.S. occurs with extrusion ratio and temperature, although there are no obvious trends. The average values of U.T.S. and 0.2% P.S. are 1158 MNm^{-2} and 1049 MNm^{-2} respectively which are approximately 12% higher than the air cooled and annealed values, which represents a significant increase in strength. The strengthening response is due to decomposition of the martensite produced on water quenching to a fine equilibrium structure of alpha+ beta.

The reduction of area values show a general decrease with increasing temperature as the proportion of alpha phase decreases and the transformed beta grain size increases. The obvious anomaly is at T = 950°C, R = 60:1 where a very high value of R. of A. is obtained.

Since only one extrusion was carried out in the beta range, and this was fully recrystallised, the influence of an unrecrystallised water quenched structure on the R. of A. value could not be assessed, however

it would be expected that a similar trough in R. of A. would be obtained and may even be accentuated by the greater inhibition of recrystallisation obtained on water quenching.

Lower values of R. of A. were obtained at R = 20:1 in the water quenched extrusions in the alpha+beta regime compared to the air cooled extrusions (Figure 4.81), however for all extrusion ratios an average value of 38.0% was obtained which is negligibly different from the air cooled value of 38.3%.

The variation of the reduction of area with the z-parameter for water quenched and direct aged material is shown in Figure 4.88. A linear relationship is assumed, the equation being given by :-

$$\text{R. of A. (\%)} = 1.852 \ln Z_I - 71.48 \qquad \text{c.c.} = 0.781 \qquad 4.14$$

The similarity of the R. of A. values for both air cooled and water quenched extrusions in the alpha+beta regime means that a single relationship can be established between R. of A. and $\ln Z_I$ which is independent of cooling rate. This is shown in Figure 4.89, the equation of the best straight line being

$$\text{R. of A. (\%)} = 1.814 \ln Z_I - 68.99 \qquad \text{c.c.} = 0.811 \qquad 4.15$$

The % elongation values are very erratic, with no trend with temperature or extrusion ratio. The average value in the alpha+beta regime is 13.0% compared to 14.7% for air cooled material, representing a percentage difference of 13%. Thus the percentage increases in strength for water quenched material is accompanied by a similar reduction in ductility.

Again no significant variation of Young's modulus was obtained with the extrusion variables, an average value of 116.7 GNm^{-2} being obtained which is a negligible increase compared to the air cooled value.

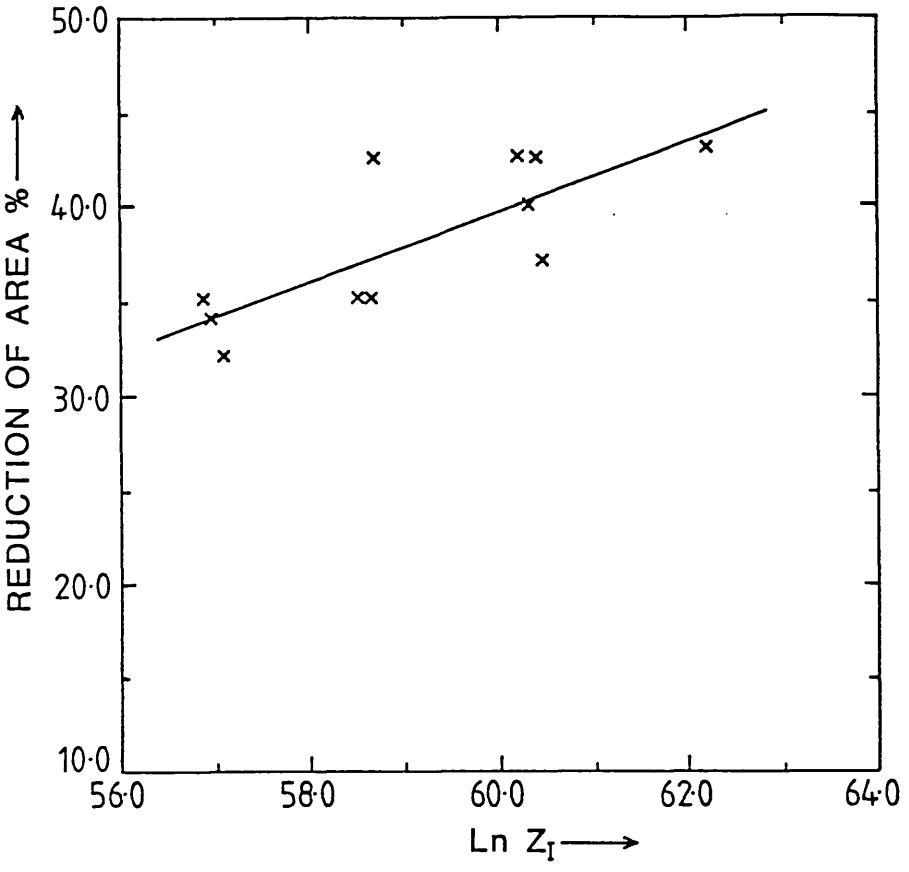

Figure 4.88 REDUCTION OF AREA VS. LN Z_I IN THE ALPHA+BETA FOR WATER QUENCHED AND DIRECT AGED MATERIAL

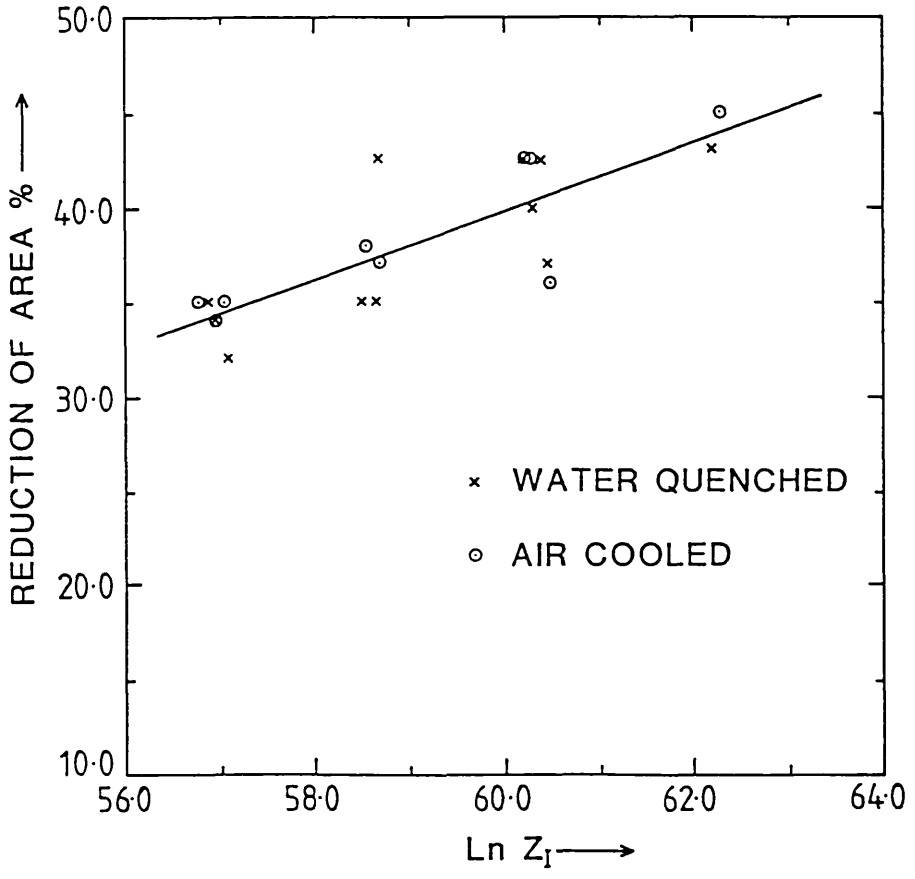

Figure 4.89 REDUCTION OF AREA VS. LN Z_I IN THE ALPHA+BETA REGIME FOR BOTH AIR COOLED AND WATER QUENCHED MATERIAL

The reasons for the variable values in % elongation and U.T.S. with temperature and extrusion ratio will now be discussed.

As was discussed in section 1.2.4.5 the strengthening response obtained on ageing of the martensite is dependent on the solution treatment temperature, which governs the proportion of martensite formed and its composition, and the ageing time and temperature.

Only one ageing treatment was investigated in the present work, 4 hours at 540°C, just to obtain some idea of the strengthening potential. This is the recommended ageing treatment following solution treatment at 950°C[7], and clearly will not represent the optimum treatment for each extrusion temperature. Thus if use is to be made of direct ageing after water quenching, ageing curves will have to be established for each extrusion temperature to identify the optimum heat treatment.

A further complication is that Ti-6Al-4V is of limited hardenability[6,7] and hence as the extrusion ratio increases the through "hardening" will increase, which may well alter the ageing response.

Although the optimum ageing conditions have clearly not been achieved for each extrusion condition, some excellent combinations of strength and ductility have been obtained, which highlight the potential for direct ageing treatments. For example, at T = 950°C, R = 60:1, a U.T.S. value of 1243 MNm^{-2} was obtained with a % elongation of 14.0% and a reduction of area of 42.5%. This is an outstanding combination of properties, with the U.T.S. being approximately 21% greater than air cooled and annealed material for similar values of % elongation and reduction of area.

Thus clearly more work needs to be done on establishing ageing curves and identifying the ageing mechanisms occurring.

As far as the potential for direct ageing of industrially sized sections is concerned, the alloy, as discussed earlier, is of limited hardenability, and hence strength increases will probably be limited to section sizes under 50 mm[6]. Obviously, for alloys of higher

hardenability, however, such as beta alloys (section 1.1.2.3) water quenching and direct ageing may well produce substantial strength increases in thick sections.

4.8.5.4 SOLUTION TREATED AND AGED PROPERTIES

Considering now the influence of a solution treatment at 950°C followed by water quenching and ageing at 540°C for 4 hours. The results for an extrusion ratio of 20:1 are given in Table 4.35 and plotted in Figure 4.80. Comparison with the as-annealed and direct aged properties are given in Figure 4.81.

The influence of the solution treatment on the structure depends on whether there is any primary alpha present in the extruded structure. If this is the case, the alpha phase formed on solution treatment has a relatively equiaxed morphology (Figure 4.90a), although some of the original elongated alpha phase does not recrystallise during heat treatment (Figure 4.90b). Electron microscopy reveals the predominantly equiaxed nature of the alpha grains (Figure 4.90c). The martensite produced on water quenching from the solution treatment temperature decomposes on ageing to a fine equilibrium structure of alpha and beta. Similar structures were produced for both air cooled and water quenched extrusions.

At temperatures of 950°C and above, where no primary alpha phase is present in the extruded structure, the alpha phase formed on solution treatment occurs in the form of plates (Figure 4.90d). The size of the plates is governed by the original martensite plate size, which in turn depends on the transformed beta grain size.

The values of U.T.S. and 0.2% P.S. for both solution treated and aged water quenched and air cooled structures are very similar (Table 4.35) and an average value is presented in Figure 4.80. The U.T.S. and 0.2% P.S. do not vary substantially with temperature, although there is a trend of a small reduction in values with increasing extrusion temperature.

(a)

PRIMARY ALPHA IN ORIGINAL STRUCTURE

TRANSVERSE SECTION

(b)

PRIMARY ALPHA IN ORIGINAL STRUCTURE

LONGITUDINAL SECTION

FIGURE 4.90

SOLUTION TREATED AND AGED STRUCTURES

(c)

PRIMARY ALPHA IN ORIGINAL STRUCTURE

- EQUIAXED ALPHA FORMED ON SOLUTION TREATMENT

(d)

NO PRIMARY ALPHA IN ORIGINAL STRUCTURE

- PLATELET ALPHA FORMED ON SOLUTION TREATMENT

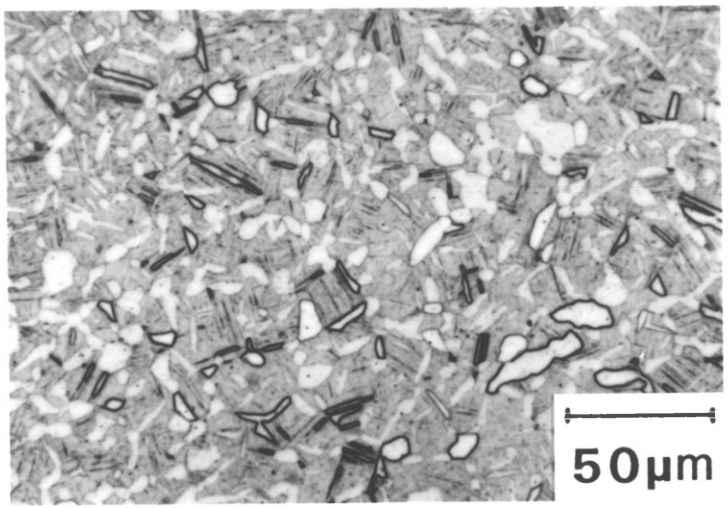
50μm

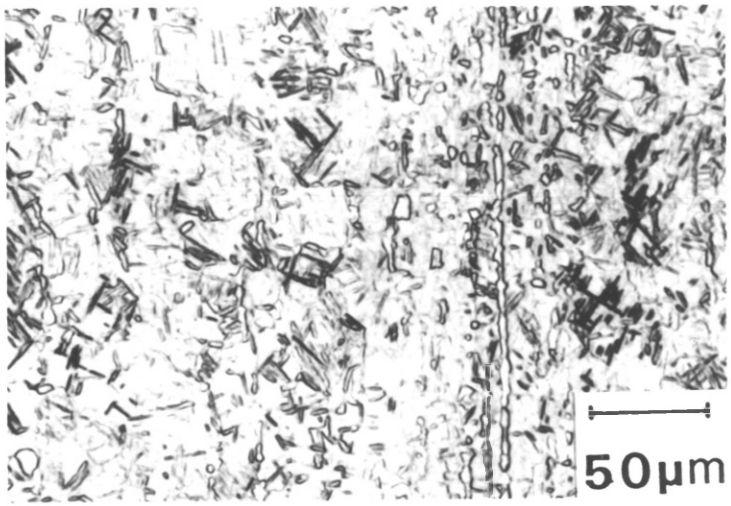
50μm

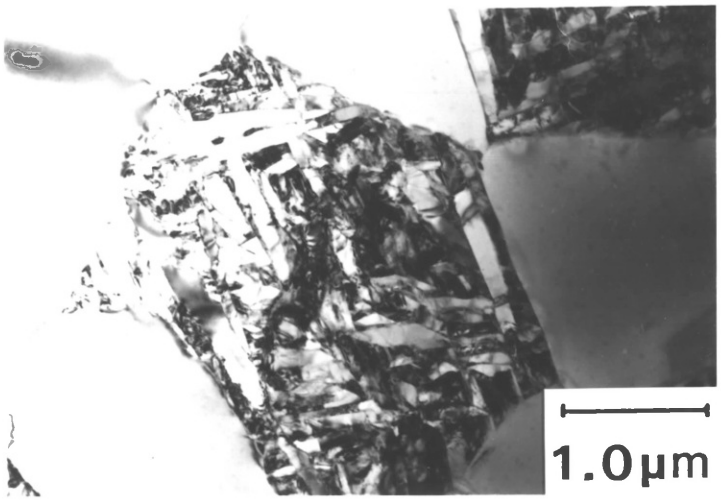
1.0μm

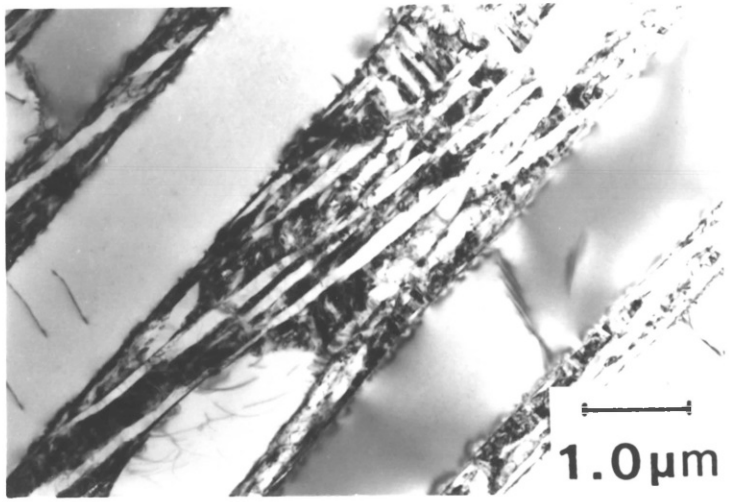
1.0μm

The average values of U.T.S. and 0.2% P.S. in the alpha+beta regime are 1221 MNm^{-2} and 1117 MNm^{-2} respectively, which are approximately 5.4% greater than the direct aged values and 18.4% greater than the as annealed results. With the correct selection of ageing conditions it would be expected that the direct aged values would more closely approach the solution treated and aged values.

The reduction of area values vary substantially with extrusion temperature, following similar trends to those observed for the other heat treatments, although the values are significantly lower (Figure 4.81).

Excellent values of reduction of area were obtained at temperatures of 900°C and below. This is associated with the primary alpha having an equiaxed morphology. Above 900°C the primary alpha occurred in the form of plates. The reduction of area values decreased markedly with increasing temperature as the transformed beta grain size and hence the platelet coarseness increased. The water quenched extrusions had significantly higher values of reduction of area than the corresponding air cooled extrusions, due to the smaller grain sizes produced on quenching. Very low values of reduction of area were again observed at 1050°C and 1100° for the air cooled extrusions, due to the presence of the unrecrystallised transformed beta, the solution treatment and ageing serving only to worsen the situation.

The % elongation values are again erratic, however they are clearly significantly lower in the beta regime, with the values in the alpha+ beta regime being generally reasonably good.

The average value of Young's modulus is 117.0 GNm^{-2}, which is negligibly different from the air cooled and annealed and water quenched and aged values.

Thus, in conclusion, in the alpha+beta regime, particularly at low temperatures when the primary alpha has an equiaxed morphology, an outstanding combination of properties can be produced on solution treatment and ageing. For example, for the air cooled extrusion at

T = 850°C, R = 20:1, a U.T.S. value of 1231 MNm^{-2} was obtained with a reduction of area of 44% and a % elongation of 13.5%. As was discussed earlier, however, the alloy is of limited hardenability and hence the strength increases will be limited to small section sizes. By contrast, solution treatment and ageing in the beta regime produces very poor values of reduction of area and % elongation, which are not sufficiently compensated for by the increased strength levels.

4.8.5.5 COMPARISON WITH GURNEY AND MALE'S RESULTS

Gurney and Male also investigated the influence of the extrusion variables on the properties of both air cooled and water quenched extrusions[30-33]. They concentrated mainly on the variation of properties with temperature at an extrusion ratio of 10:1. Thus they did not identify the crucial influence of extrusion ratio on reduction of area in the beta regime. In addition, they did not observe any unrecrystallised transformed beta on extrusion in the beta regime, and hence no reduction of area troughs were apparent. In general, however, similar property trends with temperature and cooling rate were observed.

4.8.6 SUMMARY OF THE STRUCTURE AND PROPERTIES OF EXTRUDED Ti-6Al-4V

1) Very substantial temperature rises were observed to occur during extrusion in the alpha+beta regime, the temperature rise increasing with decreasing temperature and increasing extrusion ratio. These temperature rises had a profound influence on the extrusion structures obtained. Only 30% of all the extrusions carried out in the alpha+beta regime contained any primary alpha in the extrude structures.

2) At low temperatures in the alpha+beta regime, the alpha and beta phases were elongated during extrusion. The elongated alpha phase contained an equiaxed subgrain structure indicating that dynamic recovery was the predominant dynamic restoration mechanism. Thus while in torsion dynamic recrystallisation was the predominant

restoration mechanism, in extrusion it was dynamic recovery. The different deformation textures present in the extrusion and torsion starting material was considered to be the most likely reason for this difference. The different dynamic restoration mechanisms observed in extrusion and torsion calls into question the validity of employing the hot working constants obtained from torsion in the extrusion analysis.

Future work should employ the same starting material for both extrusion and torsion, to eliminate the texture variable and to observe whether the deformation mode influences the dynamic restoration mechanism.

3) At low temperatures and low extrusion ratios in the beta regime, some areas of unrecrystallised transformed beta were apparent in the central regions of the extrude. This feature disappeared towards the periphery of the extrude where the strains were higher, and can also be eliminated by increasing the extrusion ratio, and to a lesser extent by increasing the extrusion temperature. There is thus a critical strain that has to be achieved during beta extrusion before recrystallisation occurs.

The phase transformations occurring during cooling from the beta regime eliminate any high temperature substructure. Hence while the observation of the unrecrystallised structure is conclusive evidence that dynamic recovery has occurred, the recrystallised structure could have arisen from either static or dynamic recrystallisation. Both dynamically recovered and recrystallised structures were also observed in torsion.

4) A summary of the average values of the air cooled and annealed, water quenched and direct aged, and solution treated and aged properties in the alpha+beta and beta regimes is given in Table 4.37.

5) The U.T.S. and 0.2% P.S. are relatively insensitive to variation in the extrusion variables.

	Alpha+Beta Regime				Beta Regime			
	U.T.S. MNm^{-2}	0.2% P.S. MNm^{-2}	R.ofA. %	% Elong. on $5.65\sqrt{So}$	U.T.S. MNm^{-2}	0.2% P.S. MNm^{-2}	R.ofA. %	% Elong. on $5.65\sqrt{So}$
Air Cooled and Annealed	1034	930	38.3	14.7	1028	923	30.4	12.6
Water Quenched and Direct Aged	1158	1049	38.0	13.0	-	-	-	-
Solution Treated and Aged	1221	1117	37.6	13.1	1192	1080	22.5	9.5

TABLE 4.37 SUMMARY OF PROPERTIES OF HEAT TREATED EXTRUDED STRUCTURES

6) Water quenching and direct ageing produces an increase in strength of approximately 12% compared to air cooling and annealing, however at the expense of a similar percentage decrease in % elongation. The reduction of area values are essentially independent of cooling rate.

7) A very substantial variation in the reduction of area with the extrusion variables occurred. In the alpha+beta regime the reduction of area decreased with increasing temperature as the proportion of alpha phase decreased and the transformed beta grain size increased, however the values were all relatively high. In the beta regime, however, as was illustrated for the air cooled and annealed extrusions, at low

temperatures and extrusion ratios, very low values of reduction of area were observed which are associated with the presence of coarse unrecrystallised transformed beta in the structure. Increasing the extrusion ratio, and to a lesser extent the temperature, results in a fully recrystlalised structure and an improvement in the reduction of area values. Increasing the extrusion ratio also produces a decrease in the recrystallised grain size, which further serves to improve the reduction of area values.

8) The average value of reduction of area in the alpha+beta regime is approximately 28% higher than that in the beta regime, highlighting an advantage of extruding in the two phase regime. By careful extrusion parameter control, however, the values of reduction of area in the beta regime can be substantially improved.

9) For air cooled and annealed extrusions there was a general trend of a decrease in % elongation with increasing temperature and decreasing extrusion ratio. The % elongation values were not as adversely affected by the presence of the unrecrystallised transformed beta. The average value of % elongation in the alpha+beta regime is approximately 17% higher than in the beta regime, however again the indications are that, with careful extrusion parameter control, the % elongation values in the beta regime can be improved.

10) The properties produced on water quenching and direct ageing, in particular the % elongation, varied erratically with the extrusion variables. This is because the standard ageing treatment given does not represent the optimum treatment for each extrusion condition. A further complication is that Ti-6Al-4V is of limited hardenability and hence the ageing response may well vary with section size, i.e. extrusion ratio. Although the optimum ageing conditions were not established for each extrusion condition, some excellent combinations of properties were obtained, which highlights the potential for water quenching and direct ageing treatment for thin sections.

11) Solution treatment and ageing of both air cooled and water quenched extrusions produced increases in U.T.S. and 0.2% P.S. of approximately 5.4% compared to direct aged extrusions and 18.4% compared to annealed extrusions. However, while in the alpha+beta regime, some excellent values of reduction of area and % elongation were obtained, in the beta regime very low values were observed.

12) The value of Young's modulus does not vary significantly with the extrusion variables or heat treatment, having an average value of 116.5 GNm^{-2}.

13) Relationships were established between the extrusion variables, incorporated in the z-parameter, and the reduction of area values, in both regimes. The similarities of the R. of A. values in both air cooled and water quenched extrusions in the alpha+beta regime meant that a single relationship could be established which was independent of cooling rate. The relationships are given by :-

ALPHA+BETA REGIME: R. of A.(%) = $1.852[\ln Z_I] - 71.48$ c.c. = 0.811

BETA REGIME: R. of A.(%) = $3.871[\ln Z_I] - 48.27$ c.c. = 0.901

The latter relationship only applies to fully recrystallised structures.

14) Relationships were also established between the recrystallised grain size and the z-parameter in both regimes. These are :-

(a) ALPHA+BETA REGIME

AIR COOLED: GRAIN SIZE (μm) = $- 6.626 [\ln Z_I] + 456.2$ c.c. = 0.954

WATER QUENCHED: GRAIN SIZE (μm) = $- 6.595 [\ln Z_I] + 441.2$ c.c. = 0.965

(b) BETA REGIME

AIR COOLED: GRAIN SIZE (μm) = $- 34.5 [\ln Z_I] + 847.9$ c.c. = 0.979

CHAPTER FIVE

CONCLUSIONS AND IDEAS FOR FURTHER WORK

CHAPTER FIVE

CONCLUSIONS AND IDEAS FOR FURTHER WORK

5.1 CONCLUSIONS

Each section has been summarised and hence only the major points will be reiterated from each section.

1) The die wear encountered in the extrusion programme was due to the presence of a very hard brittle oxide scale on the billet surface, formed by reaction of the alloy with oxygen during heating and transfer. The oxide scale cracked during extrusion, thereby preventing effective lubrication and insulation by the glass at the billet/die interface which resulted in die wear. The prevention of the formation of this oxide scale virtually eliminated any die wear and resulted in a marked improvement in the surface quality.

2) The lubricating behaviour of the extrusion glasses varies markedly with extrusion temperature and extrusion ratio. The viscosity of the glass at the extrusion temperature gives a good indication of the potential suitability as an extrusion lubricant, although temperature changes occurring during extrusion may well influence its lubricating behaviour.

3) The alloy exhibits markedly different hot deformation behaviour in the alpha+beta and beta regimes, as highlighted both by extrusion and torsion studies. In the alpha+beta regime, where the structure consists of fine grained two phase alpha+beta, there is a marked flow stress dependence of temperature. By contrast, in the beta regime, where the structure consists of coarse grained single phase beta, the flow stress dependence of temperature is markedly reduced. Similarly, the flow stress dependence of strain rate is much higher in the alpha+ beta, compared to the beta,regime.

4) The markedly different hot deformation behaviour exhibited by Ti-6Al-4V in the alpha+beta and beta regimes is reflected in the markedly different values of the hot working constants obtained from torsion testing. The activation energy for hot working in the alpha+beta regime is 521,697 J/mole which is approximately 3 x the value of 169,962 J/mole obtained in the beta regime.

5) The value of activation energy obtained in the beta regime is similar to that for self-diffusion in the beta phase of super-purity titanium which suggests that dynamic recovery should be the predominant dynamic restoration mechanism during beta working. Evidence of dynamic recovery was observed at low strain rates in torsion, and at low extrusion ratios at low temperatures during extrusion. However, at high strain rates during torsion, and predominantly during extrusion, fully recrystallised structures were produced, which may have occurred either as a result of static recrystallisation from a dynamically recovered structure, or as a result of dynamic recrystallisation during deformation. The phase transformations occurring on cooling from the beta regime wipe out any deformation substructure and hence this argument cannot be conclusively resolved.

6) In the alpha+beta regime the value of activation energy is substantially greater than that for self-diffusion in the alpha and beta phases of super-purity titanium and is associated with the occurrence of dynamic recrystallisation. However, while dynamic recrystallisation was the predominant restoration mechanism in torsion, in extrusion it was dynamic recovery. The different deformation textures present in the extrusion and torsion starting material was considered to be the most likely reason for this difference. The different dynamic restoration mechanisms observed in extrusion and torsion calls into question the validity of employing the hot working constants obtained from torsion in the extrusion analysis. Future work should employ the same starting material for both extrusion and torsion, to eliminate the texture variable and to observe whether the deformation mode influences the dynamic restoration mechanism.

7) In the alpha+beta regime empirical relationships were established between the peak pressure and the initial temperature, extrusion ratio and temperature compensated strain rate. A single line linear relationship was obtained between P/σ_I and ln R which enables the extrusion pressure to be predicted for any conditions of initial temperature, extrusion ratio and ram speed, using the values of the hot working constants obtained from torsion. The equation is given by :-

$$P/\sigma_I = 0.945 + 0.527 \ln R \qquad \text{c.c.} = 0.957 \qquad 5.1$$

8) In the beta regime the severity of the die wear precluded the establishment of any satisfactory relationships between the pressure and the extrusion variables. With the dramatic reduction in die wear obtained using the modified extrusion practice, future studies into titanium extrusion should allow for accurate correlations to be extablished in the beta regime.

9) All the relationships established took no account of any temperature changes occurring during extrusion. This is because the temperature rise model employed failed to give reasonable predictions of the temperature rises occurring during extrusion and hence accurate temperature compensated relationships could not be established.

10) Structural studies revealed that very substantial temperature rises occurred during extrusion in the alpha+beta regime, the temperature rise increasing with increasing extrusion pressure. As a result of these temperature rises only a small number of the extrusions carried out in the alpha+beta regime contained any primary alpha.

11) The U.T.S. and 0.2% P.S. are relatively insensitive to variation in the extrusion variables.

12) Water quenching and direct ageing produces an increase in strength of approximately 12% compared to air cooling and annealing, however at the expense of a similar percentage decrease in % elongation.

13) A very substantial variation in the reduction of area with the extrusion variables occurred. In the alpha+beta regime the reduction of area decreased with increasing temperature as the proportion of alpha phase decreased and the transformed beta grain size increased, however the values were all relatively high. In the beta regime, however, as was illustrated for the air cooled and annealed extrusions, at low temperatures and extrusion ratios, very low values of reduction of area were observed which are associated with the presence of coarse unrecrystallised transformed beta in the structure. Increasing the extrusion ratio, and to a lesser extent the temperature, results in a fully recrystallised structure, and an improvement in the reduction of area values. Increasing the extrusion ratio also produces a decrease in the recrystallised grain size, which further serves to improve the reduction of area values.

14) The average values of reduction of area in the alpha+beta regime is approximately 28% higher than that in the beta regime, highlighting an advantage of extruding in the two phase regime. By careful extrusion parameter control, however, the values of reduction of area in the beta regime can be substantially improved.

15) For air cooled and annealed extrusions there was a general trend of a decrease in % elongation with increasing temperature and decreasing extrusion ratio. The % elongation values were not as adversely affected by the presence of the unrecrystallised transformed beta. The average value of % elongation in the alpha+beta regime is approximately 17% higher than that in the beta regime, however again the indications are that, with careful extrusion parameter control, the % elongation values in the beta regime can be improved.

16) The properties produced on water quenching and direct ageing, in particular the % elongation, varied erratically with the extrusion variables. This is because the standard ageing treatment given does not represent the optimum treatment for each extrusion condition. A further complication is that Ti-6Al-4V is of limited hardenability and hence the ageing response may well vary with section size. Although the optimum ageing conditions were not established for each extrusion condition, some excellent combinations of properties were obtained, which highlighted the potential for water quenching and direct ageing treatment for thin sections.

17) Solution treatment and ageing of both air cooled and water quenched extrusions, produced increases in U.T.S. and 0.2% P.S. of approximately 5.4% compared to* annealed extrusions. However, while in the alpha+ beta regime, some excellent values of reduction of area and % elongation were obtained, in the beta regime very low values were obtained.

18) Relationships were established between the extrusion variables, incorporated in the z-parameter, and the reduction of area values in both regimes. The similarity of the reduction of area values in both air cooled and water quenched extrusions in the alpha+beta regime meant that a single relationship could be established which was independent of cooling rate. The relationships are given by :-

ALPHA+BETA REGIME	R. of A. (%) = 1.852 [ln Z_I] - 71.48	c.c.=0.811	5.2
BETA REGIME	R. of A. (%) = 3.871 [ln Z_I] - 48.27	c.c.=0.901	5.3

The latter relationship only applies to fully recrystallised structures.

direct aged extrusions and 18·4o\° compared to

5.2 IDEAS FOR FURTHER WORK

1) The die wear problem has now been essentially overcome using the modified extrusion practice developed in this work. Hence in future studies it should be possible to establish the following :-

   (a) Relationships between the extrusion pressure and the extrusion variables in the beta regime.

   (b) The optimum extrusion ranges for the glasses employed in the current work, and the variation in the thickness of the glass coating on the extrude with the extrusion variables.

   (c) Extrusion limit diagrams, and how they vary with different extrusion glasses.

2) The techniques developed for extruding Ti-6Al-4V will be appropriate to the extrusion of any titanium alloy, and hence future studies will be able to encompass the entire titanium alloy range. This should proide a fascinating study in an area which has received scant attention to date. Future extrusion programmes should preferably involve I.M.I. Titanium and Osborne Steel Extrusions (see acknowledgements), who, in conjunction, are actively pursuing titanium extrusion.

3) Extrusion at lower temperatures should be investigated. This can be achieved either with the use of conical extrusion dies using molybdenum disulphide grease as the sole lubricant (section 1.3.3.10), or using the technique developed in this work with lower softening point glasses, e.g. leaded glasses.

4) Future studies into glass lubricants for extrusion should actively involve Bayer U.K. (see acknowledgements), the major supplier, who should provide softening point and temperature-viscosity data, and also Acheson Colloids (see acknowledgements) who manufacture the Deltaglaze coatings and the molybdenum disulphide grease.

5) When investigating the suitability of glasses and other lubricants for titanium extrusion it would be more sensible to employ a cheaper billet material, with similar elevated temperature flow stress values to titanium, such as mild steel, for the initial trials.

6) When the production of simple rounds has been perfected, more complex commercial shapes should be produced with the added problems of die design considerations and increased susceptibility to die wear. H13 steel may well prove to be inadequate and hence methods of improving its wear resistance as well as alternative die materials could be looked at. Methods of improving wear resistance include surface hardening by carburising or nitriding, or flame spraying with a coating of alumina or zirconia (section 1.3.3.7). Alternative die materials that could be looked at include nimonics, cemented tungsten carbides, nickel-bonded titanium carbide, devitrium alloys and sialon (section 1.3.3.7). The use of die inserts of these material would reduce the costs of such work.

7) A new valve system has just been installed, which, when fully operational, will allow the ram speed to be controlled independently of the pressure. This will allow the variation in the extrusion pressure with the ram speed to be investigated.

8) The combination of lower temperatures, possible using lower softening point glasses or conical extrusion dies, and lower ram speeds, possible using the new value system, will mean that a more extensive investigation of alpha+beta extrusion will be possible. The lower ram speeds employed will reduce the temperature rises occurring during extrusion, and hence structures containing a larger volume fraction of alpha phase will be produced. This will allow the influence of the proportion of the alpha phase on the properties to be more extensively investigated, as well as the variation in the alpha subgrain size with the extrusion variables.

9) The newly acquired induction facility means that considerably reduced heating times can be employed. Thus in the beta regime the time for beta grain growth will be shorter, resulting in a finer starting beta grain size for extrusion. The influence of beta grain size on the properties of beta processed material has been highlighted in this work. It would be expected that with a finer starting structure, a finer recrystallised grain size would be produced on extrusion with improved reduction of area and % elongation values.

10) There is a requirement for an improved temperature rise model to predict the temperature changes occurring during extrusion and allow temperature compensated parameters to be employed in the extrusion analysis. The prediction of temperature changes occurring during glass lubricated extrusion is a particularly difficult problem and should really be tackled as a Ph.D. in itself.

11) If the best use is to be made of water quenching and direct ageing treatments for Ti-6Al-4V, ageing curves will have to be established over a wide range of extrusion temperatures to identify the optimum conditions. If use is to be made commerically of such treatment, then because of the limited hardenability of the alloy, the maximum section size that can be through strengthened will have to be established.

12) Air cooled beta extruded structures would be expected to have higher fracture toughness, and possibly creep strengths, than structures containing primary alpha (section 1.2.4.4). Further work needs to be carried out to verify this, and also establish the influence of grain size on these properties.

13) Different dynamic restoration mechanisms were observed in extrusion and torsion in the alpha+beta regime, this being attributed to the different deformation textures present in the torsion and extrusion starting material. This should be verified experimentally from texture studies of the starting material. Future work should employ the same

starting material for both extrusion and torsion to observe whether the same dynamic restoration mechanism is operative, i.e. the deformation mode is not crucial.

14) A more fundamental study is required on the hot deformation behaviour of unalloyed titanium if a greater understanding of more complex alloys is to be obtained. Unalloyed titanium is single phase b.c.c. beta above the transus and single phase h.c.p. alpha below the transus. Thus the hot deformation characteristics of the individual unalloyed phases can be clearly established and then compared with the behaviour of single phase alloyed systems and two phase systems.

15) Texture studies should be carried out on the extruded material.

APPENDIX I

MODIFICATIONS TO TORSION TEMPERATURE RISE MODEL

The torsion temperature rise model THTEMP has been modified to allow for the variation in specific heat and thermal conductivity of Ti-6Al-4V with temperature. The thermal constants were obtained from reference 75, Volume 2, Part 2.

1. Equation of specific heat Pg 1434

$$C_{J\ kg^{-1}\ K^{-1}} = 0.1172K + 468.9$$

2. Equation of thermal conductivity Pg 1440

$$K_{Wm^{-1}\ K^{-1}} = 0.02021 - 3.032$$

The density of the alloy was taken to be 4420 Kgm^{-3} (reference 6).

APPENDIX II

USE OF THE EXTEMP SUBROUTINE IN THE RESTI64 PROGRAMME TO EVALUATE THE TEMPERATURE CHANGES OCCURRING DURING EXTRUSION

The subroutine EXTEMP in the RESTI64 programme evaluates the temperature rise occurring during extrusion, having been modified to allow for the glass lubricated extrusion of titanium. Data is input into the RESTI64 programme in the normal manner using EXTDATA (procedure file Ext) and PARAM. The latter file incorporates the hot working constants file name, the number of runs and the extrusion data file name. The hot working constants file name has to be altered according to whether extrusion was carried out in the alpha+beta or beta regimes.

DATA INPUT FOR EXTEMP

The load-displacement curve is split up into increments of equal time, 10 being employed in this analysis, as described in section 4.6.2. Extrusion is assumed to commence when the accumulator is discharged, the ram speed then remaining essentially constant over the remainder of the stroke. The values of load, in MN, for each time increment are input on tape 11, starting from time t = 0. The extemp programme evaluates the area under the load-displacement curve for each time increment, using the equation

$$ALOAD = \tfrac{1}{2} (L_n + L_{n+1}) * V * DELTIME$$

where n varies from 1 to 11.

Allowance has been made in the programme for the variation of specific heat and thermal conductivity of Ti-6Al-4V with temperature, the equations employed being given in Appendix I. The tooling temperatures, evaluated experimentally, were 466°C for the container, 350°C for the die and 300°C for the pressure pad. The thermal constants for the tool steel were obtained from reference 75, Volume 3, the

constants being obtained from the steel closest in composition to H13. The values employed were :-

(a) density = 7750 kg m^{-3}

(b) thermal conductivity = 28.68 $Wm^{-1}K^{-1}$ Pg 82 Vascojet 1000

(c) specific heat = 603.6 J $kg^{-1}K^{-1}$

An average value was taken for the range 300°C - 466°C, using the data for a 9% Cr steel (Pg 65).

The properties of the borosilicate glass were obtained from reference 75, Volume 4, Part 2, although the silicate contents were higher than that of C6496. The values employed were :-

(a) density = 2520 kg m^{-3} Pg 1693

(b) thermal conductivity = 1.622 Wm^{-1} K^{-1} Pg 1699
An average value was taken of two glasses at 350°C

(c) specific heat = 951 J kg^{-1} K^{-1} Pg 1697
An average value was taken of two glasses at 350°C

To allow for the condition of no glass pad at the die face, use RESTI63.

APPENDIX III

TABLES OF EXTRUSION RESULTS

The extrusion results in the alpha+beta and beta regimes are given in the following tables. The following data has been tabulated.

1) Run Code (P) represents a partial extrusion
2) Furnace Temperature
3) Initial Average Temperature at commencement of extrusion
4) Extrusion Ratio
5) Glass Type
6) Cooling Medium
7) Die Number (n) represents nth extrusion through die
8) Peak Load Cell Pressure
9) Peak Hydraulic Pressure
10) Ram Speed
11) Time until Accumulator is Activated
12) Total Time to Extrude Billet
13) Modified Feltham's Strain Rate
14) Temperature Compensated Strain Rate at commencement of Extrusion Z_I
15) Flow Stress σ_I
16) Peak Load Cell Pressure / σ_I
17) Predicted Final Temperature with and without the Glass Pad

Run Code	Furnace Temp. °C	Initial Temp. °C	Extrusion Ratio	Glass Type	Cooling Medium	Die Number	Peak Load Cell Pressure MNm^{-2}	Hydraulic Pressure MNm^{-2}	Ram Speed mm/s	Time To Accumulator Activated S	Total Time to Extrude S
1	850	810	20	C6496	W.Q.	1(1)	1002	1328	68.7	1.36	2.48
2	850	810	20	C6496	A.C.	2(2)	1062	1469	74.5	1.17	2.15
3	850	810	20	No Glass	A.C.	1(2)	1151	1540	65.8	1.10	2.12
4(P)	900	851	10	C6496	A.C.	3(1)	506	964	108.1	0.96	1.48
5	900	851	10	K7072	W.Q.	3(2)	689	959	100.7	0.97	1.77
6	900	851	20	K7072	W.Q.	2(1)	873	1162	85.4	0.87	1.95
7	900	851	20	C6496	A.C.	5(2)	858	1153	81.1	1.17	2.32
8	900	851	40	C6496	W.Q.	6(1)	932	1290	70.7	0.81	2.04
9	900	851	40	C6496	A.C.	6(2)	873	1290	75.6	1.03	1.97
10	900	851	60	C6496	W.Q.	7(1)	1002	1380	61.3	1.07	2.17
11	950	893	20	C6496	A.C.	8(1)	683	917	103.5	1.07	1.93

EXTRUSION RESULTS IN THE ALPHA+BETA REGIME

Run Code	Furnace Temp. °C	Initial Temp. °C	Extrusion Ratio	Glass Type	Cooling Medium	Die Number	Peak Load Cell Pressure MNm^{-2}	Hydraulic Pressure MNm^{-2}	Ram Speed mm/s	Time To Accumulator Activated S	Total Time To Extrude S
12	950	893	20	C6496	W.Q.	8(2)	645	954	-	-	-
13	950	893	40	C6496	W.Q.	9(1)	808	1125	127.2	1.15	2.23
14	950	893	40	C6496	A.C.	9(2)	784	1030	130.4	0.96	1.98
15	950	893	60	C6496	W.Q.	10	843	1134	129.2	0.77	1.86
16(P)	1000	934	10	C6496	A.C.	11	322	756	121.2	0.63	0.96
17	1000	934	20	C6496	W.Q.	12(1)	560	747	133.6	0.65	1.33
18	1000	934	20	C6496	A.C.	12(2)	486	742	141.7	0.53	1.11
19	1000	934	40	C6496	W.Q.	13(1)	674	851	103.5	0.68	1.56
20	1000	934	40	C6496	A.C.	13(2)	620	851	114.1	0.64	1.46
21	1000	934	60	C6496	W.Q.	14	744	898	97.0	0.62	1.56

EXTRUSION RESULTS IN THE ALPHA+BETA REGIME (CONTINUED)

Run Code	Furnace Temp. °C	Initial Temp. °C	Extrusion Ratio	Feltham's Strain Rate s^{-1}	Z_I	σ_I	P/σ_I	Glass Pad		No Glass Pad	
								Final Temp. °C	Temp. Rise °C	Final Temp. °C	Temp. Rise °C
1	850	810	20	71.65	1.04×10^{27}	394.3	2.54	937	+ 127	868	+ 58
2	850	810	20	77.7	1.13×10^{27}						
3	850	810	20	68.6	9.99×10^{26}						
4(P)	900	851	10	86.15	1.57×10^{26}						
5	900	851	10	80.25	1.41×10^{26}	328.8	2.095	856	+ 5	804	- 17
6	900	851	20	89.1	1.57×10^{26}	332.4	2.63	918	+ 67	856	+ 5
7	900	851	20	84.6	1.43×10^{26}						
8	900	851	40	99.1	1.74×10^{26}	335.7	2.78	942	+ 91	872	+ 21
9	900	851	40	106.0	1.86×10^{26}						
10	900	851	60	103.7	1.82×10^{26}	337.2	2.97	972	+ 121	894	+ 43
11	950	893	20	108.0	2.54×10^{24}	273.1	2.50	889	- 4	833	- 60

EXTRUSION RESULTS IN THE ALPHA+BETA REGIME (CONTINUED)

Run Code	Furnace Temp. °C	Initial Temp. °C	Extrusion Ratio	Feltham's Strain Rate s^{-1}	Z_I	σ_I	P/σ_I	Glass Pad		No Glass Pad	
								Final Temp. °C	Temp. Rise °C	Final Temp. °C	Temp. Rise °C
12	950	893	20	-	-						
13	950	893	40	127.2	2.99×10^{25}	278.4	2.90	930	+ 37	867	- 26
14	950	893	40	130.4	3.07×10^{25}						
15	950	893	60	129.2	3.04×10^{25}	278.9	3.02	936	+ 43	868	- 25
16(P)	1000	934	10	121.2	4.59×10^{24}						
17	1000	934	20	133.6	5.06×10^{24}	221.5	2.53	896	- 38	842	- 92
18	1000	934	20	147.8	5.59×10^{24}						
19	1000	934	40	145.1	5.49×10^{24}	224.2	3.01	921	- 13	861	- 74
20	1000	934	40	160.0	6.05×10^{24}						
21	1000	934	60	164.0	6.21×10^{24}	228.0	3.26	957	+ 23	890	- 44

EXTRUSION RESULTS IN THE ALPHA+BETA REGIME (CONTINUED)

Run Code	Furnace Temp. °C	Initial Temp. °C	Extrusion Ratio	Glass Type	Cooling Medium	Die Number	Peak Load Cell Pressure MNm^{-2}	Hydraulic Pressure MNm^{-2}	Ram Speed mm/s	Time To Accumulator Activated S	Total Time to Extrude S
22	1050	974	20	C6496	A.C.	2(3)	407	685	146.0	0.51	1.07
23	1050	974	40	C6496	A.C.	15	526	709	123.7	0.40	1.16
24	1050	974	60	C6496	A.C.	16	595	860	114.1	0.41	1.13
25(P)	1100	1016	10	C6496	A.C.	17	303	-	152.1	0.42	0.73
26	1100	1016	20	C6496	W.Q.	18	508	709	130.4	0.6	1.25
27	1100	1016	20	C6496	A.C.	1(3)	397	671	146.7	0.43	0.99
28	1100	1016	40	C7216	A.C.	19	565	718	123.7	0.38	1.12
29	1100	1016	60	C7216	A.C.	20	570	761	116.3	0.47	1.24
30	1150	1058	10	C7216	A.C.	21	312	449	158.7	0.65	1.12
31	1150	1058	20	C6496	A.C.	5(3)	382	605	158.7	0.57	1.13
32	1150	1058	40	C7216	A.C.	22	476	624	132.7	0.51	1.14
33	1150	1058	60	C7216	A.C.	7(2)	585	869	118.2	0.495	1.18

EXTRUSION RESULTS IN THE BETA REGIME

Run Code	Furnace Temp. °C	Initial Temp. °C	Extrusion Ratio	Feltham's Strain Rate s^{-1}	Z_I	σ_I	P/σ_I	Glass Pad		No Glass Pad	
								Final Temp. °C	Temp. Rise °C	Final Temp. °C	Temp. Rise °C
22	1050	974	20	152.3	2.00×10^9						
23	1050	974	40	173.4	2.28×10^9	138.9	3.79	908	- 66	851	- 124
24	1050	974	60	192.9	2.54×10^9	141.2	4.21	938	- 36	876	- 98
25(P)	1100	1016	10	121.2	9.36×10^8						
26	1100	1016	20	136.0	1.05×10^9	122.8	4.14	933	- 83	874	- 142
27	1100	1016	20	153.0	1.18×10^9						
28	1100	1016	40	173.4	1.34×10^9	127.8	4.42	949	- 67	887	- 129
29	1100	1016	60	196.7	1.52×10^9	130.5	4.37	955	- 61	891	- 125
30	1150	1058	10	126.5	5.92×10^8	111.3	2.80	909	- 149	856	- 203
31	1150	1058	20	165.5	7.75×10^8						
32	1150	1058	40	186.0	8.71×10^8	119.1	4.00	965	- 93	902	- 156
33	1150	1058	60	199.9	9.36×10^8						

EXTRUSION RESULTS IN THE BETA REGIME (CONTINUED)

APPENDIX IV

LIST OF INDUSTRIAL CONTACTS AND SOURCES OF INFORMATION

The following people have provided very valuable advice during the course of the work, for which the author is extremely grateful. It would be hoped that in any future study into titanium extrusion greater interaction would be possible with these various parties.

1) Mr John Middleton
Osborne Steel Extrusions Limited
Low Moor, Bradford

2) Mr Brian Lowe
I.M.I. Titanium
Witton, Birmingham

I.M.I. and Osborne Steel Extrusions are, in conjunction, actively pursuing their own research and development programme into titanium extrusion.

3) Mr David Mayo
Section Leader
Materials and Development Department
British Aerospace Aircraft Group
Warton Division, Preston

British Aerospace are currently investigating the suitability of titanium extrusions for certain applications

4) Mr Bruce
Bayer U.K.
Enamels and Ceramics
Fountain Street
Penton, Stoke-on-Trent

Bayer U.K. are the major supplier of powdered extrusion glasses

5) Miss Anderskouv
Acheson Colloids
Prince Rock
Plymouth
Devon, PL4 OSP

Acheson Colloids supply Gredag 1559 molybdenum disulphide grease and the Deltaglaze glass coatings.

6) Professor C.M. Sellars et al
University of Sheffield

For any aspect of high temperature glass-lubricated extrusion.

NOMENCLATURE

A	Area
	Constant in hot working equation
A_B	Cross sectional area of billet
a	Constant
a_o, a_1, a_2	Constants
b	Constant
C	Specific heat capacity
C_G	Specific heat capacity of glass
C_S	Specific heat capacity of steel
C_{Ti}	Specific heat capacity of titanium
$C_1 - C_7$	Constants in temperature rise model
D_{AV}	Average extrude diameter
D_B	Billet diameter
D_E	Extrude diameter
d	Diameter
$d_{0.25}$	Diameter of extrude 25% along its length
$\dot{E}$	Rate of energy dissipation
$\dot{E}_{12}$	Rate of energy dissipation at velocity discontinuity separating regions 1 and 2
$\dot{E}_2$	Rate of energy dissipation within region 2
K	Thermal conductivity
K_G	Thermal conductivity of glass
K_S	Thermal conductivity of steel
K_{Ti}	Thermal conductivity of titanium
k	Shear flow stress
$k_1 - k_7$	Constants in temperature rise model
L	Extrusion load
	Thickness
L_1	Die land length
L_E	Height of control volume 2 at time t
L_m	Mean load for the nth time increment

L_n	Extrusion load at nth time increment
L_T	Height of control volume 2 at start of extrusion
m	Friction factor
n	Constant in hot working equation
P	Extrusion pressure
p	Density
p_G	Density of glass
p_S	Density of steel
p_{Ti}	Density of titanium
Q	Activation energy
$Q_1 - Q_7$	Heat flows
R	Extrusion ratio
	Gas constant
R_B	Billet radius
R_E	Extrude radius
r	Radius
$r(\theta)$	Radial distance from 0 in axisymmetric velocity field
s	Area of velocity discontinuity
	Maximum penetration distance of heat front
T	Temperature
T_B	Billet Temperature
T_{B1}	Temperature in deforming zone
T_{B2}	Temperature in non-deforming zone
T_C	Container temperature
T_I	Interface temperature
$T_{I1} - T_{I4}$	Interface temperatures
T_G	Glass pad temperature
T_P	Pressure pad temperature
T_S	Steel tooling temperature
ΔT_1	Temperature rise in the deforming zone
ΔT_2	Temperature rise in the non-deforming zone
ΔT_D	Temperature differential between the billet interface and the adjacent tooling
$\Delta T_{D1} - \Delta T_{D4}$	Temperature differentials between billet interface and adjacent tooling

ΔT_1^*	Temperature differential between the deforming zone and the tooling
ΔT_4	Temperature differential between the deforming and non-deforming zones
t	Time
Δt	Increment of time
V	Volume
	Ram speed
V_B	Ram speed
x	Depth of deformation zone in axisymmetric velocity field
	Distance
Z	Zener-Holloman parameter
Z_I	Z parameter at commencement of extrusion
α	Constant in hot working equation
	Abbreviation for alpha
	Thermal diffusivity
β	Abbreviation for beta
γ	Angle in axisymmetric velocity field
	Shear strain
$\dot{\gamma}$	Shear strain rate
δ	Angle in axisymmetric velocity field
	Displacement
$\Delta\delta$	Increment of displacement
ε	Strain
$\dot{\varepsilon}$	Strain rate
$\bar{\dot{\varepsilon}}$	Mean strain rate
ε_H	Homologous strain
σ	Flow stress
$\bar{\sigma}$	Mean flow stress
$\bar{\sigma}_y$	Mean yield stress
θ	Angle in axisymmetric velocity field
	Twist
$\dot{\theta}$	Twist rate
τ	Shear stress
τ_{ij}	Shear stress at velocity discontinuity ij

REFERENCES

1. A.S.M. Metals Handbook Vol. 1 Eighth Edition (1961) Titanium and Titanium Alloys pp. 524, pp. 1147
2. A.S.M. Metals Handbook Vol. 3 Ninth Edition (1980) Introduction to Titanium and Its Alloys pp. 353
3. I.J. Polmear, Textbook, Light Alloys-Metallurgy of The Light Metals, Edward Arnold (1981)
4. A.D. McQuillan, M.K. McQuillan, Textbook, Titanium, Butterworths, London (1956)
5. E.K. Molchonova, Textbook, Phase Diagrams of Titanium Alloys, Israel Program for Scientific Publications (1965)
6. I.M.I. Titanium 318, I.M.I. Brochure
7. Properties and Processing of Ti-6Al-4V, Timet Brochure
8. J.C. Williams, Critical Review :- Kinetics and Phase Transformations, Titanium Science and Technology, Plenum Press, New York (1973) pp. 1433
9. M.A. Zaidi, A Study of Phase Transformations in Ti-6Al-4V, M.Sc. Imperial College (1976)
10. P.J. Fopiano, M.B. Bever, B.L. Averbach, Phase Transformations and Strengthening Mechanisms in the Alloy Ti-6Al-4V, Trans. A.S.M. 62 (1969) pp. 324
11. J.C. Williams, M.J. Blackburn, A Comparison of Phase Transformations in Three Commercial Titanium Alloys, Trans. A.S.M. 60 (1967) pp. 373
12. J.M. Dupouv, M.B. Bever, B.L. Averbach, On the Ageing Behaviour of the Alloy Ti-6Al-4V, Trans. A.S.M. 52 (1960) pp. 221
13. R.G. Sherman, H.D. Kessler, Investigation of the Heat Treatability of the 6% Aluminium - 4% Vanadium Titanium Base Alloy, Trans. A.S.M. 48 (1956) pp. 657

14. A.S.M. Metals Handbook Vol. 7 Eighth Edition (1972), Microsctructure of Titanium and Titanium Alloys, pp. 321

15. J.J. Jonas, C.M. Sellars, W.J.McG. Tegart, Strength and Structure under Hot Working Conditions, Met. Rev. 14 (1969) pp. 1

16. C.M. Sellars, W.J.McG. Tegart, Hot Workability, Int. Met. Rev. (1972) pp. 1

17. H.J. McQueen, J.J. Jonas, Treatise on Materials Science and Technology Vol. 6 The Plastic Deformation of Metals, Ed. R.J. Arsenault (1975) N.Y. Acad. Press, pp. 393

18. P.G. Partridge, The Crystallography and Deformation Modes of Hexagonal Close Packed Metals, Met. Rev. 12 (1967), 118, pp. 169

19. D. Hull, Textbook, Introduction to Dislocations, Second Edition, Pergamon Press (1975)

20. F. Dyment, C.M. Libanati, Self Diffusion of Ti, Zr and Hf in their H.C.P. Phases and Diffusion of Nb^{95} in H.C.P. Zr, J. Mat. Sci. 3 (1968), pp.349

21. F. Dyment, Self and Solute Diffusion in Titanium and Titanium Alloys, Titanium '80 Science and Technology, Proc. 4th Int. Conf. on Titanium, Vol. 1, pp. 519

22. S.M.L. Sastry et al, High Temperature Deformation of Ti-6Al-4V, as above pp. 873

23. W.A. Bryant, Correlation of Data on the Hot Deformation of Ti-6Al-4V, J. Mat. Sci. 10 (1975), pp. 1793

24. A.S.M. Metals Handbook Vol. 5 Eighth Edition (1970) Forging of Titanium Alloys, pp. 142

25. London: Metals Society, Proc. Forging and Properties of Aerospace Alloys Conference (1978)

26. J.V. Scanlan, G.J.G. Chambers, Forgings in Titanium Alloys, The Science, Technology and Application of Titanium, Proc. Int. Conf. on Titanium (1970) pp. 79

27. J.E. Coyne, The Beta Forging of Titanium Alloys, As Above, pp. 97

28. T.E. Green, C.D.T. Minton, The Effects of Beta Processing on Properties of Titanium Alloys, As Above, pp. 11

29. A.F. Gerds et al, Deformation Processing of Titanium and Its Alloys, U.S. Dep. Commerce Clearing House Rep. (1966), AD-634141, pp. 337

30. F.J. Gurney, A.T. Male, The Relationship of Microstructures and Mechanical Properties of Extruded Titanium Alloy Bars to the Prior Deformation Processing History, A.F.M.L.-TR-71-28 April 1971

31. F.J. Gurney, A.T. Male, The Influence of Process Variables on the Pressure Requirements for the Extrusion of Titanium Alloy Rods, Titanium Science and Technology, Proc. 2nd Int. Conf. on Titanium (1972) Vol. 1, pp. 439

32. F.J. Gurney, A.T. Male, The Effects of Extrusion Process Variables on the Structure and Properties of Titanium Alloys, As Above, Vol. 3, pp. 1769

33. F.J. Gurney, A.T. Male, The Influence of Controlled Processing on the Yield Strength and Toughness Properties of Titanium Alloy Extrusions, As Above, Vol. 3, pp. 1755

34. A.S.M. Metals Handbook Vol. 2 Eighth Edition (1964), Heat Treating of Titanium and Titanium Alloys, pp. 301

35. Attwell M. Adair, Influence of Processing Variables on the Microstructure of Extruded Ti-5Al-2.5 Sn, Trans. A.S.M. 62 (1969) pp. 345

36. Attwell M. Adair, J.A. Roberson The Influence of Processing Variables on the Structure and Properties of Extruded Beta III Titanium, A.F.M.L. - TR-70-277 March 1971

37. Atwell M. Adair et al, The Influence of Thermomechanical Processing on the Fatigue Behaviour of Extruded Beta III Titanium, Titanium Science and Technology, Proc. 2nd Int. Conf. on Titanium (1973), Vol. 3, pp. 1801

38. K.E. Hughes, The Extrusion of Steel, M. Met. Thesis (1971), University of Sheffield

39. K.E. Hughes, Some Factors Influencing the Hot Extrusion of Steels, The Metallurgist and Materials Technologist, November 1973, pp. 572

40. K.E. Hughes, C.M. Sellars, Extrusion Limit Diagrams for the Hot Extrusion of Steel, The Metallurgist and Materials Technologist, May 1974, pp. 201

41. K.E. Hughes, C.M. Sellars, Temperature Changes During the Hot Extrusion of Steel, J.I.S.I. September 1972, pp. 661

42. K.E. Hughes et al, Temperature and Flow Stress During the Hot Extrusion of Steel, Metals Technology, April 1974, pp. 161

43. K.E. Hughes et al, Glass Lubricated Hot Extrusion of Stainless Steel, Metals Technology, August 1980, pp. 323

44. R. Cockroft, The Glass Lubricated Extrusion of Steel, Metals and Materials Technology, September 1969, pp. 351

45. R. Cox et al, Some Aspects of Steel Extrusion, J.I.S.I., April 1960, pp. 423

46. R. Cox, Recent Experiences with the 1150 Ton Extrusion Press at the Works of Low Moor Fine Steels Ltd., J.I.S.I., March 1964, pp. 346

47. J.W.R. Naden, The Extrusion of Steel Tubes, J.I.S.I., November 1959, pp. 278

48. Titanium and Steel Extrusion, Martin Marietta Brochure

49. Titanium Seamless Pipe, Martin Marietta Brochure

50. Titanium, Martin Marietta Brochure

51. I.M.I. Titanium Alloy Extruded Sections, I.M.I. Technical Report

52. P. Loewenstein, Extruding Titanium and Titanium Alloys, Soc. of MFG. Eng. Inter. Engineering Conference and Tool Exposition, Philadelphia, April 26-30, 1971, SME Paper MF-71-139

53. J. Rice, Titanium Extrusions, Precision Metal, February 1968 26(2), pp. 27

54. W. Ballentine, Titanium Extrusions, Midwest Engineer, September 1968, 21(1), pp.57

55. F.W. Fredrickson et al, Heavy Press Extrusions of Light Metals, Metals Eng. Quart., November 1968 8(4), pp. 25

56. D. Rabenold, Extruding Large Components, Metal Progress, August 1974 106(3), pp. 80

57. G. Michaelson, Big Shapes are the Backbone of Boeing 747, Metal Progress, March 1968 93(3), pp. 58

58. R. Chait, C. Stead, Fabrication and Properties of Heavy Section Extrusions of Ti-6Al-4V-2Sn and Ti-8Mo-8V-2Fe-3Al Alloys, Met. Trans. B Vol. 8B, September 1977, pp. 371

59. R. Chadwick, The Relevance of Lubrication in Extrusion, Metals and Materials Technology, May 1970, pp. 201

60. J. Sejournet, J. Delcroix, Glass Lubrication in the Extrusion of Steel, Lubrication Engineering, November-December 1955, pp. 389

61. C.E. Pearson, R.N. Parking, Textbook, The Extrusion of Metals, Chapman and Hall (1960)

62. T.H.C. Childs, Metal Flow in the Hot Extrusion of Mild Steel, Metals Technology, July 1974, pp. 305

63. L. Zagar, G. Schneider, Glass Lubrication for Hot Extrusion, Metal Forming, June 1969, pp. 168

64. J.A. Rogers, Ph.D. Thesis (1962), University of Birmingham

65. J.A. Rogers, G.W. Rowe, An Investigation of Factors Influencing Lubricant Behaviour in Hot Extrusion, J. Inst. Met. (1967), 95, pp. 257

66. J.S. Alder, The Effect of Strain Rate and Temperature on the Resistance of Aluminium, Copper and Steel to Compression, J. Inst. Met., 83, (1954-55)

67. I. Perlmutter, V. De Pierre, Extruding Refractory Metals, Metal Progress, November 1963, 84, pp. 90

68. A.S.M. Metals Handbook Vol. 4, Ninth Edition (1981), Introduction to Heat Treating of Tool Steels, pp. 561

69. A.S.M. Metals Handbook Vol. 3, Ninth Edition (1980), Selection of Materials for Hot Extrusion Tooling, pp. 537

70. R.E. Reed Hill, Textbook, Physical Metallurgical Principles, D. Van Nostrand (1973)

71. S. Hirst, D. Ursell, Metal Treatment (1958), 25, pp. 409

72. R.P. Vierod, Ph.D. Thesis (1983), University of London

73. D.S. Wright, Ph.D. Thesis (1978), University of London

74. P. Richards, Ph.D. Thesis (1984), University of London

75. Y.S. Touloukian, Thermophysical Properties of High Temperature Solid Materials, Macmillan 1967

76. S.J. Paterson, Ph.D. Thesis (1981), University of London

77. M.G. Tutcher, Ph.D. Thesis (1979), University of London

78. P.A. Tunnicliffe, Ph.D. Thesis (1979), University of London

79. P. Feltham, Metal Treatment (1956), 23, pp. 440

80. J.M. Alexander, J. Inst. Met. (1961-62), 90, pp. 193

81. A.F. Castle, Ph.D. Thesis (1974), University of London

82. T. Sheppard, E.P. Wood, Proc. 17th M.T.D.R. (1976), McMillan London, p411

83. P. Cooper, Ph.D. Thesis (1985), University of London

84. D. Pitts, L. Sissom, Textbook, Heat Transfer, McGraw Hill (1977)

85. Acheson Colloids Product Data Sheet - DAG 1559

86. I.M.I. Titanium 550, I.M.I. Brochure

87. Acheson Colloids Product Data Sheet, Deltaglaze 12

88. J.G. Tweedale, M.Sc. Thesis (1974), University of London

89. H.M. Flower, Imperial College, Private Communication

90. A.W. Bowen, The Influence of Crystallographic Orientation on Tensile Behaviour in Strongly Textured Ti-6Al-4V, Mat. Sci. and Eng., 40 (1979), pp. 31

91. A.W. Bowen, Texture Stability in Heat Treated Ti-6Al-4V, Mat. Sci. and Eng., 29 (1977), pp. 19

92. A.W. Bowen, The Influence of Crystallographic Orientation on Fatigue-Crack Growth in Strongly Textured Ti-6Al-4V, Acta Metallurgica, Vol. 23, November 1975, pp. 1401